CRANFIELD UNIVERSITY

C C ANTALOAE

FEASIBILITY OF HIGH FREQUENCY ALTERNATING
CURRENT POWER DISTRIBUTION FOR THE AUTOMOBILE
AUXILIARY ELECTRICAL SYSTEM

SCHOOL OF ENGINEERING
DEPARTMENT OF AUTOMOTIVE ENGINEERING

PhD THESIS
Academic year: 2010-2011

Supervisor: Dr. J Marco
April 2011

CRANFIELD UNIVERSITY

SCHOOL OF ENGINEERING
DEPARTMENT OF AUTOMOTIVE ENGINEERING

PhD THESIS

Academic Year: 2010-2011

C C ANTALOAE

FEASIBILITY OF HIGH FREQUENCY ALTERNATING CURRENT
POWER DISTRIBUTION FOR THE AUTOMOBILE AUXILIARY
ELECTRICAL SYSTEM

Supervisor: Dr. J Marco

April 2011

This thesis is submitted in partial fulfillment of the requirements
for the degree of Doctor of Philosophy

ABSTRACT

This study investigates the feasibility and potential benefits of high frequency alternating current (HFAC) for vehicle auxiliary electrical systems.

A 100Vrms, 50kHz sinusoidal AC bus is compared with 14V DC and 42V DC electrical systems in terms of mass and energy efficiency. The investigation is focused on the four main sub-systems of an on-board electrical network, namely: the power generation, power distribution, power conversion and the electrical loads. In addition, a system-level inquiry is conducted for the HFAC bus and a comparable 42V DC system.

A combination of computer simulation, analytical analysis and experimental work has highlighted benefits for the HFAC power distribution sub-system and for low-torque motor actuators. Specifically, the HFAC conductor mass is potentially 70% and 30% lighter than comparable 14V DC and 42V DC cables, respectively. Also, the proposed cable is expected to be at least 80% more energy efficient than the current DC conductor technology. In addition, it was found that 400Hz AC machines can successfully replace DC motor actuators with a rated torque of up to 2Nm. The former are up to 100% more efficient and approximately 60% lighter and more compact than the existing DC motors in vehicles. However, it is argued that the HFAC supply is not feasible for high-torque motor actuators. This is because of the high energy losses and increased machine torque ripple associated with the use of HFAC power.

The HFAC power conversion sub-system offers benefits in terms of simple power converter structure and efficient HFAC/DC converters. However, a significant limitation is the high power loss within HFAC/AC modules, which can be as high as 900W for a 2.4kW load with continuous operation. Similar restrictions are highlighted for the HFAC power generation sub-system, where up to 400W is lost in a 4kW DC/HFAC power module.

The conclusion of the present work is that the HFAC system offers mass and energy efficiency benefits for the conventional vehicle by leveraging the use of compact low-torque motor actuators and lightweight wiring technology.

ACKNOWLEDGEMENTS

List of Contents

List of Figures

viii

ABBREVIATIONS

AC	Alternating Current
ACRL	Actively-Clamped Resonant Link Inverter
AS	Active Suspension
AWG	American Wire Gauge
BUBI	(from German) Square Wave Voltage, Square Wave Current
BULSI	(from German) Square Wave Voltage, Sinusoidal Current with Gaps
BUSI	(from German) Square Wave Voltage, Sinusoidal Current
CSD	Constant Speed Drive
DC	Direct Current
DPA	Distributed Power Architecture
EMB	Electro-Mechanical Brakes
EHC	Electrically Heated Catalyst
EMI	Electromagnetic Interference
EPAS	Electric Power Assisted Steering
HEV	Hybrid Electric Vehicle
HF	High Frequency
HFAC	High Frequency Alternating Current
ICE	Internal Combustion Engine
IGBT	Insulated-Gate Bipolar Transistor
IG	Integrated Generator
ISG	Integrated Starter Generator
MOSFET	Metal-Oxide Semiconductor Field Effect Transistor
MMS	Modular Measurement System
MSIB	Modular System Interface Bus
NASA	National Aeronautics and Space Administration
OEM	Original Equipment Manufacturer
PDM	Pulse Density Modulation

PF	Power Factor	
PI	Proportional Integral	
PMSM	Permanent Magnet Synchronous Motor	
PUPS	Point of Use Power Supply	
PWM	Pulse Width Modulation	
SAE	Society of Automotive Engineers	
SMR	Switch Mode Rectifier	
SUBI	(from German) Sinusoidal Voltage, Square Wave Current	
SUSI	(from German) Sinusoidal Voltage, Sinusoidal Current	
SVM	Space Vector Modulation	
VCO	Voltage Controlled Oscillator	
THD	Total Harmonic Distortion	[%]
UPQC	Unified Power Quality Conditioner	
VSD	Variable Speed Drive	
VVA	Variable Valve Actuation	
VVVF	Variable Voltage Variable Frequency	
ZCS	Zero Current Switching	
ZVS	Zero Voltage Switching	

NOMENCLATURE

C_f	Output filter capacitor	[F]
C_r	Resonant network capacitor	[F]
C_s	Capacitor in series connection with L_s	[F]
C_m	Common-mode capacitance	[F]
C_o	Capacitor element acting as a circuit filter	[F]
C_p	Capacitor circuit component	[F]
$D_{1,2,3\ and\ 4}$	Diodes	
e	Error signal	
$I_{g,\ 1-4}$	Gate on/off command signals	Binary
L_s	Inductor in series connection with C_s	[H]
L_s-C_s	Series resonant network	
L_p	Inductor circuit component	[H]
$N_1{:}N_2$	Transformer winding turns ratio	constant
R_{ds}	ON-resistance of power MOSFETs $S_{1,2,3,4}$	[Ω]
R_L	Generic resistive load	[Ω]
R_r	Internal resistance of the resonant network inductor L_r	[Ω]
s	Laplace variable	
$S_{1,2,3,4}$	H-bridge MOSFET power switches	
S_{on}	Full Voltage-on Command Signal	Binary
S_{off}	Zero-Voltage Command Signal	Binary
S_r	Ramp signal	
Q_a	Thyristor switch	
Q_b	Thyristor switch	
V_{dc}	DC voltage source	[V]

V_o	Output sinusoidal voltage/ Preset decay voltage in Appendix D	[V]
V_{LF}	Synthesized AC voltage	[V]
V_{ref}	DC voltage reference	[V]
V_t	Threshold command voltage	[V]
T_a	Time constant used in the SVM algorithm	[s]
T_b	Time constant used in the SVM algorithm	[s]
T_c	Time constant used in the SVM algorithm	[s]
T	Time period corresponding to a frequency of 50kHz	[s]
T_s	Transition time	[s]
Z_r	Characteristic circuit impedance	[Ω]
α	Thyristor controller firing angle	[degree]
Δ	Time period, circuit control variable	[s]
ω_n	Natural frequency	[rad/s]
χ	Overshoot	[%]
δ	Voltage decay ratio	[%]
ζ	Transfer function damping ratio	[%]

Chapter 1

Introduction

1.1 Introduction to automotive electrical systems

The present auxiliary electrical system in passenger vehicles is based on direct current (DC) power distribution at 14V. Although auxiliary systems have become more numerous and complex over the past decades, the power architecture supplying these loads has not changed significantly since the late 1950s when the 6V DC was increased to the present 14V DC (Johnston, 1996). Although the average power demand of on-board auxiliaries has trebled over the past two decades to more than 2.5kW (Miller, 1996), the same centralised electrical network layout is still in use today.

The main limitations of the 14V DC system have been highlighted by a number of authors, including Miller et al. (1999):

- First, from a system point of view, the voltage varies from 9V to 16V. Since the loads are designed to operate at the nominal 14V DC, the variation in bus voltage could lead to less efficient or overrated load components.

- Second, the drawbacks at the load side include high losses in the brushes of 14V motors and a comparatively high failure rate of contactors.

- In addition, since the wiring is point-to-point, the harness becomes complex, heavy, and the assembly process is expensive and time consuming.

- Furthermore, state-of-the art auxiliary systems such as the integrated-starter generator (ISG), electric power assisted steering (EPAS) or variable valve actuation (VVA) have a combined power demand in excess of 5kW (Lukic and Emadi, 2002, Lukic and Emadi, 2003). This power level exceeds the capability of the present 14V DC system, which is in the order of 2.5kW (limited by the high current of up to 200A).

In an effort to keep abreast of the increasing power demand, the 42V *PowerNet* was proposed in the early 1990s by the SAE Dual/Higher Voltage Committee as a potential replacement for the 14V DC system in vehicles. The standard specifies 42V as the nominal voltage, and 50V and 60V as maximum continuous and dynamic voltage levels, respectively (Rajashekara, 2003). As will be detailed in Chapter 4, although many 42/14V DC architecture topologies have been investigated to accommodate both existing 14V loads and modern 42V systems, technical challenges such as electric arcs, corrosion and bus-to-bus faults (Keim, 2004) have tended to limit the introduction of the proposed 42V system.

1.2 Motivation for high frequency alternating current investigation

It is unlikely that a single voltage will best meet the power requirements of auxiliary consumers in vehicles, since at least three on-board supply voltage levels can be identified: 5V for instruments and electronic control units, 14V for low-power loads and 42V DC for modern applications with a power requirement in the kilowatt range. Ideally, an electrical distribution system should be capable of matching the power required by individual loads without sacrificing efficiency. It would also be desirable to have a distribution system that weighs less than the loom in cars today, provides greater design flexibility and improves efficacy of at least some electrical loads. It is argued that a suitable candidate with a realistic prospect to bring these expectations to completion is a power distribution system based on high frequency alternating current (HFAC).

The principal rationales for investigating HFAC as a possible replacement for DC as means of power distribution in vehicles can be summarised as follows:

  • HFAC cables are lightweight and efficient for power distribution (Antaloae et al., 2010) and the high frequency translates into compact passive circuit elements such as capacitors, inductors or transformers.

• In addition, smaller, lighter and more efficient electrical motors operating at 400Hz can be easily interfaced from a HFAC bus and potentially replace the existing low-torque DC motor actuators in vehicles (Antaloae et al., 2011).

• The HFAC bus has a distributed topology where power converters are employed at each point of use, making any system faults easy to track and identify. It is known that this can be problematic in current DC systems which can contain up to 600 sub-modules and contactors, 1500 wires and up to 2000 terminals (Honeywill, 2007).

• Simultaneous power regulation can be achieved for all the loads connected to the HFAC bus, unlike in some 42V/14V DC power networks where only one of the buses can be regulated at any given time (e.g. dual-stator alternator (Caliskan, 2000), dual-reference alternator or the transformer/rectifier power net (Smith, 1991)).

• Current at frequency higher than 10kHz is safer for human cells than DC or low-frequency AC current (Patel, 2005). This work proposes power distribution at a frequency higher than the upper limit of the human audible range (20kHz).

• Transformers employed in HFAC architectures tend to have a high power conversion efficiency and provide galvanic isolation for the loads connected to the bus. Furthermore, any voltage or current level is easily obtainable by appropriately choosing the transformer windings turns ratio.

1.3 Thesis aim, objectives and methodology

The research presented in this Thesis is focused on investigating the benefits of HFAC power for vehicle electrical auxiliary systems. To this end, the four main sub-systems of an electrical network are analysed: power generation, power distribution, power conversion and the electrical loads. In addition, a system-level investigation is carried out which gives an overall conclusion to this inquiry.

The objectives of this work are to investigate the advantages and potential limitations associated with the use of HFAC for the four sub-systems above and for the overall system, in terms of their feasibility for the on-board auxiliary electrical loads, energy efficiency, and potential for mass reduction.

The inquiry associated with each of the objectives is divided into two primary threads:

1. The first is directed to the investigation of existing and proposed DC electrical systems in vehicles, in order to gain an understanding of their operation and any limitations.

2. Second, the potential advantages of HFAC are explored in comparison to both the present 14V DC and the proposed 42V *PowerNet*. As part of this analysis, the comparison is conducted based on equivalent characteristics of the three systems.

The methodology employed includes modelling and simulation, analytical analysis, as well as the use of case studies and an experimental examination. These techniques are described below.

Modelling and simulation has been used to gain a better understanding of the operation of HFAC and DC power electronic circuits. The main purpose has been to observe the performance characteristics of the power transformation modules, such as the current rise time, the power capability or the voltage/current strain on the circuit elements. For the particular case of the DC/HFAC power supply, modelling and simulation has also been applied to gain an insight into the potential efficiency of the module.

The tool used to conduct the modelling and simulation is the proprietary Mathworks™ environment, namely Matlab and Simulink. Specifically, the electrical circuits presented throughout this study have been building upon the components within the Simulink SimPowerSystems toolbox. A discrete solver has been chosen for simulation, where the integration step varies from 10ns (for the particular case of power converters, which

have a very high dynamic operation) to 1ms (for the simulation of electrical machines, for example).

The analytical analysis has been utilised:

- for the evaluation of the efficiency of HFAC and DC power converters. Specifically, based on the operation of the circuit, switching and conduction losses have been estimated analytically, and also

- as part of the case study analysis, in order to approximate the mass and energy losses of the systems being compared.

Two case studies have been conducted as part of this study. First, a critical analysis has been carried out to investigate the mass and power distribution efficiency of a HFAC power distribution sub-system in comparison with both 14V DC and 42V DC topologies. Measured data of 14 electrical loads from a typical passenger vehicle have been used for this analysis. Second, a system-level case study has been conducted in order to highlight the characteristics of the HFAC bus for a large group of electrical loads. Data from the case study mentioned above and from relevant literature have been utilised for the investigation of a representative set of 98 electrical loads.

An EPAS test rig has been set up to support the analysis of HFAC power benefits for the electrical loads sub-system. The mechanical setup has been carried out as part of a supporting activity, while the actuator control has been part of this study. The column-assist EPAS system integrates a DC supply and three-phase permanent magnet synchronous motor. The purpose of the structure was to emulate realistic torque vs. speed characteristics of this actuator. The results, in turn, have been used in conjunction with EPAS models built in Simulink to investigate the feasibility and advantages of HFAC power for this application. As will be discussed in Chapter 8, the result for the EPAS system is considered representative for the applicability of HFAC power for high-torque motor loads.

1.4 Thesis outline

Chapter 2 discusses the existing work on HFAC power systems. Namely, non-automotive HFAC applications are presented, such as NASA's International Space Station programme in the 1980s, telecommunication, microgrids and commercial electronics systems. The Chapter highlights the generic potential advantages for HFAC power.

Chapter 3 includes a comprehensive account of the HFAC research in the field of automobile electric architectures. The Chapter is focused on the identification of the aspects of the HFAC technology that have not yet been addressed by the previous studies.

Chapter 4 introduces the architecture topology and the characteristics of the proposed electrical bus. The rationales underpinning the choice for specific bus features such as voltage amplitude and frequency are given.

Chapters 5, 6, 7 and 8 present the investigation of HFAC for the four electrical sub-systems, respectively: power generation, power distribution, power conversion and electrical loads. As part of the analysis in each Chapter, a brief account of the equivalent DC sub-system is given, followed by a critical comparative analysis between the HFAC and the DC sub-system.

Chapter 9 assembles the main findings of Chapters 5 to 8 in a system-level approach to determine the viability of the HFAC bus in replacing the present DC system. The discussion is centred around the case study of a representative electrical system for a passenger vehicle. Chapter 10 presents the conclusions of the present investigation and includes recommendations for further work.

Chapter 2

Survey on high frequency AC power architectures and applications

---

2.1 Introduction

The aim of this chapter is to highlight the advantages of HFAC power. These benefits form the motivation for an in-depth investigation of the technology for the automobile auxiliary electrical system. To this end, various HFAC power systems are described for applications including aerospace, telecommunication, microgrids and commercial electronics. These case studies give a comprehensive account of the previous work involving the use of HFAC power.

The Chapter introduces the reader to the typical HFAC system topologies, and discusses the system-level characteristics in parallel with DC electrical networks. In addition, several representative inverter and converter topologies are introduced. Specifically, the modules are based on typical methods employed in the transformation of DC into HFAC voltage, and conversely for HFAC/DC or HFAC/AC power conversion. Due to their simplicity and wide adoption within the relevant studies presented within the present Chapter and Chapter 3, these techniques form the basis for the DC/HFAC, and HFAC/DC and AC power management circuits presented in Chapters 5 to 8 for the automotive electrical system.

Section 2.2 presents the work reported by NASA for the International Space Station Freedom programme, which focused on the potential advantages of replacing the DC distribution system with a 20kHz, 440V AC architecture. First, the motivation behind this inquiry is outlined. Second, Section 2.2 describes the architecture of the proposed HFAC system. In addition, the topology and control of related DC/HFAC, HFAC/AC and HFAC/DC converter modules are detailed.

Next, Section 2.3 presents a HFAC network based on a sinusoidal 60V, 128kHz supply. This power system has been proposed as an alternative to DC architectures for telecommunication equipment. First, existing DC power topologies are described. Second, the Section introduces a HFAC power network concept and presents various power converter topologies which underpin the integration of the proposed technology within telecommunication power systems.

The Chapter continues with the description of a microgrid system employing 20kHz sinusoidal AC for power distribution. Section 2.4 describes the topology and control of a circuit designed to maximise the power quality within the HFAC distribution system. Specifically, the presented power quality converter compensates for reactive voltage and current distortions induced by the different electrical sources and loads connected to the grid.

Section 2.5 describes a modular measurement system (MMS) based on a distributed HFAC power bus. The MMS apparatus, operating at different voltages including 24.3V AC, 40kHz, is the sole commercially available implementation of HFAC. In addition, Section 2.5 presents the results of a comparative analysis for different types of HFAC power distribution waveforms. In particular, the comparison is focused on a square-wave voltage distribution and the effect of several transition times on the spectral power content. The motivation of this exercise for the present study is in identifying the implications of this type of waveform for the automotive environment. The finding will support the recommendation for the most suitable signal for on-board HFAC power distribution.

Finally, drawing on the presented literature review on the use of HFAC for domains other than the automotive area, Section 2.6 summarises the advantages of HFAC power and outlines the rationales for the investigation of this technology for the passenger vehicle electrical system.

2.2 NASA International Space Station Freedom programme

2.2.1 Motivation

NASA estimated in 1983 that power demand for spacecraft will extend to the megawatt level by the year 2000 (Renz et al., 1983). A power distribution system in line with this requirement implied excessive cable weight and high resistive and core losses associated with the transformers and generators. Furthermore, as indicated in the cited study, power for such a system is prone to quality issues as a consequence of load current variation.

HFAC power has been investigated by NASA as a possible alternative to DC power that can tackle the above-mentioned drawbacks. The motivation for an in-depth study of HFAC was the fact that this technology not only reduces significantly the weight and size of the cables and distribution network components (i.e. transformers, inductors, capacitors) needed for filtering and temporary energy storage, but also allows for less expensive and complex circuitry. In addition, HFAC is expected to reduce considerably the losses associated with power distribution. Furthermore, this approach eliminates the need for high voltage, high current DC switches and incorporates simpler connectors based on magnetic coupling (Renz et al., 1983).

2.2.2 HFAC system architecture and inverter/converter circuit topologies

This Subsection gives an overview of the HFAC architecture proposed by NASA and briefly presents the structure and the operation of the associated power converter topologies.

Power for the International Space Station is absorbed from solar panels and transformed into a 20kHz, 440V, single-phase supply (Hansen, 1988). One major ability of this system is to supply power at different voltage levels by using transformers to step the

voltage up or down as required by the application. By matching the voltage to the size of the user, power distribution losses can be further minimised. Therefore, as illustrated in Figure 2.1, the HFAC system emerges as a distributed network with multiple terminals and the ability to meet different voltage, frequency and power requirements (Renz et al., 1983).
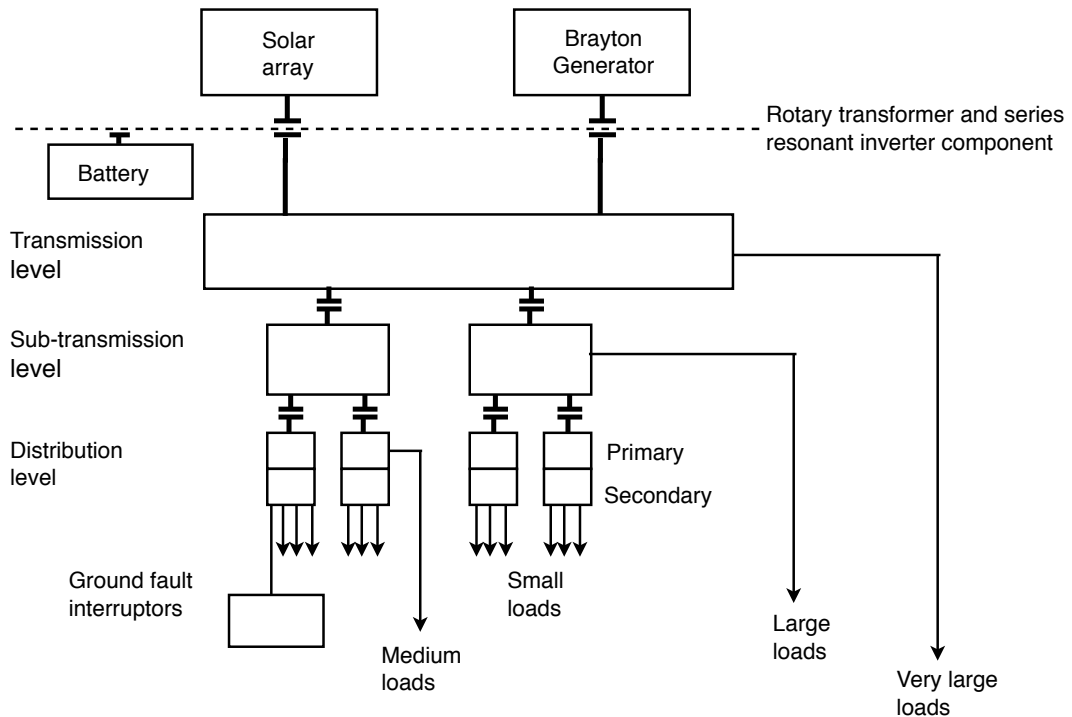
Figure 2.1 Structure of alternating current power system for the International Space Station
(Renz et al., 1983)

Alternating current is easily generated using resonant techniques or high speed generators and conveniently transformed into various voltage levels at different frequencies (Renz et al., 1983). Figure 2.2 presents the concept of a basic resonant DC/ HFAC converter in the form of a circuit diagram.
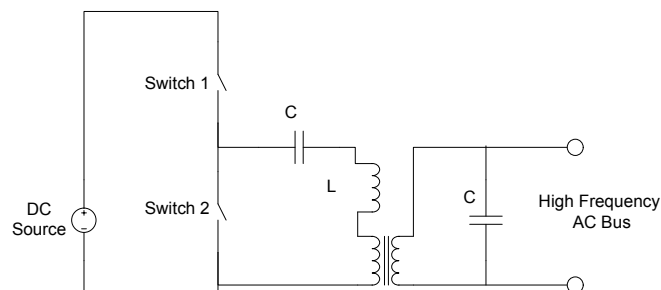
Figure 2.2 Resonant half bridge series inverter (Renz et al., 1983)

Since switches 1 and 2 can be opened when the current crosses zero, the inverter is capable of zero energy loss during power turn-on and turn-off. This aspect is noteworthy, since Renz et al. (1983) have indicated that the reliable interruption of large DC currents in aerospace applications, by other than brute force methods, can be problematic.

A different resonant DC/HFAC inverter proposed for the International Space Station has been investigated by Jain et al. (1989). Figure 2.3(a) shows the schematic of the inverter, which includes a DC voltage source, high frequency inverter, output resonant network, a transformer and a control circuit. The output resonant network includes a series LC circuit (L_s and C_s) and a parallel LC circuit (L_p, C_p). The authors claim excellent efficiency for the inverter over a wide range of power output. A full explanation of the circuit structure and operation is given by Jain et al. (1989). For reference, a brief summary of its operation is given below.
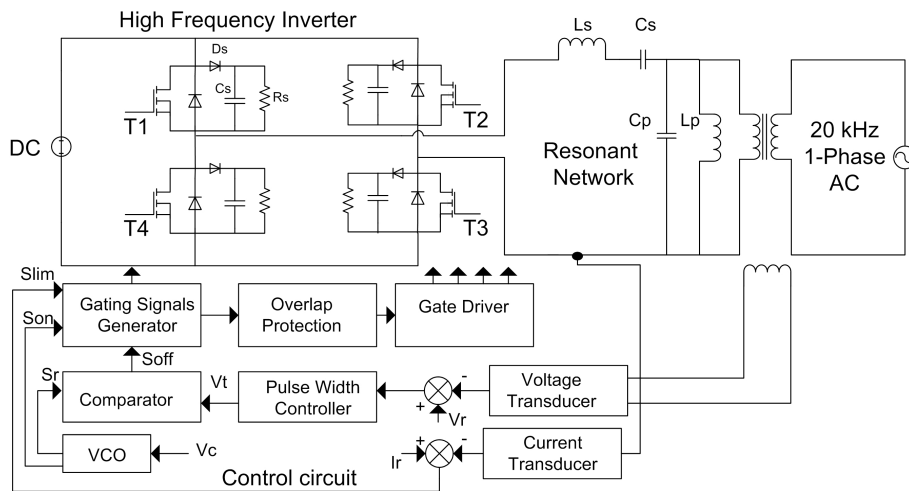
Figure 2.3a Circuit diagram of 20 kHz resonant inverter system (Jain and Tanju, 1989)

The Voltage Controlled Oscillator (the VCO block in Figure 2.3(a)) generates S_{on} and S_r which are the full voltage and pulse width ramp signals, respectively (see Figure 2.3 (b)). The comparator block matches the pulse width ramp S_r with the threshold voltage V_t derived from the output voltage feedback, and sends a signal S_{off} which is a zero

voltage command. Both the operating frequency and the pulse width can be controlled by signals V_c and V_t, respectively.
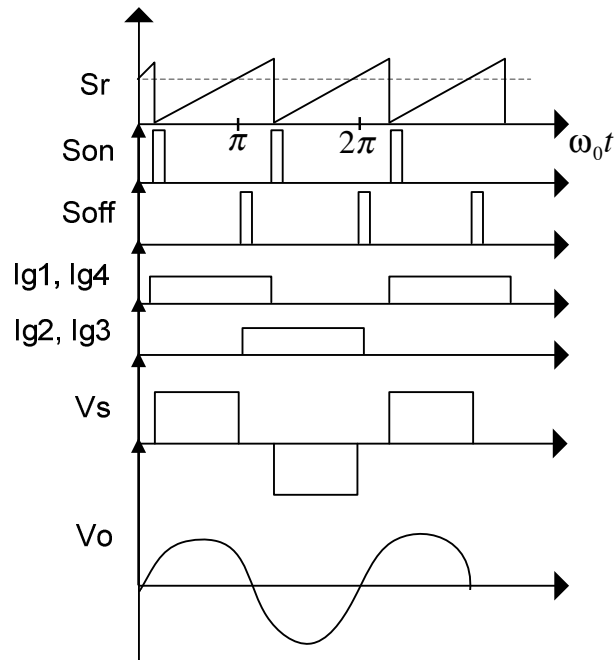
Figure 2.3b Waveforms illustrating the working principle of the hybrid
resonant inverter (Jain and Tanju, 1989)

The series and parallel branches at the output of the resonant network are tuned to match the inverter operating frequency. Therefore, the harmonics of the quasi-square voltage appearing at the resonant network input are trimmed to an acceptable level to provide a stiff sinusoidal voltage source V_o.

A zero-voltage switching (ZVS) converter has been proposed as the basic frequency converter (Renz et al., 1983). Figure 2.4 illustrates the circuit diagram of the proposed circuit. The switch pairs 1-1' and 2-2' are controlled synchronously with the input frequency, and the output is a synthesized lower frequency AC signal.

The operation of the frequency synthesis circuit is identical to the operation of a cycloconverter circuit. Chapter 7 presents in greater detail the operation of single-phase and three-phase cycloconverters.
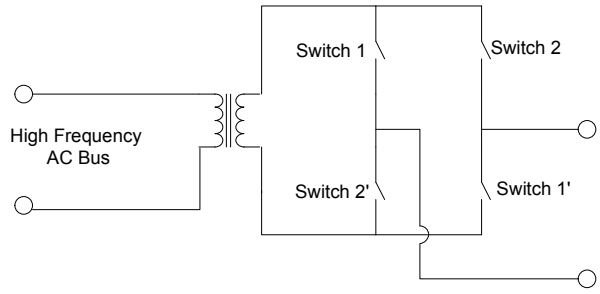
Figure 2.4 Frequency synthesis circuit diagram (Renz et al., 1983)

Sood and Lipo (1988) have proposed a high frequency power conversion system for the International Space Station, which is illustrated in Figure 2.5(a). A single phase, 20kHz voltage bus interconnects all sources and loads by means of pulse density modulation (PDM) switches. These circuits are proposed as basic interface converters for both AC or DC consumers. The temporary energy demand is supplied by the resonant *LC tank* [1] circuits , which are attached to each converter.
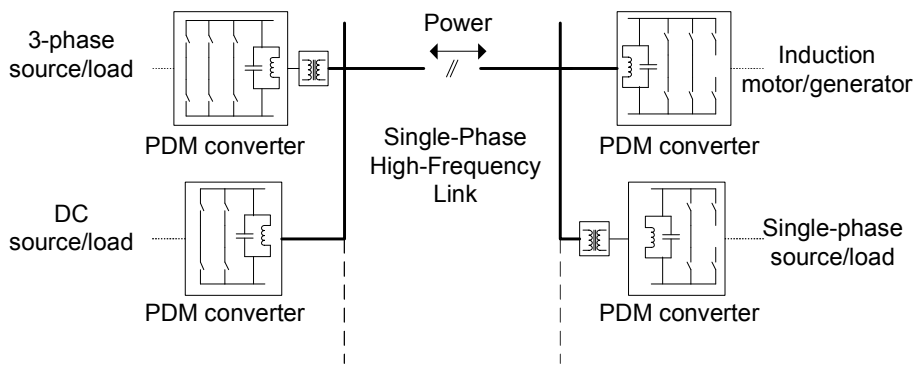
Figure 2.5a High-frequency static power conversion system (Sood and Lipo, 1988)

Figures 2.5(b) and 2.5(c) illustrate the controller diagram of the proposed PDM circuit and the associated waveforms for a DC voltage reference V_{ref}. The integrator produces an error signal $e(t)$ which is proportional to the integral of the difference between the reference and synthesized voltages, V_{ref} and V_{LF}.

---

[1] The term of tank circuit is commonly used in the field of power electronics to describe a circuit composed of parallel inductor and capacitor elements. The reason for the name is that the voltage oscillations within the circuit resemble the motion of a pendulum or the water moving back and forth within a tank.
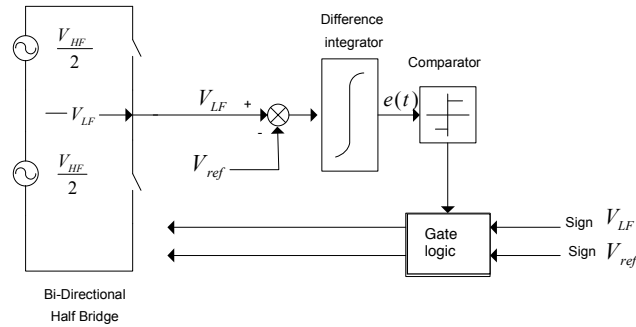
Figure 2.5b Pulse Density Modulation controller (Sood and Lipo, 1988)
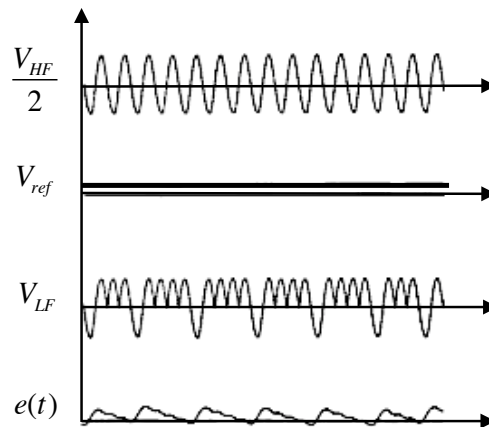
Figure 2.5c Waveforms associated with the PDM controller for a DC
reference signal (Sood and Lipo, 1988)

Half-cycle pulses of the 20kHz sinusoid are the basic building blocks used by the PDM controller. The amplitude of the DC reference signal dictates the density of the half cycles in the bi-directional half bridge.

A similar output signal to the PDM controller circuit can be produced by other types of AC to DC converters. Various techniques can be employed to convert high frequency AC voltage to a conditioned DC output voltage, for a determined power level.

Ideally, an AC/DC converter should aim for performance criteria such as: close-to-unity power factor, close to sinusoidal input current, low mass and volume, controlled output voltage, low input surge current, low electromagnetic interference (EMI) and high reliability (Jain et al., 1993). Figure 2.6 illustrates the conventional approaches to the

design of AC to DC converters: the link AC/DC converter, the switch mode rectifier and the AC/DC controlled rectifier. These converter topologies are briefly described next.

Link AC/DC converters (Figure 2.6(a)) use several conversion stages and have a high number of power components. This typically translates into high cost, weight and volume, and low reliability and efficiency. Figure 2.6(b) depicts the diagram of a switch mode rectifier (SMR). This circuit is considered inefficient because of the high switching losses in the active filter, which is essentially a buck or boost converter. In addition, it carries all the drawbacks of the link AC/DC converter. Although the active filter is redundant in the presence of the smoothing capacitor element, it is used to reduce the physical size of the latter which can be considerable at low frequency. The controlled rectifier (Figure 2.6(c)) generates large current harmonics in the supply lines, has a poor input power factor over a wide range of voltage control and is reported to emit high levels of EMI (Jain et al., 1993).

(a)

(b)

(c)
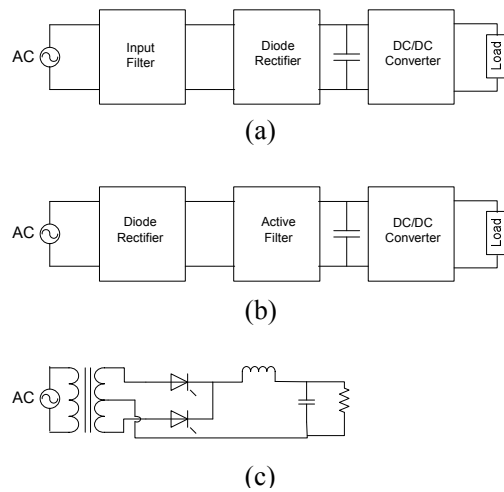
Figure 2.6 (Jain et al., 1993)

(a)   Block diagram of link AC/ DC converter
(b)   Block diagram of Switch Mode Rectifier (SMR)
(c)   Circuit diagram of AC to DC controlled rectifier

Jain et al. (1993) proposed a new class of converters with three topologies. It is stated that all have close to unity power factor (greater than 0.98), low total harmonic

distortion (THD) for the input current (less than 5%) and a high conversion efficiency (more than 96%). Figure 2.7 shows the proposed generic AC/DC converter which comprises of 4 stages: input transformer, resonant network, current controller and diode rectifier. Brief explanations of their functionality is given in the following paragraphs.
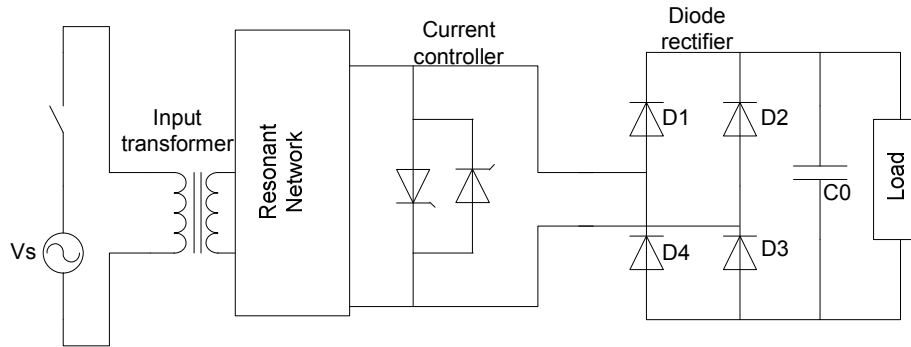
Figure 2.7 Generic AC to DC converter (Jain et al., 1993)

The role of the input transformer is to match the output voltage and also to isolate the load. The isolation is possible due to the functionality of the transformer, which allows only time-varying currents to flow between the coils. Thus, DC current flow in either of the transformer side is not transmitted on to the other winding.

The second circuit element, i.e. the resonant network, converts the high frequency AC input voltage into a high frequency bi-directional current source. The current controller, which has two independently controlled switches connected in anti-parallel, provides the required output bi-directional current. This alternating current is subsequently converted into uni-directional (DC) current by the diode rectifier stage. Finally, the role of the output filter C_O is to ensure a smooth and constant output DC voltage.

Figure 2.8 illustrates the three constituents of the proposed class of converters. Type 1-A is described in detail in this work in order to illustrate the underlying operating principle of the converter. The difference between the topologies B and C lies in the location of the C_p component, which is used to increase the power factor of the converter input current. Specifically, the component is connected in parallel with the

transformer secondary winding for topology B and in series with the primary winding for topology C. The classification of the the converters as type 1-A, 1-B and 1-C is the one used by Jain et al. (1993) and does not have a specific relevance within the context of the present study.
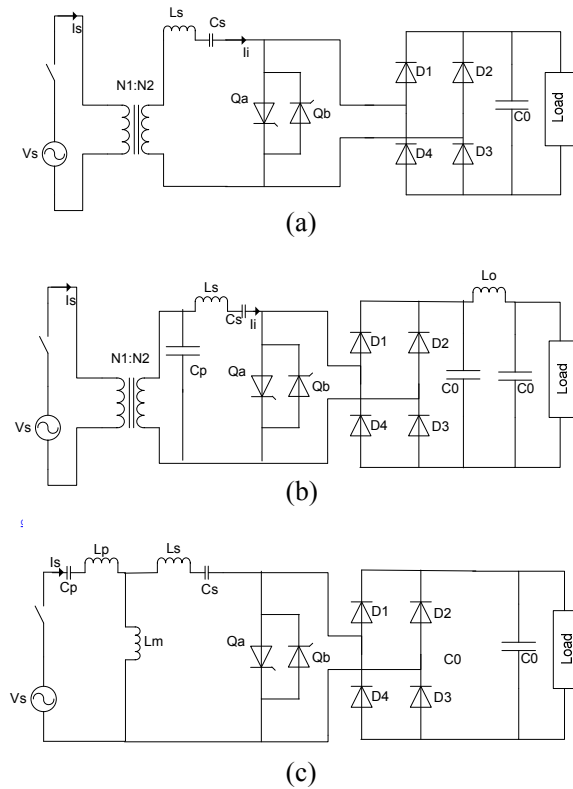
Figure 2.8. (Jain et al., 1993)
(a) Type 1-A AC/DC converter (b) Type 1-B AC/DC converter
(c) Type 1-C AC/DC converter

The previously mentioned four converter stages are realised by the following circuit components of the Type 1-A AC/DC converter, respectively: N_1:N_2 transformer, series L_S-C_S resonant network, thyristor switches Q_a and Q_b acting in anti-parallel as a current controller, the diode rectifier comprising diodes D_1, D_2, D_3 and D_4, and C_O as the output filter. L_S and C_S are tuned at the frequency of the voltage source, thus rejecting higher frequencies. This ensures a low THD of the input current. The current controller manages the amount of current flowing from the resonant network to the rectification stage, according to the output demand. Figure 2.9(a) illustrates the waveforms associated with the operation of the type 1-A AC/DC converter.
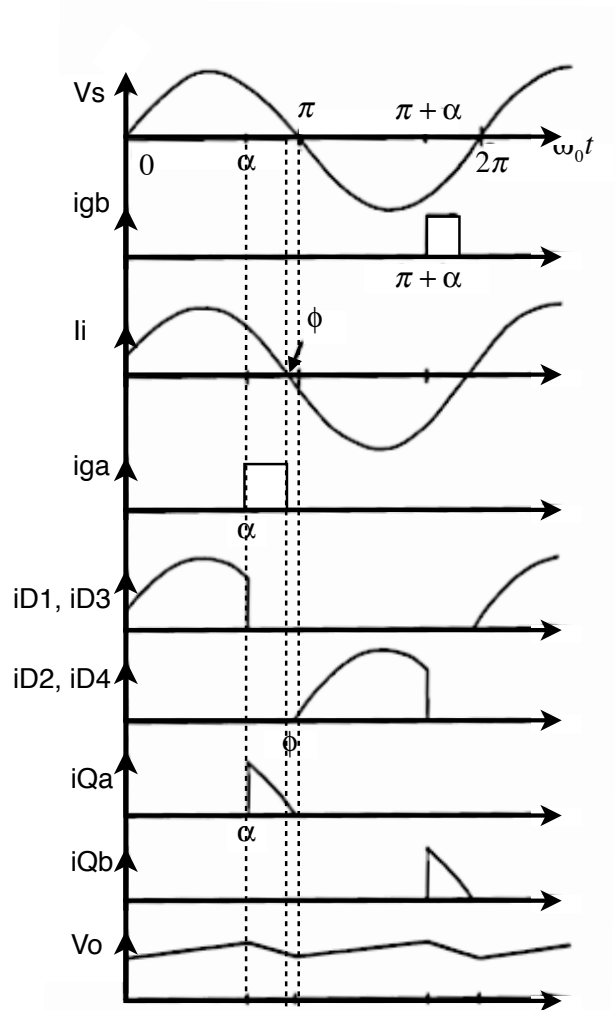
Figure 2.9a Type 1-A converter waveforms (Jain et al., 1993)

At $\omega_0 t = 0$, diodes D_1 and D_3 are conducting and the input resonant current I_i is charging the output capacitor C_o. The charging process continues until $\omega_0 t = \alpha$. At this point, the thyristor Q_a is opened and the current passes from the rectification part of the circuit to the current controller. When the input current crosses zero, at $\omega_0 t = \pi - \phi$, Q_a is forced to stop conducting since the polarity beyond this point does not allow current flow within the thyristor. Subsequently, diodes D_2 and D_4 start carrying the negative resonant current, which restarts charging the output capacitor C_o.

At $\omega_0 t = \pi + \alpha$, the current controller ends the charging period by switching on thyristor Q_b; this 'shorts' the load circuit, allowing capacitor C_o to discharge. Q_b will continue this operation until the resonant current passes again through zero, a time when the cycle re-iterates. Essentially, the output voltage control is provided by the current controller thyristor firing angle, α. Figure 2.9(b) shows the relationship between α and the converter output voltage.
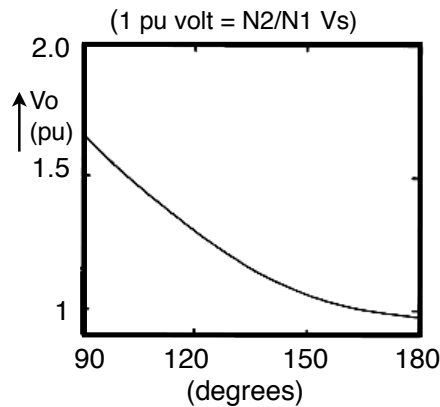
Figure 2.9b Type 1-A converter output voltage control (Jain et al., 1993)

2.2.3 Implications for the automobile electrical system

The studies presented within this Section provide indicative results for the potential benefits of HFAC power, which are of particular interest for the automobile environment. Namely, as indicated in the cited studies, a HFAC system is expected to offer advantages such as:

- low mass and size of cables and passive circuit components,
- less expensive and potentially less complex circuitry,
- low power distribution losses,
- redundancy of high voltage/current switches since HFAC connectors are magnetically-coupled, and
- HFAC network has a distributed topology. This benefit is equivalent to a certain degree of flexibility in supplying power at the most efficient voltage, current and frequency to the consumers.

In addition, the converters described in this Section are illustrative of the typical structure and control of HFAC power electronics modules:

- HFAC power can be generated using either resonant DC/AC inverters employing zero voltage switching (ZVS), or DC/AC circuits based on a hard-switching[2] method. The former is potentially more attractive for the automobile electrical system due to the higher efficiency of the module. Also, it has been indicated that high-speed generators can be used to supply AC power at high frequency. While such generators are commonly integrated within aircraft propulsion systems based on turbine engines (Renz et al., 1983), it is unlikely that this type of machine will be integrated within vehicles due to the potential high cost and space constraints.

- Similar to the DC/HFAC inverters, the HFAC/DC converter topologies can utilise either soft or hard switching methods. A PDM-based converter appears to be a good candidate for automotive applications due to its simple control and the fact that it employs ZVS. The Section has also highlighted a different type of HFAC/DC converter, which makes use of two thyristors but does not allow for ZVS. The interesting aspect to note about the two HFAC/DC converters is the different approach to obtaining the rectified DC voltage: either by PDM for the former structure, or by varying the thyristor firing angle for the latter. As will be discussed later in Chapter 7, the PDM method is adopted as part of this study due to the high efficiency of the converter.

- The HFAC/AC conversion method is based on PDM in order to synthesize a lower frequency AC signal. As will be discussed in Chapter 3, the cycloconverter appears to be the most appropriate and widely-used module for frequency transformation. Therefore, this type of circuit will be integrated as part of the present work. The implications of using a cycloconverter circuit will be highlighted in Chapters 7, 8 and 9.

Apart from the ZVS capability, the circuit topologies presented have other interesting characteristics such as:

---

[2] A soft switching method refers to the use of zero voltage switching (ZVS) or zero current switching (ZCS). Conversely, a hard switching technique does not make use of these methods.

- The integration of single or double-tuned resonant networks, which are either series or parallel combinations of circuit elements such as capacitors and inductors. Their role is first to filter frequencies outside the designed operating frequency, and second to create a high-impedance output voltage (for a load-invariable output voltage).

- Input and/or output transformers, which have two roles: first, to step up or down the voltage as required, and second to provide galvanic isolation for both the loads and the electrical bus.

2.3 HFAC power distribution for telecommunication systems

2.3.1 DC electric architectures

Two electrical architectures have generally been utilised to supply power to telecommunication systems. The first is a centralised network based on DC/AC or DC/DC power converters (Figure 2.10), and the second is a distributed system of DC/DC converters (Drobnik, 1994). HFAC power adds to this list as a potentially attractive third option.

The centralised DC power distribution system uses a common method of power supply management, based on a battery-fed converter. The alternative to this DC network is a distributed DC architecture (Figure 2.11), which makes use of Point-of-Use Power Supplies (PUPS). These units are small, dense power converters integrated into each system card that transform the battery voltage into the required output voltage.

As noted in the study by Drobnik (1994), the disadvantages associated with the two proposed configurations within the context of telecommunication equipment include:

- high resistive losses due to high DC distribution current,
- large packaging volume,
- the necessity to use forced air for cooling the centralised system, and

• the high cost of the distributed DC power system.
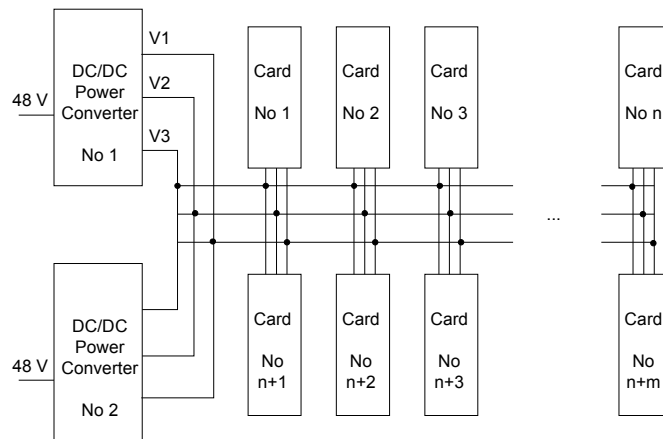
Figure 2.10 Centralised DC/DC power distribution (Drobnik, 1994)
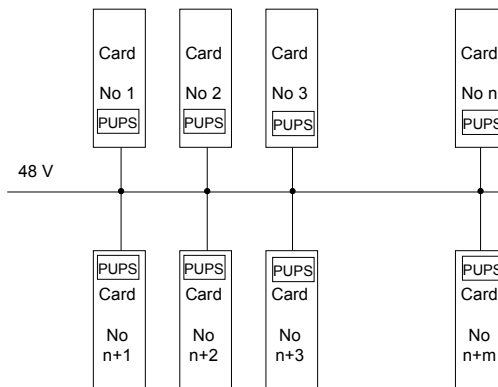
Figure 2.11 Distributed DC/DC power distribution (Drobnik, 1994)

2.3.2 HFAC power bus

Drobnik (1994) has proposed an alternative to the DC power distribution topologies; namely, a HFAC system that includes power conversion and distribution at 60V, 128kHz. Figure 2.12 shows a schematic of the proposed distributed HFAC system.

As suggested in the cited study, the advantages of the HFAC system cannot be overemphasized. Claimed benefits include low losses on the distribution path, even heat distribution throughout the cards shelf and good voltage regulation on the load side. In addition, HFAC power supplies use less components than would be necessary for the

equivalent DC PUPS and the power conversion efficiency is cited as being higher. Since resonant circuits are integrated in the inverter and within AC/DC converters as well, the inrush current is limited when the cards are inserted under power, without the need for additional voltage regulation circuits.
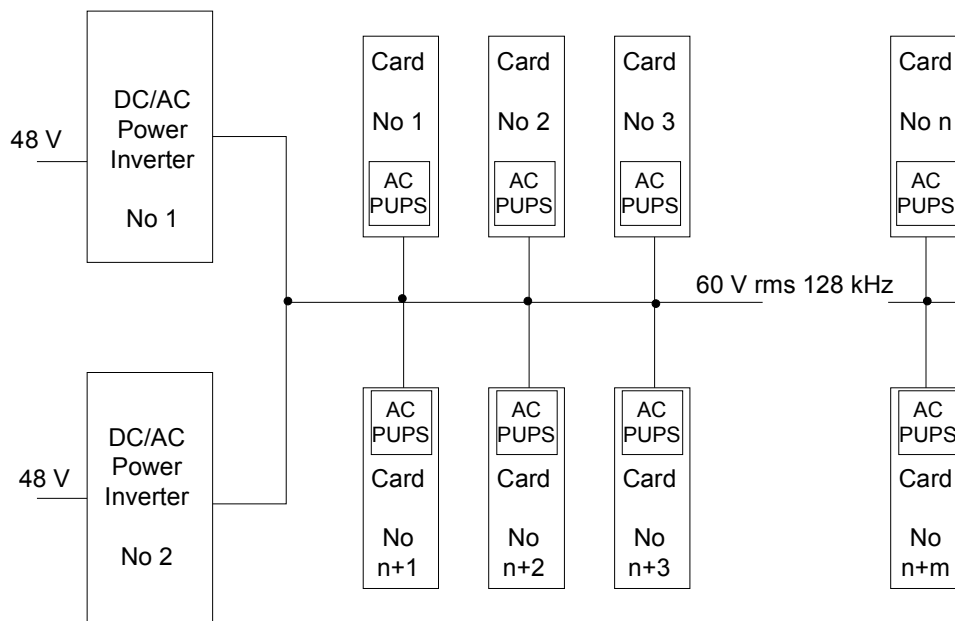
Figure 2.12 High frequency alternating current power distribution (Drobnik, 1994)

In the case of HFAC power distribution, by contrast with the DC networks, the entire output portion of the power converter which includes rectifiers, post regulators and filters is distributed to the point of use. As shown in Figures 2.13 and 2.14, the result of this approach is that there are fewer components in the centralised HFAC inverter in comparison to the centralised DC/DC converter (Drobnik, 1994).

Furthermore, as illustrated in Figure 2.15, the energy in the HFAC distribution system can be coupled by a magnetic field only. The media for magnetic coupling can be the transformers in both the inverters and converters.

Figure 2.16 shows the circuit diagram of a possible power distribution system for telecommunication equipment proposed by Jain and Pinheiro (1999). The authors have

argued low EMI and high overall system efficiency from low load to full load for the circuit.
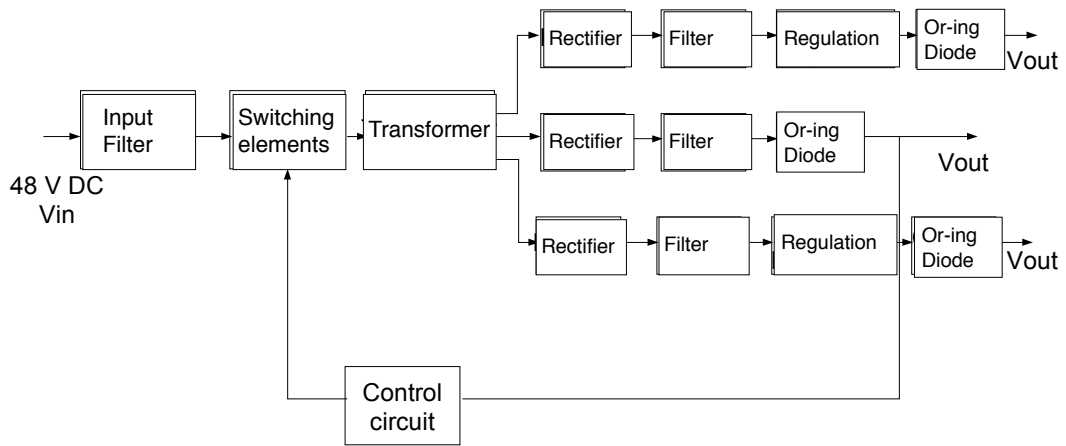
Figure 2.13 Multiple output DC/ DC (Drobnik, 1994)
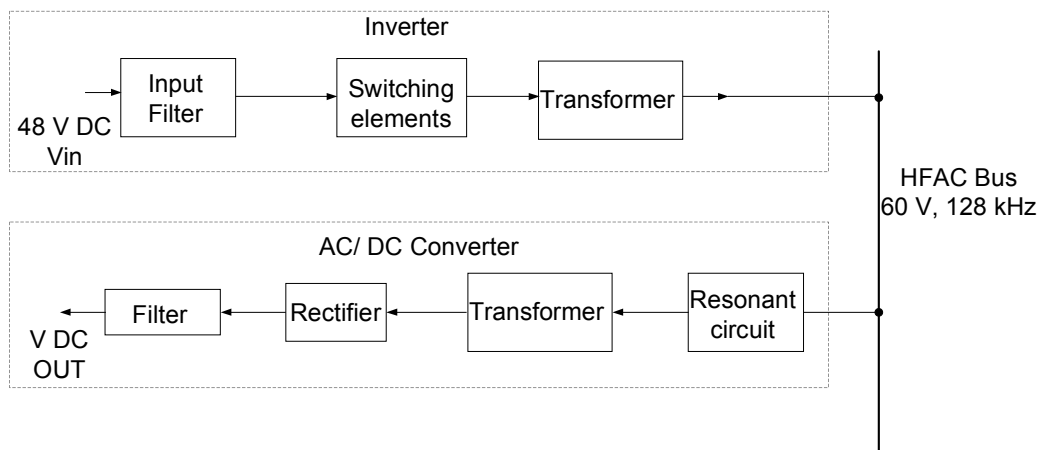
Figure 2.14 Inverter and AC/ DC converter (Drobnik, 1994)
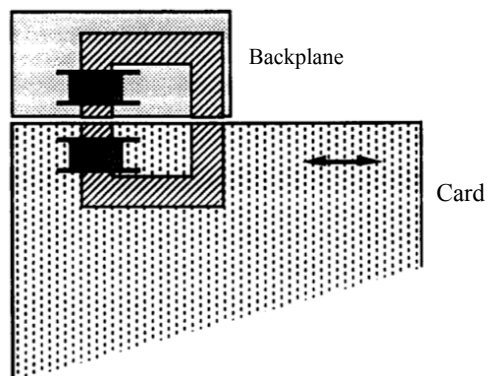
Figure 2.15 Connector-less power transfer (Drobnik, 1994)
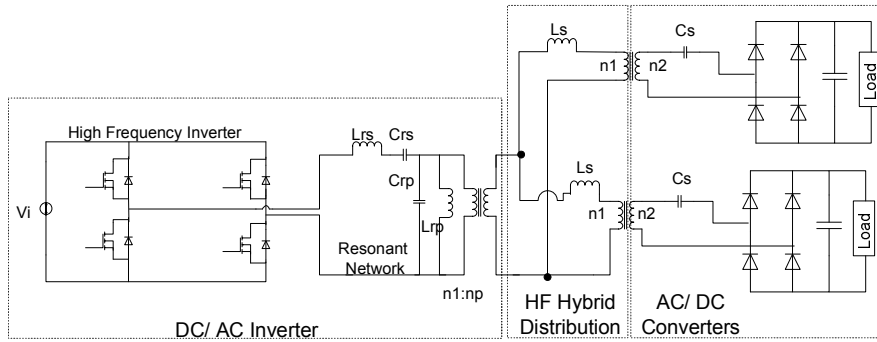
Figure 2.16 Proposed HF hybrid distribution system (Jain and Pinheiro, 1999)

As further described by Jain and Pinheiro (1999), the system illustrated in Figure 2.16 combines the advantages of high frequency sinusoidal voltage and high frequency sinusoidal current. The equivalent circuits for the two modes of operation are depicted in Figures 2.17 and 2.18, respectively. The voltage distribution system has one cited drawback; namely, it does not allow for connector-less power transfer. On the other hand, the current distribution system offers this capability, but suffers from high EMI and poor efficiency at low to medium load.
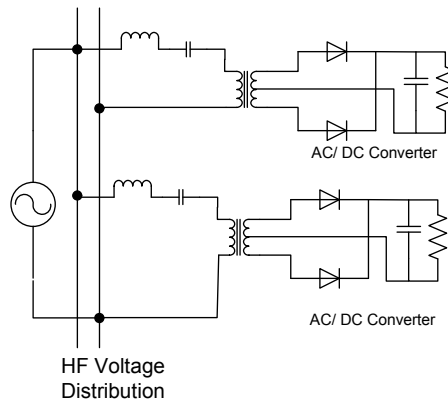
Figure 2.17 HF voltage distribution circuit diagram (Jain and Pinheiro, 1999)

The proposed hybrid power distribution system includes a DC/AC inverter, a high frequency hybrid distribution stage and AC/DC converter. These sub-systems are described in the next paragraph with reference to the circuit diagram in Figure 2.16.

The DC/AC inverter topology comprises a full bridge inverter and double-tuned series (L_{rs} and C_{rs}) and parallel (L_{rp} and C_{rp}) resonant network. The output stage includes a

transformer, which employs the phase-shift modulation technique and inherently benefits from load-independent output voltage (Jain and Pinheiro, 1999). The AC/DC converter integrates a transformer, a series resonant circuit (L_S and C_S, which are placed on the primary and secondary sides of the transformer, respectively), a diode bridge and output filter. The transformer is physically divided into two parts: the primary side and inductor L_S are part of the high frequency distribution system, whereas the secondary side and capacitor C_S are part of the AC/DC converter.
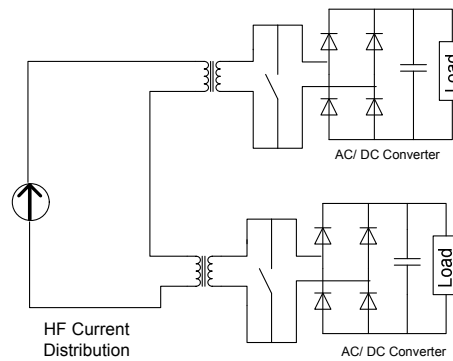
Figure 2.18 HF current distribution circuit diagram (Jain and Pinheiro, 1999)

Three operating modes are possible for the hybrid system: power transfer mode, no-load mode and short-circuit mode. These are depicted in Figure 2.19(a), 2.19(b) and 2.19(c), respectively (Jain and Pinheiro, 1999).

Bringing the two halves of the transformer together so that the primary and secondary are magnetically coupled, the power transfer mode is enabled - as shown in Figure 2.19 (a). Hence a high frequency voltage V_S is applied across L_S and the primary transformer winding, allowing maximum current transfer from the high frequency AC bus to the load.

The no-load mode is achieved by disconnecting the secondary half of the transformer (Figure 2.19(b)). V_S is thus applied only across the series inductor L_S and the transformer primary. The drawn no-load current is only a fraction of the nominal value, resulting in higher no-load efficiency and higher no-load power factor.
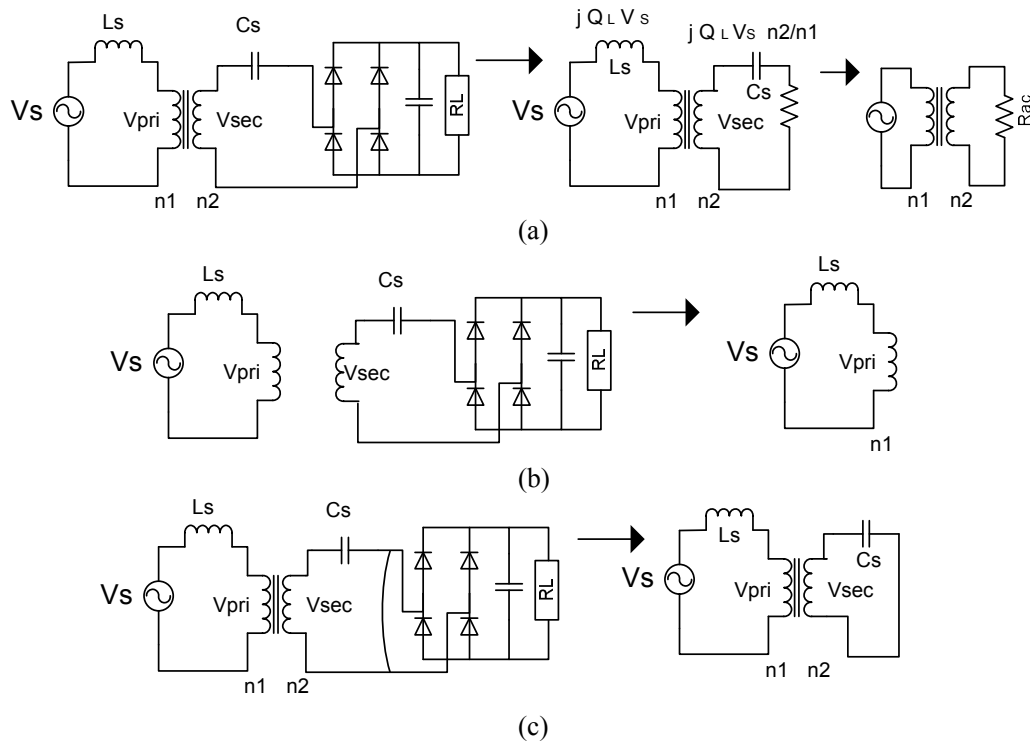
Figure 2.19 (Jain and Pinheiro, 1999)

(a) - Equivalent circuit of power transfer mode
(b) - Equivalent circuit of no-load mode
(c) - Equivalent circuit of short circuit mode

When a load short-circuit occurs and the primary and secondary windings of the transformer are coupled, the current drawn is low and limited by *Ls* and the saturation action of the transformer. This is an effective fuseless protection for the circuit (Figure 2.19(c)).

2.3.3 Implications for the automotive environment

In addition to the advantages listed in Section 2.3, the studies detailed in this Section are suggestive of more benefits for HFAC power that may be of interest for the vehicle electrical system. These include:

• An even heat distribution throughout the telecommunication cards shelf. Although not directly relevant for a specific automotive problem, this fact is nonetheless notable. With the increasing electrification of the vehicle, the integration of more

electrical loads within a confined space can potentially lead to the requirement of a complex and expensive thermal management system. As indicated for the telecommunication power system, this can be achieved simply by replacing DC with HFAC power distribution.

- The reduced number of AC PUPS components compared to DC PUPS. This characteristic can potentially increase the reliability and reduce the cost of local power supply units. From the perspective of the present study, this aspect is only relevant for a comparative analysis between a HFAC system and a distributed DC power network. However, the system employed in the majority of passenger vehicles is based on a centralised topology. Therefore, this characteristic can be further investigated if eventually a distributed DC bus topology will be proposed in the future by the automotive industry.

- The inherent capability to handle inrush current as cards are inserted. The ramification of this capability is that maintenance and repairs of the electrical system can potentially be carried out while the engine is running, i.e. without disconnecting the power supply. This can translate into a potential improved vehicle diagnostics and service time. Also, based on the trend of integrating a high-voltage mild-hybrid electric drivetrain within the conventional internal combustion engine (ICE) setup (such as the start-stop capability), the possibility to operate live the electrical systems can lead to a potentially safer working environment.

The power converters presented in this Section share the common characteristics of HFAC modules outlined in Section 2.2. The hybrid distribution system provides three modes of operation which may be of interest from an automotive perspective: power transfer, no-load and short-circuit. The short-circuit mode can potentially make the existing fuse box in vehicles redundant. As discussed in the context of the power distribution sub-system in Chapter 6, the no-load operation mode may also be beneficial for the proposed electrical system.

2.4   HFAC power distribution in microgrids

Small modular generation technologies like hydro or wind sources, photovoltaic cells and diesel sources, fuel cells, gas turbines, batteries, ultra-capacitors and flywheels, interconnected in distribution systems can shape a new type of power system: the microgrid. Correa et al. (2003) have investigated the potential of integrating all sources and loads into a high frequency AC power system with a common distribution bus operating at 20kHz. Figure 2.20 illustrates the proposed concept.
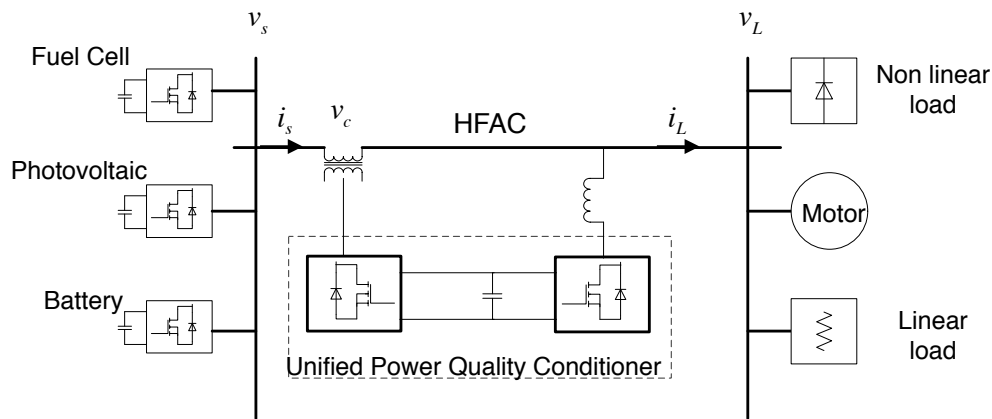
Figure 2.20 HFAC-based microgrid concept (Correa et al., 2003)

A unified power quality conditioner (UPQC) has been described within the cited study that ensures the optimum operation of the HFAC bus. The role of the UPQC, shown in the diagram of Figure 2.21, is to compensate for reactive power, voltage distortions resulting from converter nonlinearities and load current harmonics generated by nonlinear loads. The UPQC integrates a shunt active filter and a series active filter. The reference signals for the two filters are, respectively, the reference compensating current and compensating voltage obtained with the *p-q* theory. This theory is described in the Appendix A for reference.

The shunt active filter in Figure 2.22 (Correa et al., 2003) uses a current-controlled voltage source inverter with bipolar pulse-width modulation (PWM) switching. The

difference between the reference compensating current i_c^* and the bus current is the error signal minimised by the proportional-integral (PI) controller. Therefore i_c follows the reference compensating current, ensuring compensation for both current harmonics and power factor on the bus. The output filter (Lf and Rf-Cf) attenuates the harmonics originating from the converter switching.
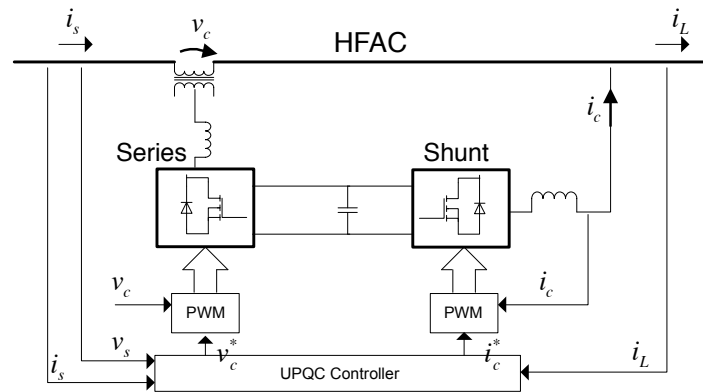
Figure 2.21 HFAC unified power quality conditioner (UPQC) (Correa et al., 2003)
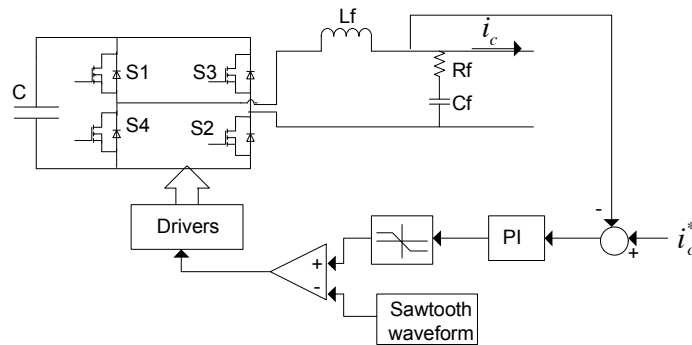
Figure 2.22 Shunt active filter with PWM converter and controller (Correa et al., 2003)

The series active filter (Figure 2.23) uses a voltage controlled source inverter with PWM bipolar switching, an external voltage control loop and an internal current control loop. The difference between the reference compensating voltage v_c^* and the bus voltage v_c, multiplied by constant K, is compared to the output current of the inverter. The PI

controller uses the difference between these two signals to adjust the PWM cycle accordingly, thus compensating for voltage harmonics.
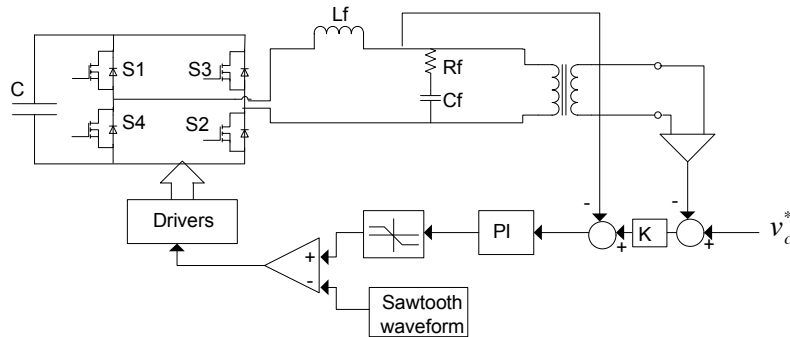
Figure 2.23 Series active filter with PWM converter and controller (Correa et al., 2003)

Figures 2.24 and 2.25 illustrate the compensating effect of the two active filters. Figure 2.24 presents the bus voltage before (part (a)) and after (part (b)) being filtered by the series active filter. Conversely, Figure 2.25(a) depicts the load current before the shunt filter control; part (b) of the same Figure shows the compensated load current.
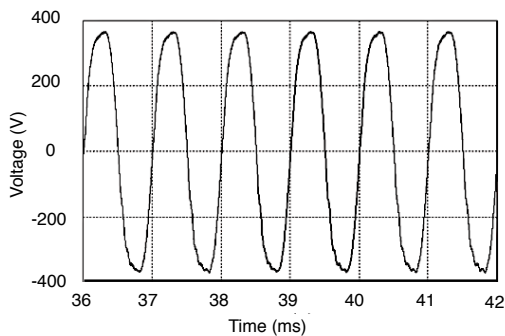
Figure 2.24a HFAC voltage without compensation (Correa et al., 2003)

Figure 2.25a HFAC load current without compensation (Correa et al., 2003)

Figure 2.24b HFAC voltage with compensation (Correa et al., 2003)
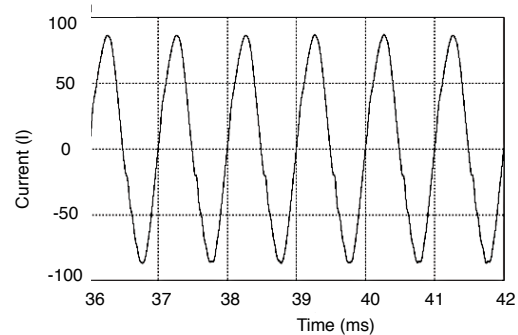
Figure 2.25b HFAC load current with compensation (Correa et al., 2003)

Conclusively, Correa et al. (2003) have suggested that high power quality is achievable for a HFAC-based microgrid system. The authors have indicated that high-order voltage and current harmonics can be filtered by the use of series and shunt active filters. In addition, it has been suggested that induction motors can be easily interfaced from the HFAC bus by frequency converters. As will be discussed later in Chapter 8, such machines can potentially be used in automotive applications such as electric pumps, engine cooling fans or windscreen wipers motors.

The findings presented in the context of the power grid application are significant for the potential integration of HFAC within vehicles, as detailed below.

- First, the two controllers presented can potentially be incorporated as part of an on-board electrical bus in order to ensure a high power distribution factor and therefore a high power transmission efficiency.
- Second, it is important that high-order harmonics can be easily filtered out, since these may cause EMI with electrical and electronic systems in the vicinity of the power distribution path.
- Third, the presented power correction modules can be used for the integration within the same electrical system of prospective regenerative sub-systems. Electrical applications based on motor-generator actuators, such as the ISG, can potentially be supervised by the shunt and active series controllers for their seamless integration onto the same AC bus.

2.5   High frequency AC power for commercial electronics

Distributed power architectures (DPA) offer increased performance over typical centralised power supplies (Watson et al., 1996). Typical cited advantages include the flexibility to supply different load voltage levels, paralleling load converters to meet high current demand, improved load regulation and better fault tolerance. The drawback of DC DPA is the high cost and complexity. However, the switching of DC to HFAC

can potentially diminish the impact of these two obstacles. Figure 2.26 illustrates the diagram of a HFAC DPA distribution network. Cp and Lp^3 are the differential mode capacitance and inductance, respectively, while Cm is a common mode capacitance formed between the bus conductors and ground.
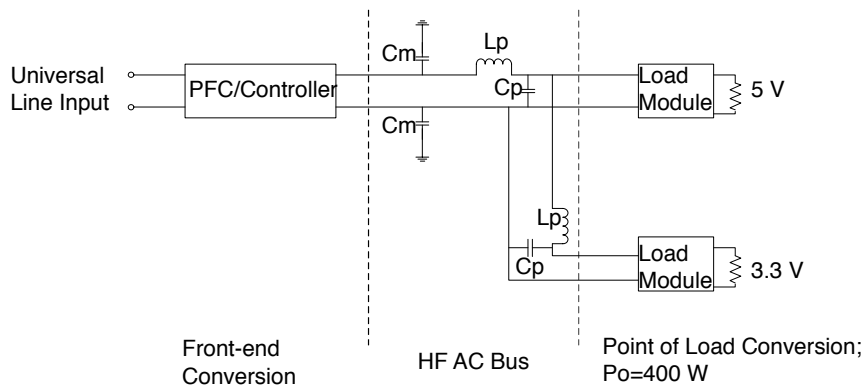
Figure 2.26 AC DPA block diagram including bus parasitic elements (Watson et al., 1996)

A commercial application of the HFAC DPA concept is the HP 70000 MMS, shown for reference in Figure A2.2 (Appendix A). The specifications from the HP 7001A manual (1999) describe the capability of the MMS: AC input power is switchable between several ranges: 90-132V AC at 47-66Hz, 199-264V AC at 47-66Hz, and 103-132V AC for a frequency interval of 356-444Hz. The mainframe power supply, pictured in Figure A2.3(a) and detailed by the diagram in Figure A2.3(b), processes the AC line power to produce:

• a regulated 24.3V at 40kHz AC power for the output modules (power up to 200W), and

• DC power for the modular system interface bus (MSIB) and the cooling fans.

The similar concept of a DPA has been highlighted in the previous two Subsections. Yet, the significance of the MMS system for the present study is to illustrate a potential

---

[3] The inductance and capacitance indicate bus parasitic elements within a simplified lumped parameter representation.

practical integration of electrical loads with different power requirements within a HFAC architecture.

Another example of a DPA based on HFAC has been presented by Watson et al. (1996). The study has detailed the development of a 300kHz AC architecture for low power applications (up to 500W per application). The analysis focused on the effects of using high-frequency (HF) square waves for power distribution on the spectral power content.

The relevance of this investigation is to have an indication of what may be the most energy-efficient waveform for HFAC power distribution. As will be detailed later in Chapter 3, some automotive-related studies have focused on square-wave HFAC power distribution. As discussed in Chapter 4, the findings presented next will support the decision for a specific HF waveform to be used as part of the present work.

The most prominent disadvantage of implementing a square wave voltage for power distribution is its rich harmonic content compared to a sine wave. The key to reducing the high frequency harmonic power contained in square waves is to soften its rising and falling edges (the voltage dv/dt rate).

Figure 2.27(a) illustrates four waveforms having a frequency of 300kHz with different transition times. The first waveform is a square voltage and the subsequent three have a rising and falling time of 5%, 10% and 20% of the voltage time period. Part (b) of the same Figure shows the spectral content of a unity amplitude square and trapezoidal waveforms (rising time of 10% of switching period) (Watson et al., 1996). It can be observed that the amplitude of the trapezoidal waveform at high frequencies is significantly reduced in comparison to the square voltage signal.

The power contained in the waveform harmonics (3rd through to the 99th, and 1MHz to 50MHz) is illustrative of the advantages of increasing the transition time. Figure 2.28

illustrates the results obtained by Watson et al. (1996) related to the power of harmonics grouped into three frequency bands: 1 to 15MHz, 15 to 30MHz and 30 to 50MHz.
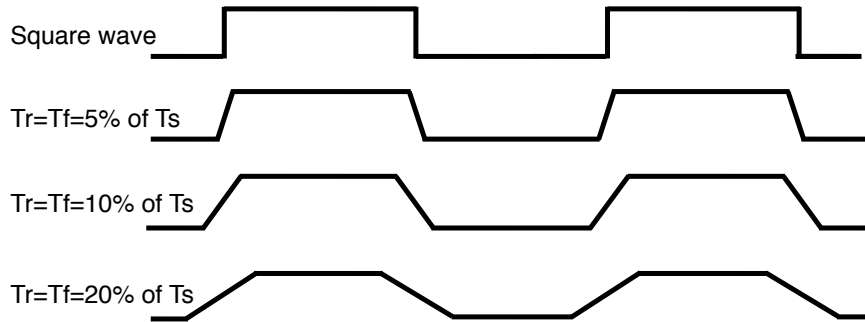
Figure 2.27a HF Voltage Transition Waveforms (Watson et al., 1996)Tr=Rising time; Tf=Falling time; Ts=period (2μs)
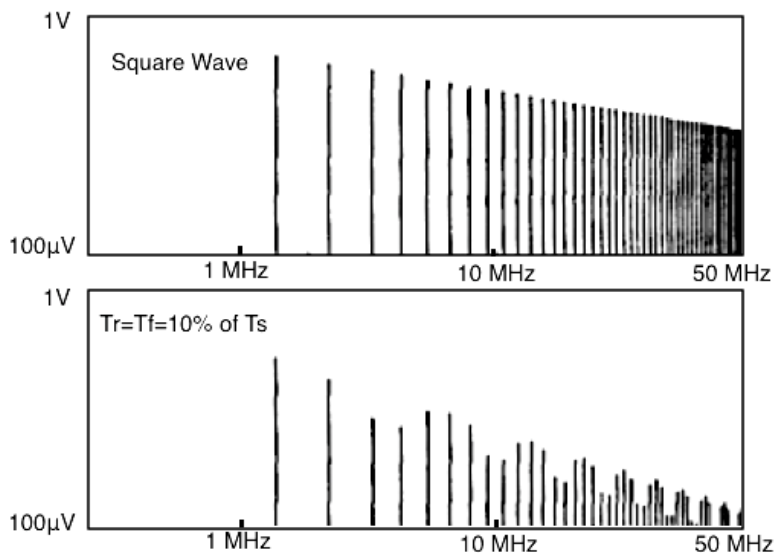
Figure 2.27b Spectral content of square wave and *soft transition* wave (Watson et al., 1996)

With reference to Figure 2.28, the bars are scaled relative to the fastest-transition square wave, whose total power in each frequency range is normalised to one. The main finding is that above 15MHz, reducing the signal transition time to 5% of the time period (denoted as T_S in Figure 2.28) lowers the harmonic power content by approximately two orders of magnitude over that of the square wave. Watson et al.

(1996) have concluded that sinusoidal or square-wave waveforms with a small rise and fall time are preferable for high frequency power distribution.
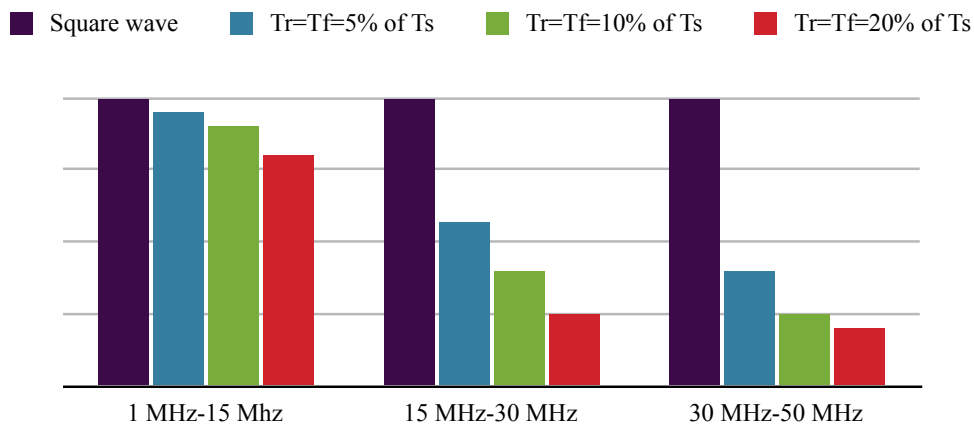
Figure 2.28 Power contained in harmonics for three frequency bands and different rise and fall time of square wave (Watson et al., 1996)

The particular frequency classification into three groups is not relevant for this study. However, it is important to note that the higher harmonics are significantly reduced by increasing the transition time. As it will be discussed in Chapter 10 in the context of future work, a low harmonic content is desirable within a vehicle environment since regulations such as the CISPR-25 (or BS EN 55025:2003) or the ISO 7627 have to be satisfied.

2.6   Summary and conclusions

The studies presented in this Chapter illustrate some of the potential advantages of HFAC for power distribution in applications such as aerospace, microgrids, telecommunication equipment and consumer electronics. The voltage waveform, amplitude and frequency are tailored for each system according to key requirements such as the power rating, power quality or power system topology.

In particular, research by NASA has focused on power distribution at 440V, 20kHz, for an electrical system with a power rating in the order of hundreds of kW. The similar

frequency of 20kHz has been considered appropriate for a very efficient power distribution system in microgrids. The focus of the research in this field has been the quality of the power transmitted between various types of sources and consumers connected to the grid. Higher frequencies have been proposed for applications with a lower power rating (up to 1kW). Specifically, a 60V, 128kHz distribution system was described in this Chapter for telecommunication equipment. Comparably, 40kHz and 300kHz AC networks employed for power distribution in DPAs have been discussed, for a power rating of 200W and 500W, respectively. Table 2.1 summarises the electrical characteristics of the HFAC systems described in Sections 2.2-2.5.

Table 2.1 Characteristics of the HFAC systems presented in Chapter 2

Application	Aerospace	Telecommunication equipment	Microgrids	Instrumentation equipment	
Voltage	440V	60V	possibly higher than 100V	24.3V	-
Frequency	20kHz	128kHz	20kHz	40kHz	300kHz
Power	hundreds of kW/ possibly megawatts	several kW	tens of kW	200W	500W

The main potential advantages of HFAC power, highlighted by the studies presented in this Chapter, can be summarised as follows:

- low mass and size of cables and passive circuit components,
- less expensive and complex circuitry,
- low power distribution losses,
- magnetically-coupled HFAC connectors,
- HFAC network has a distributed topology, where loads may benefit from the most efficient voltage, current and frequency input,
- high power quality is achievable for a HFAC-based distribution system,
- HFAC/DC converters can be operated in parallel for satisfying high load currents,

- better fault tolerance and lower cost and complexity compared to DC distributed networks,
- sinusoidal voltage or square-wave waveforms with a small rise and fall time may be more suitable for power distribution within an automotive environment compared to square-wave voltage.

The implications of these attributes for the automotive environment are significant:

- The low mass of the cables and electric circuit components may contribute to a reduction in vehicle mass. This advantage, combined with the low distribution resistive losses and high power quality, can potentially improve the fuel consumption.

- The distributed topology of the HFAC bus is potentially a better alternative to the existing centralised DC architecture in vehicles. Particularly, a HFAC DPA is expected to be less complex and more cost-effective compared to centralised DC networks. In addition, it has been indicated by the studies presented in this Chapter that the former bus topology is also fault-tolerant and more reliable since less components are needed.

- A HFAC bus offers notable advantages for the auxiliary on-board consumers. Magnetic connectors are simple, reliable and isolate galvanically the bus from the consumers. In addition, these are not expected to be prone to arc faults and corrosion like the connectors within high voltage DC networks. Chapter 4 discusses in more detail the limitations of the 42V DC connectors for vehicle applications.

- Any voltage and current amplitude are easily obtainable by choosing the appropriate transformer winding turns ratio. The effect of this attribute is that electrical consumers no longer have to operate at the nominal 14V DC, and the power input can be tailored to meet their most effective operating conditions. In addition, since the HFAC bus voltage is continuously regulated, the typical voltage range withstanding capability of on-board consumers (9V to 16V DC) can be waived.

- HFAC converter modules offer fuse-less protection for the loads. Therefore, the fuse box found in vehicles today is potentially not necessary in a HFAC system.

- Finally, frequency converter circuits can interface AC motors operating at 50Hz, 60Hz or 400Hz as in aircraft electrical systems. The latter are lighter and more compact than

the existing DC motors used in automobiles. Possible applications for AC induction machines in automobiles include compressors, fans or electrical pumps. Chapter 8 presents a critical investigation into the potential for AC induction motors to replace the existing DC motor actuators within vehicles.

Chapter 2 has highlighted the typical circuitry used to manage HFAC power. The structure and operation of the converter modules are directed to an efficient and robust operation. Their main attributes, which have been considered in the present study for the vehicle HFAC power bus, can be summarised as follows:

- ZVS or ZCS. This method eliminates the switching losses and is expected to reduce the voltage and current harmonic content of the power converters.
- Single or double-tuned *LC* resonant networks, used to filter frequencies outside the operating circuit frequency. In addition, the *LC* combinations used to create a high-impedance output voltage (for a load-invariable output voltage) are also useful as temporary energy storage units.
- Input and/or output transformers, which have two roles: first, to step up or down the voltage and second to isolate galvanically the load.

Chapter 3 continues to provide a comprehensive account of the studies related to the use of HFAC power within the automotive environment. The investigations are based on the inherent advantages of the technology, as discussed here, and aim to highlight the achievements to date within the automotive domain.

Chapter 3

Survey on high frequency AC power for automobile electrical systems

---

3.1 Introduction

The aim of this Chapter is to give a comprehensive account of the body of literature into automotive HFAC electrical systems. Due to the small and disjointed number of studies relevant to the present analysis, the literature review includes a collection of the existing case studies. The main findings of this review are compared to the cited benefits of HFAC power outlined in Section 2.6. Based on this comparison, the aim of this Chapter is to highlight areas which have not yet been considered in the literature.

It should be noted that although the studies discussed in Chapters 2 and 3 have not been published relatively recently, these reflect nonetheless the most up-to-date research related to HFAC power.

Section 3.2 presents a study into HFAC power for a HEV. The analysis includes a comparison between three possible power distribution systems: DC, resonant DC and HFAC single-phase. The latter is described in detail. In particular, the main power management modules of the HFAC architecture are presented.

Section 3.3 highlights the main findings of a study into an auxiliary HFAC system based on 48V, 25kHz. The principal characteristic of the presented architecture is the potential to transmit data signals onto the HFAC power bus for on/off load regulation.

The focus of Section 3.4 is an auxiliary 400Hz AC power network. Both one-phase and three-phase architectures are presented, which can easily interface 400Hz induction motors. In addition, several suitable DC/AC inverter topologies are discussed.

Section 3.5 details the study of an on-board HFAC power bus based on a square-wave supply voltage, sinusoidal current at 80V, 25kHz. The structure and operation of the power modules employed are described, including a DC/HFAC inverter, HFAC/DC converters and a bi-directional HFAC/DC circuit.

Section 3.6 summarises the main findings of the Chapter. Section 3.7 compares these results to the potential advantages of HFAC power, as outlined in the previous Chapter, and identifies the main novel areas of investigation for the present research study.

3.2 HFAC power distribution for a hybrid electric vehicle

Bose at al. (1996) have investigated three means of power distribution within a hybrid electric vehicle (HEV): DC, resonant DC and HFAC single-phase, which are discussed in Section 3.2.1. The conclusion of the study is that the single-phase HFAC system is more attractive compared to the DC and resonant DC alternatives. Specifically, the cited work has identified the following advantages for the HFAC network:

• The elimination of the switching losses.

• The high connector reliability, due to magnetic coupling.

• The fact that the bus voltage is independent of the power source voltage. Thus, the HFAC voltage is isolated and regulated to any amplitude and waveform type required by the loads. These benefits lead to the possibility of an optimal design for converters and electrical machines connected to the HFAC bus (Bose et al., 1996).

3.2.1 The DC power distribution system

Figure 3.1 illustrates the proposed HFAC power distribution system for a series HEV (Bose et al., 1996). A common 440V, 20kHz bus collects energy from the storage sources (battery, flywheel, ultracapacitor or super conducting magnet) and from the power source, which is a gasoline engine. The network then distributes the power to an AC machine used for vehicle propulsion, through a variable voltage, variable frequency (VVVF) converter.

DC system

In the DC distribution system shown in Figure 3.2, the engine is connected to an electrical machine that fulfills both the starter and generator functions. The starter/ induction generator is connected to the power bus by a bi-directional converter and power is supplied from the battery to the three-phase induction motor via an inverter integrating six insulated-gate bipolar transistor (IGBT) power switches.
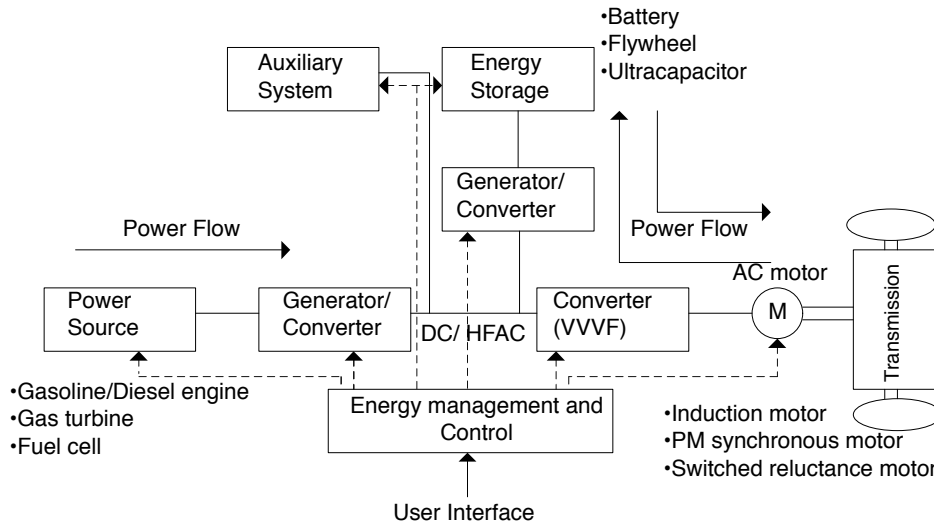
Figure 3.1 Propulsion power distribution system
for a series hybrid electric vehicle (Bose et al., 1996)
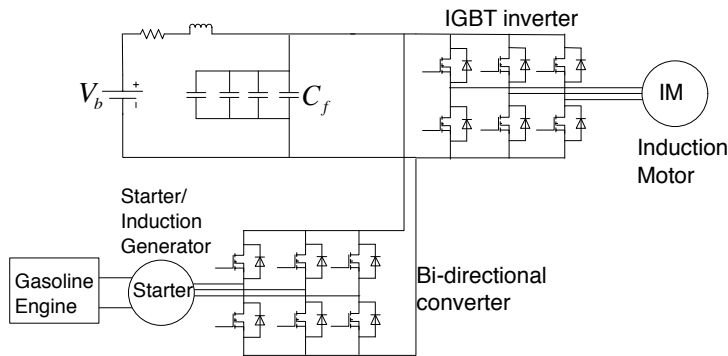
Figure 3.2 DC distribution system (Bose et al., 1996)

Resonant DC system

Figure 3.3 illustrates the schematic of the resonant link DC system. The advantage of this topology is that, unlike the DC distribution system, it employs soft switching. As discussed in Chapter 2, the potential implication for the vehicle electrical system is the

increased efficiency of the DC/HFAC power transformation in comparison to the DC topology.

However, the drawbacks cited include additional converter components and increased voltage and current strain for the circuit elements (Bose et al., 1996). The consequence of this limitation is that the reliability of the circuit may degrade in comparison to the DC distribution system. In fact, the robust topology of the latter may be preferable for the automotive environment where safety and reliability are critical, even if it is not expected to be as efficient as the resonant DC topology.

The high electrical stress on the components within a resonant circuit topology can be addressed using a common technique which limits the amplitude of the voltage and current over the circuit elements. The approach, denoted as the voltage clamping method, is amply described within the literature (Emadi, 2005, Mizhi and Little, 2006).

Figure 3.3 illustrates the resonant DC system which integrates this feature. The following components have been added to the schematic previously shown in Figure 3.2: L_r and C_r, which form the resonant network, and the power switch Q in series with capacitor C_O which undertake the voltage clamping function. In particular, switch Q is turned on when the voltage over C_r exceeds a certain threshold. This causes the C_O potential to increase, thus relieving the voltage stress on component C_r.
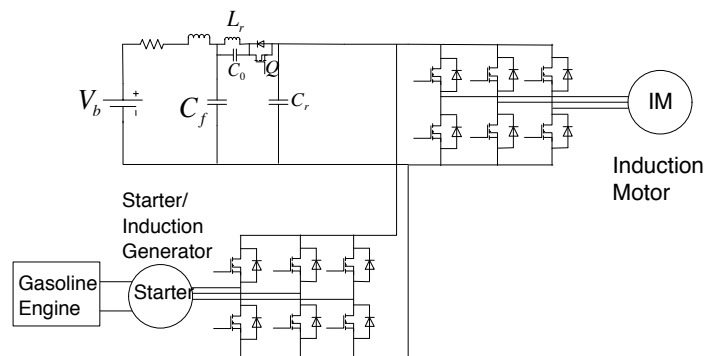
Figure 3.3 Resonant DC distribution system (Bose et al., 1996)

3.2.2 The HFAC power distribution system

Figure 3.4 presents the high frequency one-phase AC system, where the DC voltage is transformed into HFAC by the H-bridge inverter proposed by Jain et al. (1989). This circuit has been described in detail in Section 2.2, as part of the proposed 440V, 20kHz electrical system for the International Space Station.
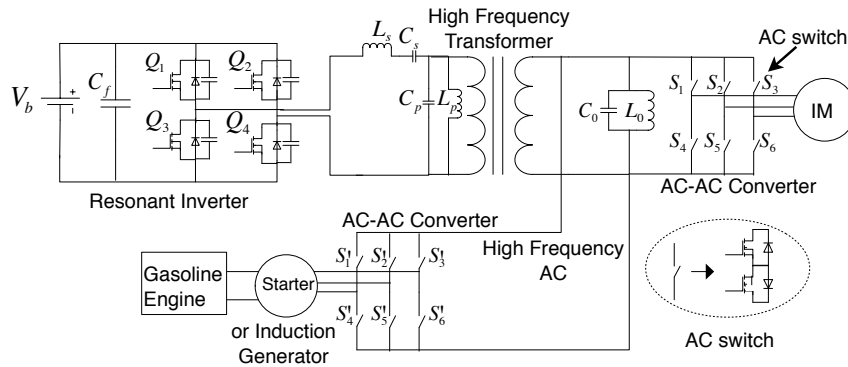
Figure 3.4 High frequency single phase AC link distribution system (Bose et al., 1996)

It should be noted that the inverter illustrated in Figure 3.4, although denoted as resonant, does not integrate the resonant circuit elements described previously (see Figure 3.3). Although the cited work indicates that the inverter is of resonant type, the schematic in Figure 3.4 and the circuit description in Chapter 2 (see Figure 2.3(a)) indicate the contrary. In fact, it is the author's opinion that the original study of the inverter (Jain and Tanju, 1989) has indicated that the circuit is resonant based on the series and parallel resonant network (L_sC_S and L_pC_p) used as output voltage filter. Based on the schematic in Figure 3.4, the proposed circuit employs a hard switching technique to transform DC into HFAC voltage.

As shown in Figure 3.4, the AC/AC converters integrate two inverse-series IGBTs or metal-oxide semiconductor field-effect transistor (MOSFET) components as the basic switching element. The reason is that the switch has to withstand AC voltage and

conduct bi-directional current. The L_0C_0 filter attenuates the current harmonic loading of the HFAC bus.

It is noteworthy that either two MOSFETs or two IGBTs are typically used as an elementary switch within HFAC power converter modules. The impact of integrating such circuits is that the energy efficiency is expected to be greatly reduced in comparison to DC power electronics performing similar operations. In fact, since the number of switches is double for the HFAC converters, the conduction losses are expected to be twofold in comparison to comparable DC circuit technologies. As it will be discussed in Chapters 7 - 9, the requirement for two inverse-series MOSFETs has a significant impact on the feasibility of HFAC power for automotive auxiliary applications.

Figure 3.5 illustrates the control strategy for the HFAC/AC converter proposed in the same study by Bose et al. (1996). The method is based on hysteresis current control and the diagram shows the half-bridge variant of the converter.

N.B. Comp=Comparator
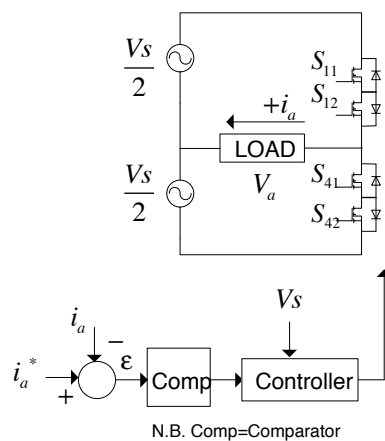
Figure 3.5 Half bridge converter with current control (Bose et al., 1996)

At the zero crossing point of Vs, one of the pairs of switches is constrained to open. Table 3.1 summarises the switching modes of the inverter according to the polarities of the load current i_a, the error signal ε and the source HFAC voltage Vs.

The important aspect to note in Table 3.1 is that, regardless of the AC machine control method (e.g. hysteresis, vector control), the polarity of the HFAC voltage has to be taken into account as well within the control algorithm. Effectively, as will be discussed in more detail in Chapter 8, this leads to a more complex control strategy for VVVF machines supplied by HFAC power.

Table 3.1 Switching modes of the half-bridge converter (Bose et al., 1996)

Mode	i_a	ε	Vs	SW
1	+	+	+	S11
2	+	+	-	S42
3	+	-	+	S42
4	+	-	-	S11
5	-	+	+	S41
6	-	+	-	S12
7	-	-	+	S12
8	-	-	-	S41

Figure 3.6 shows the block diagram of the one-phase HFAC system with the added control circuitry. The drive motor and the engine generator are torque controlled, including indirect vector control in the inner loops. Figures 3.7(a) and 3.7(b) display the phase currents of the two machines, and thus indicate a reasonable performance for the total system.
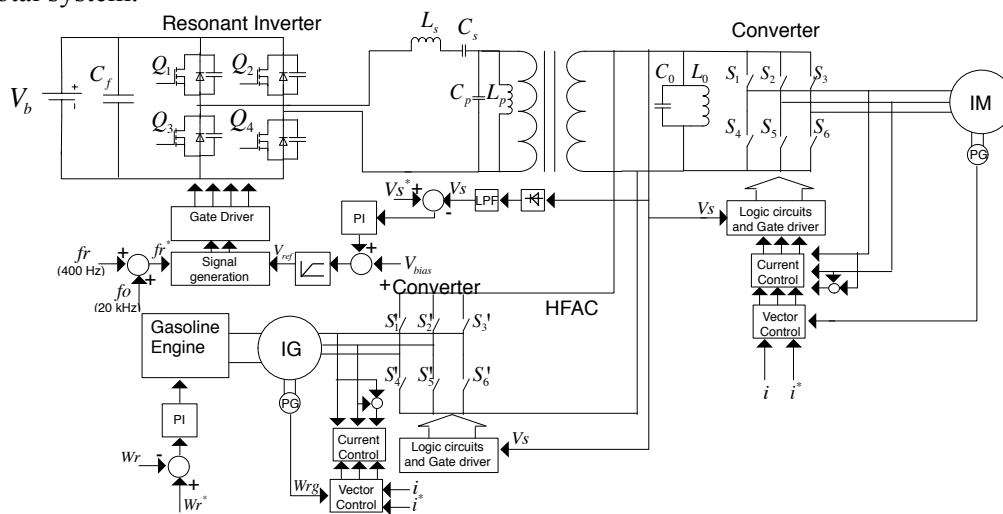
Figure 3.6 Control block diagram of the complete system (Bose et al., 1996)
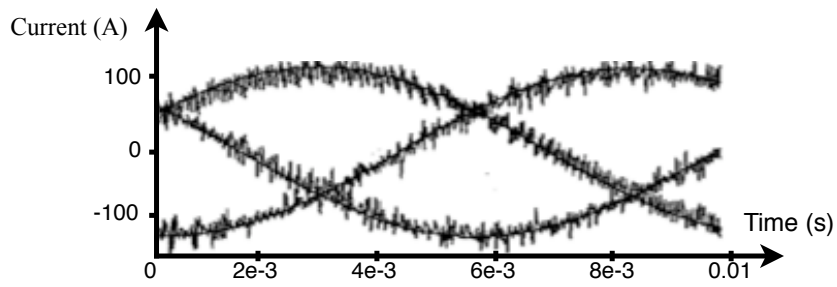
Figure 3.7a Motor phase current (Bose et al., 1996)
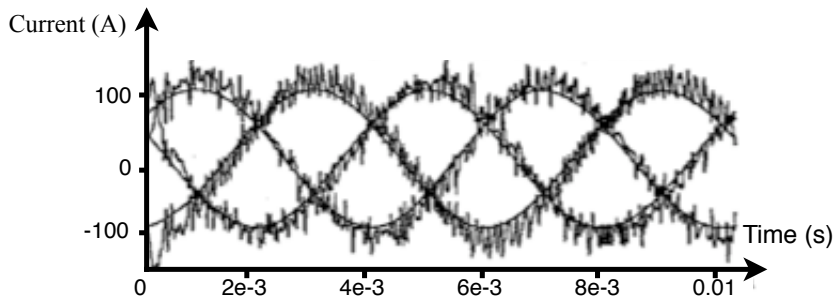
Figure 3.7b Engine starter phase current (Bose et al., 1996)

In relation to the system-level diagram in Figure 3.6, a supervisory control unit is potentially required to manage the simultaneous operation of the two AC machines. As shown in the previous Chapter for microgrid systems, it is advisable to integrate power factor control modules if several power sources and/or loads are connected to the same electrical bus.

Also, with regard to the HFAC system in Figure 3.6, it is unclear what technique has been employed for the integration of a bi-directional AC/HFAC converter. The module, which manages the AC power flow to and from the integrated generator (IG) machine, appears to convert the low frequency AC output from the generator into HFAC without an intermediary DC conversion stage. Typically, an intermediary DC transformation is required. The topic concerning the integration of regenerative electrical loads into a HFAC system will be discussed in detail in Chapters 4, 8 and 9.

In conclusion, this Section has highlighted the potential advantages of HFAC as a means of power distribution within a HEV. The investigation by (Bose et al., 1996) has suggested that the HEV HFAC system is preferable to DC or resonant DC power networks. Specifically, some of the HFAC benefits outlined in Chapter 2 have been attributed to the power distribution system in a HEV as well. These include:

- A potential increased efficiency of inverters and converters due to the soft switching technique employed.
- The reliable and galvanically-isolated magnetic connectors.
- The prospect for an optimal design of converters and electrical loads.

In addition, this Section has illustrated several possible HFAC converter topologies. Particularly, resonant DC inverters can be employed to efficiently convert the battery voltage into HFAC voltage. However, it is noteworthy that the resonant DC inverter proposed by (Bose et al., 1996) integrates a voltage-clamping mechanism which reduces the voltage stress on the passive circuit components. Unless robust circuit components are employed, this technique is likely to be of great importance for the automotive environment where reliability and safety are key.

Furthermore, HFAC/AC converters can be utilised to interface both starter motors and propulsion AC induction motors to the HFAC bus. These modules are essentially frequency converters, and the implications of supplying the AC machines with HFAC power are that:

- two inverse-series MOSFETs or IGBTs are required, which are expected to increase significantly the conduction losses in the circuit, and
- the polarity of the HFAC voltage has to be integrated within the control algorithm, which may lead to an increased complexity of the control system.

It is important to stress that while the literature cited in this work emphasizes the efficiency of the HFAC power converters due to the ZVS technique, no information is

given on the significant conduction losses in these circuits. This aspect is further discussed in Chapters 7 and 9.

Lastly, it is the author's opinion that it is unlikely for a HFAC/AC frequency converter to operate as a bi-directional power module, as suggested within (Bose et al., 1996). The main reason is that the only method to transform a low-frequency AC signal into a higher frequency waveform involves an intermediary DC conversion stage. In addition, even if such a method existed, it is unlikely that the speed of the IG machine in generation mode is constant due to the variability of typical regenerative cycles (which depend, for example, on the driving conditions and battery state of charge). As a result, the IG output frequency is not fixed in order to produce the required invariable HFAC bus frequency.

3.3 Auxiliary power and data bus

Another hypothetical HFAC electrical architecture has been proposed by Kassakian et al. (1996). Figure 3.8 shows the diagram of the electrical system, where an AC/DC/ HFAC converter supplies 48V at 25kHz from the VVVF output of the alternator. In addition, the AC/DC converter charges the 12V battery and supplies essential loads when the ignition is switched off.

The power architecture proposed by Kassakian et al. (1996) has a distributed topology, where local distribution boxes convert the HFAC power into the voltage needed by the loads. The modules, which contain MOSFET switches and fuses in this particular example, are part of a data network that transmits simple load on/off control signals. For instance, distribution boxes can be placed at the vehicle rear, serving loads such as lights, defrosters, audio and infotainment systems, power windows, door locks and cabin lighting.
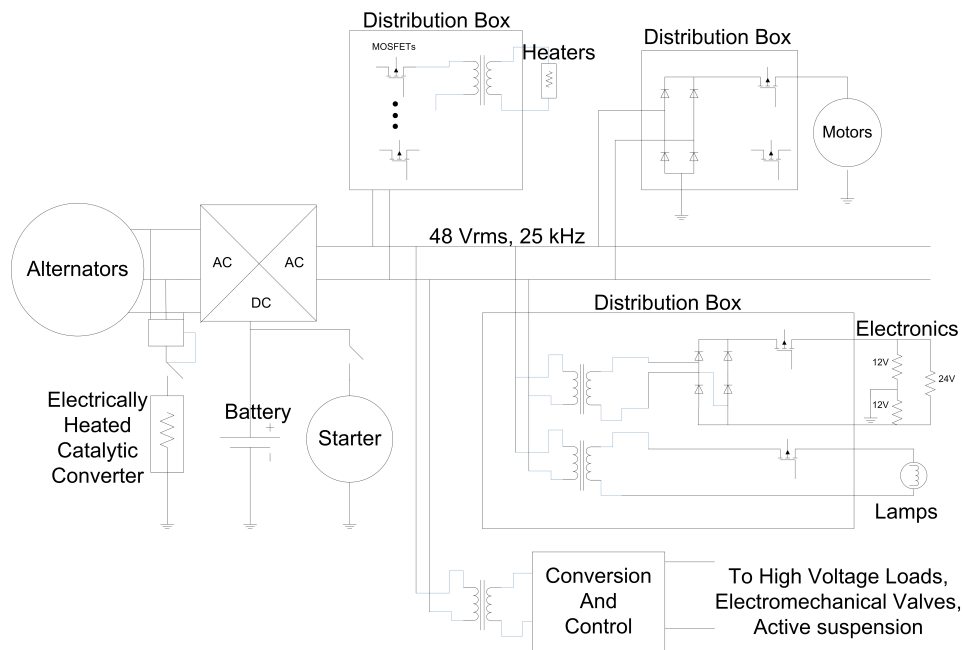
Figure 3.8 Hypothetical AC electrical distribution system (Kassakian et al., 1996)

Unlike the HFAC bus described in Section 3.2 for a HEV, the architecture presented in this Section introduces a first possible network topology for the vehicle auxiliary electrical system. The architecture includes two electrical buses operating in parallel:

- first, a centralised 12V DC bus which includes the battery and starter motor, and
- second, a distributed 48V, 25kHz AC bus where converters are allocated at the consumer location in the vehicle. It has been suggested in (Kassakian et al., 1996) that these converter modules can also serve as communication hubs for simple on/off load control.

An interesting difference between the HFAC system in this Section and the network presented in Section 3.2 is that the starter motor is not connected to the HFAC supply. For reasons detailed in Chapter 4, and subsequently in Chapter 8, this work supports an architecture configuration where the starter motor is detached from the HFAC bus.

Although it has not been explained in the study by (Kassakian et al., 1996) how data can be transmitted onto the proposed bus, it can be inferred that the HFAC sinusoid serves

as the signal carrier onto which the data signal is modulated. Amongst the main modulation techniques (amplitude and frequency modulation), it is likely that a potential implementation of a power and data bus may integrate the latter. The reason is that the bus voltage amplitude is strictly regulated by standards in the automotive industry, as indicated in Chapter 4.

A possible consequence due to the merging of both power and data onto the same HFAC bus is that new communication technology has to be developed for the specific type of carrier and modulation technique employed. This implication is a possible limitation for the proposed HFAC technology, since automotive OEMs have already invested into the development of multiplex control for the existing 12/14V DC system in vehicles. Conversely, the existing communication technology imposed onto DC power cables can potentially be adapted for the HFAC bus, although the latter has to provide a significant incentive for the industry to be willing to shift from the newly-developed multiplex systems.

3.4 400Hz AC auxiliary electrical networks

An important contribution to the study of HFAC power for vehicles is the investigation by Masrur et al. (1998a). The study addresses the question of whether a 400Hz AC electrical system can replace the existing DC system. The major parts of this study include the description of an AC architecture (single-phase and three-phase) and the estimation of the relative cost and size of additional hardware required.

In the conventional vehicle DC system, the battery is charged by a three-phase alternator. A voltage regulator converts the VVVF into DC voltage. For an AC system, however, several inverter topologies able to supply constant frequency AC from a DC source have been proposed by Masrur et al. (1998a):
• a PWM controlled inverter,
• a single-phase resonant inverter, and

• an actively clamped resonant link inverter.

The three converter topologies proposed by (Masrur et al., 1998a) are similar to the three converter modules described in Section 3.2 and hence will not be described again. It is noteworthy however, that the different studies cited within Chapters 2 and 3 revolve around the same circuit topologies for DC/HFAC power transformation. As indicated throughout this work, the same applies to HFAC/AC and HFAC/DC conversion circuits.

Figure 3.9 illustrates the 400Hz AC architecture proposed by Masrur et al. (1998a). The main components are the vehicle alternator, a three-phase AC/DC rectifier, battery and inverter - which can be any of the three topologies outlined above. Also, the architecture includes a filter circuit that prevents unwanted frequencies from distorting the AC sinusoid. A similar *tank circuit* has been integrated into the proposed HEV HFAC system. The author's view is that this type of filter should be assembled in all the adaptations of the HFAC distribution system, as a basic mechanism to ensure a high power factor and favourable transmission efficiency. The importance of this aspect has been discussed in Chapter 2 for the microgrid system.
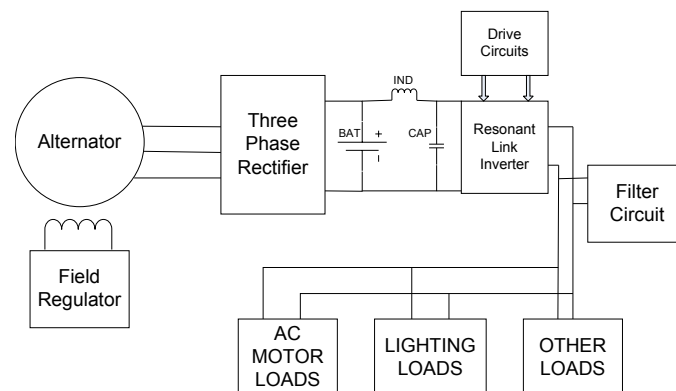
Figure 3.9 The proposed AC electrical power distribution architecture (Masrur et al., 1998a)

Figure 3.10 shows the three-phase variant of the same electrical network. This system requires an additional pair of solid-state switches and the use of three-phase machines.

The third phase adds redundancy to the system: should one line fail, the remaining two will ensure the system does not cease to function.
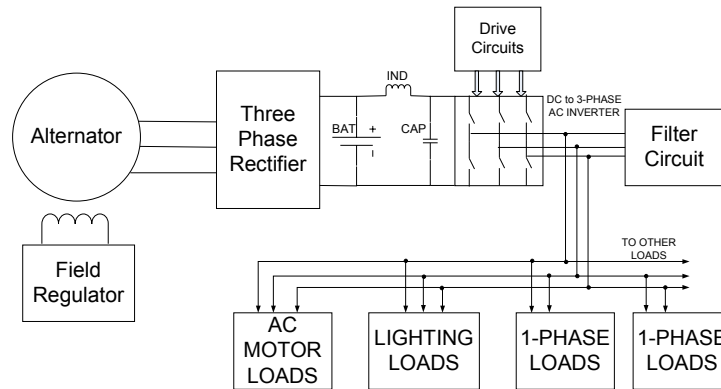
Figure 3.10 The proposed three phase AC electrical power distribution architecture (Masrur et al., 1998a)

The study indicates that induction motors are suitable candidates for the 400Hz AC bus, potentially due to the present use of such actuators within aircraft electrical systems. However, the voltage supply for these motors is of 115V, which is higher than the maximum allowed by the electrical safety standards within vehicles. This aspect is further discussed in Chapters 4 and 9.

The referenced study has also presented an estimation of cost and size for the DC/AC inverter and for the motors. The conclusion for the inverter investigated for different voltages (12V, 24V and 48V) and frequencies (400Hz, 800Hz and 1600Hz) for a 2kW power output, is that the frequency does not have a significant impact on its size and cost (Masrur et al., 1998b). It has been further shown that an overall decrease of about 8% in size of optimised single-phase AC motors compared to DC motors is possible, and up to 40% for three-phase induction motors. The motor data utilised for this analysis is shown in Tables 3.2 and 3.3. In particular, the Tables include the machine operating point (i.e. rated speed and torque, output, input and efficiency) and size

(diameter, length and weight). Chapter 8 presents a critical investigation into the potential mass and energy saving of state-of-the art 400Hz AC machines, in comparison to existing DC motor actuators in vehicles.

Table 3.2 AC induction motors (400 Hz) (US metric system) (Masrur et al., 1998b)

Application	Gear Ratio	Speed (rpm)	Torque (oz-in)	Output (watt)	Input (V)	Input (A)	Effic. (%)	Diam (in)	Length (m)	Weight (lbs)
				Operating Point					**Size**	
Cooling fan	2.5:1	5400	24	95	12.8	7.2	80%	3.1	3.1	2.3
A/C blower	2.7:1	5400	129	122	12.8	7.2	80%	3.4	3.5	3.1
Wiper	100:1	5600	11.25	29.6	12.8	2.2	80%	2.4	3.1	1.4
Washer	1	5400	1.25	4.6	12.8	0.4	50%	1.2	2.4	5 oz
Fuel Pump	1.75:1	10800	1.1	8.9	12.8	0.7	80%	1.6	1.5	6 oz
Vacuum Pump	2.25:1	5400	15	60	12.8	4.5	50%	2.7	2.9	1.7
Power Window	100:1	10800	5.2	42	12.8	3.2	50%	1.8	2.8	1
Power Seat	2 : 1	3600	11.25	30	12.8	2.3	50%	1.9	3.5	1
Door Lock	1	10800	4	30	12.8	2.3	50%	1	2	4 oz
Power Mirror	5 : 1	10800	0.2	1.5	12.8	0.11	50%	1	1	2 oz

Note: 1 Nm = 141.60 oz-in ; 1m = 39.37 in ; 1 kg = 2.205 lbs

Table 3.3 DC motors in vehicles (US metric system) (Masrur et al., 1998b)

Application	Gear Ratio	Speed (rpm)	Torque (oz-in)	Output (watt)	Input (V)	Input (A)	Effic. (%)	Diam (in)	Length (m)	Weight (lbs)
				Operating Point					**Size**	
Cooling fan	1	2150	60	95	12.8	12.7	58%	3.06	3.65	4.4
A/C blower	1	2000	108	162	12.8	21.9	68%	3.36	4.47	3.3
Wiper	56:1	2000	20	29.6	12.8	4	58%	2.4	3.71	3.9
Washer	1	6250	1	4.6	12.8	3	12%	1.2	1.2	1 oz

			Operating Point					Size		
Fuel Pump	1	6000	2	8.9	12.8	2	35%	1.6	2.1	9.6 oz
Vacuum Pump	1	2450	33	59.8	12.8	7	67%	2.74	4.04	3.9
Power Window	47:1	5200	11	42.3	12.8	8	41%	1.8	3	1.8
Power Seat	1	1600	25	29.6	12.8	6.4	36%	1.9	2.75	4
Door Lock	1	1400	7.1	7.5	12.8	1.5	39%	0.75	1.25	1.8 oz
Power Mirror	1	2000	1	1.5	12.8	0.25	47%	1	1	1.3 oz

Note: 1 Nm = 141.60 oz-in ; 1m = 39.37 in ; 1 kg = 2.205 lbs

Another interesting result presented by Masrur et al.(1998b) is the relationship between AC motor power factor and financial cost saving. The relationship between the two variables is shown in Figure 3.11. The key to the plot is the link between the power factor (*PF*) and the wiring harness volume, which changes by a factor of $\dfrac{1}{PF^2}$.

As illustrated in the Figure, the break-even point in cost savings is for a power factor of 0.737 for the three-phase system and 0.956 for the single phase system. The authors concluded that significant benefits can be achieved with a three-phase AC system in terms of cost and reliability.
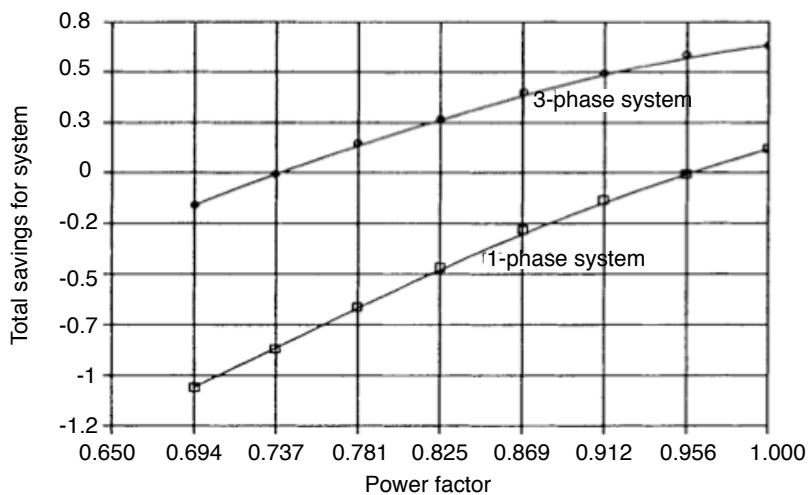
Figure 3.11 Cost saving versus power factor of AC motors (Masrur et al., 1998b)

Miller et al. (1996) indicated that the main benefits of HFAC power are related to motor loads and the distribution system. It was noted that resistive loads such as heaters can operate equally well when supplied with either DC or AC power. The cited study further examined the power architecture proposed by Masrur et al. (1998a), which has been presented so far in this Section. The recommendation is that the added cost of the third phase can be balanced by cost savings in the wiring harness and increased system flexibility.

Various multi-voltage systems with DC and AC power distribution for vehicles have been analysed by Khan (1999). Low and high frequency AC distribution systems were briefly introduced, followed by a review of advantages and disadvantages of the AC and DC power systems.

Khan (1999) proposed the low frequency AC system shown in Figure 3.12, based on a possible bus frequency of 400Hz. The energy source can be either a high-voltage battery pack or a three-phase generator. Various converters are used to transform:

• three-phase AC into one-phase AC power (constant voltage, constant frequency), or

• three phase AC into DC and vice-versa, and

• one phase AC into DC, which is useful to recharge the 12V battery and supply 12V loads. Point-of-use transformers can serve local load requirements, such as DC, or single-phase or three-phase AC power.
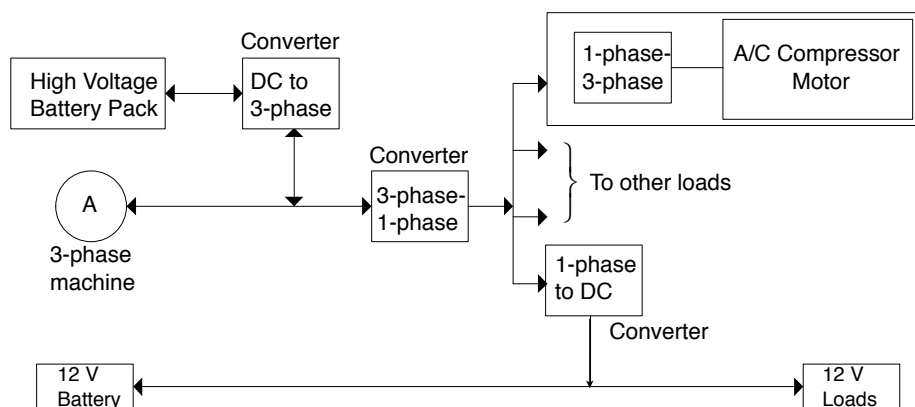
Figure 3.12 Block diagram of a low-frequency AC distribution system (Khan, 1999)

As discussed previously in the context of the HFAC system proposed by (Bose et al., 1996), the supply of regulated AC power directly from a three-phase machine as shown in Figure 3.12 may not be realisable. Also, the schematic diagram in the same Figure suggests that the three-phase machine and the DC/AC inverter can supply the loads either individually or jointly. As discussed earlier in Section 3.2 for the latter case, a system management control may be required. This may increase the complexity of the overall system and may also impose the requirement for additional power converters.

The conclusion drawn by Khan (1999) can be summarised as follows:

- Transformers in the electrical AC system add benefits such as easy voltage transformation and isolation. The higher the frequency is, the smaller their physical dimension.
- However, advances in power converters allowed DC/DC converters to successfully take the place of converters based on AC transformers.

Furthermore, the cited study has suggested that the following components add to the cost and complexity of a HFAC system:

- HFAC cables should have low inductance and capacitance, as well as reduce the skin effect[1]. As a result, HFAC conductors are potentially expensive in comparison to DC cables.
- Filters are required on the AC bus to neutralise the unwanted harmonics generated by the AC loads.

In conclusion, this Section presented two possible on-board auxiliary systems based on a 400Hz, single-phase or three-phase supply, as utilised for example in aircraft electrical systems. With regard to the architecture, the main difference between these topologies and the architectures presented in the previous two Sections is that AC machines can be directly connected to the bus without the need for additional HFAC/AC frequency converter modules. The implication is that cost and power losses can be decreased due

---

[1] Detailed in Chapter 4, the skin effect represents the effect causing current at high frequency to flow through a smaller conductor area than the one physically available.

to the reduced number of power converters. Also, the 400Hz system appears to be less complex than the HFAC electrical networks presented as yet.

However, no indication has been given as to the potential voltage amplitude for 400Hz power distribution. As will be discussed in Chapter 4, this aspect is important since the HFAC bus has to comply with automotive electrical safety regulations. Furthermore, since the network frequency advocated by (Masrur et al., 1998a, Masrur et al., 1998b) is lower by one order of magnitude than the other HFAC systems presented (400Hz, compared to 20kHz and 25kHz), the mass reduction advantages[2] associated with power distribution at frequency in the kHz range may not be realised.

The inverter topologies presented in this Section share the same resonant power transformation and voltage clamping techniques as proposed by (Bose et al., 1996) for the HEV power system (Section 3.2, Figure 3.3). Thus, it becomes apparent that a typical inverter structure and operation should be employed within all automotive HFAC systems.

This Section has also highlighted some of the possible disadvantages of HFAC. These include:
- The high cost of low-inductance HFAC cables.
- The requirement to add filters onto the HFAC bus.
- The fact that progress in DC/DC converter circuitry can possibly make this technology at least as efficient as converter modules which include AC transformers.

3.5 HFAC bus based on square-wave voltage power distribution

The research reported by Kokes (1997) has focused on the performance analysis of a DC/HFAC inverter. The study includes the mathematical description of the circuit and

_____

[2] As indicated in Chapter 2, the conductor copper mass and the mass and volume of passive circuit elements can be significantly reduced if these components are designed to operate at high frequency.

an experimental setup of a DC electrical network, used to validate the mathematical models.

Table 3.4 Possible current and voltage waveforms for a vehicle HFAC distribution system (Kokes, 1997) (SUSI,SUBI,BUBI, BUSI acronyms explained[3])

Inverter Name	Current and voltage waveform	Corresponding current and voltage equations
SUSI (sinusoidal voltage, sinusoidal current)		$u_N = \hat{U}_N \cdot \sin \omega t$ $i_N = \hat{I}_N \cdot \sin \omega t$
SUBI (sinusoidal voltage, square wave current)		$u_N = \hat{U}_N \cdot \sin \omega t$ $i_N = \begin{cases} +\hat{I}_N, 0 < t < \dfrac{\pi}{\omega} \\ -\hat{I}_N, \dfrac{\pi}{\omega} < t < \dfrac{2\pi}{\omega} \end{cases}$
BUBI (square wave voltage, square wave current)		$u_N = \begin{cases} +\hat{U}_N, 0 < t < \dfrac{\pi}{\omega} \\ -\hat{U}_N, \dfrac{\pi}{\omega} < t < \dfrac{2\pi}{\omega} \end{cases}; i_N = \begin{cases} +\hat{I}_N, 0 < t < \dfrac{\pi}{\omega} \\ -\hat{I}_N, \dfrac{\pi}{\omega} < t < \dfrac{2\pi}{\omega} \end{cases}$
BUSI (square wave voltage, sinusoidal current)		$u_N = \begin{cases} +\hat{U}_N, 0 < t < \dfrac{\pi}{\omega} \\ -\hat{U}_N, \dfrac{\pi}{\omega} < t < \dfrac{2\pi}{\omega} \end{cases}$ $i_N = \hat{I}_N \cdot \sin \omega t$
BULSI (square wave voltage, sinusoidal current with gaps)		$u_N = \begin{cases} +\hat{U}_N, 0 < t < \dfrac{\pi}{\omega} \\ -\hat{U}_N, \dfrac{\pi}{\omega} < t < \dfrac{2\pi}{\omega} \end{cases}$ $i_N = \begin{cases} +\hat{I}_N \cdot \sin(1+\Delta)\omega t, 0 < t < \dfrac{\pi}{(1+\Delta)\omega} \\ 0, otherwise \end{cases}$

---

[3] Acronyms from German: SUSI: Sinusspannung und Sinusstrom, SUBI: Sinusspannung und Blockstrom, BUBI: Blockspannung und Blockstrom, BUSI: Blockspannung und Sinusstrom.

First, the most suitable waveforms for the DC/HFAC inverter operation have been investigated. Amongst the possibilities depicted in Table 3.4, variant BULSI[4] (square wave voltage, sinusoidal current with gaps) has been chosen as the most appropriate based on the rationales described next.

Since the sinusoidal output voltage is cited as being load-dependent the first two inverter types, SUSI and SUBI, have not been investigated further. Similarly, the BUSI alternative (square wave voltage, sinusoidal current) has not been analysed in-depth due to limitations such as (Kokes, 1997):
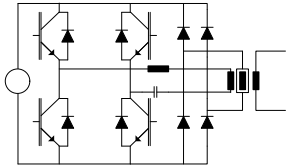
• high operating temperature,

• sensitivity to aging effects, and

• the fact that high-volume applications are not sustainable.

The remaining two alternatives, BUBI and BULSI, have both pros and cons associated with their use. The reported financial cost for the former is approximately 20% lower compared to the BULSI transformer (Kokes, 1997). However, since the BUBI circuit has shortcomings such as added circuit protection components and includes a buck converter (thus adding further losses to the system), and the fact that between the two only BULSI can offer contact-less power transfer, led to the choice of an inverter based on square-wave voltage and variable-duty sinusoidal current (BULSI).

The option for the 25kHz frequency is based on several arguments: a high frequency brings advantages of space and weight saving, but the disadvantage is a more expensive circuit transformer windings. High frequency also increases the skin effect of the conductor as well as its cost, and potentially gives rise to EMI problems. On the other hand, a frequency higher than the audible range is required (above 20kHz). Table 3.5 summarises the characteristics of the chosen concept.

_____

[4] Acronym from German: Blockspannung und lückender Sinusstrom

Table 3.5 Properties of the selected bus concept (Kokes, 1997)

Concept	BULSI	Inverter topology
Voltage	80 V	
Frequency	25 kHz	
Current gap variation factor	$0.1 < \Delta < 0.2$	

The selected concept is in accordance with the safety norm DIN VDE[5] 0800 Part 1, rated class 1B (Kokes, 1997). The norm, which is consistent with the SAE J2232 standard[6] for vehicle system voltage, states that the bus voltage must satisfy the following inequality, where m is the frequency factor (Figure 3.13):

$$U_{rms} \leq m \cdot 25V \qquad (1)$$
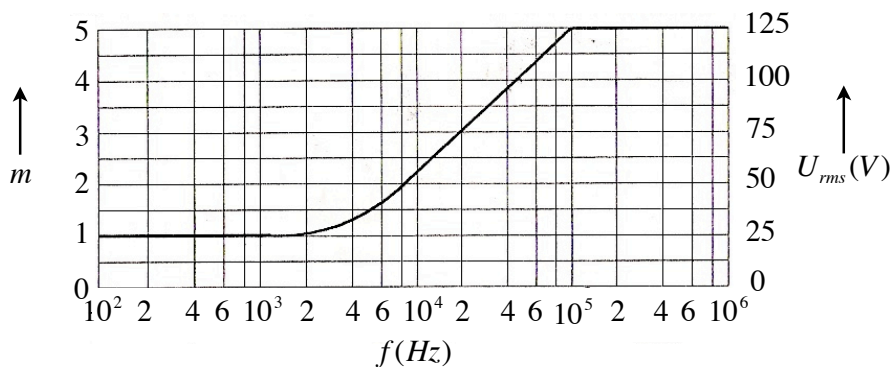
Figure 3.13 Maximum allowed bus voltage as a function of frequency (Kokes, 1997)

It is important to discuss the choice presented by (Kokes, 1997) for an inverter based on a square-wave voltage in the context of the finding presented in Section 2.5, which emphasized the rich harmonic content of such waveforms (Watson et al., 1996). The research outlined in this Section has primarily focused on the development of a robust

---

[5] The German DIN VDE standards include recommendations for power systems and power cables.

[6] The Society of Automotive Engineers (SAE) standards specifies the maximum safe operating voltages of 60V DC, 50V AC at 50Hz, 75V at 25kHz and 87.5V at 30kHz.

DC/HFAC inverter and the analysis has been primarily directed to the design and control of the circuit. As a result, the implications of the square-wave in terms of power distribution efficiency and EMI compatibility have not been addressed. Based on the findings presented in Section 2.5 of the previous Chapter, it can be inferred that the square-wave waveform chosen as part of the study by (Kokes, 1997) is not the most advantageous for the overall HFAC system. Nonetheless, the cited research is of interest to the present work for the followings reasons:

- first, it presents a potential implementation of the HFAC system within vehicles, and
- second, it provides an insight into the power capability of a HFAC electrical bus.

Kokes (1997) has proposed the electrical system shown in Figure 3.14 as a potential implementation of the HFAC bus. The components of this particular configuration are:

- An energy source, which is a battery-supplied inverter with a rated output power of 4kW.
- Four high-power consumers, each having an output voltage of 310V DC, rated power of 1.5kW and cumulative peak transient power demand of 7.5kW,
- A front module, which produces two output voltages: 13V DC and 42V DC. The front module can supply 42V DC at a rated power of 1kW, and 13V DC at 500W.
- A battery management module that can operate both as an AC inverter or DC rectifier, thereby allowing energy to flow from the HFAC bus to the battery and also supply the network from the battery.

A detailed description of the structure and operation of the network components outlined above is included in Appendix B for reference.
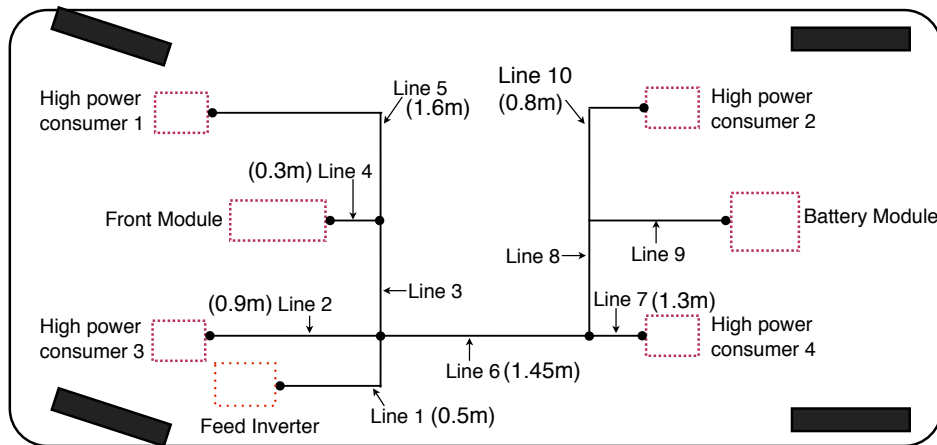
Figure 3.14 Wiring structure for HFAC bus experimental setup (Kokes, 1997)

The connections between the network components are either double conductor lines (lines 3, 4 and 5) or triple lines (1, 2, 6, 7, 8, 9 and 10). The double line type has twice the resistance and inductance per meter as the triple line, and half of its capacitance. Table 3.6 includes the electrical characteristics of the HFAC cables considered in the study by Kokes (1997). As will be detailed in Chapters 4 and 6, the electrical attributes of the HFAC conductor are dependent on the the frequency used for power distribution. In addition, these features have an effect on the power transmission efficiency and the mass of the cabling network within the vehicle.

Table 3.6 Electrical properties of the transfer lines for a temperature of $25^{o}C$ (Kokes)

Parameter	Double line	Triple line
Resistance	$6.86 m\Omega / m$	$3.43 m\Omega / m$
Inductance	$80.9 nH / m$	$40.45 nH / m$
Capacitance	$0.8 nF / m$	$1.6 nF / m$

The fist understanding from the HFAC system implementation is that the capability of the proposed HFAC bus extends up to 4kW for continuous operation and 7.5kW under transient conditions. Similar power levels are estimated for the proposed high-voltage replacement[7] of the current 12/14V DC system within vehicles, as further detailed in

---

[7] The 42V DC Power Net has been proposed as replacement for the 14V DC system since 1989.

Chapter 4. Therefore, it is expected that the HFAC system can successfully meet the high on-board power demand.

It can be inferred from the configuration of the HFAC architecture that high-power loads, in the order of 1.5kW, can potentially be supplied. This aspect is significant for the proposed technology, since several state-of-the-art applications within vehicles have a continuous power demand in excess of 1kW (e.g. the VVA system). Nonetheless, if particular electrical loads have a very high current requirement, HFAC converters can be connected in parallel in order to achieve the desired output level as suggested by (Watson et al., 1996) and previously discussed in Chapter 2.

The fact that the bus includes 14V DC and 42V DC converters illustrates:

- First, the necessity to integrate these voltage levels within the proposed system for compatibility with both applications designed for the present 14V supply, and consumers intended to operate off the 42V *PowerNet*,
- Second, the fact that the HFAC bus is effectively a multi-voltage electrical system which can easily meet various requirements of the electrical loads.

The capability of the battery management module to manage bi-directional power flow suggests that (Kokes, 1997) supports the integration of regenerative electrical loads within the HFAC architecture. This finding is consistent with the studies previously discussed in Sections 3.2-3.4. However, as it will be argued in Chapter 4, this may not be the best approach for the management of the recuperated energy.

The detailed analysis of the DC/HFAC inverter operation indicates that the transient response of the supply to step changes in load current is approximately 10ms. As opposed to the current DC system where the battery can supply a large instantaneous current, HFAC power is processed by various electronic circuits which have a limited current and transient response capability. Therefore, in order to meet the potential high current surge of electrical loads, the transient time of the bus should be as small as

possible. This discussion is continued in Chapter 5, where consideration is given to the dynamic response of the DC/HFAC inverter to step changes in the load current.

The study presented in this Section has indicated another possible disadvantage of the HFAC system. Namely, the no-load power loss of HFAC bus is expected to be higher than the DC system. However, as it will be argued in Chapters 6 and 9, this aspect may not have a great impact on the overall conclusion of the present work.

3.6 HFAC power distribution for automotive applications - summary

The pursuit of HFAC power distribution advantages for the International Space Station Freedom programme by NASA and the successful implementation of AC electrical systems in aircraft have sparked the interest of the more conservative and cost-aware automotive industry to follow suit, although not to the same extent. Frequencies ranging from 400Hz, to 20kHz and 25kHz have been analysed for automotive applications including auxiliary and propulsion systems. Specifically, (Bose et al., 1996) have investigated the feasibility of a HFAC bus for propulsion power distribution in a HEV. In addition, single-phase and three-phase 400Hz AC systems have been analysed by (Masrur et al., 1998a, Masrur et al., 1998b) for vehicle auxiliary electrical loads. Furthermore, (Kassakian et al., 1996) and (Kokes, 1997) have presented auxiliary networks based on 25kHz, and 48V and 80V, respectively. A summary of the characteristics for these power architectures is included in Table 3.7.

Possible HFAC power sources include the vehicle battery as DC supply and sundry inverter topologies. The inverter in the proposal by Bose et al. (1996) for a HFAC power distribution system in HEVs is the one customised by Jain et al. (1999) for aerospace and telecommunication applications, previously detailed in Chapter 2, Section 2.3. Other inverter topologies include the DC PWM controlled inverter and the resonant DC inverter (Masrur et al., 1998a). The simplicity and robustness of the first comes at the price of hard switching losses. The latter two solve this issue, but the potential limitation is the low module reliability caused by the high voltage stress on the

passive circuit elements. A further refinement of the resonant inverter design is to include active voltage clamping in order to reduce the high voltage strain on the circuit.

Table 3.7 Studies of HFAC power for automotive applications

Application	Voltage	Frequency	Power
HEV power distribution	440V	Possibly 20kHz	In the order of tens of kW
Auxiliary electrical system (1)	48V	25kHz	Several kW
Auxiliary electrical system (2)	up to 25V, based on norm illustrated in Figure 3.13	400Hz, 1-phase or 3-phase	Several kW
Auxiliary electrical system (3)	80V, square wave	25kHz	4kW continuous

The circuit proposed by Kokes (1997) is a series oscillatory static inverter. The author opted for mathematical modelling to describe its operation and control of the circuit, as detailed within Appendix B. In addition, Kassakian et al. (1996) referred to an AC/AC converter to produce 48V, 25kHz voltage, from the VVVF of the vehicle alternator. No description has been given of how such a high frequency was obtained from the alternator machine. Finally, Khan (1999) noted that three-phase 400Hz power can be produced by a three-phase generator machine as in today's aircraft and then distributed to three-phase, single-phase AC or DC loads.

It is noteworthy that there is no proposition for a frequency higher than 25kHz nor lower than 20kHz. As Kokes (1997) explains, the higher the bus frequency, the more expensive the transformer windings and the cables are. Additional high frequency effects are the skin effect on cables and the higher probability of EMI with nearby electronic devices. On the other hand, in order to avoid interference with signals in the audible range, the bus frequency should be higher than 20kHz.

The HFAC architecture has a distributed topology and power adjustment is performed at the point of use. Bose et al. (1996) opted for HFAC/AC converters in HEVs based on

hysteresis-band current control[8]. Good performance was noted in supplying the three-phase traction induction motor and the starter induction machine. In the hypothetical distributed network submitted by Kassakian et al. (1996) the distribution boxes are part of both power and data networks. Based on this architecture, the simple on/off control signals can be transmitted onto the power cables.

The power net suggested by Masrur et al. (1998a, 1998b) employs an alternator with three-phase rectifier as a DC supply, and resonant inverter and filter circuits synchronised at 400Hz. This study is distinctive for the investigation into matching 400Hz AC motors for automotive applications. Also, the cited studies give a useful estimation of additional cost and hardware required by an AC electrical system in vehicles. Specifically, optimised 400Hz induction motors with adequate gearing mechanisms meet the power requirements for automotive applications such as wiper and A/C blower motors. Furthermore, the inquiry into cost and size yielded interesting results. Optimised induction motors can be 8% to 40% smaller than their DC counterparts, while the break-even power factor for potential financial cost savings in the three-phase and one-phase systems is 0.737 and 0.956, respectively.

Miller (1996) noted that the main advantages for HFAC in vehicles are first for motor loads, in replacing brushed DC motors with asynchronous AC machines, and second for the power distribution system itself. However, Khan (1999) is skeptical about the success of a 400Hz AC system in vehicles. As argued within the referenced work, the advancement in DC/DC converter technology enabling better efficiency, in addition to the high cost of HFAC cables, and the extra cost of filters are the chief arguments in favour of a DC system.

---

[8] The hysteresis-band current control is described within the same study (Bose et al., 1996)

3.7 Discussion and conclusion

The present study aims to investigate the advantages of HFAC power for automotive auxiliary electrical systems. To this end, the inquiry is focused on the aspects which have not been covered by the existing studies in this field and are potentially of significant interest to the automotive industry.

Based on the review of current literature, Table 3.8 summarises the main benefits of HFAC power, the extent to which these advantages have been studied for automotive applications and the potential for further research. In particular:

- The second Table column summarises the main advantages of HFAC power, as highlighted in Chapter 2.
- The third column of the Table indicates the research conducted for automobile HFAC networks, corresponding to the items in column two, as presented in Chapter 3.
- Column four includes the prospective areas that have not yet been analysed, and are critically evaluated as part of the present work.

Table 3.8 Potential for further research into advantages of HFAC for vehicle auxiliary electrical systems

No	General HFAC power advantages (Chapters 2 and 3)	Automotive studies (Chapter 3)	Potential for further research
1	Low cable copper mass and also compact passive circuit components	Only mentioned, but not quantified	Quantify, for various possible network topologies (see Chapters 6 and 9)
2	Less expensive and complex circuitry	Only mentioned, but not quantified	HFAC converter complexity detailed as part of Chapters 5 (DC/HFAC), 7(HFAC/DC and HFAC/AC, constant speed drive) and 8 (HFAC/ AC, variable speed drive)
3	Low power distribution losses	Only mentioned, but not quantified	Quantify, for various possible network topologies and load power demand (included in Chapters 6 & 9)

No	General HFAC power advantages (Chapters 2 and 3)	Automotive studies (Chapter 3)	Potential for further research
4	Magnetically-coupled HFAC connectors	Only mentioned, but not tested.	HFAC connectors are known to offer galvanic isolation, but the required testing is not included in the present study.
5	High efficiency of HFAC power electronic circuits	Not quantified	Rigorous calculations for the losses in DC/HFAC, HFAC/DC and HFAC/AC converters. (see Chapters 5,7,8 and 9).
5	Distributed network topology, where power is converted at the point of use, and loads benefit from the most efficient voltage and current level	Only mentioned, but not detailed.	Part of the analysis in Chapter 9.
6	High power quality	Not mentioned	Not included in this work.
7	Better fault tolerance and increased reliability	Not mentioned	Can be potentially quantified based on probability theory. This study only mentions possible effects on reliability of the introduced HFAC power electronics.
8	Mass and efficiency advantages for motor loads in vehicles	Mentioned, quantified	Analyse these advantages based on present off-the-shelf machine technology. Include in analysis high-torque motor loads as well. (see Chapter 8)
9	Potential to integrate regenerative electrical loads into the HFAC bus.	Mentioned and assumed to be feasible.	Discusses in more detail. (see Chapters 4 and 9).

The analysis is directed first to the four main sub-systems of the electrical architecture. Namely, these sub-systems are:

- *power generation*, which refers to the power electronics stage of converting the battery voltage into HFAC voltage or current,

- *power distribution*, which includes only the cabling in the context of the present study,

- *power conversion*, i.e. various topologies of HFAC/DC and HFAC/AC power converters required by auxiliary electrical consumers in vehicles, and
- the *electrical loads*, ranging from low-power DC loads such as light bulbs, to state-of-the-art loads including the EPAS or the ISG applications.

Table 3.9 presents a different view on the novelty of the present study, based on the structural analysis of the HFAC bus described above. Specifically, amongst the four sub-systems, the current work aims to present original results mainly for the power distribution and electrical loads subsystems.

The power generation and conversion sub-systems have already been extensively covered in the literature. However, it is important to customise the existing inverter and converter topologies within the context of the automobile HFAC system. In addition, the assessment of energy efficiency and mass reduction associated with these sub-systems is necessary for the system-level study of the proposed technology.

Finally, the present work concludes with the system-level analysis of the HFAC bus. This investigation is based on the mass and energy assessment at the sub-system level and aims to provide an overall conclusion to this study. Table 3.10 summarises the sought-after innovation related to the two characteristics investigated at the system level: energy efficiency and mass reduction.

Table 3.9 Novelty of the present study at the sub-system level

Sub-system	Research to date	Novelty
Power generation	Many inverter topologies exist. Circuit control is not presented in detail.	Tailor an efficient inverter topology for the requirements of modern loads in vehicles. (Chapter 5)
		Present in detail the circuit control. (Chapter 5)
		Include inverter efficiency and mass assessment into system-level analysis. (Chapter 9)

Sub-system	Research to date	Novelty
Power distribution	Several HFAC architecture topologies have been proposed. These have only been generally described, and not thoroughly examined.	Analyse the benefits of possible HFAC network topologies to meet the requirements of state-of-the art electrical loads. (Chapters 5 and 9) Quantify the wiring harness mass of suitable bus topologies, and compare to mass of existing 14V system and proposed 42V PowerNet. (Chapters 6 and 9). Quantify the power distribution efficiency and compare to 14V and 42V DC alternatives. (Chapters 6 and 9).
Power conversion	Many inverter topologies exist. Circuit control is detailed.	Choose the most appropriate topology for the present study. (Chapter 7) Compare the efficiency of existing DC/DC converters in vehicles with the efficiency of HFAC/DC converters. (Chapter 7) Analyse the mass of converter modules. Include findings into system-level analysis. (Chapter 9)
Auxiliary electrical loads	Indication of the load categories which can benefit from HFAC. Quantification of packaging volume and cost saving of 400Hz motors (1996). Feasibility of high power consumers proven (cumulative power of 7.5kW).	Quantify benefits in terms of size, mass and efficiency for off-the-shelf 400Hz machines, compared to DC motors in vehicles today. Analysis is based on present technology (2010). (Chapter 9) Indicate loads which can potentially benefit from voltage supply higher or lower than the 14V present in vehicles. (Chapters 5 and 9). Analyse the feasibility of the HFAC bus to withstand load current surges. These are normally filtered by the battery in a DC system. (Chapter 5)

Table 3.10 Novelty of the present study at the system level

System-level	Research to date	Novelty
Energy efficiency	None	Quantify for several HFAC network topologies. Includes efficiency assessment of all sub-systems. (Chapter 9)
Mass saving	None	Quantify for several HFAC network topologies. Includes mass saving assessment of all sub-systems. (Chapter 9)

Chapter 4

Proposed auxiliary HFAC power system

4.1 Introduction

The aim of this Chapter is to present the topology and parameters of the proposed HFAC bus. Section 4.2 discusses the present auxiliary electrical system in vehicles, operating at 14V DC, and highlights its main disadvantages. Next, Section 4.3 outlines the main rationales for the proposal of the 42V DC Power Net within the automotive industry and the characteristics of this system. Section 4.4 introduces the HFAC power bus, and discusses the reasons for supporting the chosen topology, voltage and frequency. Finally, Section 4.5 concludes the Chapter by summarising the properties of the proposed auxiliary HFAC system.

4.2 The present 14V electrical system

Figure 4.1 shows a schematic of the present 14V DC bus employed in passenger vehicles. This system has a centralised topology and includes the following components:

- A 14V alternator with diode rectifier.
- A 12V lead-acid battery,
- 12V (key-off) and 14V (key-on) loads connected to the battery.
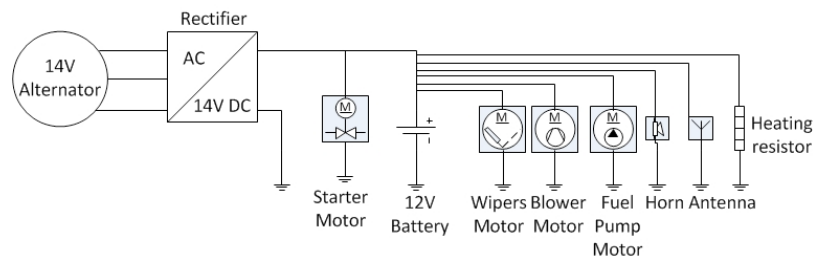
Figure 4.1 Schematic of the existing 14V DC auxiliary electrical system in vehicles

The main limitations of the current auxiliary DC system can be summarised as follows:

- Heavy and complex wiring harness, due to the point-to-point wiring topology. In fact, a typical medium size passenger vehicle can contain up to 1500 individual wires. In addition, the wiring harness mass can be as high as 50kg (Honeywill, 2007).

- Varying system voltage, typically from 9V to 16V (Miller et al., 1999) depending on the battery age and state of charge. This aspect is reflected as part of the design of different electrical actuators and sensors. For example, the specified supply voltage range for off-the-shelf steering torque and angle sensors is between 8V and 16V DC.

- Destructive high voltage transients, such as the "load dump" transient which is an exponentially decaying voltage that occurs when the battery is accidentally disconnected, while the alternator is generating charging current. In this scenario, the loads have to withstand a voltage transient as high as 120V, for a duration of 400ms (Chiu, 2002).

- High losses in the brushes of 14V DC motors (Miller et al., 1999). Typically, as will be highlighted in Chapter 8, the efficiency of bespoke DC motor actuators is within the 40% - 70% range.

- Expensive and time-consuming assembly process, fault tracing and repairing. This is due to the large number of modules within the system, which can be as high as 600 for the typical passenger vehicle (Honeywill, 2007).

In addition, an important drawback of the 14V system is that due to its limited power capability, it can not keep abreast of the present trend of vehicle electrification (Keim, 2004, Iles-Klumpner et al., 2006, Kassakian et al., 1996). Specifically, the power demand of state-of-the-art vehicle applications such as the ISG and the VVA systems exceeds the 2.5kW capability of the current on-board supply. As presented in the following Section, one possible solution to this limitation is a DC architecture based on a higher voltage.

4.3 The *42V Power Net*

It is questionable how long will the present alternator be able to keep its role in passenger cars, since the gap between the electrical power it can supply and the forecast of on-board power demand is growing larger every year. A study by Lukic and Emadi (2003) quantified the average power consumption of auxiliaries for the UDDS[1] cycle to 1,713W. The addition of *hotel* loads, comprising navigation and entertainment systems, plus state-of-the-art electromechanical applications such as active suspension, VVA and EPAS increase the figure by another 2,920W (Lukic and Emadi, 2003). Hence , the total power requirement clearly exceeds the maximum capability of the 14V alternator which is in the order of 2.5kW.

This computation, forecasted since the late 1980s, led to the proposition to upgrade the 14V to 42V DC as the next voltage standard in vehicles. Figure 4.2 shows the schematic of the proposed power bus and Figure 4.3 illustrates in detail the voltage limits of the 42V standard (Rajashekara, 2003).
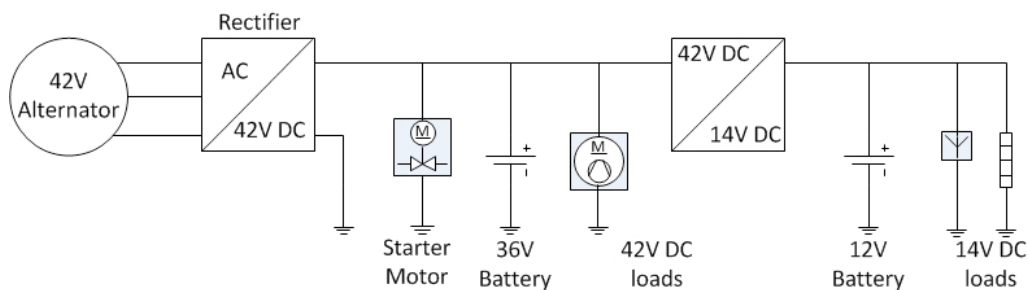
Figure 4.2 Schematic of the proposed auxiliary 42V Power Net

Since its proposal in the early 1990s, the 42V Power Net has received much attention from academia and original equipment manufacturers (OEMs), but it has not been adopted to the present day. Diverse rationales can account for this. First, technical challenges reported by Keim (2004) related to 42V electric arcs and connector corrosion

---

[1] UDDS stands for Urban Dynamometer Driving Schedule

have yet to be overcome. Second, the high cost associated with the adoption of the 42V technology seems to keep its prospect in the balance for the foreseeable future (Keim, 2004).
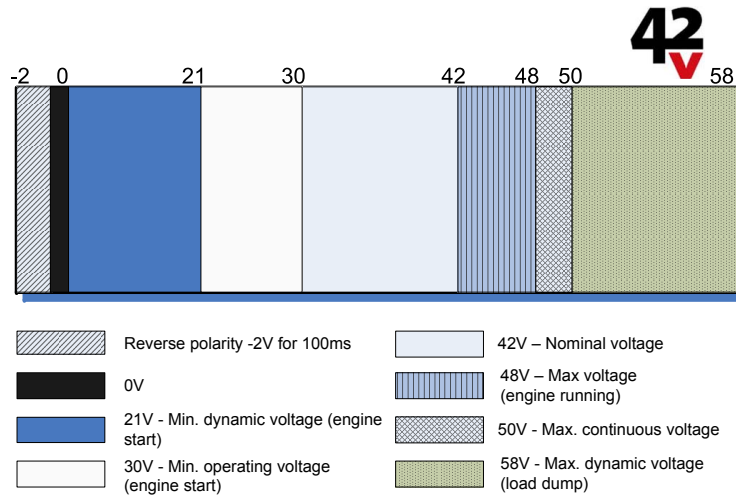
Figure 4.3 The 42V Power Net standard - voltages explained (Rajashekara, 2003)

4.4 The proposed HFAC bus

It is the view of the author that it is unlikely for a single voltage to meet the power requirements of present and future auxiliary consumers in vehicles. Ideally, an electrical distribution system should be capable of matching the power required by individual loads without sacrificing efficiency. It would also be desirable to have a distribution system that weighs less than the loom in cars today, provides greater design flexibility and improves efficiency of at least some electrical loads. It is proposed that a suitable candidate with a realistic prospect to bring these expectations to completion is a power distribution system based on high frequency alternating current (HFAC).

Figure 4.4 illustrates the schematic of the proposed HFAC power bus for vehicle auxiliary electrical systems. The main components of the proposed network are listed below, and discussed in the remaining part of this Section:

1. the power generation sub-system, comprising 42V alternator, AC/DC rectifier and DC to HFAC inverter,
2. the energy storage sub-system, which is a 42V lead-acid battery,
3. the 42V DC power distribution bus, for electrical loads which require high-torque motor actuators such as the ISG. This aspect will be further detailed in Chapter 8 as part of the electrical loads analysis,
4. HFAC power distribution bus, at 100V, 50kHz AC. The choice is justified in Section 4.4.2 of the current Chapter,
5. power converters, including HFAC/AC and HFAC/DC modules, and
6. electrical actuators, interfaced locally by power converters.
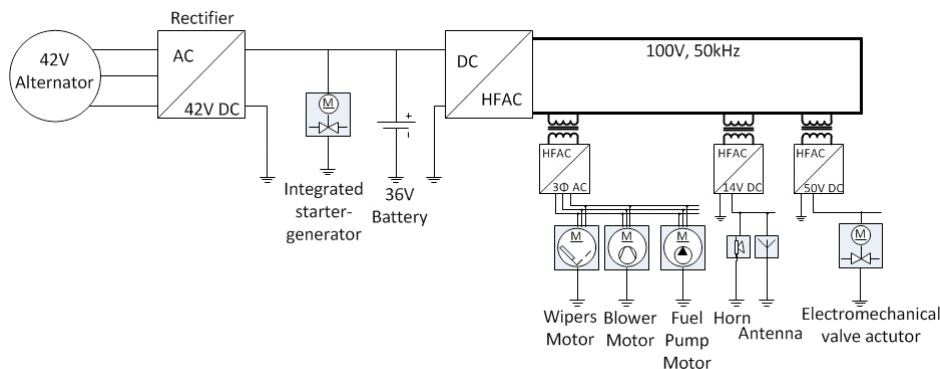
Figure 4.4 Schematic of the proposed HFAC power bus, including example loads

4.4.1 Architecture topology

Similar to the vehicle auxiliary power networks presented in Sections 3.3 and 3.4, the proposed bus includes both DC and HFAC power distribution. The necessity for the former can be justified by the following rationales:

- The on-board energy storage function is fulfilled by the battery. Therefore, the AC power from the engine-driven alternator must be converted to a DC voltage in order to recharge the battery.

- A large number of vehicles today integrate a mild hybrid electric system for energy capture during braking. Typically, an ISG machine is coupled to the engine crankshaft and fulfills two functions: first, as an engine starter, and second it generates electrical power while the vehicle is decelerating. The studies by Bose

et al. (1996) and Kokes (1997), presented in the previous Chapter, have proposed that the power generated by the ISG be converted into HFAC and subsequently used by the loads connected to the bus and/or stored in the battery. Unless all the recaptured energy is used instantaneously by the various actuators in the vehicle, the low frequency AC output of the ISG is unnecessarily following the bi-directional energy conversion process depicted in Figure 4.5[2]. Based on this argument, the present work proposes that the ISG is connected directly to a 42V DC bus, thereby removing the conversion steps 2 and 3 in Figure 4.5.
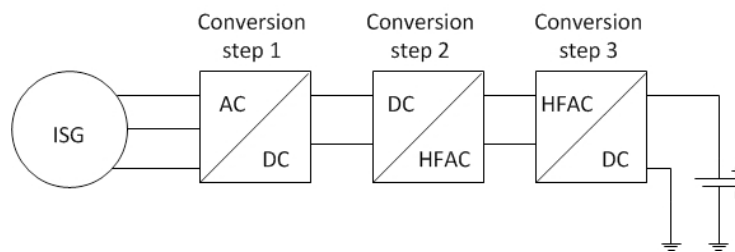
Figure 4.5 Sub-optimal connection of ISG to the vehicle electrical system

- As discussed in Chapter 8, high-torque motors (e.g. ISG, EPAS, VVA actuators) are expected to have more efficient 42V DC power drive electronics and lower torque ripple compared to a HFAC supply.
- Lastly, a DC bus is possibly a better alternative to HFAC for loads in the engine compartment, which require specific insulation of the conductors to withstand extreme temperatures and vibration. It is possible that adding such protection to HFAC cables within the engine compartment can increase their expected high cost (Khan, 1999, Kokes, 1997) even further.

---

[2] An intermediary stage of converting AC into DC prior to transforming the voltage into HFAC is required since a higher frequency AC signal cannot be obtained directly from a lower AC sinusoid. N.B. The reverse is possible, i.e. synthesize a low frequency AC voltage from a high frequency AC voltage, as discussed in Chapters 2 and 3.

4.4.2 System voltage and frequency

The choice for the 42V DC alternator and battery in the present study can be justified by the following reasons:

- First, it has been acknowledged by the automotive industry since the late 1980s that a voltage higher than 14V is required to keep abreast of the higher on-board power demand.

- Second, the higher the voltage, the lower the mass of motors and the higher the power distribution efficiency. A good design study into a 42V brushless DC motor actuator for automotive applications is described in (Jun-Hyuk et al., 2007).

- Third, as detailed in Figure 4.3, the proposed 42V is the highest DC voltage amplitude considered safe within a passenger vehicle environment.

The studies presented in Sections 3.3 and 3.4, have similarly proposed a parallel DC bus with the main HFAC network. Particularly, the work proposed by Kassakian et al. (1996) and Khan (1999) focused on a voltage amplitude of 48V DC and 12V DC, respectively. While the first does not align with the present safety regulations in vehicles, the latter is known to be too low for modern on-board applications.

The amplitude and frequency of the HFAC bus voltage have been chosen according to the SAE J2232 standard and the safety norm DIN VDE 0800 Part 1, rated class 1B. This norm, previously mentioned in Section 3.5, specifies the maximum allowed AC voltage for a range of frequencies. In particular, the voltage amplitude limit for a frequency of 50kHz is 100V. The maximum voltage amplitude has been chosen in order to minimise the AC power distribution losses and also to reduce the size of the network electronic components.

As will be discussed in Chapter 9, future potential changes in the regulations regarding the on-board voltage amplitude and frequency are not expected to have a significant impact on the benefits of HFAC power distribution within vehicles.

The justification for the 50kHz can be given as the compromise between two contrasting effects of the frequency on the HFAC bus. Specifically, on one hand, current at high frequency flows through a smaller copper area than the one physically available. This effect, known as the skin effect[3], allows for the use of thin and light cables which in turn reduces the mass of the wiring in the vehicle. On the other hand, however, the high frequency translates into a high cable impedance. This effect can be quantified by Equation 4.1, where R is the cable resistance and L is the inductance.

$$Z(\omega) = \sqrt{R^2 + X_L(\omega)^2}, \text{ where } X_L(\omega) = 2\pi f L \tag{4.1}$$

It should be noted that the cable capacitance does not have an effect on the voltage drop and the parasitic impedance losses are negligible, as discussed in (Sudipta et al., 2007).

Figure 4.6 illustrates the variation of the skin depth and cable impedance as a function of frequency, for a particular cable resistance of 5mΩ/m and three inductance values: 25nH/m, 30nH/m and 35nH/m. These values are consistent with the data from commercially available conductors.
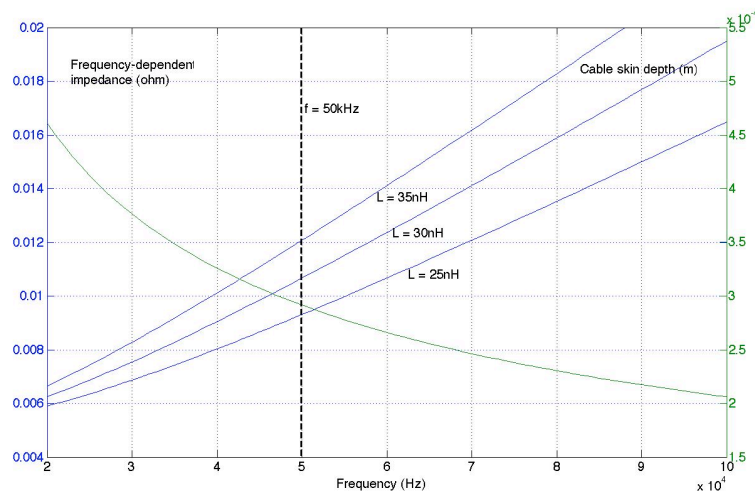
Figure 4.6 Variation of skin depth (m) and cable impedance (Ω) with frequency (Hz)

---

[3] A detailed description of the skin effect is given in Appendix C.

The lower the skin depth, the more copper mass can be saved. Conversely, the higher the cable impedance, the greater the distribution losses and the voltage drop. Consequently, as shown in Figure 4.6 for the lowest inductance cable, the optimum compromise between the two factors is for a frequency of approximately 50kHz.

Finally, Section 2.5 has indicated that the softer the transition time of square-wave voltage, the lower the harmonic power content. Therefore, based on the favourable EMI property of sinusoidal voltage in comparison to square-wave voltage, the former is the preferred choice in the present study. Kokes (1997) has suggested that sinusoidal voltage is load-dependent, and focused on the study of a 84V square-wave bus. However, all the other studies presented in Chapters 2 and 3 have investigated the use of sinusoidal HFAC, which suggests that a sinusoidal HFAC signal is feasible for applications ranging from auxiliary loads to HEVs.

4.5 Conclusion

This Chapter has introduced the architecture topology and parameters of the HFAC power bus. Table 4.1 includes the attributes of the proposed electrical system.

Table 4.1 Properties of the proposed HFAC auxiliary electrical system

Characteristic	Value
Voltage, DC	42V
Voltage, HFAC	100V (rms)
Frequency	50kHz
HFAC voltage waveform	Sinusoidal
HFAC current waveform	Sinusoidal

Section 4.4.2 has highlighted the rationales for the integration of a 42V DC bus in parallel with the HFAC system. Specifically, the former is required to facilitate the

integration of energy recuperation systems. In addition, as discussed in Chapter 8, a DC bus is preferred for the supply of high-torque machines.

Furthermore, the Chapter presented the rationales for the voltage amplitude, frequency and waveform for HFAC power distribution. In particular, 50kHz appears to be a good compromise between cable mass saving and cable impedance; the latter is directly proportional to the cable voltage drop and resistive losses. The safest on-board voltage at 50kHz, according to norm DIN VDE 0800 Part 1, rated class 1B (Kokes, 1997), is 100Vrms. This voltage level is consistent with the SAE J2232 standard on vehicle system voltage. Therefore, this amplitude has been chosen for the present study, based on the fact that a high voltage translates into low power distribution losses.

Finally, the choice for high frequency sinusoidal voltage and current is based on the low EMI property of the waveform. The EMI aspect is of particular importance within the vehicle environment, since interference with other electronic systems can possibly obstruct their normal operation.

The following five Chapters discuss the feasibility and advantages of the proposed electrical system for auxiliary electrical systems. In particular, Chapters 5 to 8 evaluate the proposed technology for the four main sub-systems in vehicles: power generation, power distribution, power conversion and electrical loads. Subsequently, Chapter 9 brings together the findings in a critical system-level evaluation of the technology.

Chapter 5

HFAC power generation sub-system

5.1 Introduction

Figure 5.1 illustrates the schematic diagram of the proposed HFAC power generation sub-system, which includes two components:

- a DC power generation module, and
- a DC/HFAC inverter module.

HFAC power generation sub-system

Mechanical power from the internal combustion engine → DC power generation → DC/HFAC inverter → To the power distribution sub-system
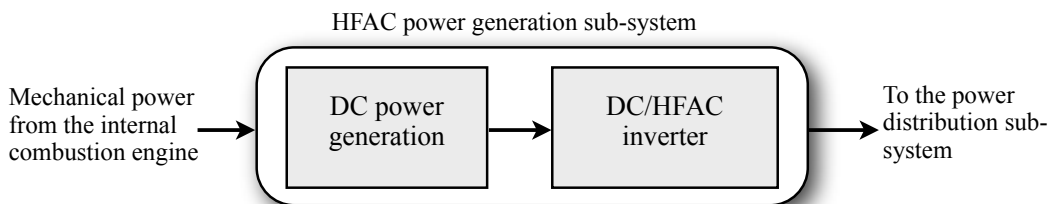
Figure 5.1 Components of the HFAC power generation sub-system

The role of the DC power generation module is to convert mechanical power into electrical power and integrates:

- an engine-driven generator, which can be either a conventional claw-pole alternator or an ISG, and
- an AC/DC rectifier. For the alternator, the rectification function is fulfilled by a full-wave diode rectifier. Conversely, due to its dual functionality[1], the ISG integrates a six-switch bi-directional AC/DC converter.

The regulated output voltage of the DC power generation stage is the input to the DC/HFAC inverter. The latter transforms the DC voltage into a high frequency AC voltage for efficient power distribution within the vehicle.

_____

[1] The ISG operates as an alternator, converting electrical power into mechanical power to crank the ICE, and also as a generator, i.e. transforming mechanical power into electrical power to recharge the battery.

First, the requirements of the power generation sub-system are outlined in Section 5.2, and further detailed in Section 5.3. Section 5.4 describes briefly the 42V DC power generation component, and Sections 5.5 and 5.6 present the proposed DC/HFAC inverter. Section 5.7 includes the summary and conclusions of the present Chapter.

5.2 Requirements of the auxiliary power generation sub-system

Several performance and safety criteria have to be met by the vehicle power supply. Specifically, the on-board electric power source should:

1. Meet the electrical safety standards in vehicles, including norm DIN VDE 0800 Part 1, rated class 1B, and the SAE J2232.
2. Satisfy the power requirement of auxiliary electrical loads.
3. Minimise the power conversion losses.
4. Supply a load-invariant output voltage.
5. Minimise the THD of the output voltage.

Regarding the first requirement, Sections 4.3 and 4.4 in Chapter 4 have discussed the voltage and frequency of the proposed bus in the context of the electrical safety standard. In particular, Section 4.3 has indicated that 42V is the highest allowed on-board DC voltage. In addition, Section 4.4 has discussed the feasibility of power distribution at 100V, 50kHz. Therefore, the electrical safety aspect will not be further examined in this Chapter.

The second requirement, related to the power demand of auxiliary applications, is presented in Section 5.3. Subsequently, prerequisites 3, 4, 5 are detailed in the context of the two components of the power supply in Sections 5.4 and 5.5-5.6, respectively.

5.3 Power demand of auxiliary electrical loads

With regard to the power requirement of auxiliary applications, there are two aspects to take into consideration. Specifically, the power supply must:

- satisfy the cumulative average power of the loads, and

- cope with the transient current requirement of dynamic systems such as the ISG or the VVA.

Table 5.1 illustrates the power requirement of the main existing and currently state-of-the-art[2] applications within passenger vehicles. The numerical values related to the maximum power requirement for each system vary from approximately 300W for the lighting system, to more than 10kW for the active suspension system.

Table 5.1 Peak and estimated average power requirement of electrical loads in vehicles (Lukic and Emadi, 2002, Lukic and Emadi, 2003)

Electrical load	Peak power [W]	Average power [W]
Electromechanical valve actuator (VVA)	2,400	800
Engine cooling fan	800	300
Electric power assisted steering	800	100
Heated rear and front screen	600	150
Electrically heated catalyst	2,500	60
Integrated starter generator (starter function)	3,000	not applicable
Electric fuel pump	150	100
Electric water pump	500	500
Electric oil pump	500	500
Electromechanical brakes	1,800	400
Active suspension	12,000	360
Engine management system (cylinder charge control, air-fuel mixture formation, secondary ignition, intake air preheating, sensors)	250	250
Air conditioning	3,000	300
Lighting system	300	50
Telematics (on-board laptops, fax machines, sound and navigation systems, internet connection)	up to 1,000	100
Total estimated average power demand		**3,970**

---

[2] It is expected that some of the state-of-the-art electrical loads have a high power demand compared to the majority of the current on-board applications.

The average power demand, however, depends on the operational duty cycle of each application. In particular, while loads such as the oil and water pumps have a continuous operation, other systems including the air conditioning, engine cooling fan or electromechanical brakes operate on an intermittent basis.

With regard to the values specified in Table 5.1, it must be stressed that these are only indicative of the potential maximum and average power demand for the most demanding electrical loads in the vehicle. Although these figures are consistent with the reported studies by Lukic and Emadi (2002, 2003) and also with the analyses presented in (Eki et al., 2007, Iles-Klumpner et al., 2006, Jain et al., 2006), the simplistic assumption has been made that the average power demand is a fraction of approximately 0.1 of the peak power demand. A sensible method to compute these average values would have to account for the specific drive cycle (i.e. motorway or urban), the type and class of the vehicle, as well as the very specific driving style and weather/traffic conditions. As a result, a very precise approximation of the cumulative average power requirement of vehicle auxiliary electrical systems implies the employment of a sophisticated and in-depth analysis which is out of the scope of the present work. Consequently, the cited cumulative average power of the electrical loads in Table 5.1 has been chosen in the present work as the desired power rating for the auxiliary HFAC power supply.

The consequence of this result is that both modules, i.e. the DC generation system and the DC/HFAC inverter, must manage this continuous power level. The implications of this aspect are discussed further in Sections 5.4 and 5.6. In addition to meeting the aggregate power demand, the on-board power supply has to cope with the load current transients. For reference, the voltage and current demand of some of the most dynamic applications within passenger vehicles are briefly presented in Appendix D. Table 5.2 summarises the dynamic power requirement of the four applications[3] described in

---

[3] ISG, EMB, EHC and VVA

Appendix D. Amongst the presented loads, the most demanding system is the ISG, with a current requirement in excess of 400A.

Table 5.2 Summary of the dynamic requirements for the applications presented in Appendix D

Application	Current amplitude	Current profile	
		Rise time	*Duration*
ISG	more than 400A (at 42V)	1.5ms	250ms
Electro-mechanical Brakes (EMB)	40A (at 42V)	5ms	not specified, but at least a few seconds
Electrically Heated Catalyst (EHC)	175A (at 14V)	not critical	up to 30s
	more than 200A (at 14V)	not critical	at least 4s, and up to 15s
VVA	18A (at 14V)	1ms	5ms

It should be noted that the EHC, which draws current in excess of 150A, is operated at 14V DC. Therefore, the EHC current load in a 42V system is expected to be reduced by a factor of three. The same analysis is equally applicable to the VVA system.

Section 5.3 has highlighted the cumulative and dynamic or transient power requirement of auxiliary loads in vehicles. The finding is that the power generation sub-system in passenger vehicles must have a continuous power rating of approximately 4kW. In addition, the supply must cope with the current demand profile of dynamic applications, such as the ISG, VVA, EMB or EHC. Essentially, a transient time as low as 1ms and current as high as 400A can be considered as sensible design characteristics for the on-board power generation sub-system.

5.4 DC power generation

This Section discusses the DC power generation module of the HFAC power supply. As previously indicated in Section 5.1, this module is the first component of the proposed power source, while the second component is analysed in Sections 5.5 and 5.6. The aim

of this Section is to present typical systems which can fulfill the DC power generation function and to highlight how these meet the requirements outlined in Section 5.2.

5.4.1 Module description

A possible DC power generation component for the proposed sub-system is the technology found in vehicles today. Figure 5.2 shows the diagram of the HFAC generation sub-system, based on Figure 5.1, including the schematic diagram of the existing on-board DC power generation module.

The conventional DC power generation system includes a belt-driven claw-pole alternator and a three-phase AC/DC full-wave diode bridge rectifier. The alternator, pictured in Figure 5.3 for reference, integrates a voltage controller which supervises the power conversion from 14V or 42V, three-phase 60Hz AC into a constant 14V or 42V DC voltage.
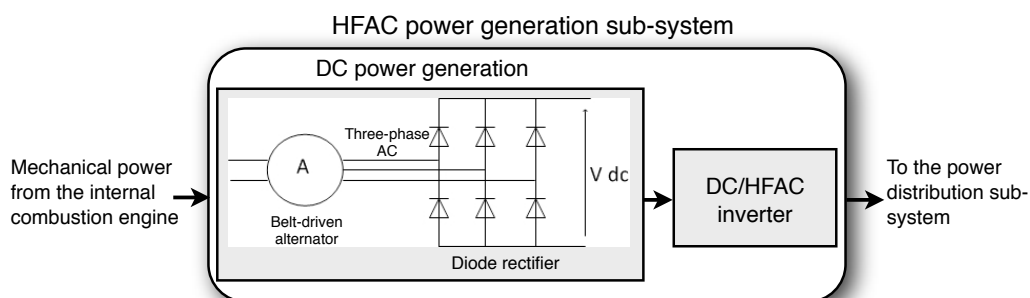
Figure 5.2 Possible HFAC power generation sub-system, including
schematic diagram of the conventional vehicle DC power generation component
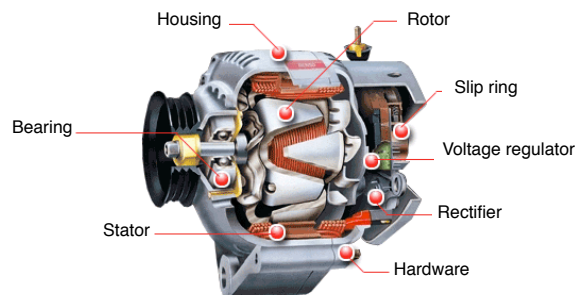
Figure 5.3 Claw-pole alternator (Denso, 2010)

Conversely, the DC power generation function can be fulfilled by a crankshaft-mounted ISG system. Figure 5.4 illustrates the diagram of the HFAC power generation sub-system, integrating an ISG and a MOSFET/IGBT bridge.

Since the ISG can operate either as engine starter or generator of electrical power, the bridge functions both as an AC/DC converter and as a DC/AC inverter. Figure 5.5 shows an example of an ISG system connected to the crankshaft of a passenger vehicle ICE (Jain et al., 2006).
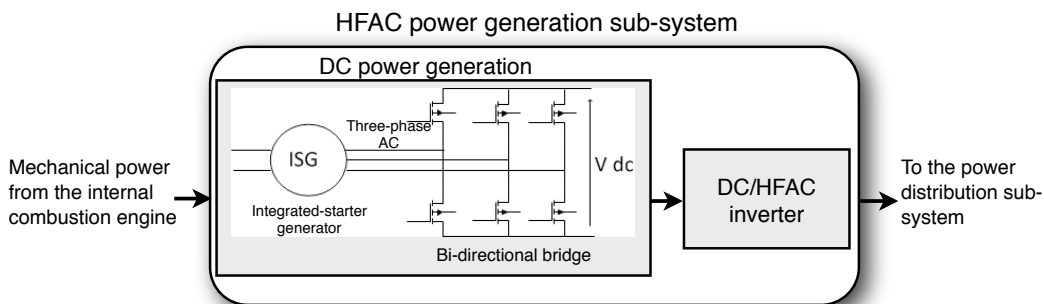
Figure 5.4 Possible HFAC power generation sub-system, including
schematic diagram of the ISG-based vehicle DC power generation component
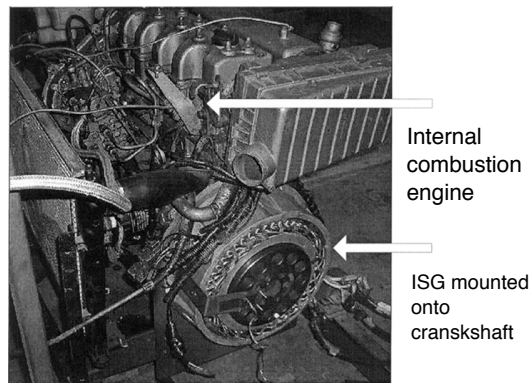
Figure 5.5 Illustration of ISG mounted to the engine crankshaft (Jain et al., 2006)

5.4.2 Feasibility of the DC power generation module

This Subsection discusses the characteristics of the DC power generation module in relation to the requirements outlined in Section 5.2. Specifically, the Section details

aspects including the power capability, efficiency and voltage control of the DC power generation unit.

The alternator with a diode rectifier offers a cost-effective solution for the on-board power requirement. As illustrated in Figures 5.6 and 5.7, the maximum efficiency of the Lundell alternator is 60% for 14V operation, and approximately 65% for 28V and 42V operation (Whaley et al., 2004). Also, Figure 5.8 indicates that the maximum power capability of 14V and 42V machines is approximately 2kW and 5kW, respectively. Therefore, the 42V alternator with diode rectifier meets the 4kW requirement specified in Section 5.3. As illustrated in Figure 5.9 for an example ISG motor, similar efficiency figures are expected for the machine operating as a generator. The power output, however, is higher compared to the former alternator-based system.
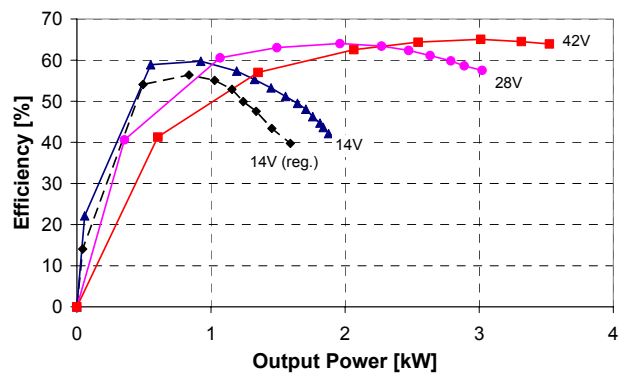
Figure 5.6 Alternator efficiency vs output power (Whaley et al., 2004)
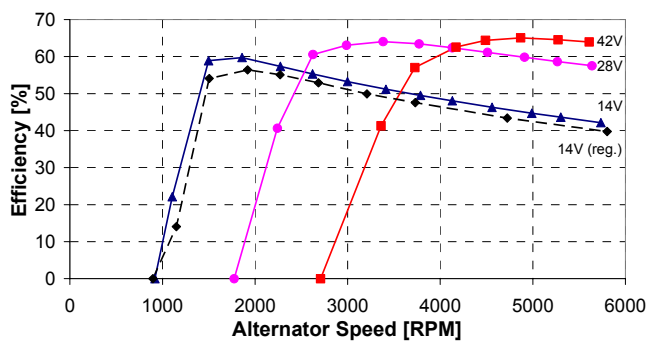
Figure 5.7 Alternator efficiency vs speed (Whaley et al., 2004)
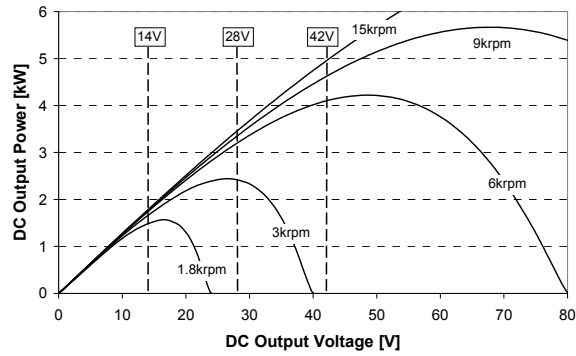
Figure 5.8 Alternator output vs voltage, for several alternator speed values
(Whaley et al., 2004)
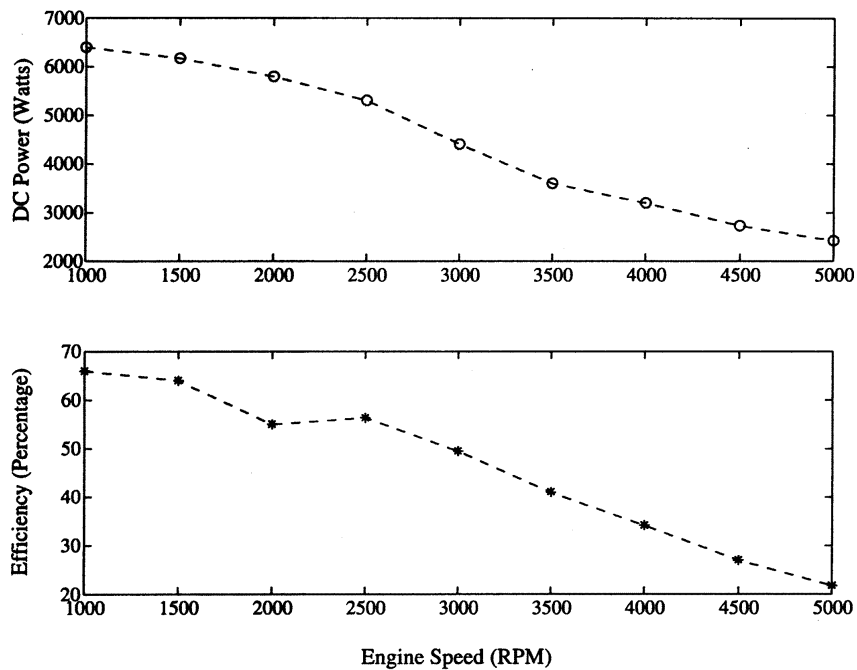
Figure 5.9 ISG induction motor efficiency and power output,
vs engine speed (Jain et al., 2006)

It should be noted that the specific ISG example presented here is based on an induction machine. However, other motor technology is suitable for this application as discussed in the study by (Cai, 2004). As indicated, ISG systems integrating permanent magnet motors may be more efficient than the induction motor (up to 80%). For reference, Table A5.2 in Appendix D tabulates the machine types analysed and their specific characteristics (Cai, 2004).

In particular for the application described by Jain et al. (2006), the ISG power output exceeds the 4kW required for vehicle auxiliaries, for an engine speed of up to 3,000rpm. The efficiency for this specific scenario appears to be above 50%. It is interesting to note that, unlike the Lundell alternator, the efficiency of the induction generator is inversely proportional with speed.

This Subsection has so far indicated that the existing 42V generator technology meets the 4kW power requirement of auxiliary loads in vehicles. In addition, the DC bus is able to withstand high current slew rates, due to the battery acting as a large capacitor in parallel with the loads. In fact, this requirement is specifically related to the ability of the DC/HFAC inverter to meet the high dynamic profile of the electrical current. The aspect is detailed in Section 5.6, which is dedicated to the second module of the HFAC power supply.

Therefore, the DC power generation unit meets the cumulative and transient vehicle power requirement presented in Section 5.3. Furthermore, the efficiency of the conversion process from mechanical power input to electrical power output is expected to be approximately 50% - 60%.

With reference to the fourth requirement (outlined in Section 5.2), the voltage control function of the Lundell alternator is fulfilled by a field current controller. Figure 5.10 illustrates the schematic diagram of the control implementation. Specifically, the rectified DC voltage is continuously monitored and the alternator field current is adjusted as part of a closed-loop setup to maintain a constant output voltage.

Conversely, the power generation process of an ISG includes a more complex control structure. Figure 5.11 shows the control diagram for the case study presented within this Section of an induction machine ISG. In generation mode, a voltage control loop is closed around the torque comparator loop, which manages the 42V DC bus voltage (Jain et al., 2006). The torque reference is negative in generation mode.
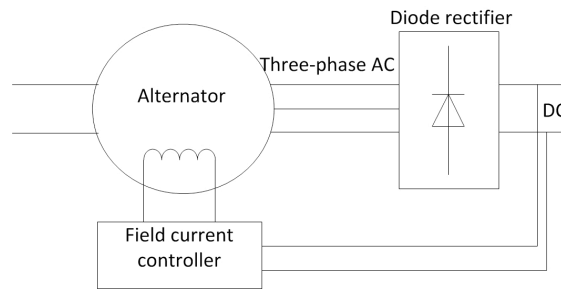
Figure 5.10 Diagram of alternator output DC voltage control
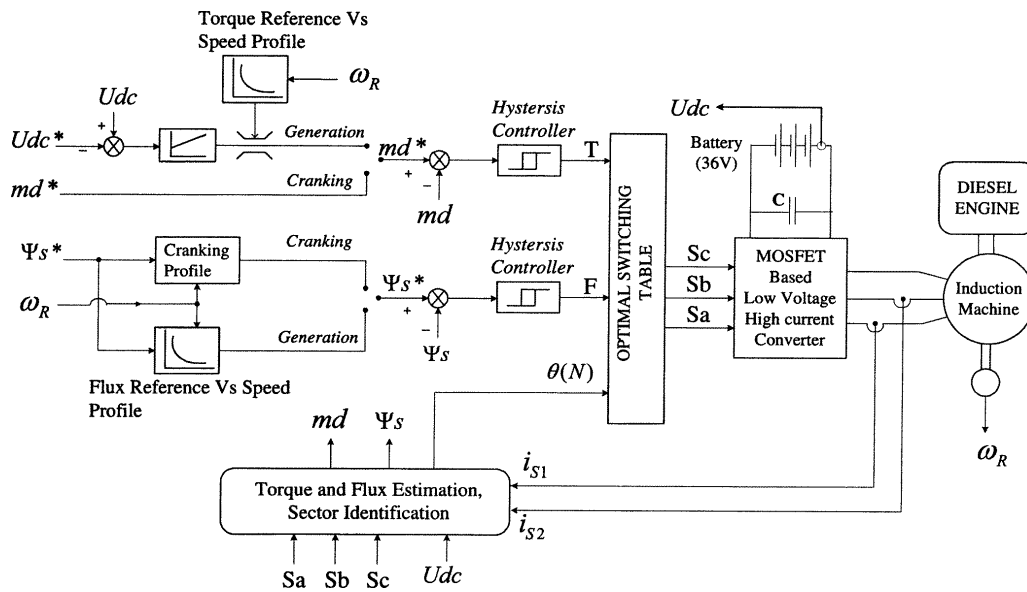
Figure 5.11 Example of control scheme for an ISG application (Jain et al., 2006)

Conclusively, this Subsection has demonstrated that the 42V DC power generation module meets the requirements outlined in Sections 5.2 and 5.3. In particular, the 42V alternator and the 42V ISG:

- Satisfy the cumulative on-board power demand.
- Are able to cope with the current transient rates of highly dynamic loads.
- Supply a load-invariant output voltage.
- Have an efficiency of approximately 65%, possibly up to 80% for permanent magnet-based ISG systems. In order to minimise the power conversion losses, the alternator and ISG have to operate close to their optimum speed. Specifically, the

efficiency of the Lundell alternator exceeds 60% for a speed above 4,500rpm. Unlike the alternator, the ISG exhibits a high efficiency for a rotational speed below 1,750rpm.

5.5 DC/HFAC inverter topology

This Section presents the chosen topology for the DC/HFAC inverter and justifies the decision. To this end, the characteristics of the DC/HFAC inverter modules presented in Chapters 2 and 3 are included in the discussion.

Based on the switching method employed to transform the DC into HFAC voltage, the inverter topologies presented in Chapters 2 and 3 can be grouped into two categories. Specifically, an inverter can have either a topology based on a *hard*-switching technique, or employ a *soft*-switching method.

The inverter topology chosen in the present study is based on a *soft*-switching method. The main advantage of this approach is the elimination of the switching losses. In addition, the voltage harmonic content is reduced since the power switches are turned on and off only at the point where the voltage or current have an amplitude equal to zero (i.e. when the AC voltage or current change polarity).

The chosen inverter topology is suitable for the voltage, frequency and power rating of the HFAC system proposed in this work (100V, 50kHz, 4kW, respectively). In fact, the feasibility of resonant soft-switching inverters has been demonstrated for a number of different applications with voltage, frequency and power varying from 60V to 440V, 400Hz to 128kHz and several kW to tens of kW, respectively. The studies include applications such as:

- The 440V, 20kHz electrical system for the NASA International Space Station Freedom system (Section 2.2).
- The 60V, 128kHz power supply for telecommunication equipment (Section 2.3).

- The 440V, 20kHz inverter in a HEV (Section 3.2).

- The 400Hz auxiliary electrical system in vehicles (Section 3.4).

Figure 5.12 illustrates the main components of a *soft*-switching inverter:

- The DC power supply.

- The resonant network.

- The MOSFET or IGBT bridge.

- The output filter and step-up[4] transformer.

DC power supply	Resonant network	MOSFET/ IGBT bridge	Output filter and step-up transformer
Stage 1	Stage 2	Stage 3	Stage 4
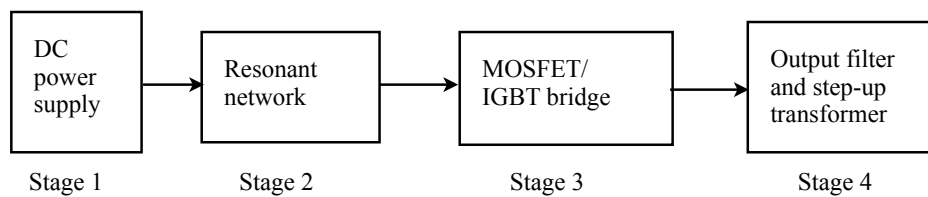
Figure 5.12 Building blocks of the DC/HFAC soft-switching inverter

Figure 5.13 exemplifies the role of each of the four stages outlined above. As discussed in Section 5.4, the DC power supply integrates either a 42V DC alternator or an ISG. The regulated DC voltage is subsequently converted by the resonant network into positive pulsating DC voltage at stage 2[5]. The MOSFET/IGBT bridge, in turn, operates synchronously with the resonating DC voltage (i.e. switches are turned on/off when the voltage amplitude is equal to zero) and transfers the pulsating DC voltage to the output filter with alternate polarities. The role of the filter (stage 4) is to attenuate the voltage frequency below and above 50kHz. Finally, the step-up transformer increases the voltage amplitude from 42V HFAC to 100V HFAC. Optionally, the resonant network stage can incorporate a voltage clamping circuit. This component, which has been discussed in Section 3.4 for an actively-clamped resonant link inverter (ACRL), is useful in reducing the voltage and current stress on the inverter components.

---

[4] Generally, a transformer can step the voltage up or down. For this particular case, the transformer performs a step-up function since the HFAC voltage amplitude (100V) is higher than the 42V DC source.

[5] The shape of the pulsating DC voltage is sinusoidal, since it represents the variation of the voltage across the resonant capacitor.
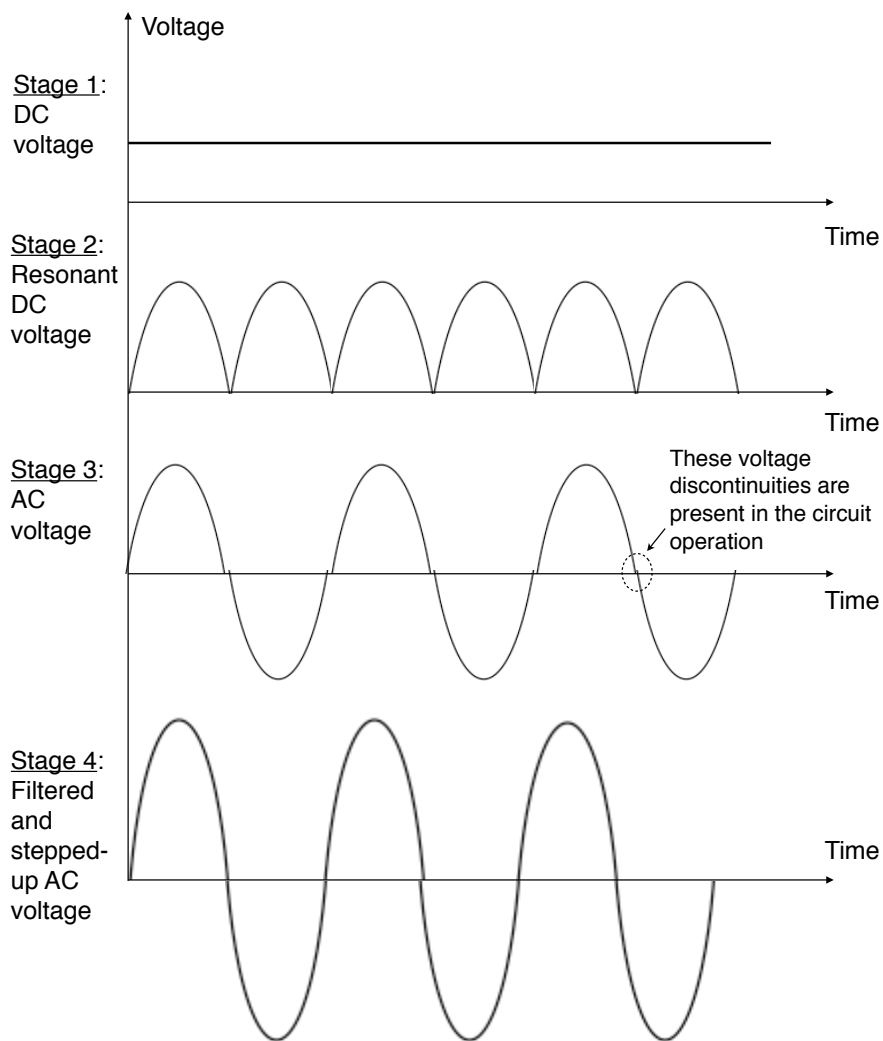
Figure 5.13 Operating principle of the resonant soft-switching inverter

Section 5.6 presents the topology of the DC/HFAC inverter and the control of the output voltage. Also, the Section highlights the steady-state and transient power capability of the inverter and its efficiency, and thus demonstrates its feasibility for the on-board electric power supply.

5.6 DC/HFAC inverter operation and control

5.6.1 Circuit structure and control

Figure 5.14 illustrates the detailed circuit diagram of the proposed HFAC power generation sub-system. As discussed in Section 5.4 (and highlighted in Figure 5.12), the power supply includes four stages:

1. DC power generation, presented previously in Section 5.5,
2. $L_r C_r$ resonant network, detailed in Appendix D.2,
3. MOSFET bridge, and
4. Output filter (series $L_s C_s$ and parallel $L_p C_p$) and step-up transformer.
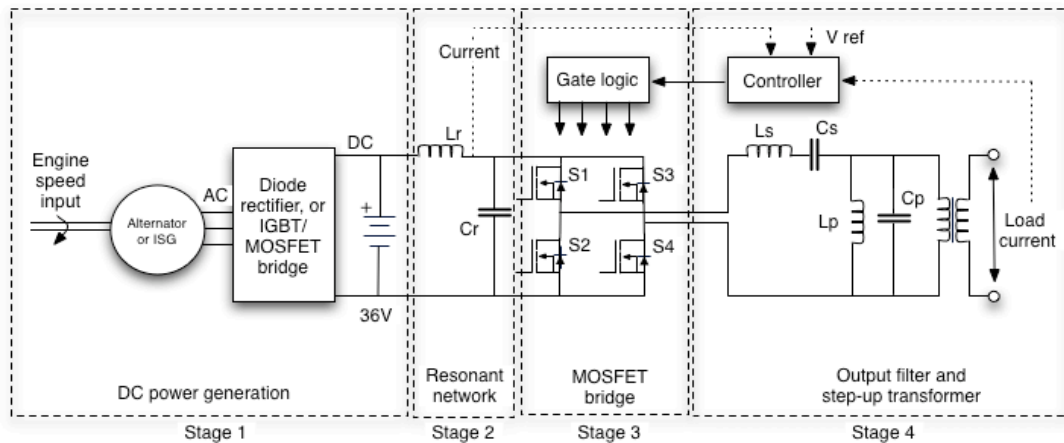
Figure 5.14 Proposed vehicle auxiliary HFAC power supply

The operation of the resonant circuit (stage 2 of the inverter) is described in Appendix D.2 using frequency and time-domain analysis. Also, the main variables required for the circuit design are highlighted.

The analysis presented in Appendix D revealed that in order for the circuit to perform under the desired conditions, a set of requirements should be met by the resonant inductor L_r under limited power output. Essentially, the higher the rated current of the inductor and the lower its internal resistance, the higher the power capability of the inverter. On the other hand, a high inductor current increases the stress on the circuit elements and increases the resistive losses. As a result, the available semiconductor

technology will play an important role in the performance and efficiency of the proposed power supply.

Equation 5.1 is the expression used to control the output HFAC voltage. The derivation of the voltage regulation technique for the proposed power supply is presented in detail in Appendix D.2.

$$V_{ref}(t) = \frac{V_{DC}(R_r + 2R_{DS})}{C_r L_r^2}\frac{\Delta^2}{2} + \frac{1}{C_r}\int_{\Delta}^{T/2}(i_{L_r}(t) - i_{load}(t))dt \qquad (5.1)$$

The key variable in Equation 5.1 is denoted by Δ, which is the time duration when switches S_1 and S_2 (see Figure 5.14) are simultaneously conducting. The other symbols in Equation 1 correspond to the following circuit variables:
- V_{DC} is the DC supply voltage for the inverter,
- Rr is the resistance of the resonant inductor Lr,
- Cr is the resonant circuit capacitor,
- T is the time period corresponding to the required frequency of 50kHz,
- R_{DS} is the *on*-resistance of the H-bridge MOSFETs,
- i_{load} is the load current, and
- i_{L_r} is the resonant inductor current.

The expression in Equation 5.1 is implemented in the Matlab Simulink model of the inverter (shown in Figure A5.10, Appendix D.3) to control the output HFAC voltage. Figure 5.15 shows the desired waveforms of the output HFAC voltage and current, together with the switching control signals and the resonant voltage over capacitor *Cr*. Δ, the overlap duration of switches S_1 and S_2, is also emphasized in the second subplot down.

5.6.2 Feasibility and benefits for automotive applications

The proposed power generation sub-system has been modelled and simulated using
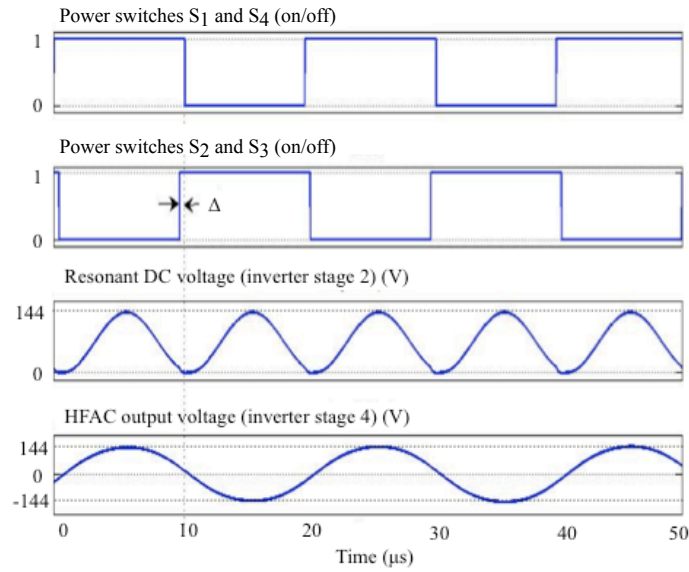
Figure 5.15 Waveforms illustrating the desired operation of the HFAC inverter

Matlab Simulink and the SimPowerSystems toolbox set. Figure A5.10 shows the Simulink model and also highlights the four stages of the power source outlined in Section 5.6.1. In addition, the inverter control strategy detailed in Appendix D.2 is included in the Matlab Simulink model.

The simulation tests for the proposed HFAC power source indicate the suitability of the system for the on-board cumulative and transient power demand. Specifically, as detailed in Section 5.3, a continuous power capability of 4kW and current transient response as low as 1ms are tested. The parameters of the power supply for the tests carried out are listed in Table 5.3.

Figure 5.16 illustrates the HFAC voltage and current waveforms for three tests including the resistive load range from 500W to 4kW. Variables associated with each test are shown in Table 5.4, including the approximate value for the control variable Δ as a percentage of the corresponding switching frequency time period (equal to 10µs). Each test represents a step change in power output; indexes 1 and 2 in Table 5.4 refer to the time prior and after the step time, respectively.

Table 5.3 HFAC generation sub-system, simulation variables and parameters [4]
(corresponding to the model shown in Figure A5.10)

Internal combustion engine model	1.4 L
Alternator	42V, 60Hz 3-φ synchronous machine
Battery	42V, lead-acid. Capacity of 95 Ah
Frequency of output voltage and current	50kHz
HFAC voltage output	100Vrms
Resonant circuit frequency	100kHz
H bridge switching frequency	100kHz
Decay voltage for resonant circuit (V_0)	0.5V
L_r	Coiltronics High Frequency Power Inductor FP1107: Open circuit inductance=150 nH; DCR=0.29mΩ, Ferrite Core loss negligible
C_r	17.2μF
$S_{\overline{1,4}}$	Internation Rectifier IRFSL4115PBF HEXFET Power Mosfet; Vds 150V, Id 99A. Rds 10.3mΩ
L_p, L_s	23μH, DCR=0.29mΩ
C_p, C_s	440 nF
Transformer magnetization resistance and reactance, respectively	2055Ω and 2.29mH, respectively
Transformer turns ratio	1:1.68

Table 5.4 Variables associated with each test

Test	1	2	3
Vrms 1	100	100	100
Vrms 2	100	99	100
Irms 1	5	5	10
Irms 2	20	40	20
Δ1	7%	7%	9%
Δ2	11%	16%	11%
Pout 1	500W	500W	1kW
Pout 2	2kW	4kW	2kW

The maximum current in the simulation tests carried out is 40A, which is lower than the current requirement of some modern loads such as the EHC or ISG (as detailed in Appendix D.1). Nonetheless, the proposed HFAC bus operates at a much higher voltage than 12/14V DC. Consequently, loads which require a high current can either be interfaced by HFAC/DC converters as will be discussed in Chapter 7, or can be

---

[4] The battery voltage (42V DC) is transformed into resonant DC pulses with an amplitude which is twofold the DC voltage, i.e. 84V, or 59.4Vrms. In order to step up 59.4V to 100V, the transformer windings ratio should be equal to 1.68.

connected to the DC bus directly as pointed out in Section 4.4.
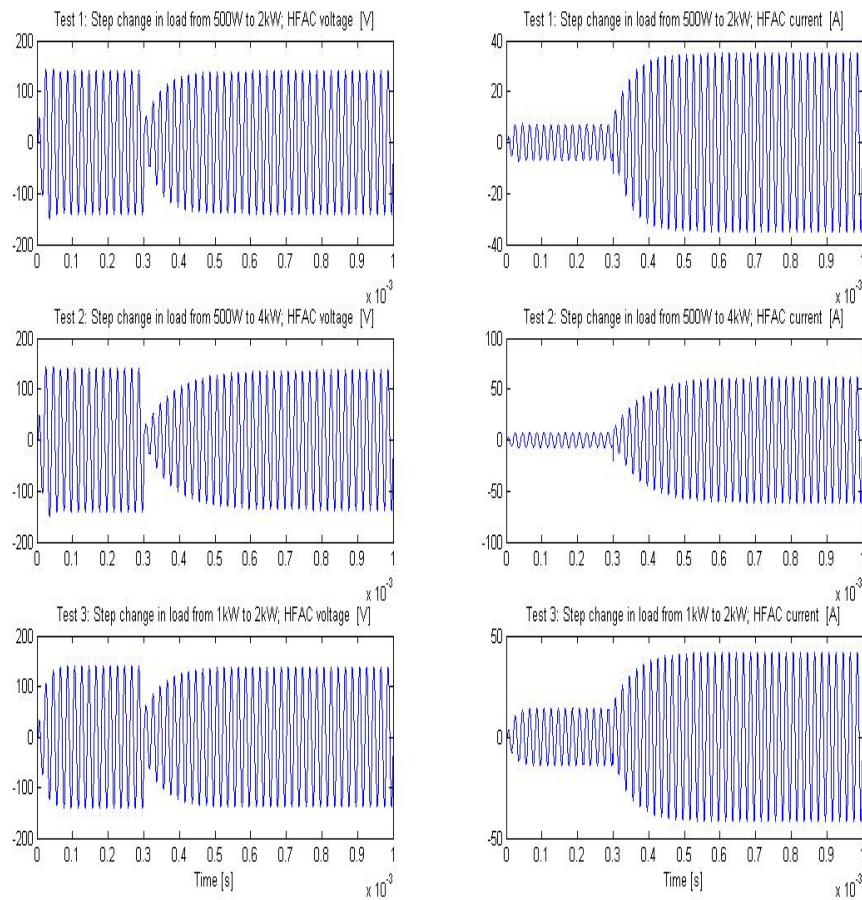
Figure 5.16 HFAC voltage and load current for three load change tests
(Test 1: 500W to 2kW, Test 2: 500W to 4kW, Test 3: 1kW to 2kW)
(Matlab Simulink simulation results)

As a step increase in power output is applied, the transient supply voltage drop can be explained by the change in the load impedance. Under steady state, simulation results demonstrate the feasibility and very good performance (transient response under 300μs) of the proposed power source for the entire power output range. As shown in Figure 5.17, low THD figures are returned by the simulation for the output voltage (1.49%) and current (1.21%) for 2kW power output. The results satisfy the steady state and dynamic requirements outlined in Sections 5.2 and 5.3 for the automotive auxiliary power supply.
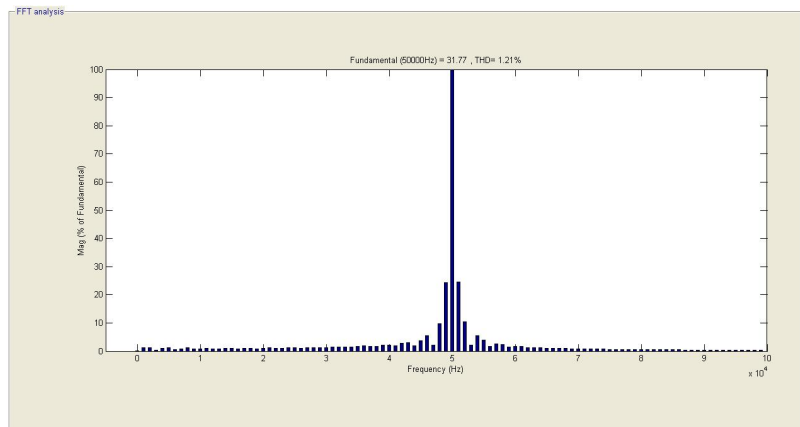
Figure 5.17(a) Total harmonic distortion of HFAC current (1.21%)
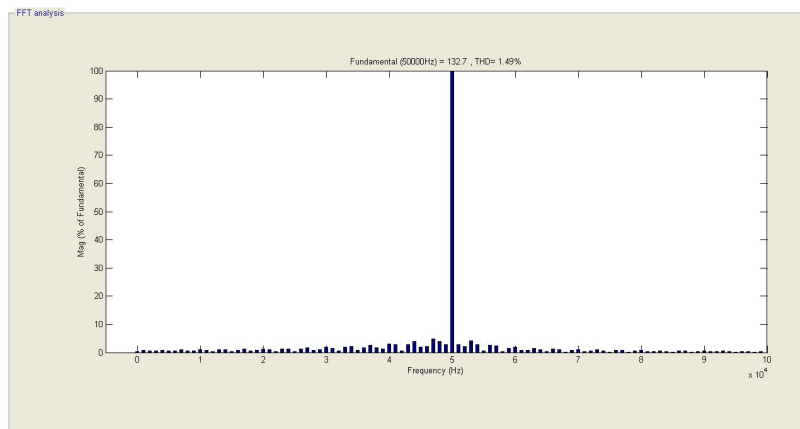
Figure 5.17(b) Total harmonic distortion of HFAC voltage (1.49%)

In relation to the power capability of the proposed HFAC supply, it should be noted that the impedance of the HFAC conductor used for power distribution within the vehicle plays an important role. Specifically, the ability of the power source to supply up to 4kW depends on its impedance matching the cable characteristic impedance (Sudipta et al., 2007). Since the HFAC voltage supply impedance is equal to the impedance of the L_pC_p parallel network[6] (as shown previously in Figure 5.14), the values of these components should be chosen to match the conductor characteristic impedance. Furthermore, it should be stressed that the AC voltage amplitude of the supply under open circuit operation can vary between zero and double the nominal voltage rating of the power source. This effect, which is caused by the infinite-impedance load reflecting

---

[6] The impedance of the parallel LC circuit is equal to $\dfrac{j\omega L}{1-\omega^2 LC}$

the AC waveform back to the source, can potentially represent a safety hazard in an automotive setting. Therefore, as further discussed in Chapter 7, careful consideration should be given to the design stage of the power converter modules in order to avoid this potential electrical safety risk.

The efficiency of the HFAC power source can be divided between the DC generation and the HFAC inverter sub-systems. The efficiency of the former, with reference to the engine mechanical power input, has been discussed in Section 5.4.

For the resonant ZVS inverter presented in this Chapter, simulation results indicate a high efficiency. As shown in Figure 5.18, efficiency higher than 90% is observable above 650W, with a peak of 94% in the mid-output range (2kW). At full load the efficiency decreases to approximately 92%.
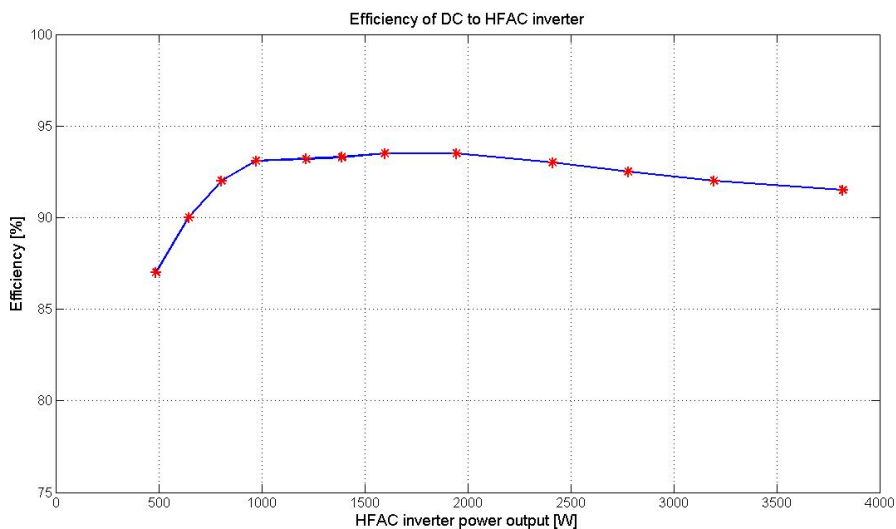
Figure 5.18 Efficiency of ZVS HFAC inverter vs. power output (W)

The shape of the efficiency curve can be accounted for by the conduction losses within the H-bridge, which increase exponentially with the load current. For a load power equal to 4kW at 100V HFAC, the load current (i.e. current in the secondary winding of the output transformer) is equal to 40A. However, the current in the primary transformer winding is higher, since the voltage across this winding is equal to 59.4V as discussed

in Appendix D.2. Therefore, for the maximum power rating of the HFAC power supply, the current in the H-bridge is equal to 67.3A.

Figure 5.19 illustrates the power input versus the combined conduction losses of two MOSFETs. The reason for including the resistive losses of only two MOSFETs is that at any moment in the operation of the H-bridge only two power switches are conducting current.
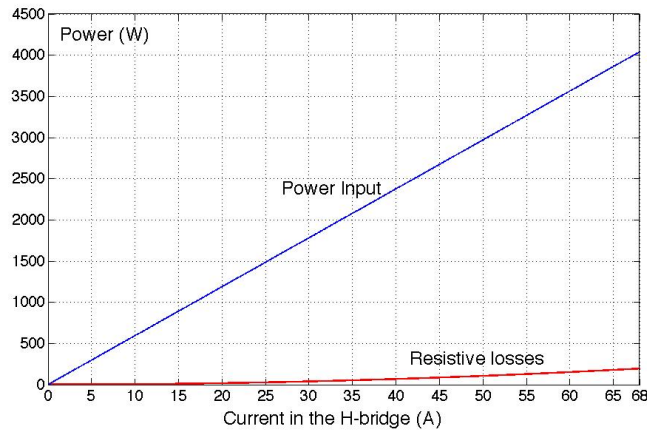
Figure 5.19 Power input (W) and H-bridge resistive losses (W)

For a very low load current, in the vicinity of zero, the circuit efficiency is very low. As soon as current is supplied to the load, the efficiency of the power source starts to increase. However, once the current is very large, the exponential increase of the I^2R losses is higher than the constant increase of the input power. Therefore, after a peak point, the efficiency starts to decrease again.

For the HFAC supply proposed in this Chapter, the peak efficiency is observed for a load power between 1kW and 2kW. This interval corresponds to a H-bridge current between 17A and 34A. It is observable in Figure 5.19 that for this particular interval, the I^2R losses are still very low while the input power is increasing - which translates into a high efficiency value. However, beyond the 34A mark, the losses start to increase at a higher rate than the linear input power, which causes a decrease in efficiency.

5.7 Conclusion

Chapter 5 has presented, in detail, the structure and operation of the auxiliary HFAC power supply. In particular, it has been demonstrated that the two main components of the supply (DC power generation and DC/HFAC inverter) meet the requirements of the auxiliary electrical system in vehicles.

Specifically, Table 5.5 shows the on-board power requirements, which have been presented in Sections 5.2 and 5.3. In parallel, the characteristics of the HFAC power supply meeting the outlined requirements are also included in Table 5.5.

The Chapter has proposed a viable HFAC power supply, which satisfies the requirements of the on-board consumers. The following Chapter discusses the feasibility and advantages of HFAC power distribution within the vehicle. The role of this sub-system is to distribute efficiently the HFAC voltage output of the power generation sub-system to the loads.

Table 5.5 Characteristics of the HFAC power supply, mapped onto the requirements of the automobile auxiliary power source

Vehicle auxiliary power supply requirements	HFAC power supply	
	Module 1: DC power generation	**Module 2: DC/HFAC inverter**
Meet the electrical safety standard in vehicles	Discussed in Chapter 4	Discussed in Chapter 4
Satisfy the power requirement of auxiliary electrical loads: 4kW, transient current response under 1ms.	- 42V alternator max. power output of 5kW - ISG max. power output of 6kW - 36V battery capable of handling high current transients	- inverter power rating of 4kW (100V, 40A) - transient current response under $300\mu s$
Minimise the power conversion losses	- alternator efficiency highest at high speed (65%, possibly up to 80%) - ISG efficiency highest at low engine speed	- simulation results indicate efficiency above 90%
Supply a load-invariable output voltage	- alternator integrates a field current controller - ISG voltage output is controlled using a voltage and torque closed-loop control.	- inverter converts the regulated DC voltage into controlled HFAC voltage - HFAC voltage regulated by control circuit which allows for ZVS
Minimise the total harmonic distortion of the output voltage	36V battery filters DC voltage distortions	-the output filter minimises current and voltage THD (under 2%)

Chapter 6

HFAC power distribution sub-system

6.1 Introduction

The present Chapter investigates the benefits of HFAC for the power distribution sub-system in vehicles. Within the context of this Chapter, power distribution refers to the wiring connecting the power source to the loads or power converters.

The main attributes of the HFAC system discussed in this Chapter are related first to the distributed topology of the architecture and second to the conductor required for high frequency power distribution.

The advantages of the proposed power bus are presented in comparison with the present 14V and proposed 14/42V DC electrical networks. First, the topology and the main drawbacks of the mentioned DC architectures are outlined in Section 6.2.1. Conversely, the proposed topology of the HFAC network is presented in Section 6.2.2. This Section highlights the benefits of the proposed architecture and how these characteristics can potentially solve the issues regarding the DC systems.

Section 6.3 highlights the mass and power distribution efficiency advantages of a commercially available HFAC conductor in comparison with 42V DC and 14V DC cables. Section 6.4 extends this critical analysis to the case study of a group of auxiliary loads in a representative C-segment passenger vehicle. Finally, Section 6.5 includes the conclusions of the Chapter, with regard to the potential benefits of replacing the existing DC wiring layout with an equivalent HFAC system.

6.2 DC and HFAC auxiliary power distribution systems

6.2.1 DC power distribution

The present 14V DC network has a centralised topology as illustrated in Figure 6.1 (Miller et al., 1999). Most electrical loads are connected to the main bus in a point-to-point architecture by switches and relays, whereas the ignition and cranking systems have direct power links.
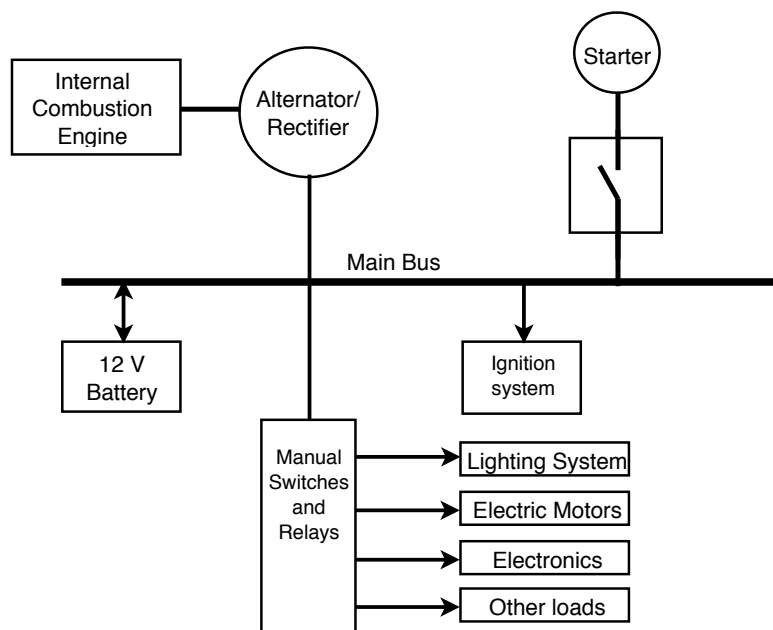
Figure 6.1 Conventional 14V DC distribution
architecture (Miller et al., 1999)

As described in Chapter 4, the 14V DC distribution system has several limitations. First, the point-to-point topology leads to expensive, intricate and heavy wiring. Second, the bus voltage can vary from 9V to 16V depending on the alternator output current, battery age and state of charge. This leads to an overrated design of the load components since the auxiliaries, designed to operate at the nominal bus voltage, have to cope with the bus current variation (Miller et al., 1999). Other disadvantages include the expensive and

time consuming process of assembly, fault tracking and repair as further noted by Miller et al. (1999).

The proposal for the 42V Power Net, described in Chapter 4, has motivated the investigation of dual voltage networks employing both 14V and 42V DC as an intermediate step towards a potential future adoption of the 42V network. As detailed in the following paragraphs, several architecture topologies have been presented in the literature.

Six network topologies are the main candidates for the dual DC voltage power bus (Caliskan, 2000, Smith, 1991, O'Dwyer et al., 1996):

1. a DC/DC converter architecture, which is considered the most suitable;
2. a dual stator/alternator architecture with both high and low three-phase AC voltage output;
3. a dual-rectifier topology, where two different rectifiers share the three-phase voltage output of the alternator;
4. an architecture employing two three-phase rectifiers, each for a different DC voltage output, denoted as the transformer/rectifier topology;
5. the dual-reference alternator topology, and lastly
6. the dual-voltage alternator architecture.

Architecture topologies 1, 2 and 3 are illustrated in Figures 6.2, 6.3 and 6.4, respectively (Caliskan, 2000). The DC/DC converter topology includes a high voltage alternator and rectifier that supplies 42V DC to the loads. In addition, a DC to DC converter steps down the voltage to 14V for lower voltage consumers. Batteries are attached to each bus, as this arrangement permits a smaller converter volume for a given power rating (Caliskan, 2000).
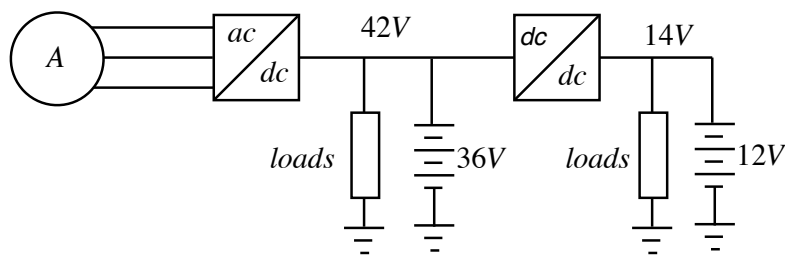
Figure 6.2 DC/DC converter architecture (Caliskan, 2000)
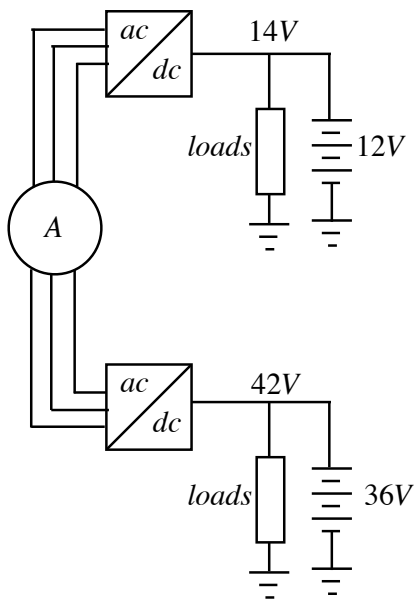
Figure 6.3 Dual stator alternator
architecture (Caliskan, 2000)
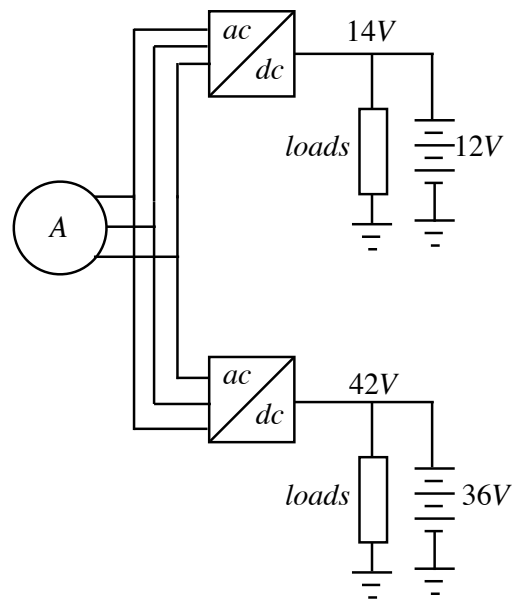
Figure 6.4 Dual rectifier alternator
architecture (Caliskan, 2000)

The cited study indicates two possible disadvantages associated with the DC/DC
architecture:

- First, the DC/DC converter has to satisfy the regulations highlighted in the SAE
  J1113 standard in relation to the EMI of the module. Whilst the specified standard
  applies to all electrical and electronic systems within vehicles, it is especially
  relevant for the DC/DC converter due to the potential high current.

- Second, a DC/DC module design in line with the SAE J1113 standard is
  potentially expensive.

The dual stator architecture shown in Figure 6.3 is based on a dual winding machine, each supplying a three-phase voltage signal, subsequently rectified by AC/DC converters. The major drawback of this topology is the difficulty of voltage regulation under high load conditions (Caliskan, 2000). The reason is that two different voltage regulation methods are employed simultaneously within the same electrical machine, one for the 42V system (e.g. field control) and the other for the 14V bus (e.g. phase control).

Figure 6.4 depicts the dual rectifier alternator scheme, where the alternator AC voltage output is distributed to two converters, for 42V and 14V rectification. The main limitation of this topology is that the current output from the alternator flows alternately in the two rectifiers, causing very large current ripple at each rectifier output (Caliskan, 2000). This issue can be overcome by substantial filtering, at the cost of additional module mass.

The remaining three architectures have been proposed for potential dual 14V/28V DC electrical networks in lorries and commercial vehicles, for example. Although lorry voltage levels are in general at a single level (28V), the features of the bi-voltage concepts are illustrative for potential problems related to dual DC voltage architectures.
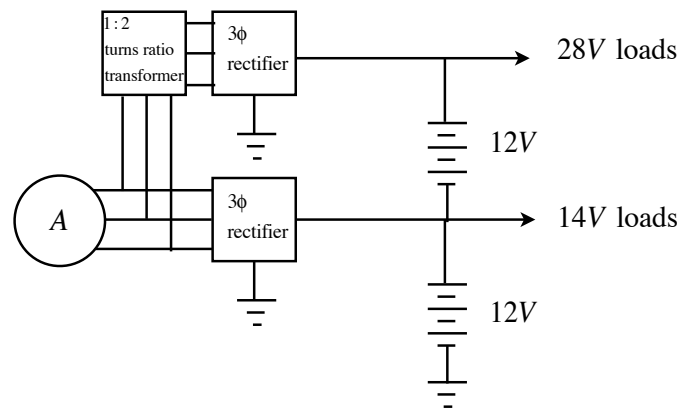
Figure 6.5 Transformer/ rectifier dual voltage network topology (Smith, 1991)
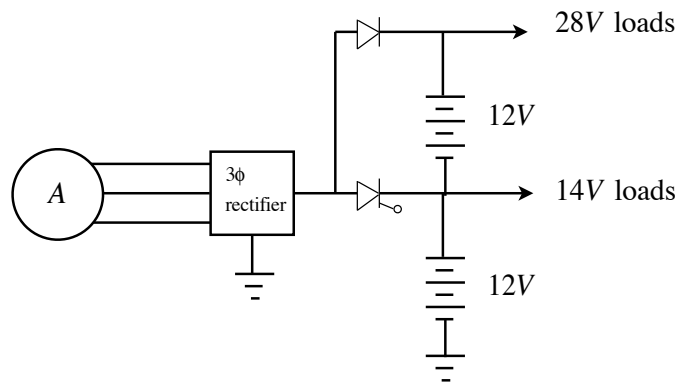
Figure 6.6 Dual reference alternator network topology (Smith, 1991)
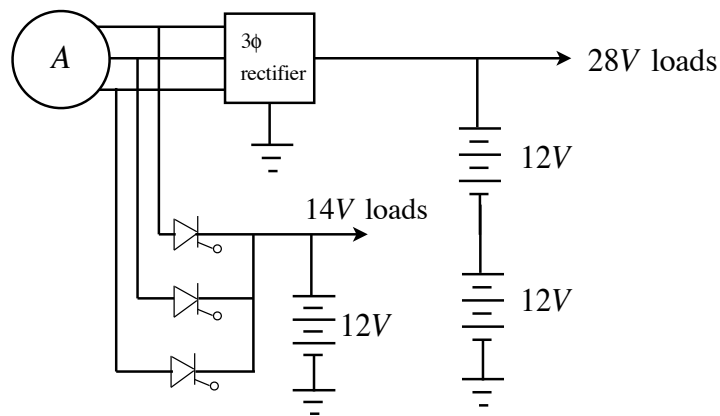
Figure 6.7 Dual voltage alternator network topology (O'Dwyer et al., 1996)

In the transformer/rectifier network in Figure 6.5 (Smith, 1991) the output of the 14V alternator is directed first to a rectifier module and second to a three-phase transformer that steps up the voltage to 28V AC. A second rectifier transforms the higher AC voltage into 28V DC. Notable is the simplicity of the voltage transformation. However, the current in the secondary winding is stepped down by a ratio of two (assuming no losses, the power in the primary and secondary windings of the transformer is the same). As a result, it is potentially difficult to design a control technique for maintaining a constant charge within the 28V battery.

Also presented by Smith (1991) is the dual-reference alternator architecture, shown in Figure 6.6. As the name suggests, this topology uses two voltage references for the

alternator. First, until the 28V battery is fully charged after having supplied the starter motor, current from the alternator is directed only to this battery and the high voltage loads. Once the 28V battery is charged, the thyristor is fired to set the new reference for the alternator, which starts supplying the 14V branch of the network. Disadvantages of this topology include the fact that only one of the two buses can be regulated at any given time and also the high conduction losses associated with the diode and the thyristor (Smith, 1991).

The latter of the proposed topologies is the dual-voltage alternator architecture shown in Figure 6.7 (O'Dwyer et al., 1996). This architecture is a particular case of the dual rectifier alternator scheme in Figure 6.4 and hence it is potentially characterised by high ripple currents.

Conclusively, the main disadvantages of the proposed dual voltage power networks can be summarised as follows:
• The potential high current ripple within DC/DC converters. DC/DC modules complying with the SAE J1113 standard related to on-board EMI emissions can be expensive.
• The difficulty in maintaining the charge in the battery pack.
• The large current ripple at the AC/DC rectifier output and hence the need for filters.
• Difficulty in achieving simultaneous voltage control for two parallel DC networks.
• For some topologies, only one of the two DC buses can be controlled at any given time.

Additional issues with 14/42V DC architectures reported in the literature include (Keim, 2004) the 42V connectors arcs and corrosion, and the possible bus-to-bus electrical faults (e.g. short circuit between 42V and 14V).

6.2.2 HFAC power distribution

Figure 6.8 illustrates the concept architecture proposed by the author for HFAC power distribution. As opposed to the DC power networks briefly presented in Section 6.2.1, the proposed architecture employs a distributed topology where AC power is transmitted onto the main bus at high frequency. Converter modules including transformers, rectifiers and filters are allocated at each point of use. Therefore, the system can potentially benefit from a better design (as noted by Drobnik (1994) for telecommunication power systems) and also from easy fault detection. The assembly and maintenance process of the HFAC system is also potentially less time-consuming and less expensive compared to a 14V DC or a dual-voltage bus.
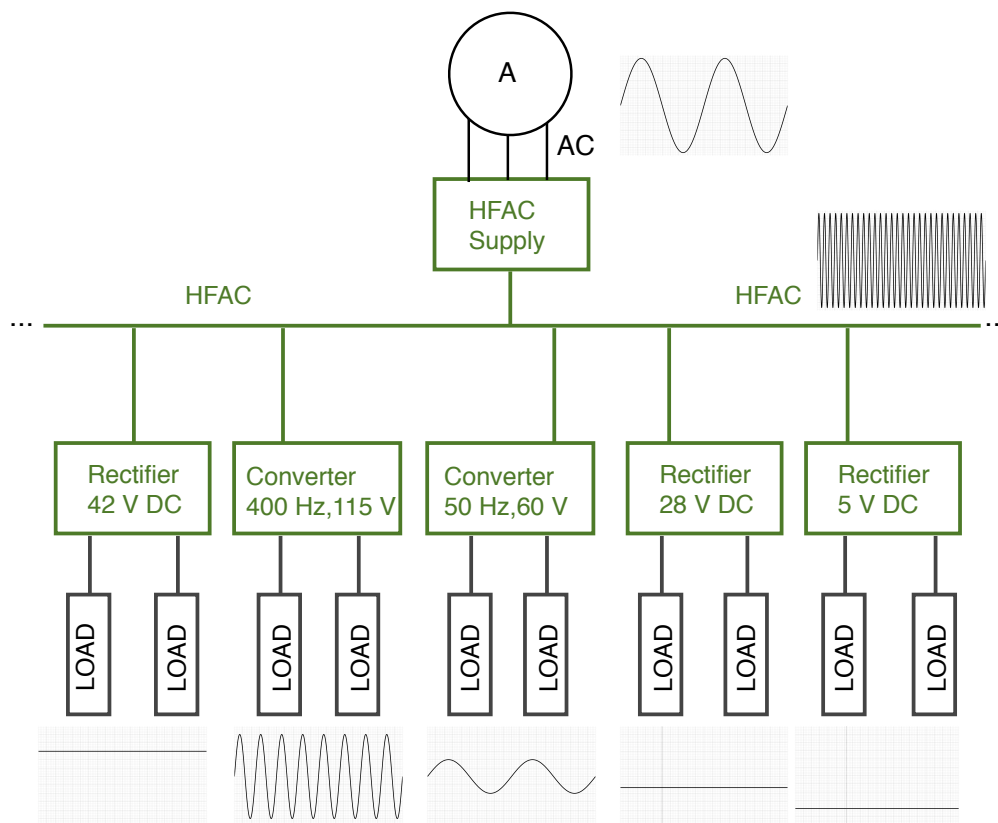
Figure 6.8 Proposed HFAC power distribution network topology

HFAC power can be easily converted into the voltage and frequency required by the loads by appropriately selecting the turns ratio of the transformer windings. In addition, power regulation can be achieved simultaneously for all the loads connected to the bus through local rectification. Specifically, as presented in Chapter 2 for microgrid power systems, converters can interface low and high voltage AC or DC consumers, as well as low frequency (50/60Hz) or medium frequency (e.g. 400Hz for induction motors) AC loads. Furthermore, different power sources can potentially be integrated onto the same bus, including generator motors and batteries. This capability of the HFAC bus contrasts with some of the dual DC voltage architectures presented in the previous Section, for which simultaneous control of varying voltage levels and maintaining the charge in the battery pack are reportedly difficult to achieve.

Another advantage of using high frequency is that any bus voltage or current harmonics are of high order and can be easily filtered out (Sudipta et al., 2007). Unlike filter modules required for the dual voltage power networks, high frequency filter circuits are potentially smaller, lighter and cost-effective.

As the cut-off frequency of the filter increases, the passive circuit components such as inductors and capacitors become more compact and lightweight . In particular for a capacitor component, Figure A6.1 (Appendix E) illustrates the variation of the element volume as a function of the capacitance[1], for a power rating of 50W and 100W. The data shown has been collected from a single manufacturer and is intended to show the downward trend of the capacitor physical dimensions with an increase in operating frequency. The actual numerical values may differ for different manufacturers, but the trend remains valid.

Finally, power transfer in the proposed power distribution system benefits from the inherent contact-less capability of HFAC connectors. This characteristic has been

---

[1] The smaller the capacitance (or inductance), the higher the operating frequency of the capacitor (or inductor) as the two variables are connected by the following relationship: $f = \dfrac{1}{2\pi\sqrt{LC}}$

presented in Chapter 2 for power distribution in telecommunication systems (Figure 2.15). Therefore, the difficulties related to DC connectors (such as arcs and corrosion) are potentially easily overcome. The galvanic isolation provided by these connectors ensures that any local faults are not transmitted onto the main bus. It can be argued therefore that as opposed to the DC system, electrical faults are less probable to occur for the HFAC bus.

6.3 Comparison between DC and HFAC conductors

Figure 6.9(a) illustrates the typical cylindrical DC conductor type utilised today for power distribution within the vehicle. The diameter and mass of this type of cable are proportional to the power rating of the conductor. For reference, Table A6.1 in Appendix E includes the American Wire Gauge (AWG) information related to these parameters.

Conversely, Figure 6.9(b) shows a possible HFAC conductor, which is composed of two parallel flat strips of copper isolated by a lightweight material. As discussed in Chapter 4, power distribution at high frequency is subject to the skin effect (current flows through a smaller conductor area than the one physically available). The consequence of this fact is that a flat conductor is best suited for HFAC power distribution. Particularly for 50kHz power distribution, the skin depth is equal to 291μm[2] and thus the conductor thickness should not exceed 0.3mm.
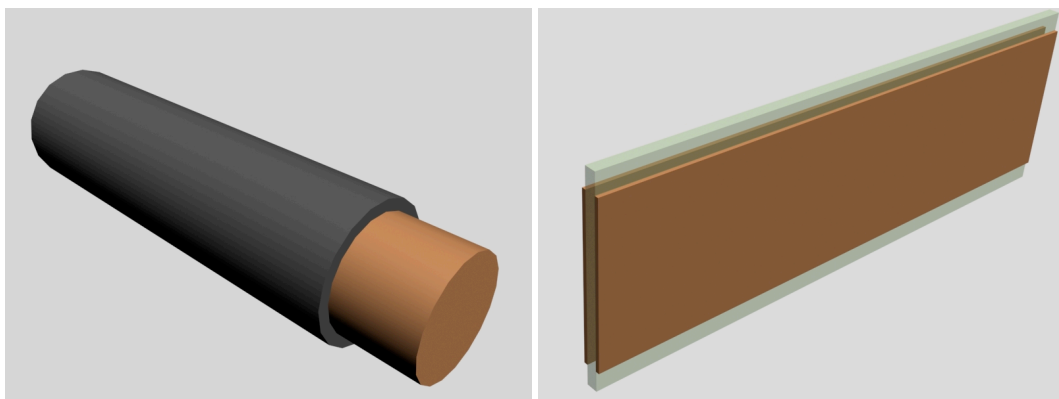
Figure 6.9 DC ((a), left) and HFAC ((b), right) power conductors

---

[2] Result obtained based on Equation A4.1 in the Appendix C

A suitable commercially-available HFAC conductor (Juice, 2008) is reported as having the following properties:

- dimensions of 0.2mm by 10mm
- resistance of 5.8mΩ/m at 50kHz
- inductance of 25nH/m

The analysis in this Subsection looks first at the power distribution losses per unit length for 14V DC, 42V DC and 100V HFAC cables. Next, a comparison between the mass of the three conductors is presented.

Considering the power transfer capability as the basis for this comparison, and the information on wire resistance for different current ratings from the AWG data table (Table A6.1), Figure 6.10 shows the losses of the three candidates expressed in W/m for a power distribution of up to 4kW.

It can be observed that not only is the 14V DC power distribution limited to less than 3kW (due to the very large current), but it also has the highest losses amongst the three. A HFAC cable with a resistance of 5.8mΩ/m is possibly the best choice for power distribution below approximately 1.6kW, and comparable to the 42V DC system between 1.6kW and 2kW. Since most of the loads in vehicles today consume less than 2kW (Lukic and Emadi, 2002, Lukic and Emadi, 2003), it can be argued that the replacement of the existing DC loom with HFAC wiring (based on the same network topology) can potentially reduce the distribution losses in 14V system by at least 50% (as shown in Figure 6.11) and also offer significant efficiency improvements over the proposed 42V PowerNet.

The erratic variation of the curves indicating the DC resistive losses in Figure 6.10 is caused by the AWG cable resistance data. In particular, specific resistance values are representative for intervals of conductor current rating, and the sudden decline observable in the Figure mark the transition from one current rating interval to the next.
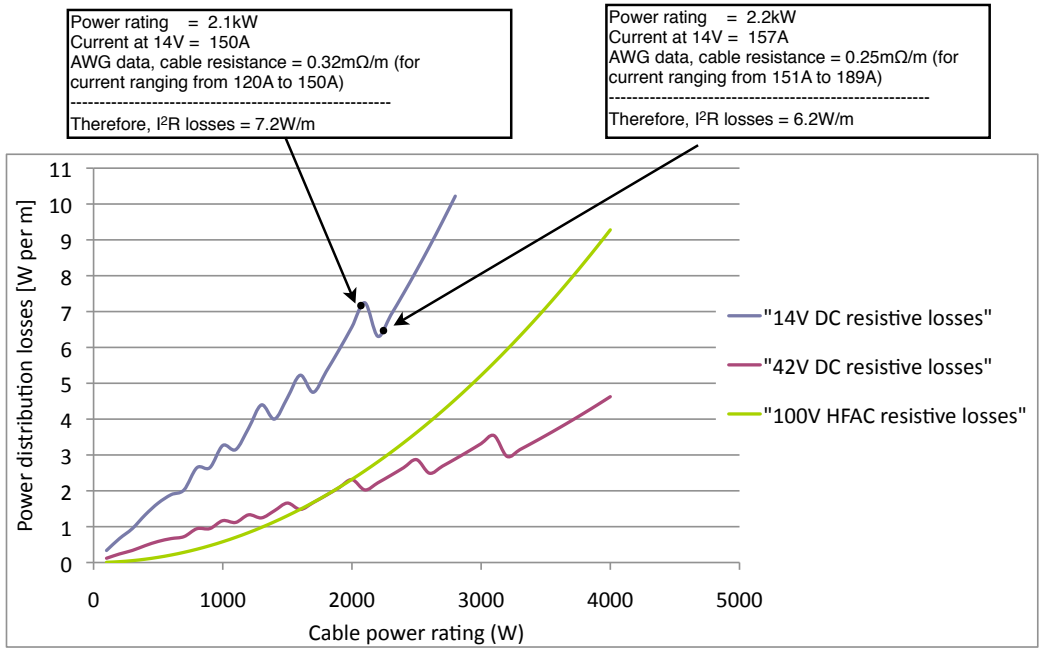
Figure 6.10 Power distribution losses for 1m of 14V, 42V DC and 100V HFAC conductors
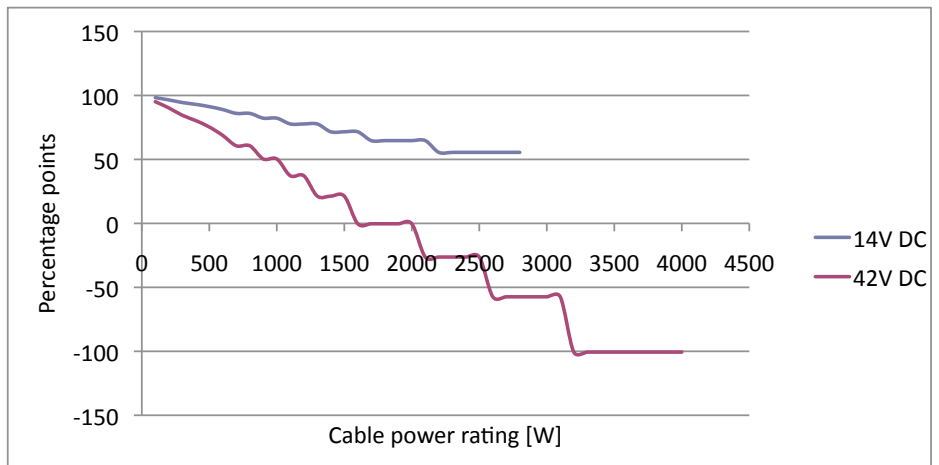
Figure 6.11 Percentage gain in power distribution efficiency for HFAC wiring compared to DC wiring (14V DC and 42V DC), per metre

In addition to the power distribution losses, the voltage drop also has to be considered. This aspect is particularly important for the HFAC cable, since the conductor impedance plays an essential role in the voltage drop as explained in Chapter 4 (see Equation 4.1). For the HFAC conductor characteristics considered in this study, Figure 6.12 illustrates the voltage drop for DC and HFAC power distribution, expressed as volts per metre.
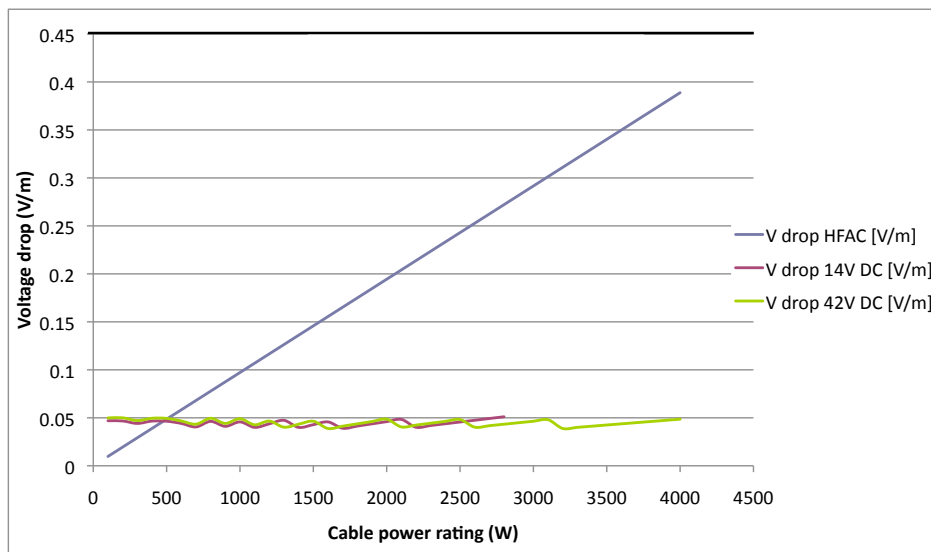
Figure 6.12 Voltage drop for 14V, 42V DC and 100V HFAC conductors (V/m)

Figure 6.12 shows that the HFAC voltage drop is higher compared to the DC counterparts starting with a power rating of approximately 500W. Although the voltage drop has a component which is proportional to the inductance of the cable, and thus is not dissipated as resistive losses but returns to the power source, the voltage decrease is up to eight times higher compared to DC wiring (for an output power of 4kW). Consequently, this result suggests that the HFAC network topology should be composed of power rings or loops with a low power rating (preferably under 1kW) in order to minimise the voltage drop. As will be discussed in Chapter 9, this finding is a potential limitation for the overall HFAC system.

The information needed to calculate the DC conductor copper mass is taken from the AWG data table. In particular, the cable diameter for various current rating values is extracted from the AWG table. Subsequently, the mass of each conductor is calculated as the product of the cylindrical conductor volume (in cm^3) and the copper density of 8.96g per cubic cm. The copper mass of the flat HFAC cable is computed in a similar manner, but this time the volume of the flat conductor of dimensions 0.2mm by 10mm is utilised.

Following the procedure described in the previous paragraph, the copper mass for 1m of HFAC versus DC cables is calculated, for power distribution capability of up to 2.5kW. As displayed in Figure 6.13, the mass advantage per metre for the HFAC cable is significant [3].
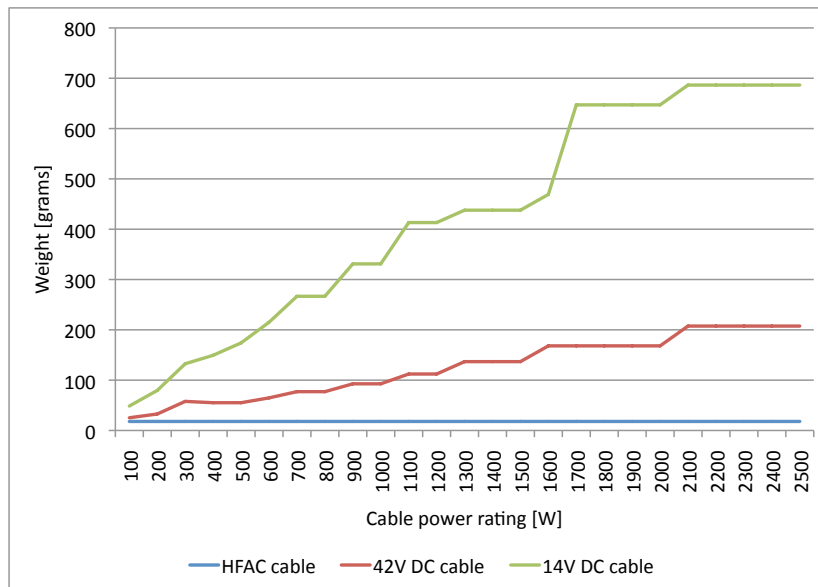
Figure 6.13 Copper mass for 1m of HFAC (17.92g), 42V DC and 14V DC conductors, as a function of power rating

However, several factors should be considered in the analysis of power distribution and mass reduction. These include:

• The fact that the chassis cannot be used as a return path for the HFAC current as in the DC system. Essentially, two strips of HFAC flat cable are required to power each electrical load off the HFAC bus.

• The fact that the HFAC system has a distributed topology where loads are supplied from a HFAC power loop (as indicated in Chapter 4) and not by individual connections from the DC/HFAC inverter. Hence, the wiring length of HFAC and DC topologies is expected to differ significantly.

---

[3] The comparison is based on the assumption that the wiring isolation material has an approximately equal mass for both cable technologies.

Consequently, a broader analysis is required for the power distribution and mass comparison between DC and HFAC systems, to include an investigation of these aspects for a group of loads. The following Section presents such an analysis for the case study of 17 auxiliary loads in a C-segment vehicle.

6.4 Case study: analysis of DC and HFAC network topologies

The analysis in this Section aims to highlight the advantages of HFAC at the distribution level, where the power transfer efficiency is expected to be higher compared to 14V and 42V DC networks and the wiring mass is anticipated to drop considerably. To this end, the case study of a group of electrical loads in a medium-sized passenger vehicle has been considered. The investigation is targeted towards quantifying the efficiency and the copper mass of the wiring interconnecting these loads.

The first Subsection describes the set of loads considered, followed by the introduction of the DC and HFAC topologies in Section 6.4.2. The efficiency and mass reduction assessment are presented in Sections 6.4.3 and 6.4.4, respectively.

6.4.1 Auxiliary electrical loads

Measurements of the battery voltage and current have been taken for loads with intermittent operation in a representative C-segment vehicle. These include the starter motor, air conditioning, blower motor, heated front screen, heated rear screen, main and high beam, power windows, front and rear fog lights, turn signal lights, brake lights, front wipers and washers, rear wiper and the central locking system.

Table 6.1 illustrates the current and voltage waveforms, which have been measured at the vehicle battery terminals. For some electrical loads, the data have been acquired whilst the vehicle engine was running (idle speed). Examples of such key-on systems

include the heated front and rear screen, or the high beam light. As a result, the current consumed by these applications is calculated as the difference between the actual current measured and the current value before the load was switched on. For the particular case of the heated rear screen, for example, the engine-idle current is approximately 13A before the load is turned on, and the measured value is in the order of 28A while the load is active. Therefore, the current drawn by the load is equal to 15A. Conversely, the power demand of other electrical sub-systems has been measured with the engine stopped, such as the central locking application.

Table 6.1 Voltage and current measurements for 14 auxiliary electrical loads (representative C-segment vehicle)
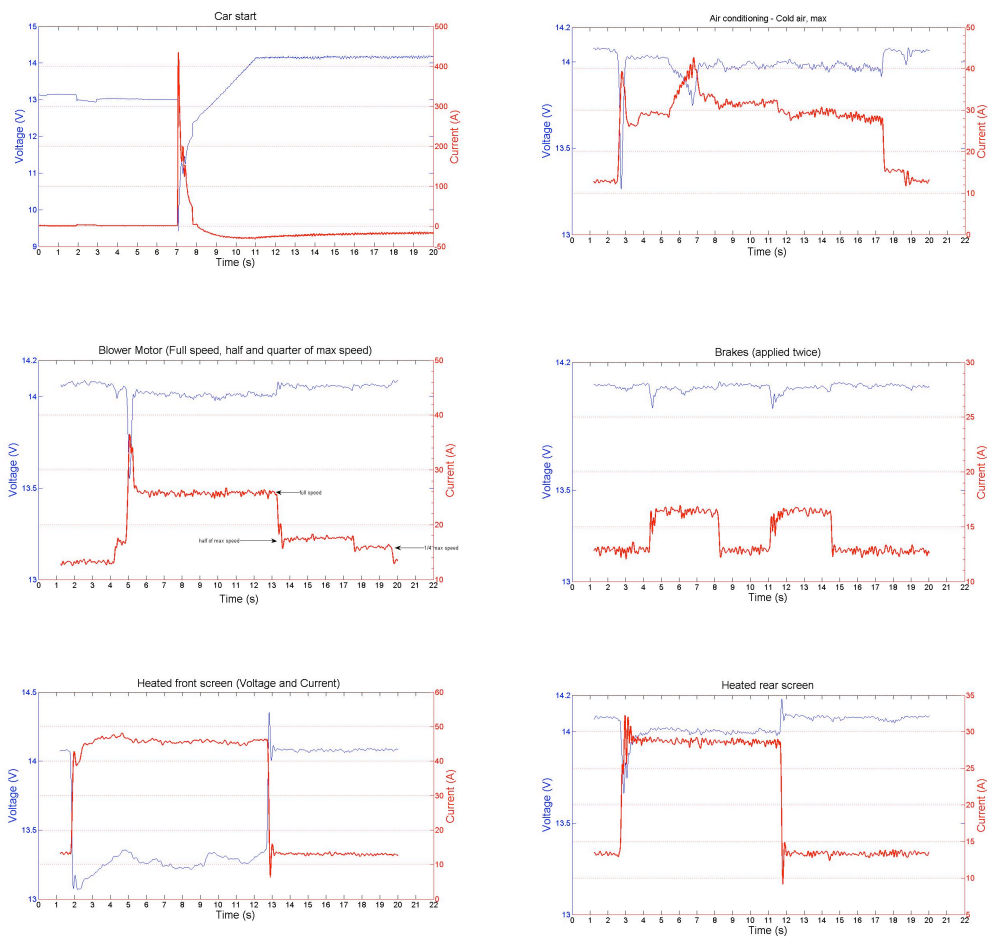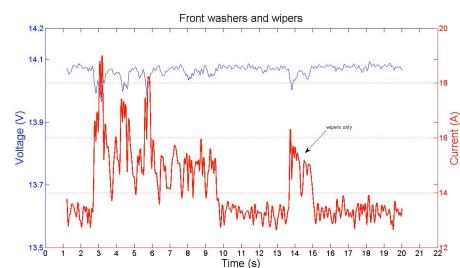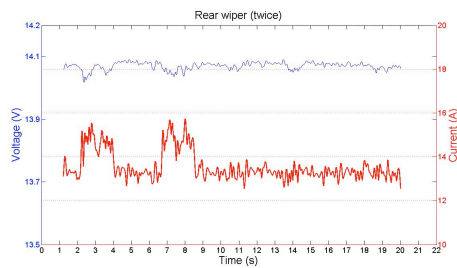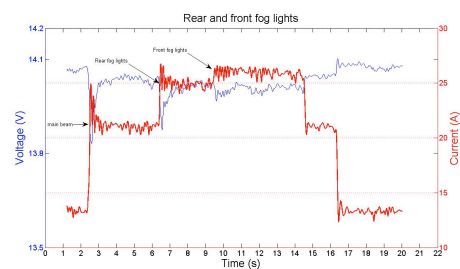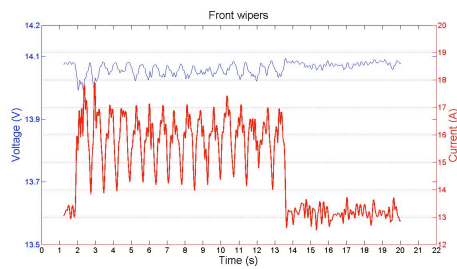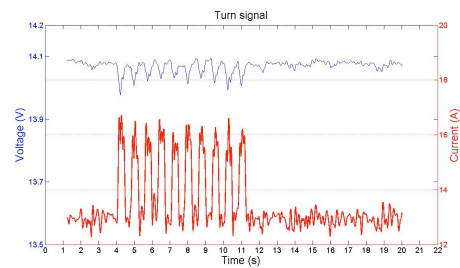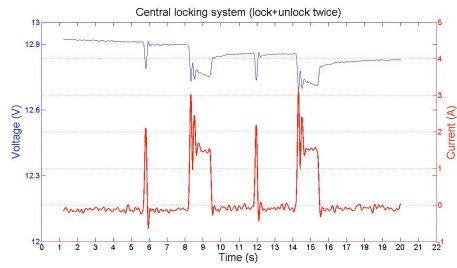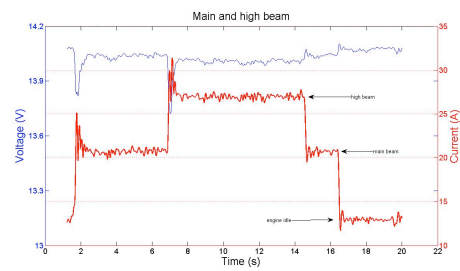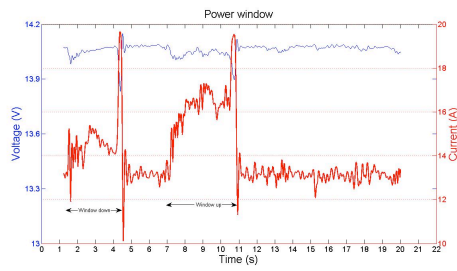
In addition to the intermittent loads in Table 6.1, the electrical auxiliaries in Table 6.2 with a continuous duty cycle are also considered in the present analysis.

Table 6.2 Auxiliary loads with continuous operation (Lukic and Emadi, 2002, Lukic and Emadi, 2003)

Load	Continuous power consumption (W)
Engine electric water pump	500
Fuel pump	100
Engine cooling fan	100

6.4.2 Power architectures and topologies

DC power architecture

The centralised topology of the DC network is illustrated in Figure 6.14, where the loads are represented by numbered circles from 1 to 17. Table 6.3 summarises the approximate length[4] and current rating of each cable connecting the loads to the battery.
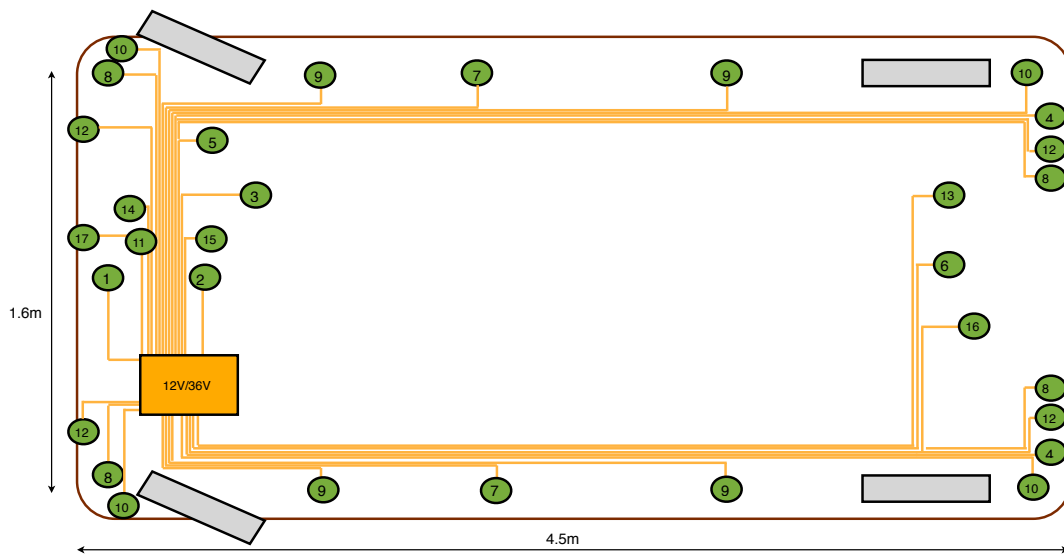
Figure 6.14 Diagram of DC electrical network

_____

[4] The length of the conductors has been calculated based on the 3-D representation of the electrical wiring in vehicles presented in Chapter 9 (Figure 9.4)

Table 6.3 Properties of cables connecting the loads to the battery for 14V and 42V DC bus

Load no.	Description	Cable length (m)	Cable current rating (A)	
			14V bus (AWG)	42V bus (AWG)
1	Starter motor	0.5	500 (0000)	167 (00)
2	Air conditioning compressor motor	1	30 (7)	10 (20)
3	Blower motor	1.5	15 (10)	5 (14)
4	Braking lights	5(left)+6(right) = 11	2.5 (17)	0.8 (22)
5	Heated front screen	2	25 (7)	8.5 (12)
6	Heated rear screen	5.5	15 (10)	5 (14)
7	Front power windows	2.5(left)+3.5(right) = 6	7 (13)	2.3 (18)
8	Main and high beam	5.5(left)+7(right) =12.5	2.5 (17)	0.8 (22)
9	Central locking motors	2.5+3.5+4+5=15	0.75 (22)	0.25 (27)
10	Indicator lights	1.5+3+5+6=15.5	1.5 (20)	0.5 (24)
11	Front wipers	1	5* (11)	1.7 (19)
12	Front and rear fog lights	1+2+5+6=14	1.5 (20)	0.5 (24)
13	Rear wiper	6	3 (16)	1 (21)
14	Front washers	1+1.5=2.5	1.5 (20)	0.5 (24)
15	Engine electric water pump	1.5	35 (6)	12 (11)
16	Fuel pump	6	7 (13)	2.33 (18)
17	Engine cooling fan	2	7 (13)	2.33 (18)
	Total current, excluding starter motor		204A	68A

In relation to the current amplitude outlined in Table 6.3, the values shown for 14V operation are taken from the measured data. However, the indicated current amplitude for 42V DC operation is estimated as one third of the value at 14V. This evaluation is based in the assumption that the actuators are suitable for 42V operation, and that the power consumed does not change with the increase in the voltage supply.

Proposed HFAC power architecture

The topology illustrated in Figure 6.15 is a possible concept for a vehicle AC bus. This specific layout is based on the location within the vehicle of the applications included in the case study. An alternative HFAC topology will be presented as part of the analysis in Chapter 9.

The proposed architecture within this Chapter is composed of several HFAC loops, each interconnecting a smaller group of loads based on their co-location in the vehicle. Table 6.4 indicates the loads connected to each of the six HFAC power loops, their approximate length[5] and cumulative power. In addition, the maximum possible voltage drop for each power loop is indicated. It is observable that for the proposed HFAC topology, the voltage drop is no larger than 0.4V. In fact, this amplitude is the equivalent of just 0.4% of the nominal HFAC bus voltage. The voltage drop calculation is based on equation 4.1 in Chapter 4 used for the conductor impedance, which is equal to 9.7mΩ/ m.

Table 6.4 HFAC subsystems - loads connected and cable length of each subsystem

Loop no.	Loads connected	Cable length (m)	Maximum power (W)	Maximum possible voltage drop (V)
1	1	1	3,000	0.291
2	8, 10, 11, 12, 14, 17	6	266	0.175
3	2, 3, 5, 15	1.7	1,470	0.25
4	4, 7, 8, 9, 10, 12	11	220	0.22
5	4, 7, 8, 9, 10, 12	9	220	0.18
6	6, 13, 16	10	350	0.39

---

[5] The length for each loop includes the combined length of two parallel conductors required for HFAC power distribution.

6.4.3 Power distribution efficiency

The resistive power losses are compared for the distributed HFAC network topology in Figure 6.15 and the centralised DC counterpart previously shown in Figure 6.14. For the latter, both 14V DC and 42V DC operation are taken into account.
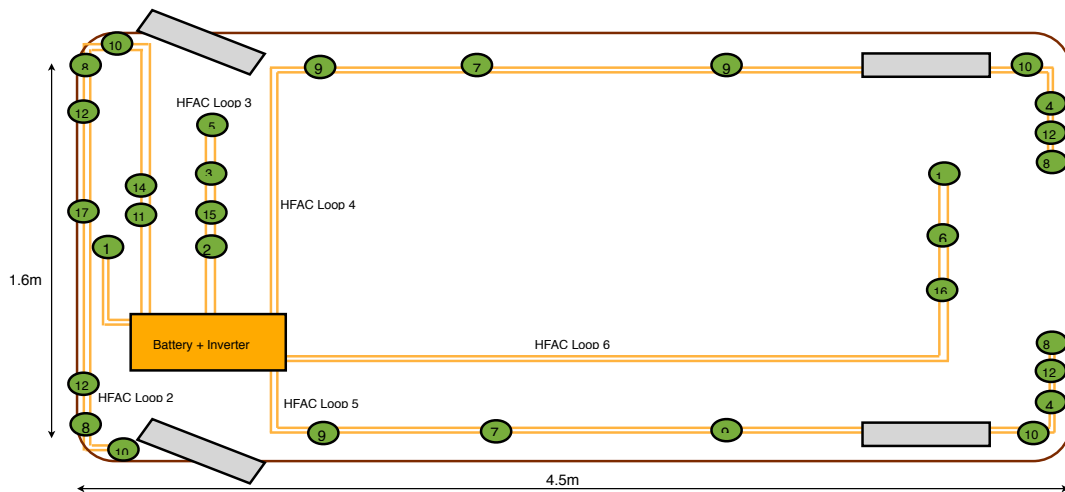
Figure 6.15 Diagram of HFAC electrical network

Two duty cycles are considered for the intermittent loads in Table 6.3 over a time period of 1200s, which is comparable to the efficiency gain of the HFAC bus over the time duration of the NEDC[6] drive cycle. The first duty cycle considers vehicle operation during the summer, implying frequent use of the A/C system, and the second aims to reflect winter driving conditions, which is equivalent to the repeated use of the heating, lighting and screen defrosting systems. The electrical loads previously shown in Table 6.2 have a continuous duty cycle in both cases.

Figure 6.16 shows the energy losses associated with each bus for the two scenarios (summer and winter driving). As expected, the 42V bus is more efficient compared to the lower voltage DC network, but the calculations show that a further significant improvement in power distribution efficiency can be achieved by the HFAC bus.

---

[6] NEDC stands for New European Drive Cycle

Indeed, since the distribution voltage for the latter system is considerably higher, the current is low and therefore the I^2R losses much reduced. In fact, for the summer duty cycle, losses can potentially be reduced by approximately 92% and 80% compared to the 14V and 42V buses, respectively. For the winter driving cycle the reductions are in the order of 91% and 81%, respectively.
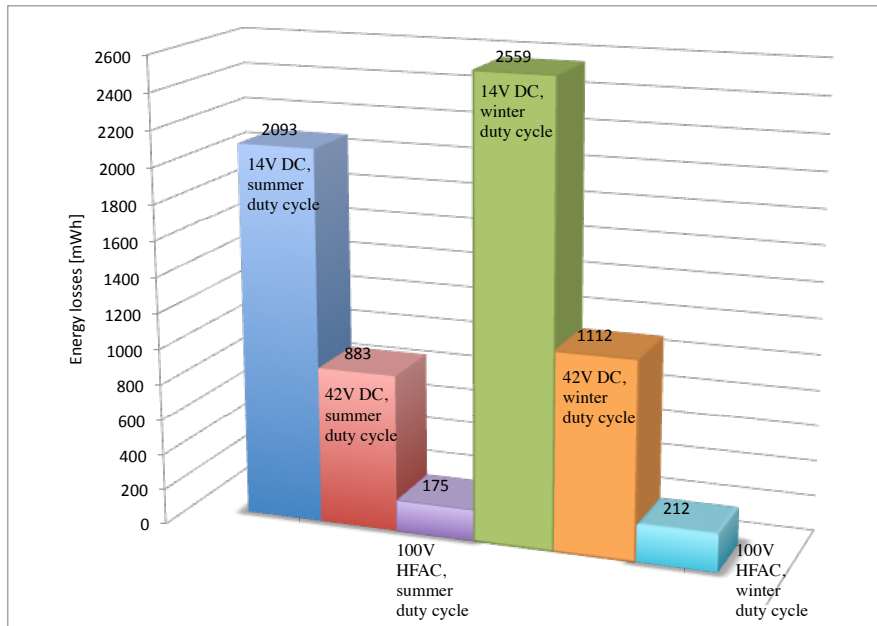
Figure 6.16 Comparison of distribution energy losses for 14V, 42V DC and 100V HFAC buses over 1200s drive cycle

6.4.4 Wiring copper mass

Each cable detailed in Table 6.3 has a different power rating and therefore a different mass. Repeating the same process as above to determine the copper mass for each of the wires connecting the 17 loads, the total mass figures are 2.27kg for the 14V system and 0.99kg for the 42V bus with a total wiring length of 103.7m.

Conversely, the HFAC cabling has a length of 38.7m and a mass of 0.693kg [7] (Figure 6.17). Therefore, a HFAC cabling system for the case study considered in this Chapter

---

[7] Result based on the mass of 1m HFAC conductor equal to 17.92g, as presented in Section 6.3

is expected to weigh approximately 70% less compared to the 14V system and be approximately 30% lighter compared to the 42V network, which is a noteworthy benefit.
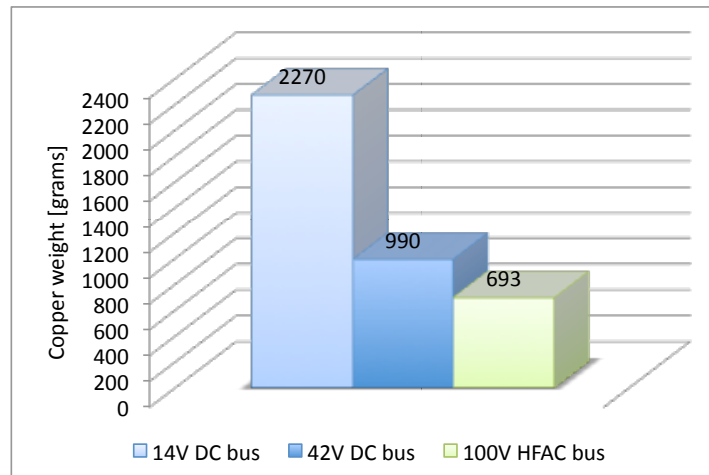
Figure 6.17 Copper weight for the three power systems (grams)

6.5 Conclusions

This Chapter has presented the advantages of HFAC power for the distribution sub-system in vehicles. These benefits can be attributed first to the distributed topology of the proposed power bus, and second to the inherent features of the high frequency network components including magnetically-coupled connectors and compact and lightweight conductors and passive circuit components.

The distributed topology of the HFAC architecture can potentially lend the proposed system to a better design, which in turn may improve the reportedly time-consuming and expensive assembly process of DC on-board wiring (Miller et al., 1999). In addition, since the HFAC bus is galvanically isolated from the remaining system components, electrical faults between network branches operating at different voltage levels are less likely to occur compared to equivalent dual voltage DC architectures.

Due to the distributed HFAC architecture, the requirement for applications to withstand the typical voltage variation from 9V to 16V in the 14V network can be waived. This, in turn, may lead to a reduced design and manufacturing cost for the electrical actuators. Moreover, local power conversion addresses the case of simultaneous multiple voltage control, which is indicated as a problem in some dual voltage architectures.

Since the HFAC connectors are magnetically-coupled, the issues regarding the 42V DC connector arcs, corrosion and thus reliability can be solved. Also, high frequency power management modules employ small and lightweight passive circuit elements. This fact implies that HFAC converter modules and filters are potentially more suitable for the automobile environment than similar DC power management units, due to their lower mass and smaller packaging volume.

The Chapter has also highlighted the benefits of HFAC at the distribution level in terms of power distribution efficiency and wiring copper mass saving in comparison to on-board 14V DC and proposed 42V DC power networks. First, the investigation has shown that for a commercially-available HFAC conductor, the benefits in terms of copper mass saving and power distribution efficiency are considerable for the same length and cable power rating.

However, since DC and HFAC systems are expected to employ wiring of different length for the same set of electrical consumers, a comparative analysis of a group of loads has been carried out. Fundamental to this analysis has been the case study of 17 intermittent and continuous electrical auxiliary loads in a representative C-segment passenger vehicle. The cumulative power of the network is approximately 2.8kW. The analysis has shown a potential efficiency gain in power distribution of 90% and 80% for the HFAC bus compared to 14V and 42V power networks over a drive cycle of 1200s, respectively, and copper mass saving of 70% and 30%. These results are indicative of the benefits of HFAC power for automobiles over a driving cycle such as the NEDC,

which ultimately translate into lower vehicle mass, reduced fuel consumption and lower CO_2 emissions.

Chapter 9 includes a similar analysis to the case study presented in Section 6.4. The examination looks at the potential HFAC power distribution benefits from a system-level perspective.

Chapter 7

HFAC power conversion sub-system

7.1 Introduction

The HFAC power conversion sub-system includes the power electronics modules which transform the HFAC power into a suitable form usable by the auxiliary electrical loads. Specifically, these modules include the HFAC/AC electrical circuits (single-phase or three-phase) and the HFAC/DC converters.

Chapters 2 and 3 have given a comprehensive overview of the HFAC converter topologies proposed for application areas including aerospace, microgrids, telecommunication equipment and automotive electrical systems. Although applied in different domains, these circuits share common characteristics such as resonant power conversion and ZVS or ZCS, which are relevant for the analysis in the current Chapter.

With regard to the HFAC/DC power converters, Figure 7.1 presents a diagram of the common stages found in the topologies presented in Chapters 2 and 3. There are five specific parts of a HFAC/DC converter:

1. An input transformer, which has the role of isolating the power conversion stage from the HFAC bus and also to step the voltage up or down as required by the load.
2. A resonant network that is used to minimise the harmonic distortion of the input voltage and current.
3. A controller that adjusts the load current flow to maintain the output DC voltage at the reference level. The controller will typically be based on a ZVS or ZCS method and can employ the PDM technique (presented in Section 2.2).
4. A diode rectifier, which transforms the AC current into DC current.
5. A smoothing capacitor acting as a filter for the output voltage and current.
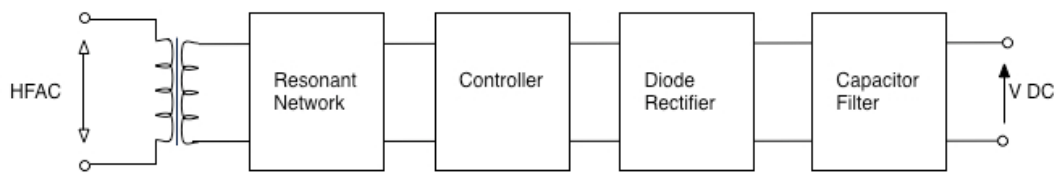
Figure 7.1 Typical stages in HFAC to DC converters

Figure 7.2 illustrates the main structure shared by the HFAC/AC converters presented in Chapters 2 and 3. Part (a) of Figure 7.2 represents a HFAC/AC single-phase frequency converter, and part (b) of the same Figure shows the typical connection of a star-type three-phase AC load to the HFAC bus.
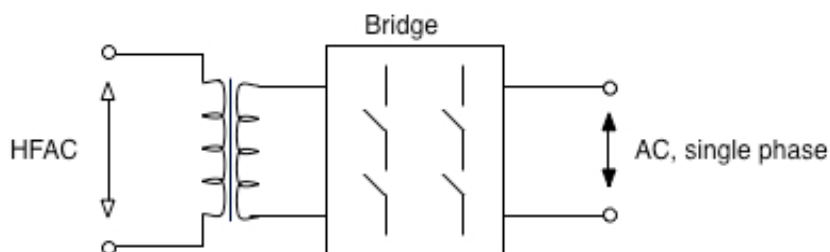
Figure 7.2a Structure of HFAC to single-phase AC converter
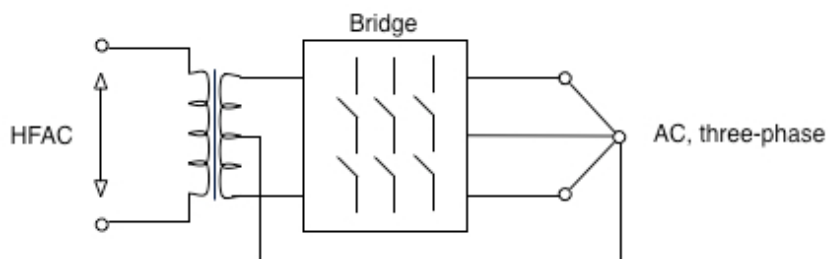
Figure 7.2b Structure of HFAC to three-phase AC converter

The role of the input transformer is similar for the HFAC/DC and HFAC/AC converters. However, unlike some topologies of the former converter type (Dhar et al., 2002), the HFAC/AC circuit always operates synchronously with the input AC sinusoid (i.e. ZVS or ZCS is constantly applied). Furthermore, specific to this type of converter are the following characteristics:

• Each switch in the bridge is composed of two inverse series MOSFETs or IGBTs. The justification for this design has already been given in Section 3.2,

• The frequency of the output AC voltage is always smaller than the input frequency, since the building blocks of the output voltage are the half sinusoids of the input voltage (PDM is applied, as discussed in Section 2.2),

• For AC motor loads which require a constant input frequency, the HFAC/AC drive is also known as a constant speed drive (CSD) and the bridge control is a preset sequence of gate signals. Conversely, for machines demanding a variable frequency (variable speed drives (VSD)), specific control techniques must be employed such as vector control. The application of HFAC for the two types of motor drive is discussed further in Chapter 8.

7.2 HFAC to DC power conversion

Figure 7.3 shows the diagram of the proposed synchronous rectifier topology. The circuit includes:

• an input transformer, for stepping down the voltage from 100V AC to 14V or 42V DC,

•a synchronous rectifier, composed of two pairs of inverse-series MOSFETs, and finally

• a smoothing output capacitor.

Within the present work, an output filter (as in Figure 7.1) is considered redundant, since it is assumed that the bus voltage and current have a low THD value. This assumption is based on the fact that, as discussed in Chapter 6, the HFAC supply voltage is continuously monitored and regulated.

As detailed in Section 7.1, the input transformer and the output capacitor are common components of the AC/DC converters discussed in the literature. Unlike the majority of these converters, control of the proposed converter operates synchronously with the input HFAC current and is based on active MOSFET switching. This technique is different from the typical converter topology, as it does not make use of the diode rectification stage. This aspect is particularly important for the automotive electrical system, since the diode conduction losses have a significant effect on the efficiency of

the power converter. Therefore, the HFAC/DC converter topology illustrated in Figure 7.3 has been chosen primarily for its high efficiency potential.
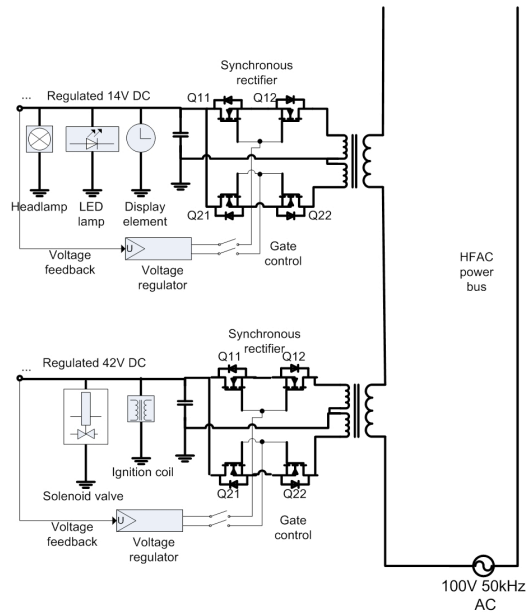
Figure 7.3 Electrical diagram of synchronous rectifiers supplying 14V (top)
and 42V DC loads (bottom) off the HFAC bus

The rectification stage includes two pairs of inverse series MOSFETs for AC bi-directional switching control, performed at zero current crossing to minimise the circuit losses. The majority of vehicle loads which operate off 14V DC can be connected to the corresponding converter, while state-of-the art loads demanding a higher voltage such as the ISG or engine VVA can be attached to the higher DC voltage bus. Moreover, as noted throughout the present work, any voltage other than the 14V or 42V DC can be easily obtained by HFAC/DC converters. To achieve this, the circuit changes required include new/modified components (such as an input transformer with a different winding turns ratio). The role of these parts is to accommodate for the load power demand, while the modular structure remains unchanged.

Figure 7.4 illustrates the three operational modes of the proposed HFAC/DC converter. In mode 1, shown in Figure 7.4 (a), all four power switches are turned off and no

current is transferred to the load. The other two modes of operation, illustrated in Figures 7.4 (b, c), are activated alternately by the voltage controller (shown in Figure 7.3) for the positive and negative polarity of the input HFAC current, respectively.
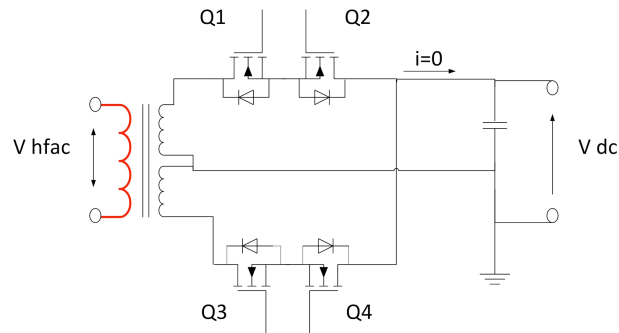
Figure 7.4a Mode 1 of the converter module operation
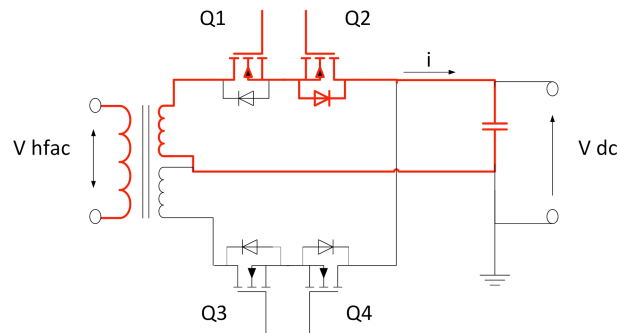
Figure 7.4b Mode 2 of the converter module operation (positive HFAC current)
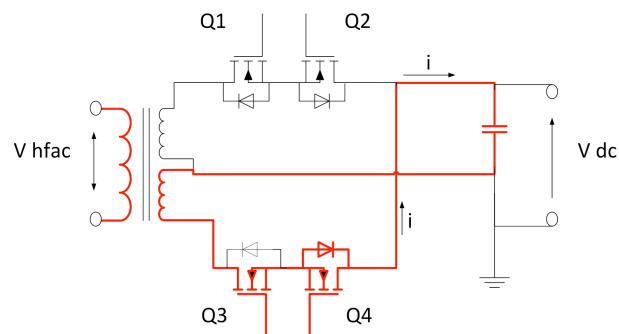
Figure 7.4c Mode 3 of the converter module operation (negative HFAC current)

With reference to modes 2 and 3 of operation Q1 and Q3 are forward biased, respectively, whilst Q2 and Q4 are reverse-biased. For the latter two MOSFETs, as long as the voltage drop is lower than the body diode, conduction losses are proportional to the MOSFET internal resistance. However, if the voltage amplitude reaches the diode forward bias threshold, circuit losses are proportional to this constant diode voltage drop. For the low-power rectifier operation discussed in this work, the MOSFET body diode is not expected to become forward biased and therefore the losses are proportional to the MOSFET internal resistance.

Figure 7.5 shows the waveforms of the HFAC current and output DC voltage for the three modes of operation.
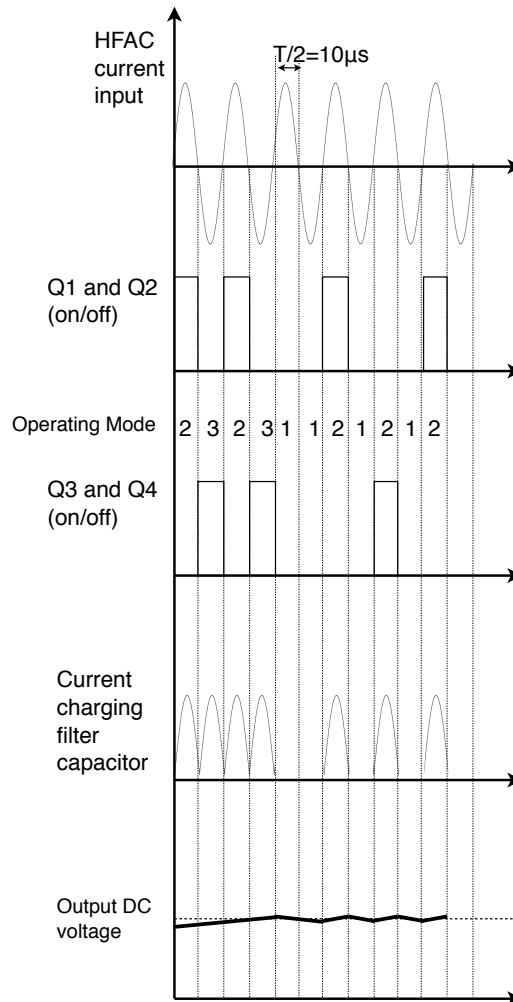
Figure 7.5 Waveforms illustrating the operating principle of the HFAC/DC converter

For illustrative purposes, the Figure captures only a particular case of circuit operation. Under varying load conditions, the circuit control scheme switches continuously between the thee operating modes.

In order to evaluate the efficiency of the converter module, the losses of the synchronous HFAC to 14V DC rectifier are examined in relation to 42V/14V DC converters. Figure 7.6 illustrates the circuit diagram of the resonant switch buck converter, which is considered very efficient for a power output of up to approximately 300W (Emadi, 2005). For loads up to several kW, Figure 7.7 shows the diagram of a suitable topology: the full-bridge DC/DC converter (Emadi, 2005, Erickson and Maksimovic, 2001).
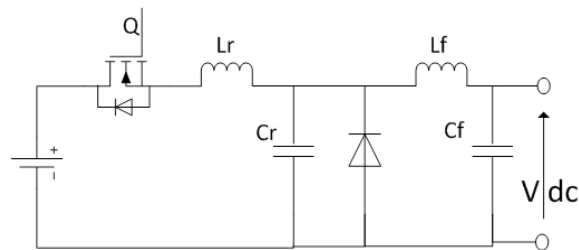
Figure 7.6 Resonant switch buck converter
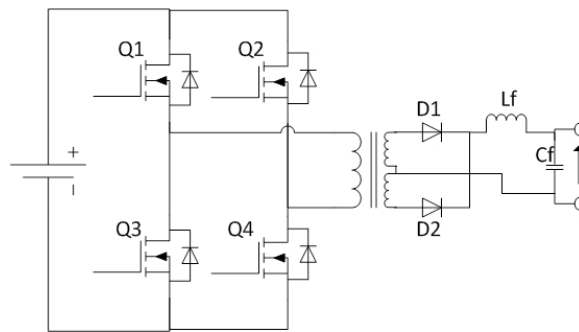
Figure 7.7 Full bridge DC step-down converter

With reference to the resonant switch buck converter, the resonant capacitor (C_r) provides a zero-voltage condition for the switch to turn on and off. The output voltage is regulated by changing the switching frequency, which can be as high as several MHz (Rashid, 2007). The full-bridge DC converter is considered a more versatile converter than the resonant switch buck converter due to its robustness and switching frequency in

the kHz range (Rashid, 2007). Diodes D_1 and D_2 conduct alternately, according to the polarity of the voltage in the transformer primary winding. Thus, the voltage is maintained at a constant level across the output filter capacitor C_f.

The efficiency of the HFAC/DC converter is estimated and compared with the efficiency of the DC/DC converters. Although the former converters are necessary modules in a HFAC network for interfacing with DC loads, DC/DC converters are less common in a DC architecture since the loads operate directly off the DC bus voltage. In fact, the comparison between the two types of circuits is only meaningful for the proposed 42V/14V DC converter in a dual voltage bus (as discussed in Chapter 6 for the DC/DC converter dual voltage architecture). Therefore, the losses of the three circuit topologies are estimated and compared for 42V/14V DC and 100V HFAC/14V DC operation:

1. First, the losses in the resonant switch buck converter have been calculated. In order to estimate the losses for different load current values, the current waveforms in Figure A7.1 (within Appendix F, illustrating the operation of the circuit) have been used (Rashid, 2007). Specifically, with reference to Figure A7.1, the current amplitude in the power MOSFET is equal to:

$$i_{\max} = i_0 + \frac{V_i}{Z_r}, Z_r = \sqrt{\frac{L_r}{C_r}} \tag{7.1}$$

where Z_r is the characteristic impedance of the circuit.

Consequently, since the MOSFET operates on a ZVS basis, the circuit efficiency is only a function of the resistive conduction losses. Equation 7.2 has been used to estimate the losses in the resonant-switch buck converter:

$$Losses = \left(\frac{i_{max}}{\sqrt{2}}\right)^2 \cdot R_{MOSFET} \cdot \delta + (1-\delta) \cdot 0.7 \cdot \frac{i_{max}}{\sqrt{2}} \tag{7.2}$$

where R_{MOSFET} is the internal resistance of the power MOSFET, the diode voltage drop is equal to 0.7V and δ is the duty cycle of the switch. Typically, the latter varies from 20% to 60% (Mathworks, 2009).

2. The efficiency of the full-bridge converter is dependent on both switching and conduction losses in the circuit.

Equation 7.3 has been used to calculate the switching losses in the H-bridge. P_{loss_on} and P_{loss_off} in equation 7.3 are the power losses in the MOSFET during switch turn-on and turn-off. As shown in Figure 7.8 (Lourdes, 2010), these values can be obtained from the measurement of a typical voltage and current waveform in a power MOSFET. It was found that P_{loss_on} and P_{loss_off} are equal to approximately $\frac{2}{3} \cdot V \cdot \frac{2}{3} \cdot I$, where V is the voltage across the MOSFET before it changes state, and I is the current in the MOSFET. Similar values for the power loss variables have been indicated in the study by (Graovac et al., 2006). The switch-on and off times (T_{on} and T_{off} in Eq. 7.3) have been measured as 118ns and 51ns, respectively.

$$Losses_{Switching} = f_{Switching} \cdot (\frac{1}{2} \cdot P_{loss\_on} \cdot T_{on} + \frac{1}{2} \cdot P_{loss\_off} \cdot T_{off}) \cdot 4 \tag{7.3}$$

The total power losses in the full-bridge converter are, therefore, the sum of the conduction for two MOSFETs and switching losses for four MOSFETs (as indicated in Equation 7.3):

$$Losses = Losses_{Switching} + 2\left(\frac{I}{3}\right)^2 R_{MOSFET} + 0.7 \cdot I \tag{7.4}$$

where the current is equal to one third of the load current (due to the 3:1 voltage step-down function of the transformer). Similarly to the resonant switch converter, 0.7V has been assumed for the diode voltage drop.
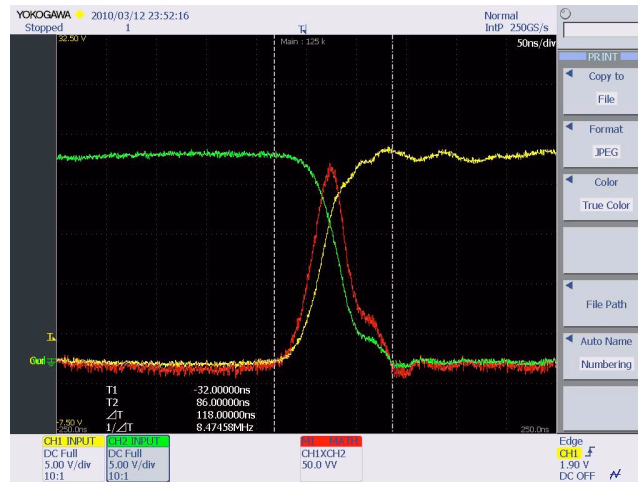
Figure 7.8 MOSFET turn-on: voltage, current and switching losses (MOSFET: IRF S4229PBF N channel, 250V, 45A, on-state resistance 0.042 ohm) (Lourdes, 2010)

3. The losses in the proposed ZCS HFAC/DC circuit are due to the conduction losses in the two MOSFET switches connected in series [1]:

$$Losses = 2\left(\frac{I}{3}\right)^2 R_{MOSFET} \tag{7.5}$$

Figure 7.9 illustrates the losses in the three converter topologies against a load current of up to 60A at 14V DC. The loss figures of the DC/DC converters are consistent with other studies presented within the literature (Gerber et al., 2005). The following circuit parameters and assumptions have been made for the calculation of the losses:

(i) The duty cycle of the resonant switch buck converter increases from 20% to 60% for the maximum power output of 280W. The frequency in the L_r-C_r circuit is 2MHz.

---

[1] The reason for the HFAC rectifier current being 1/3 of the load current (see Equation 7.5) is that the voltage across the MOSFETs is stepped down from 100V of the HFAC bus to 42V. The purpose of opting for 42V instead of 14V in the rectifier is to minimise the MOSFET conduction losses.

(ii) The isolating transformer included in the full bridge DC/DC converter steps down the input 42V signal to a 14V, alternating square voltage.

(iii) The transformer in the HFAC synchronous rectifier steps the voltage down from 100V to 42V (to minimise the current, and therefore the conduction losses), and the 14V DC is obtained by varying the switching duty cycle. ZCS is maintained.

(iii) The diodes in the DC/DC converters have a forward voltage drop of 0.7V.

(iv) The MOSFET internal on resistance is equal to 42mΩ.

(v) The switching frequency for the H-bridge converter is 20kHz.
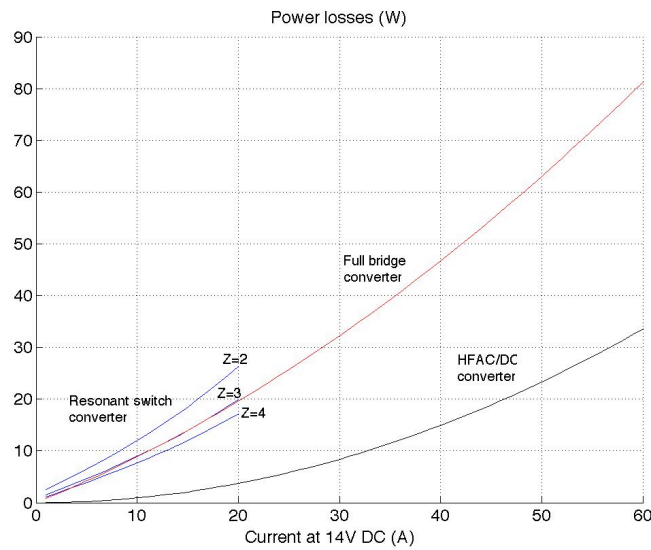
Figure 7.9 Losses in the three step-down converters, as a function of current

Although switching losses occur only in the-full bridge DC/DC converter, its advantage lies in the voltage step-down function of the transformer. This causes the current in the primary winding to be just one third of the current on the load side of the transformer. Hence, both the switching and conduction losses on the left-hand side of the transformer are minimised, making it more efficient than the resonant switch converter for a characteristic impedance (Z_r) smaller than 3.

The HFAC synchronous rectifier has the lowest losses amongst the three topologies. For the maximum load current considered in the present analysis (60A at 14V DC), the efficiency of the HFAC/DC converter is expected to be approximately 96%, while the

efficiency of the full-bridge converter is in the order of 92%. Table 7.1 shows the efficiency figures of the three candidates for the maximum power capability of the resonant switch converter of 280W.

Table 7.1 Efficiency of the three converters for a power output of 280W

Converter topology	Power output	Efficiency
Resonant switch buck	280W	91%
Full bridge buck	280W	93.5%
Synchronous HFAC/DC	280W	98%

The two main implications of the efficiency findings presented above for the automobile electrical system are described below:

1. As indicated in the current Section, a relevant comparison can be drawn between the full-bridge DC/DC and HFAC/DC converters only for 42V/14V DC operation. For this particular scenario, calculations suggest that the latter topology can potentially save up to 110W for a converter power rating of 2kW (or current of 140A at 14V DC). Table 7.2 includes the losses of the two converters for several power output levels, based on Equations 7.3 - 7.5.

2. Apart from the converter discussed at point (1) above, the proposed HFAC/DC bus employs HFAC/DC converters which do not have an equivalent in the DC power distribution system. Therefore, for the HFAC system to become a viable alternative, the losses at the power conversion stage should be minimised.

Table 7.2 Efficiency of the full-bridge DC/DC converter and HFAC/DC synchronous rectifier, for several load current values

Load current (A)	Power losses (W)		Efficiency	
	DC/DC	HFAC/DC	DC/DC	HFAC/DC
100	173	94	87%	93%
110	200	113	87%	92.5%
125	245	146	86%	91.5%
140	295	183	85%	90.5%

The efficiency analysis has indicated that the losses in the HFAC/DC converter module are very low (below 2.5% for a load power of 500W, at 14V DC).

The present Section has presented a suitable HFAC/DC converter topology for automotive applications. Particularly, the structure, operation and efficiency of a synchronous HFAC/DC rectifier based on ZCS have been discussed. The proposed module can potentially save up to 110W, compared to DC/DC converters, for a rated power of 2kW. For applications within the 500W range, the ZCS synchronous rectifier losses are lower than 2.5%. These results indicate that the HFAC is potentially a feasible and desirable technology for power conversion modules.

7.3 HFAC to AC power conversion

Figure 7.10 illustrates the proposed HFAC/AC converter diagrams[2]. The two modules, which are suitable to interface three-phase and single-phase AC loads, use the inverse-series MOSFETs as the basic switching element. Also common for the two topologies is the input transformer. The role of these two circuit components has already been discussed in Section 7.1 and therefore will not be repeated here.

A HFAC to single-phase AC frequency converter, similar to the one in Figure 7.10, has been presented in Section 2.2. Comparable to the circuit in Figure 2.4 (a), the proposed converter acts as a frequency converter or cycloconverter. The difference however, is that the proposed HFAC/AC circuit employs power MOSFETs and not thyristors. Thyristors are typically used for high voltage applications (several hundred volts, similar to IGBT power switches) and have a constant forward voltage drop (similar to diodes). Since efficiency is of particular importance for the proposed HFAC network, a cycloconverter employing power MOSFETs is preferable since these components act as resistors in conduction mode, and therefore the voltage drop is proportional to the load

---

[2] Similar to the HFAC/DC power conversion diagram in Figure 7.3, a series LC combination should be integrated with the conductor for contact-less power transfer.

current[3]. Moreover, switch-on and switch-off transition times of MOSFETs (typically under 200ns) are significantly lower compared to thyristors and IGBTs (typically in the order of hundreds of μs), which makes them suitable for high frequency operation.
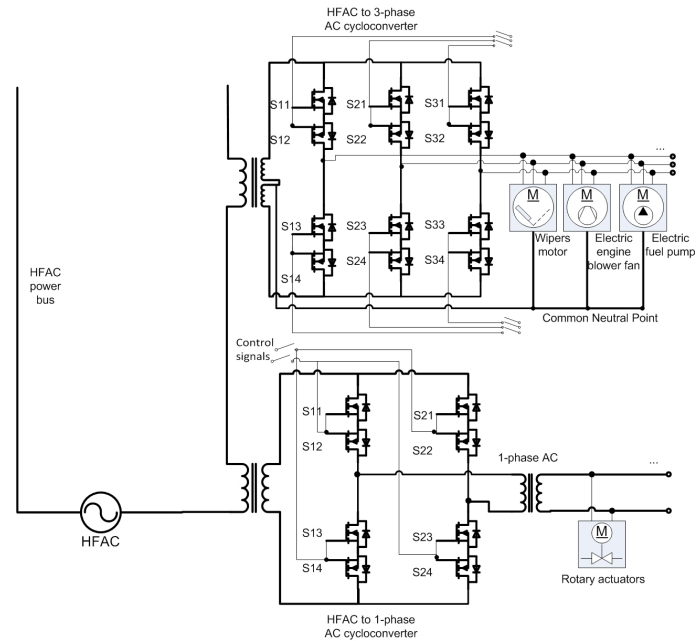
Figure 7.10 HFAC to 3-phase and 1-phase AC power converters

With regard to the three-phase converter presented in Figure 7.10, the neutral point of the motor loads with a star connection is coupled to the centre of the secondary transformer winding. Such a cycloconverter, integrating thyristors as the basic switching element, has been presented in (Agrawal et al., 1992). For the same reasons discussed above, the topology chosen for the present work employs power MOSFETs instead of thyristors.

As indicated in Section 7.1, the HFAC/AC circuit can operate either as a constant frequency drive or as a variable frequency drive for AC machines. The former operating mode is presented in this Section, while the latter is included as part of the discussion on electrical loads in Chapter 8.

---

[3] This statement is valid under all conditions. The voltage drop across the MOSFET is similar to the voltage drop across a typical resistor, sine the MOSFET is acting as a resistor while in conduction mode.

Figures 7.11 and 7.12 illustrate the circuit diagrams and the waveforms, respectively, explaining the operation of the single-phase HFAC/AC converter. Specifically:

- Figure 7.11 (a) shows the operation mode 1 in which the current path is highlighted in the Figure. Within this mode, the polarity of the output voltage is the same as the polarity of the input sinusoidal signal.

- Conversely, Figure 7.11 (b) shows the second mode of operation. The output voltage polarity changes with respect to the input HFAC voltage.
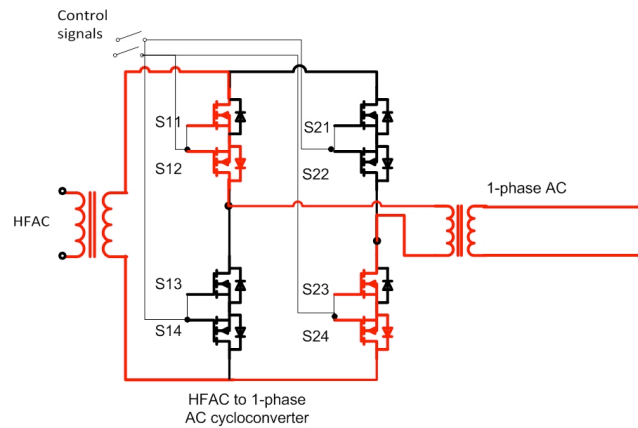
Figure 7.11a HFAC/AC, single phase, operation mode 1
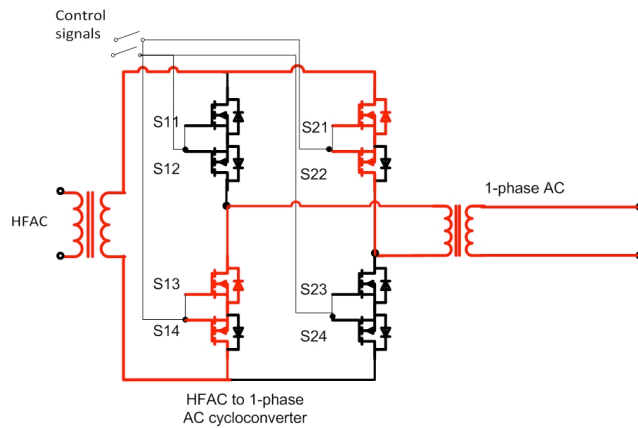
Figure 7.11b HFAC/AC, single phase, operation mode 2

Figure 7.12 shows the waveforms associated with the operation of the cycloconverter for the particular case of frequency transformation to one quarter of the input sinusoidal signal. The diagonal pairs of inverse-series MOSFETs are switched on and off simultaneously and the switching sequence is determined by the input voltage polarity and the desired output frequency.

The HFAC to three-phase AC cycloconverter operation is very similar to the equivalent single-phase circuit. As a result, the diagrams and waveforms related to the functioning of the three-phase constant speed drive have not been included.

T/2=10µs

HFAC voltage input

S11, S12, S23, S24 (on/off) (mode 1)

S13, S14, S21, S22 (on/off) (mode 2)

Output AC voltage
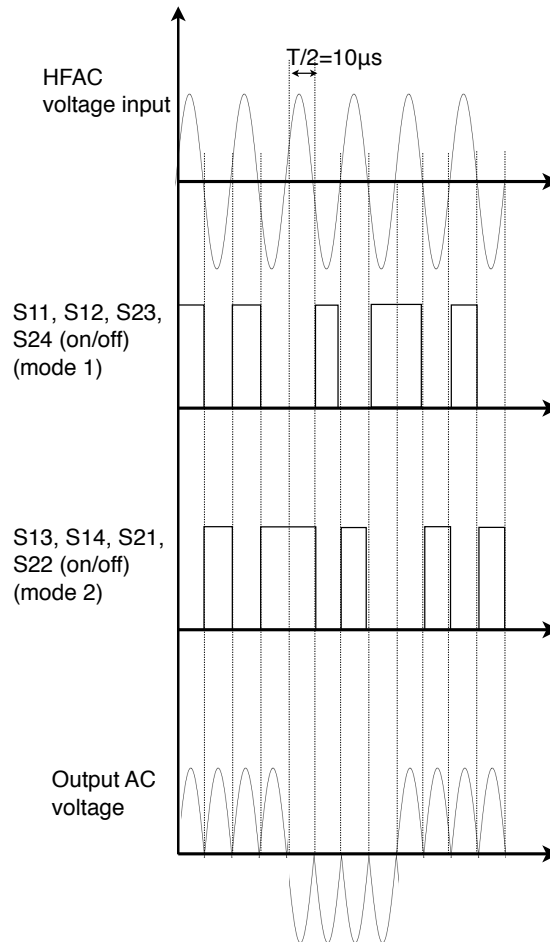
Figure 7.12 Waveforms illustrating the operation of the HFAC to single-phase AC converter (particular case, output voltage frequency is equal to 1/4 of the HFAC frequency input)

For completeness, an equivalent electrical circuit model of the three-phase cycloconverter has been built using the Matlab modelling and simulation environment, and the Simulink SimPowerSystems toolbox. Figure A7.2 in Appendix F illustrates the model. Figure 7.13 shows the synthesized 400Hz AC voltage waveform from a 50kHz input AC voltage. This particular frequency and voltage amplitude (115V rms) are typically employed for lightweight and compact electrical machines used as actuators in

aircraft applications. This aspect is further discussed in Chapter 8, which is dedicated to the feasibility of HFAC for electrical loads within vehicles.
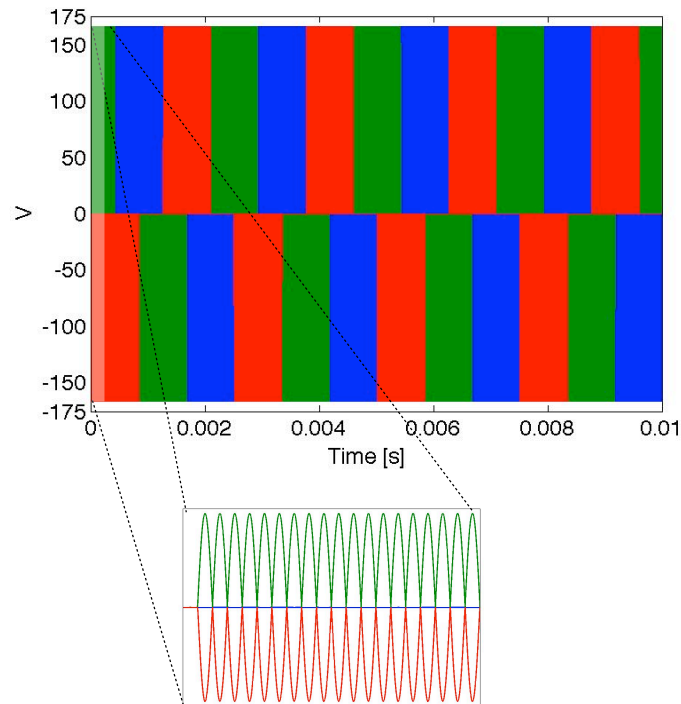
Figure 7.13 400Hz three-phase synthesized AC voltage (Matlab Simulink model shown in Figure A7.2 in Appendix F)

Next, the analysis is focused on the efficiency of the proposed AC converters. For the result to be meaningful, the losses of the HFAC/AC modules should be compared with the losses in DC/AC converters with equivalent functionality. Since most of the on-board AC motors operate as three-phase machines (e.g. three-phase permanent magnet synchronous motor (PMSM) for the EPAS application) and based on the fact that the investigation is similar for the single and three-phase converters, the following efficiency review is focused on the comparison between HFAC/3-phase AC and DC/3-phase AC circuit topologies.

For reference, Figure 7.14 illustrates the circuit diagram of the standard DC to three-phase AC inverter. The module integrates six power switches which, depending on the

target application characteristics can be either IGBTs, MOSFETs or other switching devices. For the present study, the MOSFET is the most suitable due to the rationales outlined at the beginning of this Section. The specific characteristics of the power switch are the same as the MOSFET features considered in Section 7.2 (resistance of 42mΩ and rise and fall time of 118ns and 51ns, respectively).
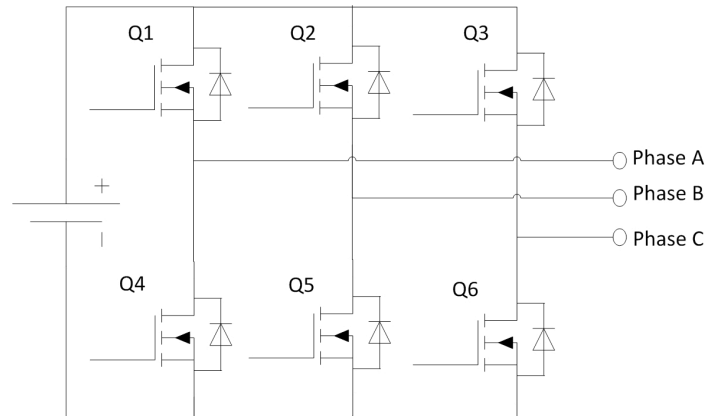
Figure 7.14 Circuit diagram of DC to three-phase AC inverter

The losses in the DC/AC inverter include:

- switching losses for all six MOSFETS, calculated using Equation 7.6:

$$Losses_{Switching} = f_{Switching} \cdot (\frac{1}{2} \cdot P_{loss\_on} \cdot T_{on} + \frac{1}{2} \cdot P_{loss\_off} \cdot T_{off}) \cdot 6 \qquad (7.6)$$

- conduction losses for three MOSFETs, since only one switch per inverter *leg* is conducting at any given moment:

$$Losses_{Conduction} = 3I^2 R_{MOSFET} \qquad (7.7)$$

Similarly, the losses in the HFAC/AC bridge include only conduction losses, but for a double number of switches compared to the DC counterpart circuit. Figure 7.15 illustrates the losses in the two converters[4]:

---

[4] A frequency equal to 20kHz has been considered for the calculation of the switching losses.
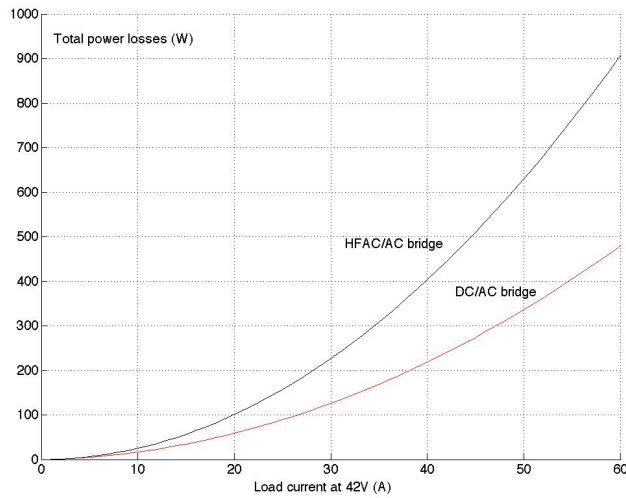
Figure 7.15 Power losses in the HFAC/AC and DC/AC inverter modules

It is observable in Figure 7.15 that the HFAC/AC bridge is less efficient than the DC/ AC circuit. Specifically, for a load current of 20A at 42V, the difference between the two is of approximately 50W. Table 7.3 includes the figures for several values of the load current as well as the estimated efficiency of the two drives.

Table 7.2 Efficiency of the HFAC/AC and DC/AC inverters, for several load current values

Load current (A)	Power losses (W)		Efficiency	
	DC/AC	HFAC/AC	DC/AC	HFAC/AC
10	17	25	96%	94%
20	50	100	94%	88%
30	126	227	90%	82%
40	218	400	87%	76%
50	336	630	84%	70%
60	480	907	81%	64%

The losses in the HFAC/AC circuit are approximately double the losses in the DC/AC drive. This is because the conduction losses in HFAC module are effectively double the conduction losses in the equivalent DC/AC circuit. Also, although the DC circuit has

the disadvantage of the switching losses, these are much lower in comparison to the conduction losses. Therefore, the DC/AC inverter appears to be the better of the two topologies for interfacing three-phase AC loads. Consequently, in order to avoid losses of up to 900W (the value corresponding to the HFAC/AC drive for a load of 60A at 42V), it is preferable to connect these loads directly to a DC bus within the vehicle. This reason, along with other rationales presented in the next Chapter, underpins the proposal for a 42V DC bus alongside the HFAC bus as suggested in Section 4.4.

7.4 Conclusions

Chapter 7 has presented potential HFAC/DC and HFAC/AC power converter modules. First, a prospective synchronous HFAC/DC power converter topology based on ZCS has been discussed. The rationale underpinning this choice is the high efficiency of the module. Power MOSFETs have been selected as the switching components of the circuit, due to their low conduction losses and fast transition times.

A candidate HFAC/AC (single-phase and three-phase) power converter has been analysed. The circuit uses MOSFETs and, alike to the HFAC/DC converter, two inverse-series switches are employed as the basic switching element.

The two HFAC power converters discussed are not novel within the area of power electronics. Nonetheless, these topologies have been chosen as being the most suitable for the present study due to their high efficiency. Since the integration of a HFAC bus aims to reduce significantly the on-board energy losses, the efficiency aspect is of great importance. Calculations presented in Section 7.2 indicate that the efficiency of the HFAC/DC converter is higher compared to the efficiency of a comparable DC/DC converter. Specifically, up to 110W can potentially be saved at the power conversion stage by replacing a 2kW 42V/14V DC converter with a 100V HFAC/ 14V DC converter.

The investigation of the HFAC to AC power conversion suggests that the present cycloconverter technology is less efficient compared to DC/AC inverter drives. Although the latter has the disadvantage of incurring switching losses compared to the HFAC drive, the fact that it employs only six MOSFETs compared to twelve in the equivalent HFAC/AC circuit makes the DC/AC inverter a more efficient alternative. In fact, calculations presented in Section 7.3 indicate that the losses of the HFAC circuit are almost double and can potentially peak at 907W for an AC load of 42V, 60A.

The results for the two types of HFAC converters are different. On one hand, the HFAC/DC converter appears to be a suitable candidate for the power conversion sub-system, while the present HFAC/AC converter technology is not yet a feasible replacement for the DC/3-phase AC drive. It should also be noted that although the HFAC/DC converter is more efficient in comparison to the equivalent DC/DC converter, most of the DC loads in the current vehicle electrical architecture do not require this power conversion stage and therefore HFAC may again be at a disadvantage.

The conclusion of this Chapter is, therefore, that a system-level analysis of the auxiliary electrical system is required in order to estimate the overall efficiency. Such an investigation, which is based on the advantages and disadvantages of HFAC for all the sub-systems within the vehicle is presented in Chapter 9.

Chapter 8

The electrical loads sub-system

8.1 Introduction

Chapter 8 presents the investigation of HFAC benefits for the fourth and last component of the vehicle electrical system; namely, the electrical loads subsystem. The aim is to indicate whether the current actuators employed in the vehicle can be replaced by more efficient and/or lightweight mechanisms which are based on, or can be introduced by, the exploitation of HFAC power.

As a guide to the analysis in the present Chapter, the following general characteristics of the on-board electrical applications have been considered:

- the power demand,
- the duty cycle, and
- the energy regeneration capability.

The reason for choosing the three characteristics detailed above as a guide to the present analysis is that these define the interface between the applications and the electrical system. The three features are further detailed below.

The power demand attribute refers to:

- the average, peak and transient voltage and current requirement,
- the type of power, such as AC or DC,
- the type of power electronic drive employed, such as voltage or current power drives.

The duty cycle relates to the proportion of time a load is being supplied power, to the duration the vehicle is being operated. For example, applications such as the electric oil pump have a continuous duty cycle. Conversely, intermittent duty-cycle loads operate

on a discontinuous basis. Examples of intermittent loads include the windscreen wipers or the brake lights.

The third feature is characteristic to electrical applications which have a dual functionality. On one hand, these operate as actuators, transforming electrical power into mechanical power. On the other hand, under different vehicle operating conditions, the same application transforms mechanical power into electrical power. This energy is stored in the on-board battery for later utilisation.

The investigation of HFAC power benefits for loads integrating rotary actuators is of particular importance due to the potential seamless integration of AC machines onto the proposed bus. The potential benefit of HFAC power for other electrical loads, such as heaters and the lighting system, is in supplying the voltage or current amplitude that improves their functionality compared to the conventional 14V DC supply[1]. However, there are yet no potential actuators to replace the existing heating resistors or lighting bulbs/LEDs that can benefit from HFAC power. This argument is supported by other studies (Masrur et al., 1998a, Masrur et al., 1998b), which indicate that DC loads operate equally well with an AC or a DC supply.

Load properties including power level demand, power electronic drive, transient current, duty cycle and regenerative capability are discussed in Section 8.2. Next, an in-depth study into the applicability of HFAC for motor-actuated loads is included in Section 8.3. Section 8.4 includes the main findings and presents the conclusions of the Chapter.

8.2 General aspects related to the applicability of HFAC power for auxiliary loads

This Section focuses on the following four points:

---

[1] The 14V DC supply is standard in the majority of passenger vehicles. Commercial vehicles typically require a 28V DC supply.

1. The feasibility of HFAC power for high voltage and current loads, as well as the suitability of the technology for fast-transient applications.

2. The implications of the load duty cycle for the proposed power bus,

3. The HFAC power converter modules for voltage or current fed loads,

4. The potential integration of regenerative electrical loads onto a HFAC architecture.

The first item above has been addressed in Chapter 5. Specifically, the Chapter has presented arguments which advocate the applicability of HFAC power for applications with a cumulative demand of 4kW at 100V. Also, modelling and simulation results have indicated that a suitable design of the HFAC power supply can successfully cope with a current rise time as low as 300μs. This result suggests that the dynamic capability of the proposed bus satisfies the transient time constant of state-of-the art applications (e.g. ISG or VVA), which is typically in the order of milliseconds (Chang, 2003, Qiu et al., 2004, Klode et al., 2006).

With regard to the duty cycle feature of electrical applications, the HFAC distribution system is expected to dissipate more power under no-load conditions compared to the DC network. The reason is that the HFAC bus incurs a constant resistive power loss, regardless of whether the load is being operated or not. As shown in Figure 8.1(a), current flows from the DC source to the load only when the latter is active. Conversely, as illustrated in Figure 8.1(b), power is transmitted onto the HFAC ring continuously. Thus, when the load is *off*, the HFAC system dissipates energy due to the following operations:

- DC/HFAC power conversion,
- HFAC power distribution, and
- HFAC/DC power conversion.
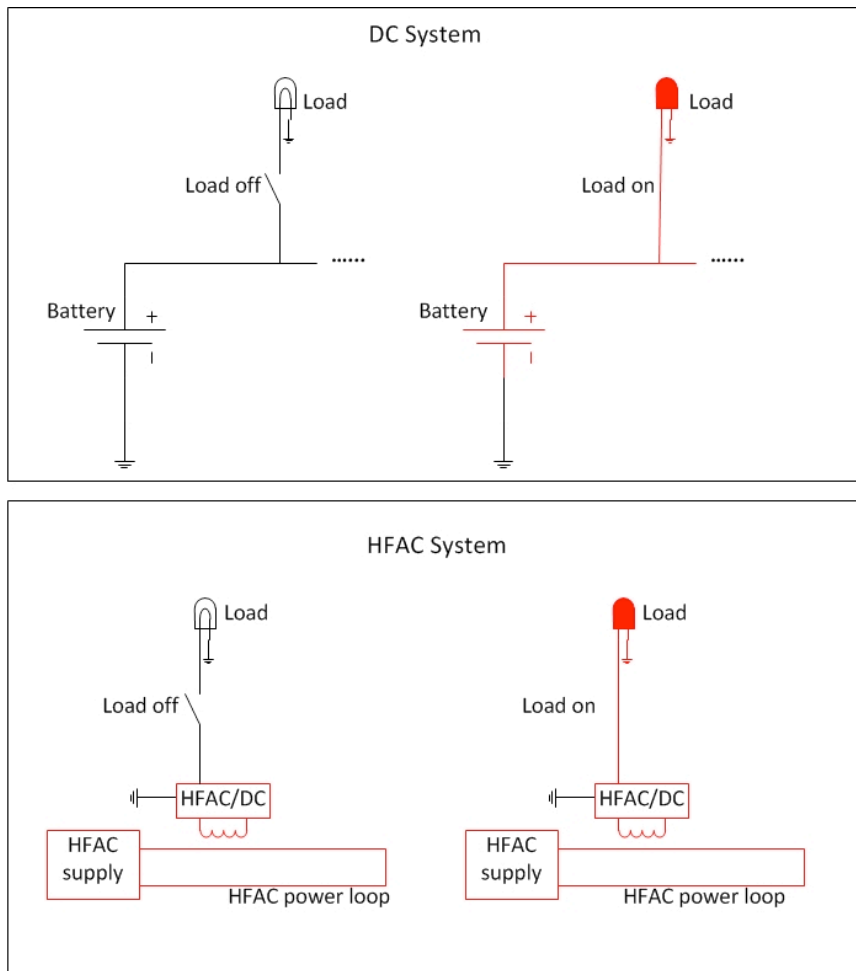
Figure 8.1 (red colour indicates current flow)
(a, top) Intermittent load operating on a DC electrical system
(b, bottom) Intermittent load operating on a HFAC electrical system

The no-load power loss aspect has also been reported in the study by (Kokes, 1997). For the specific case study of a 4kW bus presented in the referenced work, the quiescent or no-load power loss has been shown to be higher than 50W.

The HFAC system presented in this work includes components aimed at minimising the energy losses. Particularly, the power generation sub-system discussed in Chapter 5 is based on a soft-switching technique in order to maximise the efficiency of the DC/ HFAC conversion process. In addition, as shown in Chapter 6 for the power distribution sub-system, HFAC conductors are more energy-efficient compared to the existing DC

cable technology. Moreover, the main rationale for the proposition of ZCS converter topologies in Chapter 7 is their high power transformation efficiency. Therefore, the proposed HFAC system is arguably the most efficient configuration.

It can be argued that the no-load power loss is not relevant, since a set of loads are operated on a continuous basis. This aspect has been indicated in Chapter 6. The measurements of the battery current have shown a steady current consumption equal to 13A for an idle ICE while no loads have been operated by the driver.

Within the context of the type of power electronic drive, it is important to distinguish between voltage or current supplied loads since the interfacing circuitry employed can differ considerably. Voltage fed loads include, for example, heater elements, while white LED lamps require a constant current supply. The main reason for this prerequisite is the requirement to maintain the same luminous intensity for each LED within the lamp (DallasSemiconductor, 2004).

Figures 8.2 (a, b) show typical DC voltage and current drive circuits, respectively (Emadi, 2005). The difference between the two topologies is the circuit output impedance. Namely, while the voltage-fed circuit has a low impedance, the current-fed module impedance is theoretically very large.
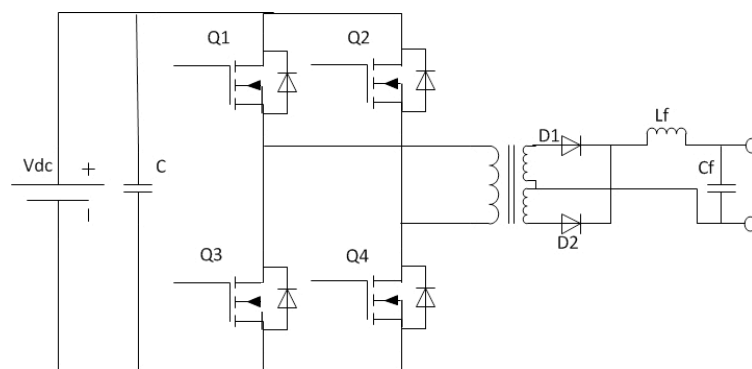
Figure 8.2a Schematic diagram of voltage-fed DC/DC converter

Practically, by removing the output filter inductor from the voltage fed circuit, and adding a *link* inductor in series with the DC voltage source, the current-controlled circuit can be obtained. The role of the attached inductor in Figure 8.2 (b) is to provide the high impedance of the DC bus at high frequency, while the capacitor in parallel with the voltage source in Figure 8.2(a) aims to secure the opposite effect, i.e. to minimise the impedance of the circuit (Pressman, 1998).
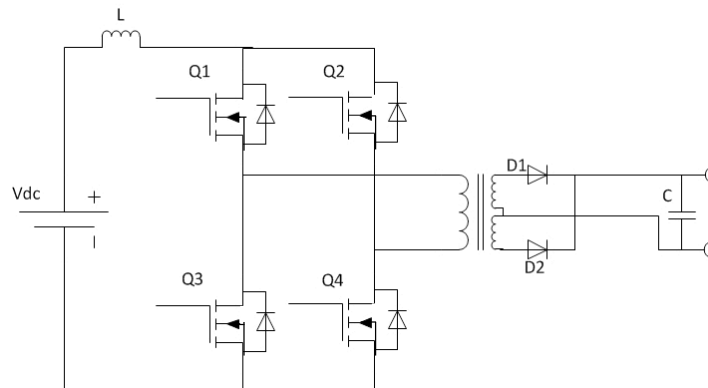
Figure 8.2b Schematic diagram of current-fed DC/DC converter

Unlike the DC/DC converter topologies, where the current-fed and voltage-fed circuits have a different structure, the HFAC/DC converter proposed in Chapter 7 supplies voltage and current loads alike. Since the circuit is based on a regulated DC bus control, it can integrate either a voltage-based control or a current control loop, depending on the requirement of the application. Therefore, within an on-board HFAC bus, the same module structure can interface the two types of electrical loads. This can be achieved by simply updating the circuit firmware for voltage or current control and using the appropriate sensors.

The implication of this finding for the vehicle auxiliary electrical system is dependent on the number of applications which utilise voltage and/or current supply modules. As indicated in Chapter 7, most DC consumers in today's automobile do not require a DC/DC converter. Consequently, an assessment regarding the ramification and importance of this characteristic is dependent upon the specific vehicle configuration. Potentially, a benefit can be identified for high-end automobiles employing a large and diversified

number of electrical auxiliaries. From the perspective of the OEM, it can be argued that the production costs can be reduced as a result of an increased circuit functionality.

The fourth and final aspect discussed in the current Section refers to the possibility of integrating loads with an energy recuperation capability onto the HFAC bus. Such applications include, for example, the ISG (discussed in Chapter 5). Equally, systems with a similar functionality include state-of-the art components such as the photovoltaic cells which transform the thermal and light energy into electrical energy (as employed for example in the third generation Toyota Prius).

The best integration of this category of loads into the electrical system is the approach that manages most effectively the produced electrical power. The energy can be:
• either distributed to the electrical consumers directly, or
• accumulated in the on-board storage sub-system for later use.

The former has been suggested by (Bose et al., 1996) for a HFAC electrical system in a HEV (presented in Chapter 3, Section 3.2). Figure 8.3 illustrates the electrical power flow suggested in the cited work.
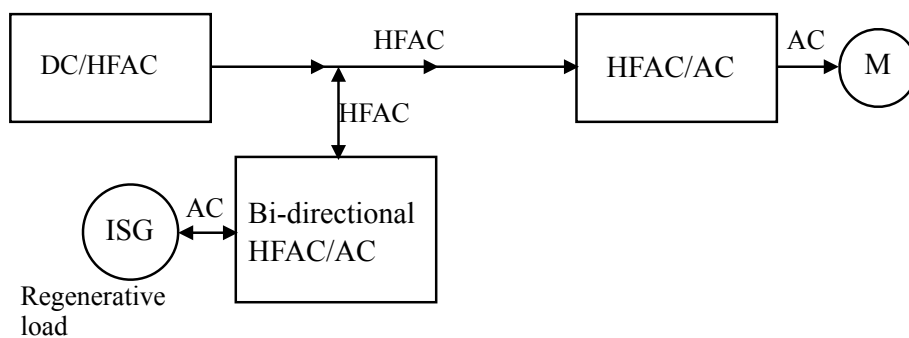
Figure 8.3 Power flow in the HFAC system proposed by (Bose et al., 1996)

Figure 8.3 shows that the energy recuperated from the ISG can only be distributed to the consumers connected to the HFAC bus. There is no indication in the study by (Bose et

al., 1996) on the operation of the system when the recuperated energy is higher than the consumed energy.

With reference to Figure 8.3, in order to make effective use of the captured energy from the ISG, a mechanism should be implemented to allow the surplus of recuperated energy to be stored in the vehicle battery. Although this option cannot be always exercised, for example when the battery is fully charged, it is essential for all the electric and hybrid electric powertrain configurations.

Figure 8.4 presents the two possible options of connecting regenerative loads to the bus:
1. the load can either be connected to the HFAC bus, or
2. the load can be attached to the parallel 42V DC bus.
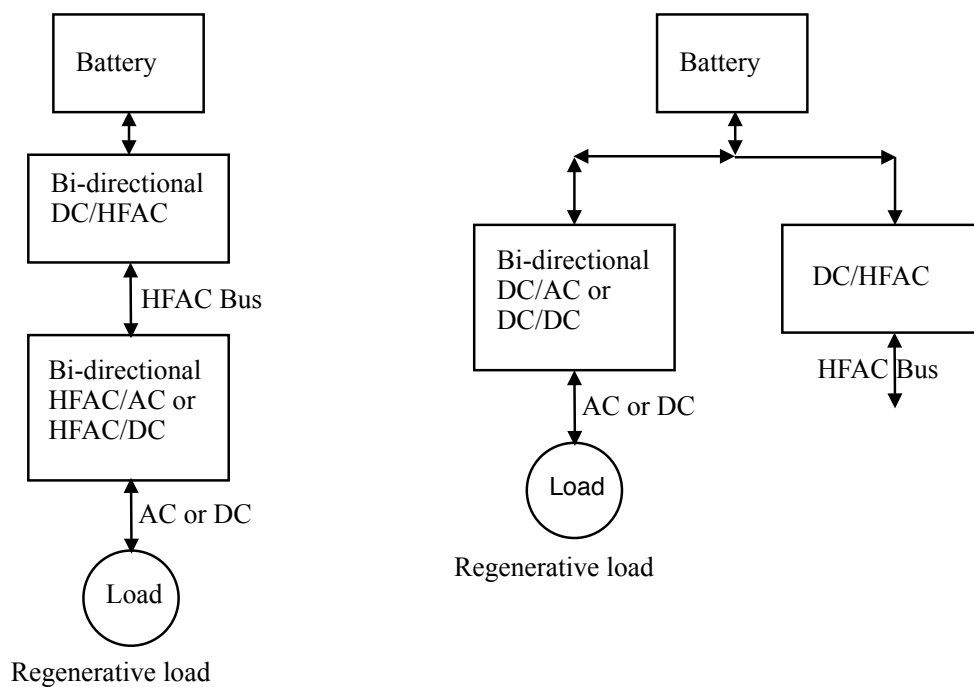
Figure 8.4
(a, left) First possible connection of regenerative loads to the HFAC bus
(b, right) Second possible connection of regenerative loads to the proposed bus

The second option for integrating regenerative loads onto the HFAC bus is proposed. The reasons underpinning this choice can be summarised as follows:

1. Option 1 (Figure 8.4 (a)) has several disadvantages. Namely:

    a. The recuperated energy which is not consumed instantaneously by the loads must be converted first to HFAC and subsequently to DC. This process is not optimal, since two power conversion stages are necessary in order to save the surplus energy.

    b. In addition, two bi-directional power converters are required. As previously discussed in Chapter 7, HFAC power converters employ twice the number of power MOSFETs compared to equivalent DC modules. Hence, power conduction losses, which are higher than switching losses, are effectively doubled. Consequently, part of the recuperated energy will be dissipated unnecessarily within these power transformation stages.

    c. Lastly, the two converter modules shown in Figure 8.4(a) must be synchronised to operate in-phase with the HFAC bus voltage. Thus, in addition to the control of the two converters, a third supervisory control unit may be required thus adding further complexity and cost to the system.

2. The advantages of Option 2 (Figure 8.4 (b)) over Option 1 are outlined below:

    a. Only one power transformation stage is required, compared to two for Option 1.

    b. Existing technology can be utilised for the bi-directional DC/AC or DC/DC converter, since HFAC is not employed in this part of the electrical system.

    c. The ISG is an application which employs a high-torque electrical motor. As will be discussed in the following Section, such actuators should be supplied by a DC power source rather than a HFAC supply.

This Section has discussed four aspects related to the feasibility and advantages of HFAC for electrical loads. Amongst the benefits, it can be argued that:

1. HFAC is feasible for high voltage or current loads. Also, the dynamic of the bus is appropriate for the current slew rate of state-of-the art applications.

2. HFAC/DC converters are suitable for both voltage and current supplied loads. This contrasts with the DC modules, which have a function-specific structure.

Conversely, the analysis has indicated that the present technology imposes the following limitations for the HFAC bus:

1. The existence of a quiescent power loss. This aspect is further discussed as part of the system-level analysis in the following Chapter.

2. Regenerative loads benefit from a direct connection to the DC bus, rather than an integration via the HFAC bus.

8.3 Motor loads

This section discusses the feasibility and potential benefits associated with the use of HFAC power for motor actuators within vehicles. Consideration is first given to low torque actuators as used in electric radiator fans and pumps, before extending the discussion to take into account the integration of HFAC within high-torque applications as employed in the EPAS system.

8.3.1 Low torque motor loads

Automotive applications such as electrically driven cooling fans, pumps and windscreen wipers generally employ 14V DC motors with a rated torque characteristic that peaks under 2Nm. As previously discussed in Chapter 7, such actuators can be replaced by more compact 400Hz, AC induction machines interfaced from the HFAC bus by either three-phase or single-phase frequency converters.

If 400Hz AC motors are to feasibly replace the present low torque DC motors in vehicles, they must offer the same torque-speed characteristics that are found within today's DC machines. It is known that the starting torque output of a DC machine can be considerably higher than that found within a comparable AC induction motor

(Masrur et al., 1998a), and therefore it is necessary to determine under what conditions AC machines may successfully take the place of DC motors.

For this purpose, performance data has been collected from commercially available AC (SL-MTI, 2010, ArcSystems, 2008) and DC machines (BoschMotors, 2010), appropriate for use within automotive applications. Tables 8.1 and 8.2 include the operating point, size and potential use within the vehicle for the DC and AC induction machines, respectively.

For the particular case of a 40Ncm DC motor, as employed for example in a throttle valve control actuator (Iles-Klumpner et al., 2006), Figure 8.5 presents the process of matching the operating envelope of the DC and AC motors. The graph includes the torque-speed characteristic for a 160W DC motor, with the nominal operating point at 40Ncm, 3,700rpm (denoted as point 2 on the graph). The similar characteristic curve for the 425W induction motor, which has a nominal torque of 34Ncm at 11,100rpm, is denoted as point 1.

Table 8.1 Specification of commercially-available DC motors

Operating Point						Dimensions			Application
Rated Power (W)	Rated Speed (rpm)	Rated Torque (Stall) (Ncm)	Voltage (V)	Current (A)	Efficiency (%)	Diameter (mm)	Length (mm)	Mass (kg)	
34.5	3,360	10 (49)	12	6.8	42	52	110	0.44	Windscreen Wipers
84	4,000	20 (97)	12	12	58	59	100	0.7	Power Windows
100	3,800	20(183)	12	12	70	73	100	1.1	Radiator Fan
120	4,600	25(198)	12	15	67	73	100	1.1	Heating system, Blower
140	5,250	25(194)	12	17	69	73	100	1.1	Electric Rooftop Actuator
160	3,700	40(190)	12	18	74	73	110	1.12	Throttle Valve Actuator
181	3,450	50(400)	12	20	75	74	74	1.5	Fuel Pump

Table 8.2 Specification of commercially available 400Hz AC motors

Operating Point						Dimensions			Possible Application
Rated Power (W)	Rated Speed (rpm)	Rated Torque (Stall) (Ncm)	Voltage (V)	Current (A)	Efficiency (%)	Diameter (mm)	Length (mm)	Gear Ratio	
179	3,375	50 (84)	115	1.1	81	45	54	3.2:1	Windscreen Wipers
246	4,000	59 (95)	115	1.4	87	46	59	2.7:1	Power Windows
425	3,800	99(214)	115	2.4	88	46	75	2.9:1	Radiator Fan
647	4,600	132 (219)	115	3.3	95	46	86	2.35:1	Heating system, Blower
647	5,350	114 (188)	115	3.3	95	73	100	2:1	Electric Rooftop Actuator
425	3,700	102 (222)	115	2.4	88	46	75	3:1	Throttle Valve Actuator
725	3,367	207 (411)	115	3.7	95	66	80	3:1	Fuel Pump
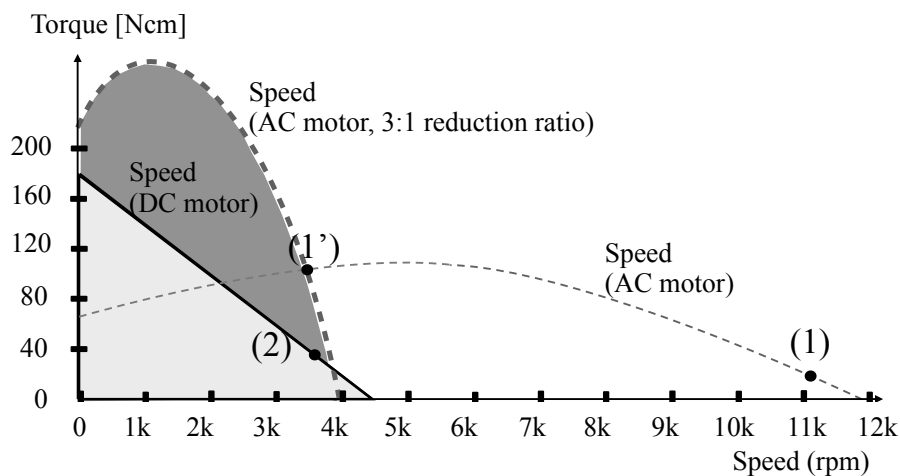
Figure 8.5 Operating torque vs. speed envelope of 160W DC and 425W AC machines

It is noteworthy that the starting torque of the two machines differs by a ratio of approximately 3:1. As shown in Figure 8.5, if a suitable gear reduction ratio is integrated within the AC motor, its nominal operating position shifts from point (1) to point (1') and the starting torque increases to more than 200Ncm. Figure 8.5 highlights also that with the inclusion of a fixed gear reduction, the torque capability of the AC motor increases up to threefold compared to the DC counterpart in the 1,000rpm to 3,000rpm region. In particular, the torque capability of the two candidate machines for a

rotational speed of 2,000rpm is 255Ncm and 85Ncm, respectively. High torque values can be a potential benefit for the throttle valve actuator[2]. Since the throttle valve controls the air flow within the ICE (and therefore the power output of the ICE), the actuator must manage a larger volume of air for more powerful engines. Therefore, a single actuator type based on a 400Hz induction motor can potentially be used for a wide range of ICE capacities. The implication is that OEMs can simplify the product line without any limitation to the scope of the actuators.

Table 8.3 presents a summary of the relevant data-set for this exercise and shows that with the appropriate gear ratio a 425W AC machine can successfully meet the specified stall and nominal torque requirements for the automotive application.

Table 8.3 Comparison between 160W DC and 425W, 400Hz AC motors

Motor type	Voltage[V] (line to line rms for AC)	Nominal Power [W]	Nominal Current [A]	Nominal Speed [rpm]	Nominal Torque [Ncm]	Peak Stall torque [Ncm]	Length [mm]	Diameter [mm]	Mass [kg]
DC	12	160	18	3,700	40	190	110	73	1.12
AC	200	425	2.41	11,100	34	74	75.3	45.7	-
AC, with gear reduction of 3:1				3,700	102	222			

Repeating the steps above for a wider selection of motors, the study shows that 400Hz induction motors satisfy the torque specification of DC machines of up to approximately 180W. Beyond this limit, AC motors fail to meet the high starting torque requirement of the DC motors, while providing the same torque vs. speed envelope as the latter at the same time. If a larger gear reduction mechanism is integrated, the proposed motor technology can handle a higher starting torque, although this comes at the price of greatly reduced speed which may be below the base speed of the equivalent DC motor. As a result, a balance is required when choosing the gear ratio, as both the starting torque and the operating area of the machine have to match the comparable DC actuator.

---

[2] For reference, a picture of a throttle valve system is shown in Appendix G, Figure A8.1

This conclusion is supported by other studies contained within the literature (Masrur et al., 1998b). Although the majority of motor loads require less than 200W, including fuel pumps, electric cooling fans, window and seat motors, blower and windscreen wiper motors (Bosch, 2004), there are also DC machines with a higher power rating than the above threshold. For example, the power rating of motors found in electric water pumps and oil pumps can extend to as much as 500W (Lukic and Emadi, 2002, Lukic and Emadi, 2003, Miller and Nicastri, 1998).

Therefore, based on present motor technology, off-the-shelf 400Hz machines can feasibly replace DC motors with a maximum stall and nominal torque capability of 4Nm and 2Nm, respectively. However, it should be noted that future technological improvements can possibly extend these limits, since the suggested nominal torque limit for a similar study conducted more than a decade ago was only 0.9Nm (Masrur et al., 1998b).

Benefits of 400Hz induction motors

For equivalent 400Hz AC machines, Figure 8.6 illustrates the potential reduction in packaging volume within the vehicle as a function of the machine's power rating. The Figure shows that a significant reduction, in the order of 60%, is realisable by replacing DC motors with AC motors with a power rating of up to 181W. Based on a 1:1 relationship between machine volume and mass, it is expected that a similar reduction of approximately 60% in the mass of the electrical machine can also be achieved via the transition from a DC machine to an AC induction motor (Masrur et al., 1998a).

As previously shown in Table 8.1, within an automotive context, the mass of individual DC machines was found to be typically between 0.4kg – 1.5kg. Therefore, considering an average mass of 1kg per DC motor[3], and that up to 50 such devices may be integrated within a typical passenger vehicle, the potential vehicle mass saving can be

---

[3] The specific value of 1kg has been chosen as being both the average and median value for the DC machines listed in Table 8.1. This assumption is required to simplify the analysis in this Section.

estimated at approximately 30kg, which is a noteworthy advantage. It should be highlighted that this is only a first-order approximation and it is based on the assumption that the AC machines detailed in Table 8.2 include the required gear reduction mechanism.
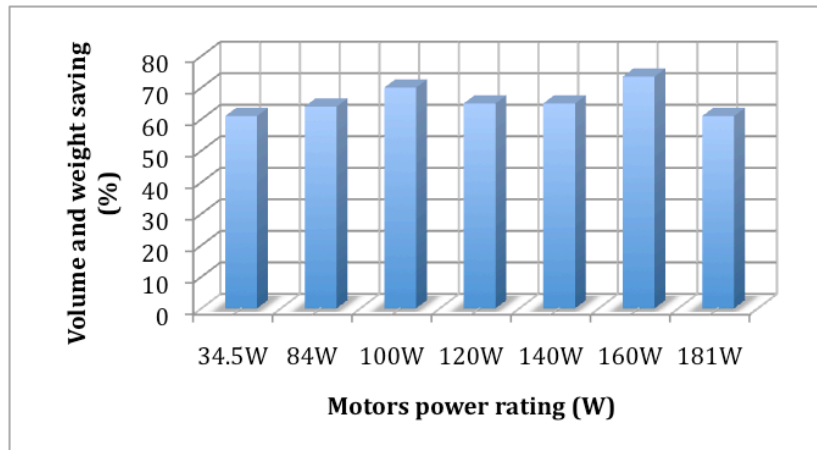
Figure 8.6 Potential packaging volume and mass saving of 400Hz AC machines compared to DC motors, vs. power rating (W)

In addition to the possible reductions in system mass and packaging volume, Figure 8.7 highlights efficiency improvements between 25% and 100% associated with the use of 400Hz induction motors as compared to DC machines. Efficiency data for commercially available motors are available only for their respective nominal operating points. It can be assumed that the machines will operate in a close vicinity of their nominal, i.e. most efficient, operating region. Assuming an average power rating of 100W for continuously operating low-torque DC motors, and considering the possible mean energy saving of 30% (based on Figure 8.7), the potential power saving for such machines is in the order of 30W per device.

In order to determine a more accurate estimate of the system efficiency, consideration should be given to the duty cycle of the different motor actuators. Specifically, whereas loads such as the fuel pump have a continuous duty cycle, applications including windscreen wipers or power windows are only operated on an intermittent basis. A duty

cycle of 0.3 has been indicated in (Bosch, 2004) as an appropriate value for motors running intermittently. Consequently, a potential individual saving of approximately 10W for such machines can be achieved.
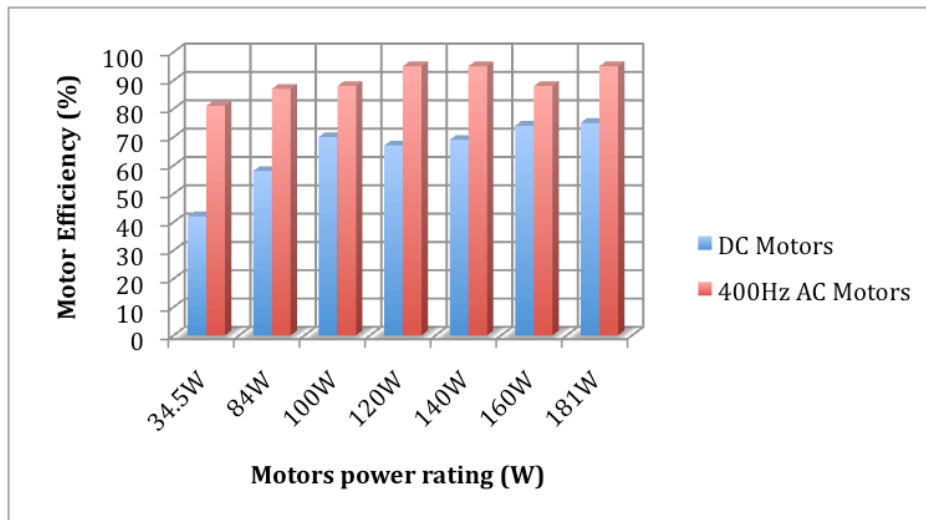
Figure 8.7 Efficiency of 400Hz and DC motors at the nominal operating point vs. power rating (W)

As a result, considering the estimated potential saving of 30W and 10W for each continuous and intermittent machine, respectively, and noting that only a small proportion of the motor loads have a continuous operation, the total potential power saving for a typical vehicle may be in the region of 500W.

The efficiency improvements shown do not take into account the small losses caused by the gear reduction integrated with the AC motors, nor the conduction losses within the cycloconverter. However, the efficiency of a fixed ratio transmission is typically high, in the order of 97% (Jordan, 1994). Also, for the maximum output power of 181W considered in this exercise, the cycloconverter current is 1.6A at 115V; since only the upper or lower side in each converter leg is conducting at any given moment, only 6 power MOSFETs are simultaneously in the on-state. As a result, for a current value of 1.6A and for a MOSFET with an internal resistance equal to 40mΩ, the total I^2R losses for the circuit peak at just 0.62W.

The HFAC/three-phase AC cycloconverter can be either integrated with each AC motor in modules operating as separate entities, or a single cycloconverter can be used and all motors connected to the 3-phase 400Hz AC bus. Although the latter method is initially less expensive, due to the employment of a single frequency converter, the former approach is potentially more attractive since the modules can be used in a plug-and-play mode. This can lead to an effective maintenance procedure, which in turn may save cost over the lifetime of the vehicle.

Conclusively, based on a number of assumptions regarding the number of electrical motors in the vehicle and the duty cycle of the majority of these, potential vehicle mass and electrical power saving in the region of 30kg and 500W can be realised, respectively.

Based on the fact that approximately 5% of the fuel consumed in a medium-sized automobile is used to drive the alternator and transport the combined weight of the starter, battery and alternator, approximately 0.1L/100km can be attributed to every 10kg added to the vehicle or 100W of drive power (Bosch, 2004). Mapping the figures above to these potential savings in terms of terms of mass and electrical power associated with the use of 400Hz motors, a possible fuel consumption saving of approximately 0.8L/100km (or extended vehicle range by 5 miles per imperial gallon) is feasible.

Several aspects should be noted with regard to the three-phase AC system supplying the 400Hz AC motors. First, additional weight and packaging volume can potentially be saved at the power distribution level, since the three-phase AC system requires less copper than a DC system to distribute the same amount of power (Miller, 1996). Also, the three-phase system is more fault-tolerant: if one of the lines fails, power distribution is degraded but nonetheless can be maintained by the remaining two lines. The implication is that three-phase AC motors are preferable to DC or single-phase AC machines for the safety-critical systems such as the EPAS or the EMB. However, a

possible issue related to the three-phase system is that it may require a load-balancing mechanism amongst the phases.

8.3.2 High torque motor drives

Within the context of the present analysis, high torque refers to applications with a rated requirement above the 2Nm capability of 400Hz AC induction machines. Such loads include, for example, existing consumers such as the EPAS (7Nm), air-conditioning (6Nm) and proposed state-of-the-art systems such as brake-by-wire, VVA, electromechanical active suspension or the full electric gearbox. All of these applications integrate motors with a rated torque of 3Nm, 4Nm, 50Nm and 120Nm, respectively (Iles-Klumpner et al., 2006, Murakami et al., 2001).

As a result, high torque actuators are used within these applications. These may include permanent magnet (PM) DC or three-phase interior or surface-mounted machines. For example, a 320W PM DC motor has been shown to be feasible as a possible VVA actuator for one valve (Chang, 2003). Also, it has been reported that a three-phase, surface-mounted PM AC machine rated at 3.1kW is suitable for the heating, ventilation and air conditioning (HVAC) system in vehicles (Naidu et al., 2003).

It is noteworthy that these high torque applications require a higher voltage than the current 14V. Particularly, for the two examples above, a 42V DC supply has been considered a pre-requisite.

In order to interface such actuators from the HFAC bus, two methods can be employed. A first possibility is to transform the HFAC into DC, using ZCS synchronous rectifiers as described in Chapter 7, which in turn supplies a high-torque PM DC motor. The alternative approach is to utilise an existing three-phase AC machine, but replace the standard DC/AC inverter with a HFAC/AC drive. Such an inverter can synthesise the low-frequency AC from the HFAC based on ZVS and PDM.

The second solution is preferable to the former as the intermediary stage of converting HFAC to DC can be eliminated. In addition, since soft switching is used, a HFAC/AC converter is expected to offer benefits such as lower voltage EMI and reduced motor torque ripple in comparison to the equivalent DC/AC bridge (Bendyk et al., 2007).

In order to test these assumptions, a typical high torque load has been considered; namely, the EPAS application, which is a standard technology on the majority of vehicles today either as a full-electric or electro-hydraulic option. Both PM DC and PM AC motors are suitable for EPAS, although the latter in the form of a surface-mounted PM synchronous motor (PMSM) is the preferred choice due to its high specific torque, coupled with high efficiency and low torque ripple (Liu et al., 2004, Hur, 2008). The torque oscillation is a performance attribute of particular interest, since it causes not only an audible noise, but also mechanical vibration within the steering column which is propagated through to the steering wheel (Bianchi and Bolognani, 2000).

To support this study, an experimental test-rig of a production EPAS system is employed to create a realistic load profile for the PMSM actuator. This setup is described further in Section 8.3.2.1. Subsequently, in Sections 8.3.2.2 to 8.3.2.6, a mathematical model of the experimental apparatus is described and used to extend the study by providing an insight into the operation of HFAC/AC and DC/AC drives for the EPAS application. In particular, the model is used to compare the voltage harmonic content and the PMSM torque ripple associated with the operation of the two power electronic drives.

8.3.2.1 *EPAS Experimental Apparatus*

The experimental column-assist EPAS system is shown in Figure A8.2 in Appendix G. It includes a variable load in the form of a hydraulic circuit that emulates the typical road forces associated with different steering manoeuvres. The design of the mechanical and hydraulic components of the test rig is described in (Tonius, 2009), while the control of the electrical motor has been developed as part of the present study and is described below.

A detailed description of the column-assist EPAS test rig is included in (Tonius, 2009) and therefore only a brief account of the concept used to emulate the tyre load is included here for reference. The hydraulic circuit setup used to emulate the typical damping forces within the EPAS system includes the following components:

- a hydraulic cylinder within the steering rack[1],
- two needle valves[2], which are valves with an adjustable orifice used to control the flow and hence the pressure within the circuit,
- a fluid reservoir, and
- two pressure gauges, for left and right steering manoeuvres, respectively.

The needle valves have the same adjustment in order to emulate similar forces experienced by the driver while steering in both directions. In order to emulate the steering forces present in vehicles of different mass, the orifice of the two valves can be adjusted accordingly. For example, for vehicles with a higher front-axle mass, the valve orifice can be reduced in order to restrict the flow of hydraulic fluid and consequently increase the pressure within the circuit.

The original production motor attached to the steering column was a 14V, 300W PM DC motor. As part of the study, this machine was replaced with a bespoke three-phase 440W PMSM machine. Information relating to the design of this machine, which is shown in Figure A8.2 (Appendix G), is discussed in (Wang et al., 2010) and will therefore not be repeated here. The full list of machine parameters is included in Table A8.1 in Appendix G. The relevant machine parameters appropriate for this study are summarised below for reference:

- open-circuit phase voltage 12.5V;
- phase current 13A;
- base speed 62.8rad/s (600rpm);
- nominal torque 7Nm;

---

[1] Aston Martin ZF Servotronic 7800. No. turns from lock to lock: 3.04. Maximum travel of rack: 139mm. Outer hydraulic cylinder diameter: 41mm. Inner piston diameter: 26mm. Pinion diameter: 14mm.
[2] Hoke Milli-Mite Forged Metering Valve 1300 Series, type 1335G4Y, 316 Stainless steel material, 1/4 inch Gyrolock connections. Max operating pressure: 5000 PSIG, orifice size 1.19mm.

Figure 8.8 presents a schematic diagram showing the main components, connections and control of the EPAS system. An off-the-shelf device controls the PMSM torque based on two inputs; first, a reference motor current is set using the associated computer software, and second the rotor position signal from the encoder attached to the PMSM.

Using the experimental apparatus, discussed above, a comprehensive test programme was undertaken using a 48V DC power supply. The reason for a higher voltage level than 42V DC is that 48V is the minimum required by the current controller. The results of this activity were used to validate the equivalent EPAS DC model built within the Matlab Simulink environment. The following Section describes the construction and implementation of the mathematical model.
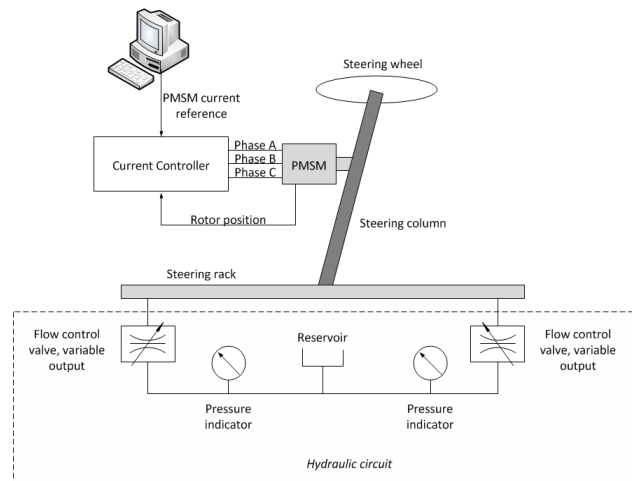
Figure 8.8 Diagram of EPAS experimental apparatus (N.B. the controller is a physical module)

8.3.2.2 Description of the EPAS Model with DC/AC Drive

The EPAS model includes three main sub-systems. A high-level diagram of the model is shown in Figure 8.9 and includes:
- the representation of the PMSM motor, described in Section 8.3.2.1;
- the power electronics sub-system, which implements both the motor control scheme and the DC/AC bridge, and finally
- the sub-system that emulates the load torque for the PMSM,

The latter component of the model is represented as a torque vs. speed lookup table that has been derived from experimental results.
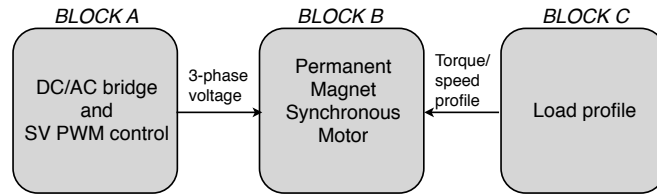
Figure 8.9 Block diagram of the EPAS model

The torque control is achieved via the vector control technique, which is considered superior to other regulation methods such as Volt/Hz, sensorless or flux control and has been extensively described in the literature (Emadi, 2005). For reference, a schematic diagram of this control method is illustrated in Figure 8.10.
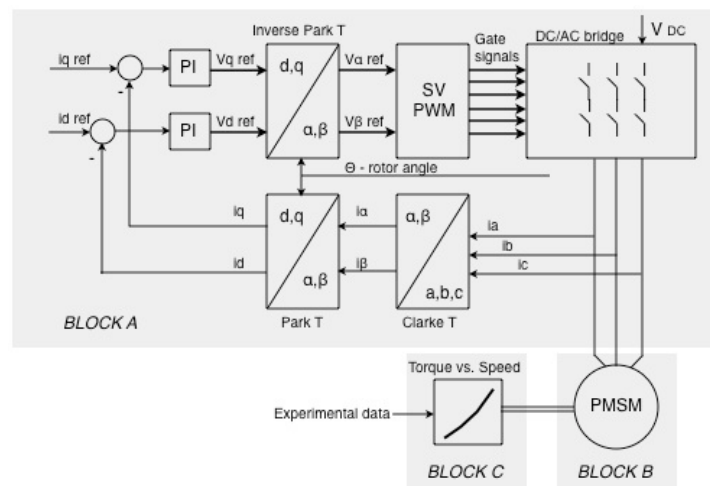
Figure 8.10 Detailed block diagram of EPAS model

Block A, which relates to the vector control, is based on the Clarke and Park transformations method of converting the three-phase motor currents into the *d* and *q* axes components. The current component along the *q-axis* is directly proportional to the motor torque and the current component along the *d-axis* is directly proportional to the motor flux. Therefore, *iq ref* shown in Figure 8.10 represents the torque command to the control system. In addition, since the rotor flux is fixed (determined by the physical

properties of the magnets employed within the PMSM), the current reference along the *d-axis* is set to zero (Emadi, 2005).

An important block in the control scheme in Figure 8.10 is the modulation model. Typical strategies include sinusoidal and space vector (SV) methods, based on pulse width modulation (PWM). It has been reported in the literature that the latter (SV PWM) offers superior performance in terms of low voltage THD, torque ripple, switching losses and high output-to-input voltage ratio (Emadi, 2005, Tsung-Po et al., 1999). Therefore, this modulation technique has been implemented within the control model.

8.3.2.3 Validation of the EPAS Model with DC/AC Drive

Several tests have been carried out in order to validate the Simulink mathematical model. Experimental and simulation waveforms associated with four tests are illustrated in Figure 8.11, and include steady state motor current of 1A and 2A, and current step tests from 3A to 4A, and 4A to 6A.
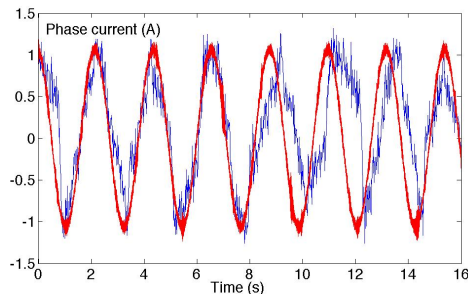
Figure 8.11a 1A motor phase current (A)   Figure 8.11b 1A motor active current (A)
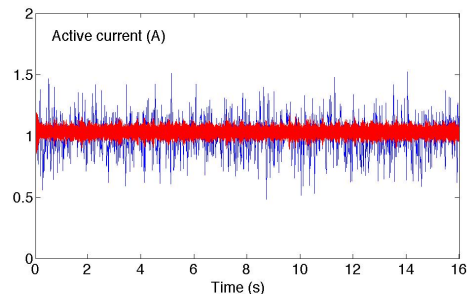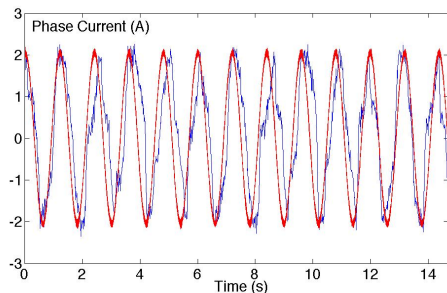
Figure 8.11c 2A motor phase current (A)   Figure 8.11d 2A motor active current (A)
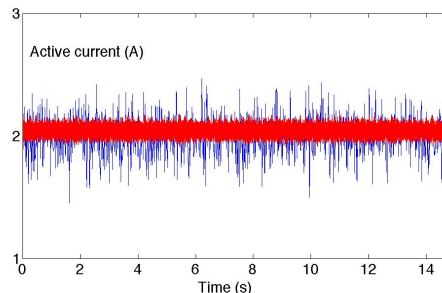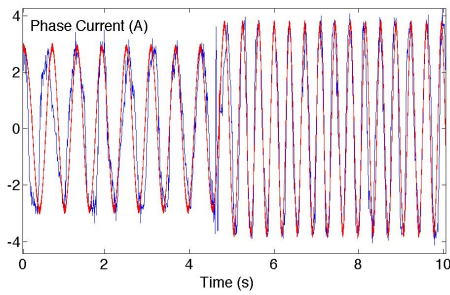
Figure 8.11e 3A-4A motor phase current (A)
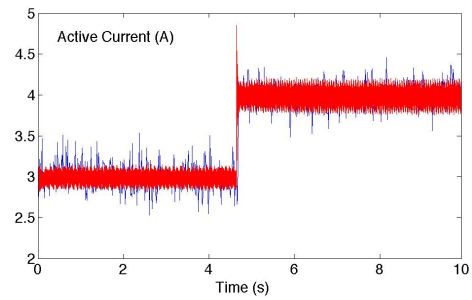
Figure 8.11f 3A-4A motor active current (A)
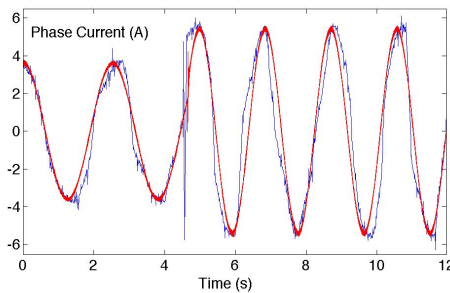
Figure 8.11g 4A-6A motor phase current (A)
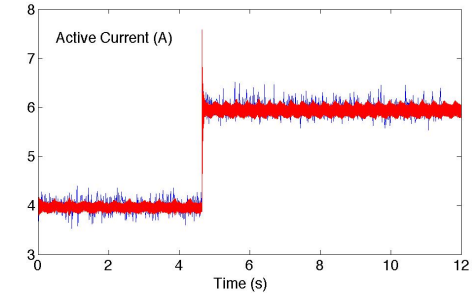
Figure 8.13h 4A-6A motor active current (A)

Figure 8.11 Phase (left) and active (right) motor current, experimental (blue) and simulation (red) results for four tests: 1A, 2A, 3A-4A and 4A to 6A.

The tests have been performed at different pressure levels within the hydraulic circuit, and are representative for the varying load conditions within the EPAS system[3] (e.g. high or low motor load for parking manoeuvres or urban driving, respectively). In particular, the flow in the hydraulic circuit has been adjusted using the needle valves orifice (as previously indicated in this Section) in order to emulate a light load for the first three tests (1A, 2A and 3A-4A motor current) and an incrementally higher road load for the last test. As a result, the different road load characteristics shown in Figure 8.12 have been obtained for the four test scenarios and were implemented as the torque vs. speed load characteristics in the model (Block C in Figure 8.10).

The first two test cases (1A and 2A motor current) and the latter two experiments (3A-4A and 4A-6A) are representative for low-level and medium-level motor assist within EPAS systems for small to medium size vehicles (Eki et al., 2007). Specifically, since a motor torque constant of 2.6 has been identified as the ratio between motor current (A)

---

[3] The specific forces within the steering rack are discussed further in this Section.

and torque (Nm), the active current waveforms in Figure 8.11 (right) correspond to a torque range between 0.38Nm and 2.31Nm.
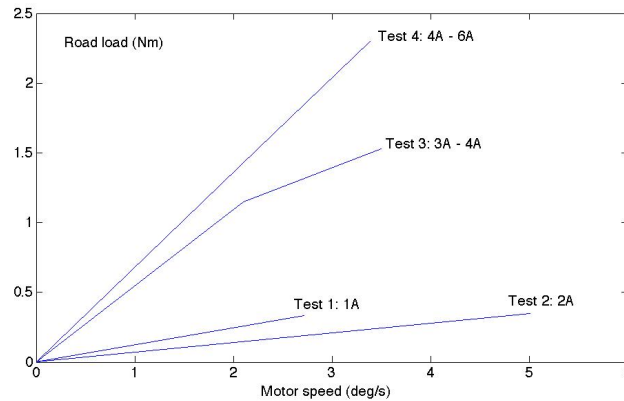
Figure 8.12 Load profile (*road* torque vs. motor speed) for four case studies

Consequently, based on the gear ratio of 12 to 1 between the motor shaft and the steering column, and that the pinion radius in the rack-and-pinion connection equals 7mm, the forces exerted in the hydraulic circuit for the four trials are: 650N (for 1A motor current), 1.3kN (2A), 1.95kN (3A), 2.6kN (4A) and 3.9kN (6A). It should be noted that although the motor rated torque is equal to 7Nm, the present analysis is limited to 2.31Nm due to the high stress observed on the mechanical components in the EPAS apparatus (Figure A8.2, Appendix G).

As it can be seen in Figure 8.11, for EPAS motor torque levels appropriate for use within both small and medium-sized vehicles, a high degree of correlation exists between the experimental and simulation results. This in turn implies that the mathematical model of the DC system is representative of the physical realisation of the technology.

8.3.2.4 Modification of the EPAS Model to include a HFAC/AC Drive

The validated EPAS model described in Section 8.3.2.2 has been extended in order to integrate a HFAC/AC drive that replaces its DC/AC counterpart. The aim of this study is to derive a comparison between the operation of the two inverter technologies, in

terms of both the output voltage harmonics and the motor torque ripple. Both of these parameters, as discussed in (Bianchi et al., 2005, Graovac et al., 2008), are key to satisfactory system performance within a vehicle application.

The modifications made to the model are related only to block A of Figures 8.10 and 8.11 and are illustrated in Figure 8.13. The enhancements consist of replacing the 6-switch DC/AC inverter with a 12-switch HFAC/AC circuit (detailed in Figure 8.14). The rationale for this design decision has already been discussed in Chapter 7. The enhancement of the SV PWM algorithm for ZVS is described below.
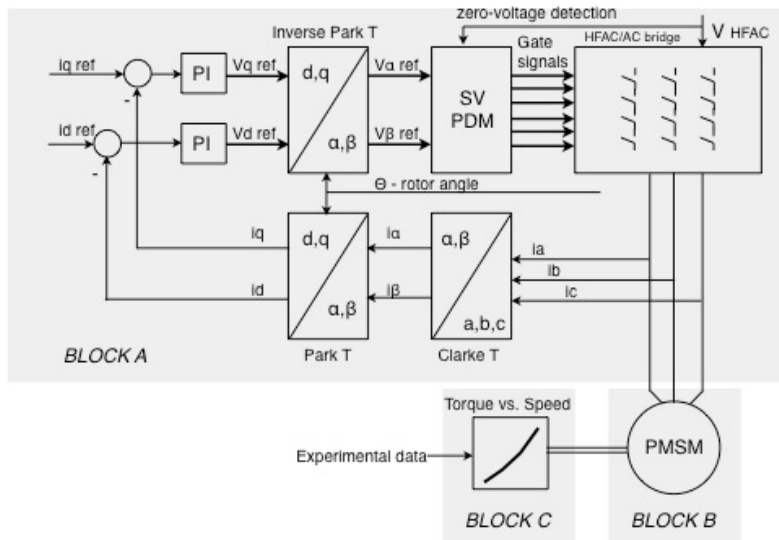
Figure 8.13 Diagram of EPAS model integrating HFAC supply and SV PDM
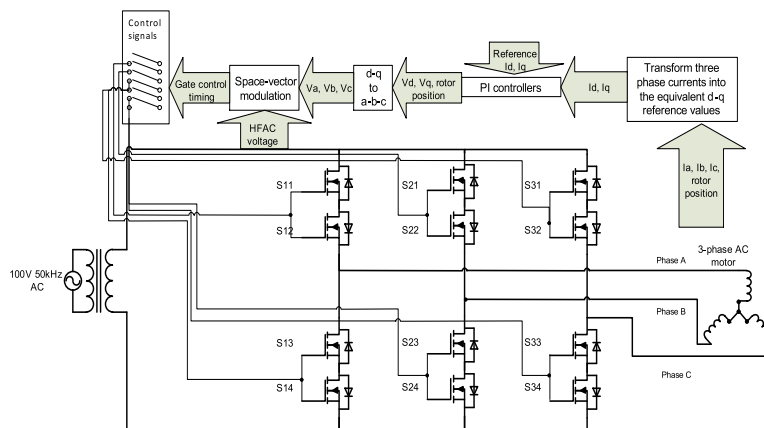
Figure 8.14 Representation of the modified HFAC/AC bridge and SV PDM control

A common way to represent the three phase machine voltages is by using a space vector model. This technique has been extensively covered in the literature (Emadi, 2005). The main principle of this model is that the eight vectors, corresponding to the eight different states in a 3-leg DC/AC bridge, are used in pairs of two adjacent vectors to produce the desired output voltage. Every time period, the controller computes the three time variables required to bias the output voltage amplitude and direction according to the reference voltage or current. Consequently, the bridge changes state (i.e. MOSFETs are switched *on* and *off*) at these predefined time moments.

The SV PWM model can be replaced by a SV model based on PDM of half-wave AC sinusoids, to allow for ZVS in the HFAC/AC drive. Specifically, the proposed method is based on the original SV principle and the only difference is that the three variables (denoted as *Ta*, *Tb* and *Tc*) are determined as multiples of half the fundamental time period of the high frequency AC voltage. For the present analysis, this entails that *Ta*, *Tb* and *Tc* are calculated every time period in multiples of 10μs.

Figure 8.15 (a) illustrates the typical state change of the three legs in a DC/AC inverter for one time period, where the *zero* state is equivalent to the low-side MOSFET conducting and state *one* indicates when the high-side MOSFET is switched *on.* As it can be seen from Figure 8.15 (b), for the same scenario, the proposed SV PDM algorithm ensures that switching is aligned with the 50kHz bus frequency.

8.3.2.5 Comparison between the DC/AC and HFAC/AC Drives for the EPAS system

Figure 8.16 shows the comparison between voltage, current, torque, speed and the voltage harmonic content associated with the DC drive (left hand side) and the HFAC drive (right hand side of the Figure) for the case study of a step motor current from 4A to 6A. For reference, Figures A8.4 (a, b) illustrate the implementation of the model within the Matlab Simulink environment.
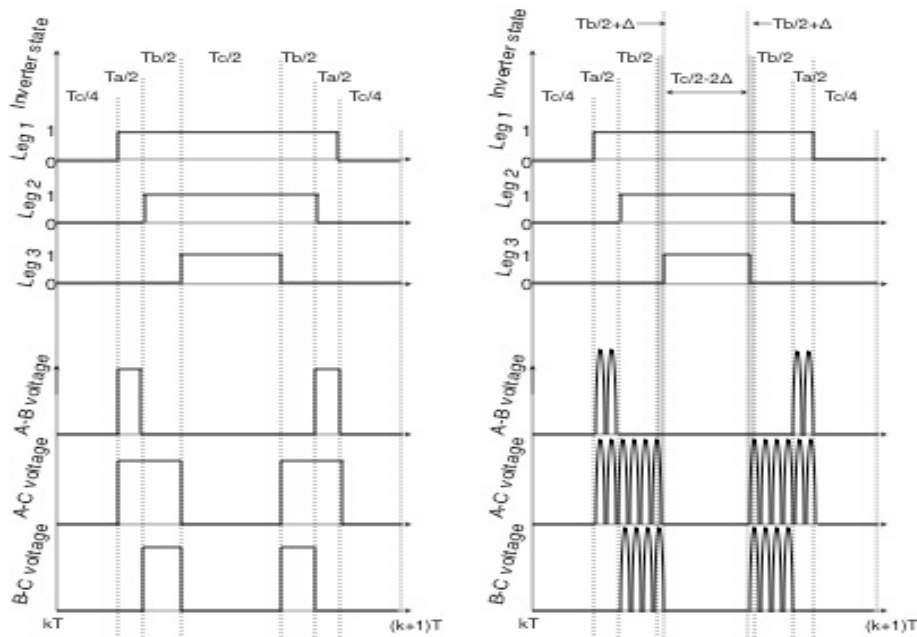
Figure 8.15a (left). Typical logic and associated phase-to-phase motor voltage for standard SV PWM control method

Figure 8.15b (right). Modified SV PDM control based on zero voltage switching

As it can be seen from Figures 8.16 (e) and 8.16 (f), although the SV PDM algorithm is feasible for the EPAS HFAC/AC drive and allows for ZVS, the motor torque ripple appears to be higher compared to the DC/AC inverter. The Figure shows that for a steady-state torque output, the peak-peak motor torque is in the order 0.07Nm when controlled via HFAC drive. This is 1.7% and 1.2% greater than that observed before and after the time step when the machine is supplied from the DC/AC inverter. This implies that a higher mechanical vibration will be present within the steering column and therefore in the steering wheel. However, the overall torque ripple for the HFAC drive is 5% and 3.1% for a PMSM torque of 1.53Nm and 2.31Nm, respectively, which is within the 5% requirement for an EPAS implementation (Hur, 2008).

The higher motor torque ripple associated with the HFAC drive can be accounted for by the modification of the SVM technique for loss-less switching of the AC voltage. As described in Section 8.3.2.4, the three time constants *Ta*, *Tb* and *Tc* are computed at the beginning of each time period and are constrained to be multiples of 10μs. The

consequence is that the HFAC voltage applied to the PMSM has a lower resolution in comparison to the DC voltage. Small differences between the two drive voltages can also be observed in Figures 8.16 (a, b).
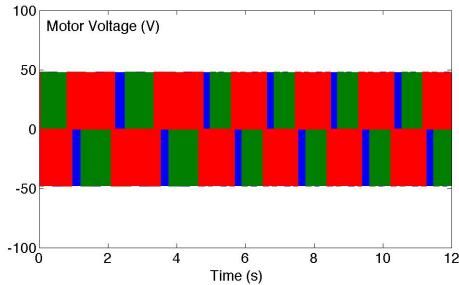
Figure 8.16a DC/AC drive 3-phase voltage (V)
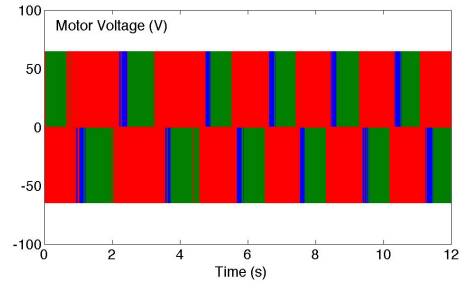
Figure 8.16b HFAC/AC drive 3-phase voltage (V)
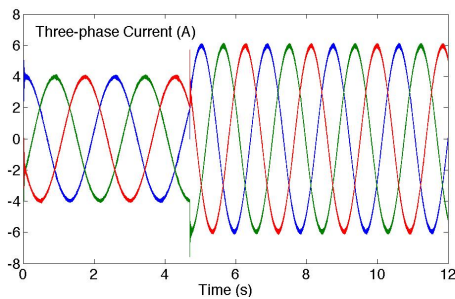
Figure 8.16c DC/AC drive 3-phase current (A)
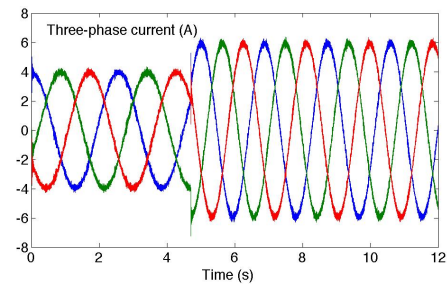
Figure 8.16d HFAC/AC drive 3-phase current (A)
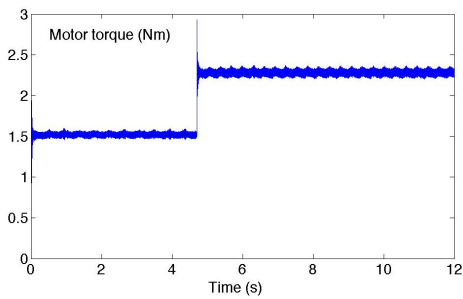
Figure 8.16e DC/AC drive, PMSM torque (Nm)
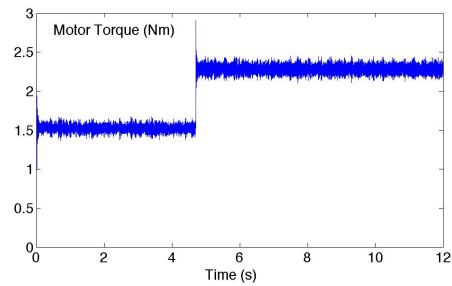
Figure 8.16f HFAC/AC drive, PMSM torque (Nm)
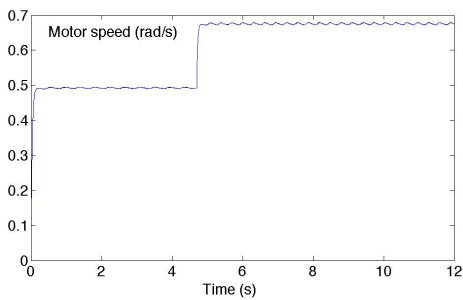
Figure 8.16g DC/AC drive, PMSM speed (rad/s)
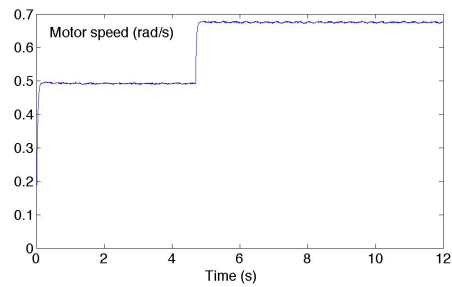
Figure 8.16h HFAC/AC drive, PMSM speed (rad/s)
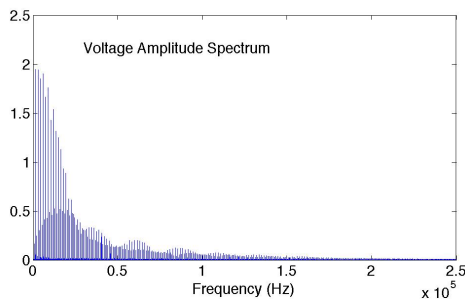
Figure 8.16i DC/AC drive, voltage harmonics (relative to base value 1)
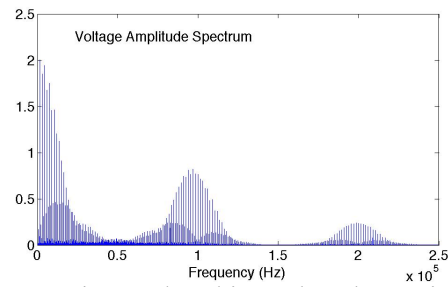
Figure 8.16j HFAC/AC drive, voltage harmonics (relative to base value 1)

Figure 8.16 Comparison of DC/AC drive (left) and HFAC/AC drive (right) voltage, current, motor torque and speed, and voltage amplitude spectrum

It should be noted that it is possible to achieve the same level of output torque ripple by applying the non-modified SVM algorithm to the HFAC/AC converter. While this has the advantage of reducing the torque oscillations, the disadvantage is that it requires the use of non-ZVS within the HFAC/AC drive, which in turn degrades the efficiency of the electrical sub-system by adding switching losses to the overall bridge losses.

The frequency spectrum of the hard-switched and synthesized AC voltage (sampled at a frequency of 500kHz) across the motor windings is illustrated in Figures 8.16 (i) and 8.16 (j), respectively. The plot includes frequencies up to 250kHz, and it shows that although the frequency spectrum of the DC voltage is lower than the equivalent of the HFAC/AC system above 50kHz, it includes comparatively lower frequency components below this threshold (by approximately 10%). It has been indicated in the literature that the high frequency harmonics can be easily filtered out (Sudipta et al., 2007). Furthermore, it has been suggested that reduced harmonics in the lower frequency range can potentially reduce the motor copper losses, especially for high machine torque levels (Venkatesan and Lindsay, 1982).

It has been indicated so far that the HFAC/AC drive based on soft switching techniques offers simultaneous advantages such as low voltage harmonic content below a frequency of 50kHz and no switching losses. Figure 8.17 illustrates the associated switching losses for a DC to three-phase AC drive circuit for several switching frequencies and load current up to 60A. The method applied for the calculation of

switching losses has been previously detailed in Section 7.2. It can be observed that the maximum switching loss per MOSFET, which occurs at 60A and 20kHz switching frequency, is approximately 13W.
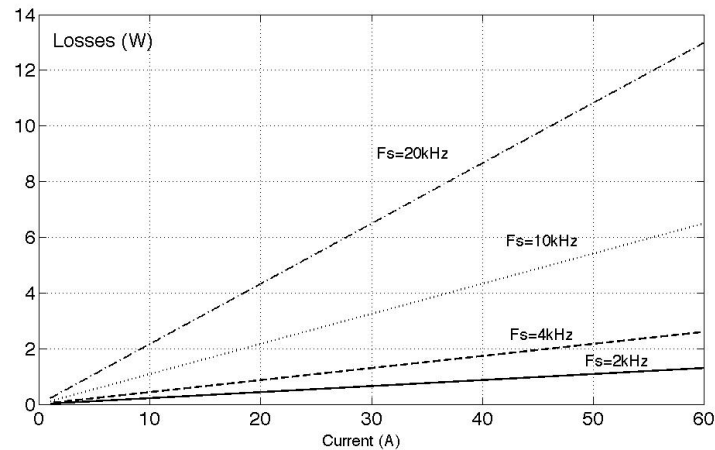
Figure 8.17 Switching losses associated with the operation of a DC/AC drive (W) vs. load current (A) for several switching frequencies (Fs)

As presented in Chapter 7, regardless of the elimination of switching losses, the conduction losses of the HFAC/AC drive are effectively double. A typical MOSFET for the EPAS application with an internal resistance of 42mΩ will dissipate 4.2W at 10A, and 16.8W for a load current of 20A, which is higher than the maximum possible saving of 13W at 60A in switching losses. This limitation becomes more apparent when all the 12 switches are considered. Specifically, for a load current of 6A, the I^2R losses are 4.5W and 9W for the DC/AC and the HFAC/AC converters, respectively. The same figures are 50W and 100W, respectively, for a load current of 20A, which is a significant disadvantage for the use of a HFAC drive.

In summary, this Section has highlighted that HFAC can provide both advantages and disadvantages for high-torque motor electrical loads. The main advantage is a reduced low-frequency harmonic content in the supply voltage to the actuator. Although switching losses can be avoided, the conduction losses, which are predominant, are effectively double in comparison to the DC/AC drive since. Although this disadvantage is inherent in the physical design of the system and can therefore not be mitigated

against by the use of novel switching strategies, potential motor energy savings are still feasible due to the reduced voltage harmonics in the lower frequency range (under 50kHz).

The limitations associated with the use of a HFAC/AC system stem from the need to satisfy the conflicting requirements of high performance and high efficiency. If a ZVS strategy is employed to increase system efficiency, the side-effect of this is a higher torque ripple at the output of the electrical machine. In order to reduce the magnitude of the torque oscillations (to a value comparable to that associated a DC/AC drive) a hard switching strategy must be employed. It is noteworthy, however, that the increase in output torque ripple is still below the 5% maximum threshold, cited by (Hur, 2008) for an EPAS application.

Based on the results of the study presented in this Section 8.3.2, it is concluded that, as yet, there are no tangible performance or efficiency benefits associated with the use of HFAC instead of DC for high-torque motor applications. In addition, the level of control complexity required to manage the HFAC drive may further negate its future adoption by the automotive sector. Therefore, either HFAC/DC synchronous rectifiers or HFAC/DC/AC converters are recommended for use with high-torque DC or AC machines, respectively.

8.4 Conclusions

The following electrical load characteristics have been analysed within this Chapter:
1. the load power demand, including:
      1.1 voltage/current level;
      1.2 transient current demand;
      1.3 AC or DC power;
      1.4 voltage or current fed loads;
2. the load duty cycle, and
3. the energy recuperation capability.

Regarding characteristics 1.1 and 1.2, the analysis in Chapter 5 has indicated that a suitable HFAC power supply design can successfully meet the steady-state and transient voltage/current requirement of electrical loads. In particular, it was shown within Chapter 5 that a power level up to 4kW can be supplied at 100V, 50kHz. Also, simulation results presented in the same Chapter indicate that the HFAC current rise time is in the order of 300µs.

With reference to point 1.4 above, it was shown that the HFAC converter topology is potentially a better alternative to existing DC converter topologies. The reason is that the former employs the same circuit structure for both voltage and current supplied loads. However, the DC modules have a function-specific structure. This finding may have a positive impact on the component supply base for automobile electrical systems, and is directly linked to the diversity of voltage and current loads within the vehicle.

Related to the duty cycle of the electrical loads (point 2 above), it has been indicated in the literature that a no-load power loss occurs on the HFAC distribution path (Kokes, 1997). The level of the power loss suggested in the referenced work is higher than 50W, although no specific value has been cited. However, it can be argued that this aspect is not significant since there is a minimum set of electrical loads with a continuous operation. Thus, a comparison between a DC and a HFAC bus based on this aspect is not expected to be relevant.

The third and last item of the list of characteristics is the applicability of HFAC for regenerative loads. The analysis in this Chapter has presented the main rationales in favour of a DC bus integration of these applications. Specifically, connecting regenerative loads to a 42V DC bus simplifies the structure and control of the energy management system. In addition, since less power conversion modules are needed, less power is lost in the conversion stages. Therefore, more energy can be stored in the battery or distributed to the loads.

With regard to point 1.3, Section 8.3 has been dedicated to the investigation of HFAC benefits for AC loads. The reason for omitting DC loads from this analysis is that DC

loads are expected to operate equally well of DC and HFAC power, as indicated in the study by Masrur et al. (Masrur et al., 1998a, Masrur et al., 1998b).

Therefore, the feasibility of HFAC power for two main categories of motor-actuated electrical applications has been analysed in Section 8.3: low torque (2Nm nominal, 4Nm peak) loads and high torque (above 2Nm) loads. The rationale for this division is the limited torque capability of present 400Hz AC machine technology, which can potentially be replaced by DC motors with a rated torque below 2Nm.

It was shown that a significant benefit in efficiency (up to 100%[4]), packaging volume and weight (above 60%) is feasible by replacing DC motors with commercially available AC induction motors with a nominal torque of up to 2Nm. This limit is dictated by the low starting torque capability of the AC machines, since their operating torque vs. speed profile must match the profile of the DC motors to be replaced. Based on the assumptions described in Section 8.3.1, relating to the number of electrical motors employed and their respective duty-cycles, the potential weight and electrical power saving for a typical medium size vehicle is in the region of 30kg and 500W respectively.

Section 8.3.2 illustrated that a HFAC/AC frequency converter based on ZVS may degrade the performance of high-torque motor actuators and lead to considerable losses in the conversion process due to the high number of power MOSFETs required. Nonetheless, forgoing ZVS within the bridge, standard modulation techniques can be applied with no penalty in motor performance at the cost of added switching losses. Also, it is possible that the lower voltage harmonics (below 50kHz) of the HFAC/AC circuit compared to the DC/AC bridge may reduce the copper losses in the three-phase motor and partially compensate for the higher conduction losses. Furthermore, it has been argued in the literature that the higher harmonic content of the 12-switch HFAC/AC inverter above 50kHz can be easily removed via appropriate filtering.

---

[4] i.e. twice as efficient

In conclusion, significant benefits of HFAC can be claimed for applications integrating low-torque DC motors. Since these loads are predominant in the vehicle in comparison to high-torque actuators, a preliminary verdict for the motor loads analysis is favourable for the adoption of a HFAC bus architecture. Advantages in terms of weight and efficiency are obtainable, which in turn support the overall strategy of many OEMs towards the market introduction of more fuel-efficient vehicles.

Chapter 9

9.1 Introduction

Chapter 9 presents a critical evaluation of the suitability of HFAC power for the automobile auxiliary electrical system and provides a conclusion for the present work. To this end, a system-level analysis is carried out that integrates the findings presented in Chapters 5 to 8 for the four main electrical sub-systems within the vehicle.

As detailed in Section 9.2, more information is needed in addition to the findings presented in Chapters 5 to 8 in order to conduct the HFAC system-level investigation. Section 9.3 introduces the information supporting the system-level analysis, which is required to complete this study.

Section 9.4 presents a case study of a HFAC auxiliary electrical architecture, which is compared to a 42V DC network from a mass and energy efficiency point of view. The rationale for comparing the proposed bus with a 42V DC, as opposed to the existing 14V DC system within vehicles, is that the two systems have a similar power capability of approximately 4kW.

Section 9.5 includes a discussion of the findings presented in Section 9.4. Also, the Section highlights the main conclusions related to the viability of HFAC system for the automobile auxiliary electrical loads.

9.2 Main results of the sub-system level analysis

Table 9.1 includes the main findings at the sub-system level, as presented in Chapters 5 - 8. The investigation has been focused on three main aspects of the proposed technology:

1. the feasibility of HFAC power for the auxiliary electrical system,

2. the energy advantage of the HFAC bus, compared to DC networks, and

3. the mass benefits resulting from a potential replacement of the DC system with a HFAC architecture.

Table 9.1 Main results of the present analysis at the sub-system level

	Power generation sub-system	Power distribution sub-system	Power conversion sub-system	Electrical loads sub-system
Advantage of HFAC compared to DC networks	none	- HFAC conductor is lighter and more energy-efficient up to a power rating of 2kW.	- HFAC/14V DC converter more efficient than 42V DC/14V DC converter.	- 400Hz AC motors substantially lighter and more efficient than comparative low-torque DC machines - potential advantage for current and voltage-fed applications.
Disadvantage of HFAC compared to DC networks	- approx. 10% power loss in DC/HFAC power conversion - added mass	- HFAC conductor expected to be less energy efficient above 2kW compared to equivalent 42V DC cables	- a larger number of HFAC/DC converters may counterbalance the efficiency advantage above, and add extra mass to the vehicle. - HFAC/AC converter less efficient than equivalent DC/AC inverter.	- HFAC not feasible for high-torque motor actuators - the mass and energy of 400Hz converters should be considered in the system-level analysis.

Table 9.1 indicates that there are both advantages and disadvantages linked to the use of HFAC power within vehicles:

1. at the power generation level, the analysis has focused on:

   • first, the feasibility of the proposed bus for supplying state-of-the-art loads, and

   • second, on finding the most efficient power supply design in order to minimise the energy losses in the DC/HFAC power conversion process. As

explained in Chapter 5, this aspect is significant since this power transformation stage is a net disadvantage for HFAC compared to a DC system. The analysis has indicated an energy loss in the order of 10% for the proposed power supply.

2. for the power distribution sub-system, it can be argued that:

    • HFAC conductors are lighter than comparable DC conductors, and

    • HFAC flat cables are also more energy-efficient compared to DC cable technology for a rated power of up to 2kW.

3. for the power conversion sub-system, the analysis has indicated that:

    • for the particular case of HFAC/14V DC and 42V DC/ 14V DC converters, the former is expected to be more efficient.

    • However, as suggested in Chapter 7, the benefit indicated above may be counterbalanced by the fact that a larger number of such converters is required for the HFAC bus, compared to the DC bus, and

    • based on today's technology, whereby a HFAC power switch must integrate two MOSFETs or IGBTs, DC/AC inverters are more efficient compared to HFAC/AC frequency converters.

4. for the electrical loads sub-system, the investigation has shown that:

    • significant mass benefits can be claimed by replacing low-torque DC motors with 400Hz AC machines. However, for the system-level analysis, the mass and energy efficiency of HFAC/400Hz AC converters should also be taken into account,

    • also on the upside, Chapter 8 has indicated that a single HFAC/DC converter topology can potentially meet the different requirements of current and voltage-fed loads within the vehicle (as opposed to two different topologies required in a DC system setup).

    • however, HFAC is not feasible for high-torque motor loads, and also the proposed technology does not allow for the seamless integration of regenerative electrical loads.

In order to conduct a system-level analysis into the feasibility and advantages of HFAC power, all the relevant information related to the feasibility, energy efficiency and mass of HFAC and comparable DC modules is required. Table 9.2 highlights the information available up to the current stage for the system-level analysis. The question marks indicate that the specific information is required for the proposed study, as summarised below:

- Q1: the added mass of the HFAC power generation sub-system,
- Q2: an indication of whether HFAC/DC power converters have a positive or negative impact on the bus energy efficiency (due to the number of these devices within a HFAC bus). This aspect is discussed in Section 9.4.
- Q3: the mass of HFAC/DC and HFAC/AC converters.

The colour code[1] in Table 9.2 indicates whether the analysis outcome is positive, negative or uncertain at this stage for each of the HFAC sub-systems and for the overall system.

Table 9.2 Indication of the data required for the system-level analysis

	Power generation sub-system	Power distribution sub-system	Power conversion sub-system	Power consumption sub-system	Overall system
Feasibility	Chapter 5	Chapter 6	Chapter 7	Chapter 8	Chapter 9
Energy analysis	Chapter 5	Chapter 6	Q2 ? (Section 9.4)	Chapter 8	Section 9.4
Mass analysis	Q1 ?	Chapter 6	Q3 ?	Chapter 8	Section 9.4

9.3 Data required for the system-level analysis

Commercially-available power electronics modules integrating HFAC are limited to a power level in the order of 200W - 300W (for the consumer electronics market, as

---

[1] The colour code in Table 9.2 indicates whether the findings for the different sub-systems are a benefit (green) or a disadvantage (red) for HFAC in comparison to DC sub-systems. Cells with a gradient background color indicate that the respective characteristic is uncertain at this stage and question marks have been placed to indicate that more information is required.

indicated in Chapter 2), and the most relevant data available are for lower frequency (50/60Hz) AC power modules. Based on this limitation, the present analysis is underpinned by the assumption that the mass of DC/HFAC modules is approximately equal to the mass of DC/AC inverters. The same hypothesis has been considered for HFAC/DC converters and HFAC/400Hz AC converters, i.e. that the information for the present AC/DC and DC/400Hz AC technology, respectively, is relevant for the present study of the HFAC system.
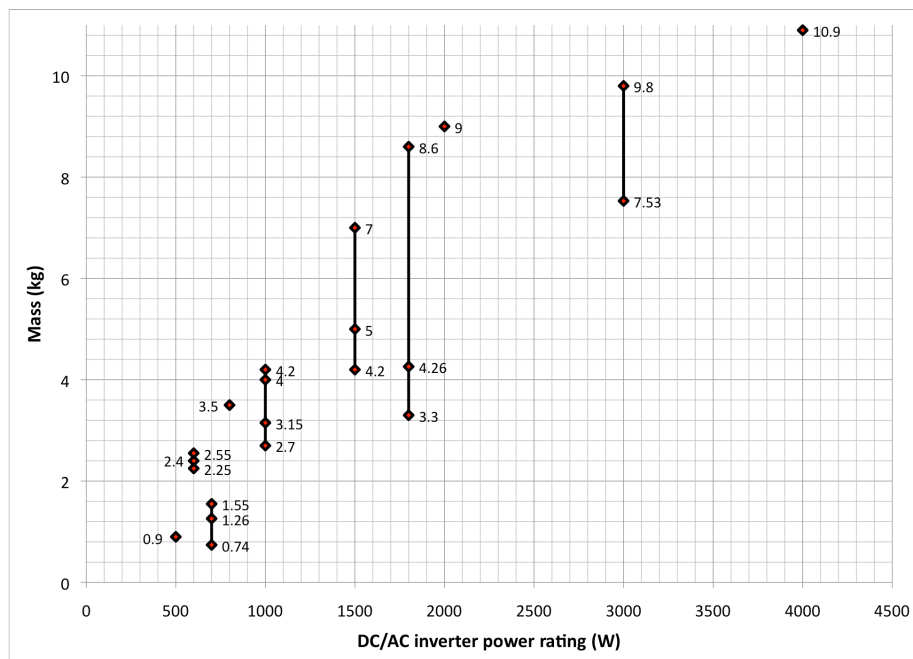
Figure 9.1 Mass (kg) vs. power rating (W) for commercially-available DC/AC inverters (Xantrex, 2010, TrippLite, 2010).

First, data related to the mass of the HFAC power supply is required. This information relates to the first question in Table 9.2 (Q1). Figure 9.1 illustrates the representative mass of commercially-available DC/AC inverters, as a function of the module power rating (Xantrex, 2010, TrippLite, 2010). The Figure indicates that for each of the power levels included, the mass of the DC/AC modules can vary significantly from one manufacturer to the next. This variation is due to several factors, including the power and energy surge capability of the power supply and whether the output voltage waveform is a pure sinusoid or a quasi-sine wave (the latter is easier to build, and

therefore the circuit is potentially lighter). In addition, due to the high expected heat generated in the conversion process, the higher mass of the high-power inverters can potentially be explained by the requirement of a liquid cooling system.

The study presented by (Ng, 2010), which focused on the design of a high frequency AC power supply, specifies that the mass of a 1kW HFAC power supply (50kHz, 84V peak-to-peak) is approximately 5kg for the initial prototype and possibly lower if the module is further optimised for weight reduction. This is consistent with the data shown in Figure 9.1, which supports the assumption that the available information on the mass of low frequency DC/AC inverters can be used within the present analysis.

Information on the mass of AC/DC converters has been collected (MurataPower, 2010, TracoPower, 2010b). Figure 9.2 shows the mass vs. power data for commercially-available AC/DC converters up to a rating of 1kW. The data, which relates to the third question in Table 9.2 (Q3), illustrates typical mass intervals for AC/DC converters from several manufacturers.

The mass difference for converters of the same power rating can be attributed to specific module characteristics. These can include the power conversion method (such as soft or hard switching), cooling technique and the capability of the circuit to withstand various vibration, humidity and/or temperature conditions.

In addition, information related to the mass of 400Hz AC converters is necessary. Data for off-the-shelf DC/115V AC converters have been collated and is illustrated in Figure 9.3 (Xantrex, 2009). Due to the limited information available, data obtained from a single manufacturer is shown to provide guidance. The rationale for the limited power output to 250W is the restricted torque of DC motors that can potentially be replaced by 400Hz AC induction machines. This aspect has been previously discussed in detail in Chapter 8.
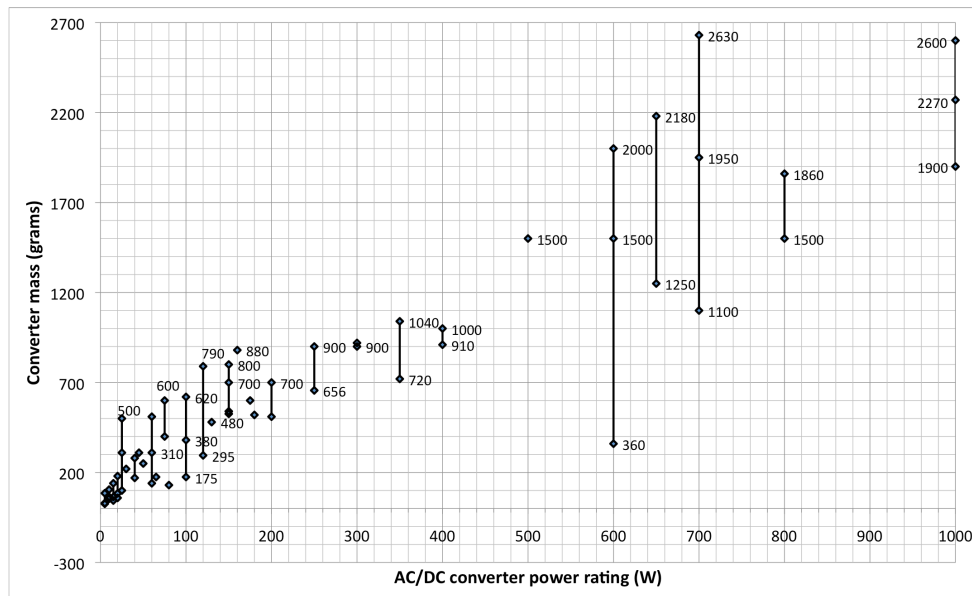
Figure 9.2 Mass (grams) vs. power rating (W) for commercially-available AC/DC converters (MurataPower, 2010, TracoPower, 2010b)
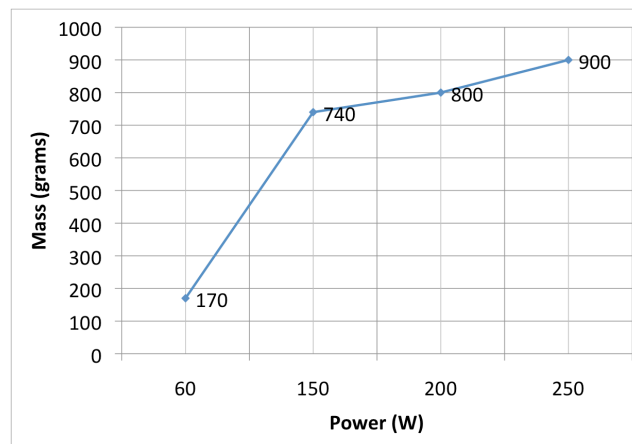
Figure 9.3 Mass (grams) vs. power rating (W) of commercially available DC/ 115V AC inverters (Xantrex, 2009)

9.4 Case study analysis

The method employed for the HFAC system-level analysis includes a case study of 98 auxiliary electrical loads. The investigation looks at the overall mass and energy efficiency of a HFAC bus in parallel with a 42V DC system. As already mentioned, the reason for choosing the 42V system for comparison is the similar power capability of

the two candidates, which is in the order of 4kW. A similar system-level comparison with the 14V DC network would not be appropriate, due to the limited capability of the present DC bus to a maximum of 2.5kW.

Table 9.3 includes the list of the electrical applications included in the proposed case study. The set of loads in Table 9.3 is considered a representative group of loads within a typical passenger vehicle. This assumption is supported by a similar analysis conducted by (Afridi, 1998) for the comparative study between 14V and 42V DC electrical systems. The cited work included the investigation of 100 loads (39 of which were electrical motors). Unlike the cited work, the present study includes modern loads such as the ISG or the EPAS systems.

Table 9.3 Auxiliary electrical loads considered for the present case study

No.	Load name	No.	Load name
1	Starter motor/ISG	50	Rear parking sensor 3
2	A/C compressor	51	Rear parking sensor 4
3	Blower motor	52	DVD player 1
4	Braking light 1	53	DVD player 2
5	Braking light 2	54	GPS navigation system
6	Braking light 3	55	Electric roof
7	Heated front screen	56	Climate control sensor 1
8	Heated rear screen	57	Climate control sensor 2
9	Front power window 1	58	Radio
10	Front power window 2	59	Instrument cluster
11	Rear power window 1	60	12V cigarette lighter
12	Rear power window 2	61	HUD display
13	Main/high beam 1	62	Interior light 1
14	Main/high beam 2	63	Interior light 2
15	Central locking motor 1	64	Interior light 3

No.	Load name	No.	Load name
16	Central locking motor 2	65	Interior light 4
17	Central locking motor 3	66	Seat 1, motor 1
18	Central locking motor 4	67	Seat 1, motor 2
19	Central locking motor 5	68	Seat 1, motor 3
20	Front left indicator light 1	69	Seat 1, motor 4
21	Front left indicator light 2	70	Seat 2, motor 1
22	Front right indicator light 1	71	Seat 2, motor 2
23	Front right indicator light 2	72	Seat 2, motor 3
24	Rear left indicator light	73	Seat 2, motor 4
25	Rear right indicator light	74	Seat 1 heater
26	Front wipers motor	75	Seat 2 heater
27	Front washer pump	76	Lane departure warning sensor 1
28	Rear wiper motor	77	Lane departure warning sensor 2
29	Rear washer pump	78	Adaptive cruise control radar
30	Front fog light 1	79	Throttle-by-wire motor
31	Front fog light 2	80	Brake-by-wire 1
32	Rear fog light 1	81	Brake-by-wire 2
33	Rear fog light 2	82	Brake-by-wire 3
34	Electric water pump	83	Brake-by-wire 4
35	Fuel pump	84	Active suspension 1
36	Cooling fan	85	Active suspension 2
37	Tire pressure monitoring system 1	86	Active suspension 3
38	Tire pressure monitoring system 2	87	Active suspension 4
39	Tire pressure monitoring system 3	88	Boot open motor
40	Tire pressure monitoring system 4	89	Boot 12V supply
41	Airbag sensor (accelerometer)	90	Electrically heated catalyst
42	Airbag sensor (accelerometer)	91	Electric mirror 1
43	Rear view camera	92	Electric mirror 2

No.	Load name	No.	Load name
44	Parking sensor front 1	93	Steering angle sensor
45	Parking sensor front 2	94	Steering torque sensor
46	Parking sensor front 3	95	Barometric air pressure sensor
47	Parking sensor front 4	96	Vehicle angular rate sensor
48	Rear parking sensor 1	97	Variable valve actuation
49	Rear parking sensor 2	98	Electrical power assisted steering

The analysis in Chapter 8 has suggested that HFAC power may not be feasible for high torque motor loads. Nonetheless, Table 9.3 includes electrical loads integrating high torque actuators such as the VVA and the EPAS systems. The rationale for this decision is that the present analysis is intended to be relevant for potential future improvements of the HFAC technology, which may turn the proposed bus into a viable supply for high torque machines.

For the set of electrical loads, a similar analysis to the study presented in Chapter 6 is necessary in order to quantify the mass and energy loss of the cable network. Therefore, the approximate position within the vehicle of the proposed loads has been derived.

Figure 9.4 is a graphical representation of the location within the vehicle of some of the applications listed in Table 9.3[2]. To aid clarity, the Figure depicts only a subset of the 98 electrical loads as the inclusion of the entire set would make the drawing illegible.

Within a DC system, the conductor length can be easily approximated based on the location of the load in the vehicle (as shown in Figure 9.4), since each application is supplied by separate conductors. However, a HFAC power distribution system offers the flexibility of interconnecting the loads in rings of different power rating and length that maximise the mass saving and power distribution efficiency. Figure 9.5, which is a top-

---

[2] Acronyms are explained in Appendix H, Table A9.1.

view representation of all the 98 electrical loads considered, highlights all the possible connections between the loads and the battery/inverter module within a HFAC network.
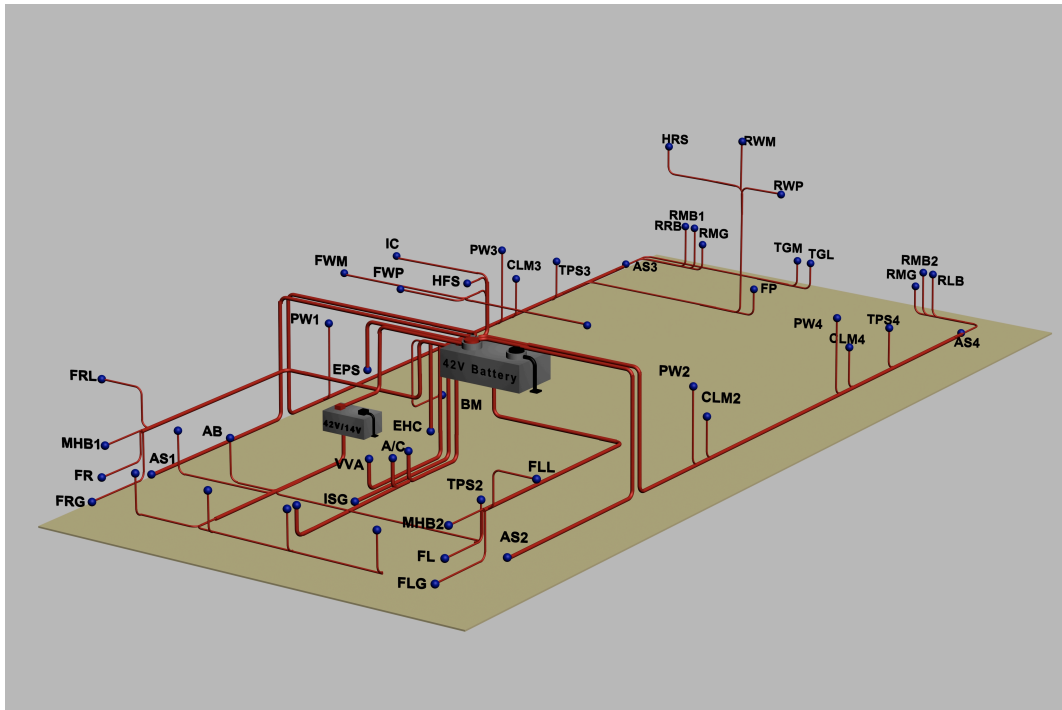
Figure 9.4 Spatial representation of the location of various loads within the vehicle

The analysis focuses next on finding the layout of the HFAC power distribution system which is the most advantageous for the comparison with the 42V DC bus. In order to investigate all the possible connections between the 98 loads, the mass and energy efficiency of more than 2^{98} possible configurations would have to be examined.

Given the computational demands of this investigation, a simplification is required in order to analyse the proposed system. To this end, the investigation is divided into the examination of three main categories of loads:

    a. high-power loads (applications with a power demand in excess of 1kW),

    b. low-torque (up to 2Nm) motor loads, and

    c. the remaining resistive loads (typically with a cumulative power of up to 2kW).
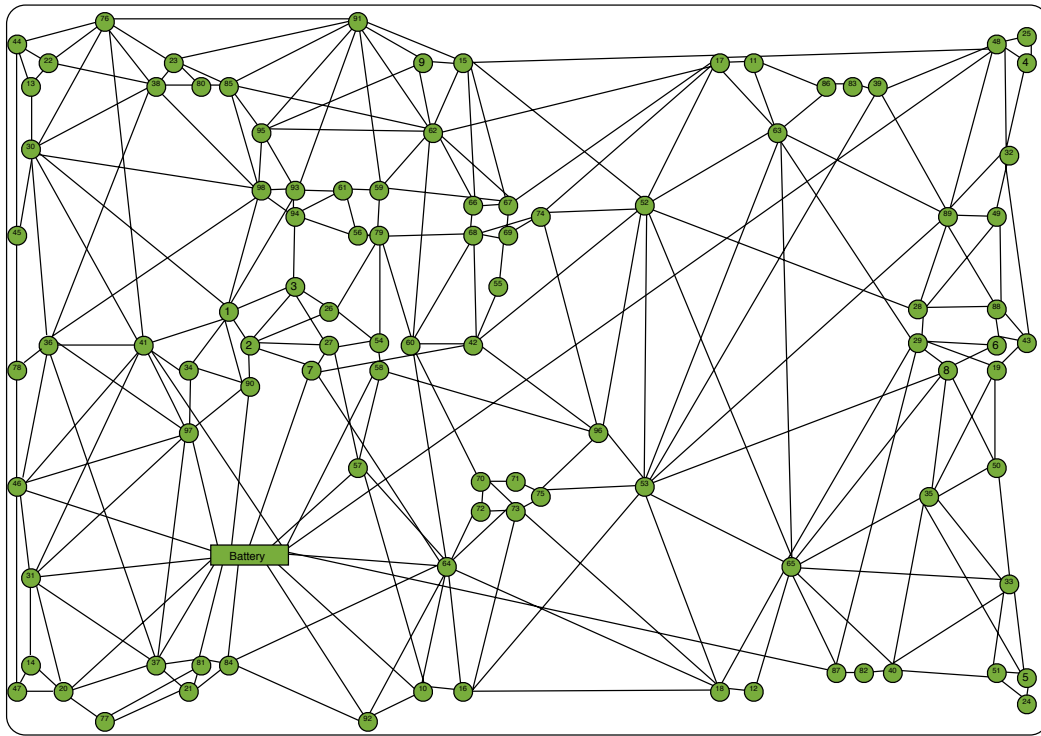
Figure 9.5 Top-view of the location within the vehicle of the loads considered in the case study, and potential connections between these and the battery/inverter module

Justification for the proposed division is presented below:

a. DC conductors supplying high power applications have a high current rating capability, hence are characterised by a high copper mass. Conversely, the HFAC conductor mass is constant across the power spectrum. As a result, the mass saving of HFAC cables is expected to be significant for high power conductors. However, a high power load increases exponentially the resistive losses for the specific HFAC power ring that the application is supplied by. In addition, as previously shown in Section 9.3, the mass of the HFAC power supply units increases significantly with the rated power. Therefore, the analysis for high power loads aims to indicate whether the advantages offered by HFAC outweigh the disadvantages specified above.

b. Chapter 8 has indicated that significant mass saving can be achieved by replacing low-torque (up to 2Nm, 200W) DC motors with 400Hz AC machines. Therefore, the analysis in the present Chapter takes this study further to include

the mass and energy efficiency of the HFAC supply, HFAC conductors and HFAC/AC converters.

c. Lastly, the analysis focuses on loads with a low power rating which can by integrated within a single HFAC power ring. The main advantage of such a configuration in comparison to a DC bus is the flexibility of the cable layout. This, in turn, can translate into potential cost savings for maintenance and manufacturing.

9.4.1 High power loads analysis

Table 9.4 includes the list of the high power applications and their expected power consumption as previously outlined in Chapter 5. These loads are typically the modern and state-of-the-art applications which have motivated the automotive industry to investigate higher voltage alternatives to the 14V DC bus.

Table 9.4 High power electrical loads (as detailed in Chapter 5, Section 5.2)

No.	Load	Power rating
1	Active Suspension (1)	3kW
2	Active Suspension (2)	3kW
3	Active Suspension (3)	3kW
4	Active Suspension (4)	3kW
5	Brake-by-wire (1)	0.45kW
6	Brake-by-wire (2)	0.45kW
7	Brake-by-wire (3)	0.45kW
8	Brake-by-wire (4)	0.45kW
9	Electric Power Assisted Steering	0.8kW
10	Integrated Starter Generator	3kW
11	Air conditioning	3kW
12	Variable Valve Actuation	2.4kW

Power generation sub-system

Considering a duty cycle of 0.1 to 0.3, as indicated in (Bosch, 2004) for intermittent-operating loads, the average cumulative power rating of the loads listed in Table 9.4 is in the order of 2.33kW to 7kW. Based on this expected power rating, and considering the information presented in Section 9.3 related to the mass of DC/AC inverters, it can be estimated that the mass of a DC/HFAC inverter for high power loads is potentially higher than 10kg.

In addition, based on the analysis presented in Chapter 5, an energy loss of approximately 10% can be attributed to the DC/HFAC module. This claim isg supported by efficiency figures in the order of 90% for commercially-available DC/AC inverters (Sinergex, 2010).

Therefore, the HFAC power generation sub-system is expected to increase the mass of the vehicle by at least 10kg, and dissipate between 256W and 770W in the power transformation process[3].

Power distribution sub-system

At the basis of the analysis conducted in this Section are the results detailed in Section 6.3 related to the mass and energy efficiency of the HFAC conductor. Figure 9.6 illustrates a possible HFAC bus topology for connecting the 12 applications.

Loads 5 - 8 in Table 9.4 can be supplied by a single HFAC loop, since their cumulative power rating of 1.8kW is within the advantageous interval of up to 2kW indicated in Figure 6.11. The remaining eight applications are optimally supplied by point-to-point links due to their high power rating which is outside the optimal range.

---

[3] Since the DC/HFAC inverter losses are 10%, the actual losses are equal to approx. 11% of the power that the module has to supply: $P_{out} = P_{in} - P_{in} \cdot 10\%$
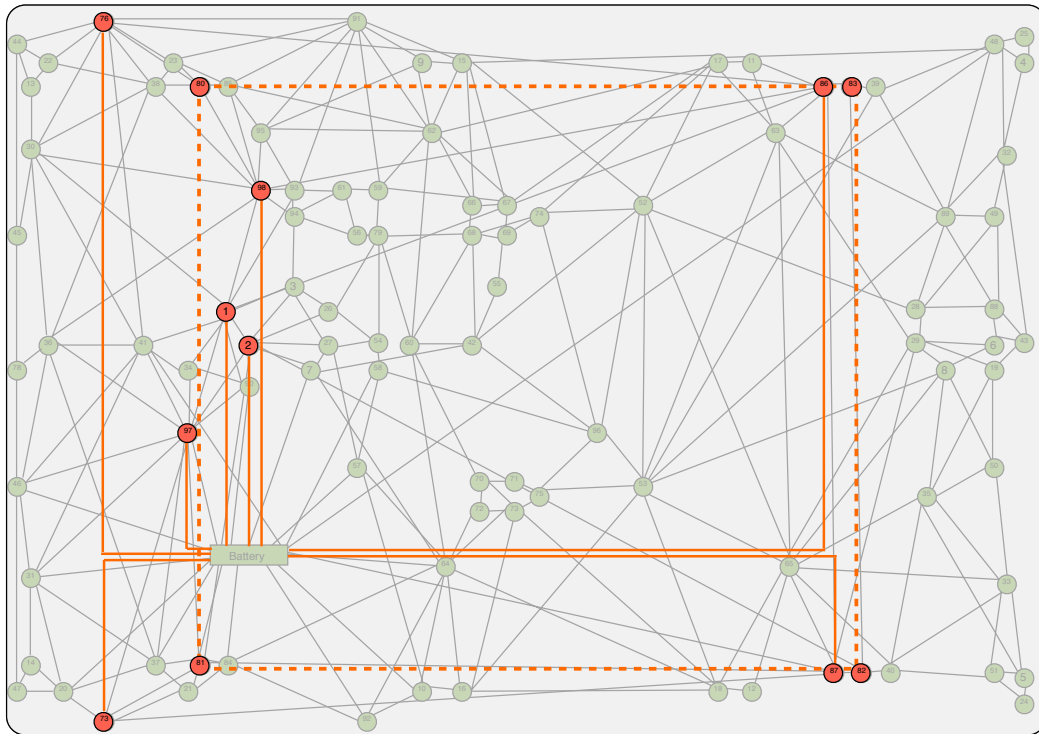
Figure 9.6 Optimum HFAC cabling setup for high power electrical loads
(the interrupted line indicates the only HFAC power loop within the topology)

For the mass and power distribution efficiency calculation, a similar analysis as detailed in Chapter 6 has been used. Table 9.5 lists the characteristics of the proposed HFAC power rings, including the copper mass, the expected resistive losses and the voltage drop for each loop (given the cable characteristics of: copper mass of 17.92g/m, a resistance of 5.8mΩ/m and an inductance of 25nH). Conversely, Table 9.6 includes the results for the integration of the similar load set into a 42V DC system. It should be noted that consideration is restricted to the continuous operation of the loads. However, these applications have an intermittent duty cycle which may suggest that the actual resistive losses represent only a small fraction of the total figures indicated.

The finding for the power distribution stage is that the 42V DC cabling is expected to have a higher copper mass than the HFAC conductors. In particular, the latter offers a potential total weight saving in the order of 2.8kg.

Table 9.5 HFAC cabling setup for high power electrical loads

Loop no.	Loads	HFAC conductor length (m)	HFAC conductor copper mass (g)	Resistive energy losses (W)	HFAC ring voltage drop (V)
1	Active Suspension 1	4	72	21	1.16
2	Active Suspension 2	2	36	10.5	0.58
3	Active Suspension 3	7	125	37	2
4	Active Suspension 4	8	143	42	2.29
5	Brake-by-wire 1-4	22	395	41.5	3.84
6	Electric Power Assisted Steering	3	54	1.1	0.23
7	Integrated Starter Generator	2	36	10.5	0.58
8	Air conditioning	2	36	10.5	0.58
9	Variable Valve Actuation	2	36	10	0.38
	Total		**933**	**184.1**	**not relevant**

However, the investigation suggests that the HFAC system losses are higher by approximately 140W compared to the DC bus. As mentioned previously, these figures represent the losses within the conductors for a set of continuous loads. Since the applications considered have an intermittent operation, the expected power distribution disadvantage of HFAC is potentially between 14W and 42W (corresponding to a duty cycle interval of 0.1 to 0.3).

Table 9.5 has also highlighted the estimated voltage drop values for each of the nine power rings[4]. The power level of the HFAC loops considered exceeds the 1kW limit indicated in Chapter 6 (see Figure 6.12) for an acceptable voltage drop within the HFAC system. As a result, the maximum voltage drop is in the order of 4V for the ring supplying the brake-by-wire application. However, as discussed in Chapter 5, any decrease in the HFAC voltage amplitude is expected to be adjusted by the proposed

---

[4] As previously indicated in Chapter 6, a cable impedance value of 7.9mΩ/m has been considered

control scheme of the HFAC supply. Therefore, this aspect will not be considered within the analysis in Sections 9.4.2 and 9.4.3 for the remaining two groups of applications.

Table 9.6 42V DC cables characteristics for the high power electrical loads

Load	DC conductor length (m)	DC conductor copper mass, based on AWG data (g)	Resistive energy losses (W)
Active Suspension 1	2	476	6.62
Active Suspension 2	1	238	3.31
Active Suspension 3	3.5	833	11.585
Active Suspension 4	4	952	13.24
Brake-by-wire 1	1.75	65.1	0.84
Brake-by-wire 2	1	37.2	0.48
Brake-by-wire 3	5.25	195.3	2.52
Brake-by-wire 4	4	148.8	1.92
Electric Power Assisted Steering	1.5	88.8	1.425
Integrated Starter Generator	1	238	0.8
Air conditioning	1	238	0.8
Variable Valve Actuation	1	190	2.67
Total		**3,700**	**46.21**

In conclusion, the HFAC cabling system is expected to offer the benefit of a reduced wiring mass compared to the 42V DC loom by 2.8kg. However, the power losses associated with the former are higher, in the order of 14W and potentially as high as 42W.

Power conversion sub-system

The applications investigated within this Section integrate high-torque electrical machines as actuators. This aspect has been described in Section 5.3 for the ISG, VVA

and brake-by-wire applications. In addition, the studies presented by (Iles-Klumpner et al., 2006) and (Eki et al., 2007) are indicative for the high-torque motors incorporated within active suspension (AS) and EPAS systems.

The high-torque actuators can be either DC or permanent-magnet AC machines, which require either a DC/DC or a DC/AC power conversion and control stage, respectively. For the present case study, the implications of this aspect are summarised below:

- first, if DC motors are employed, a total of 12 DC/DC and HFAC/DC converters are required for the DC and HFAC architectures, respectively (one for each of the high-power loads considered). Based on data in Figure 9.2 (for the mass of commercially-available AC/DC converters), the total mass value for the converters is higher than 30kg. However, similar mass values can be attributed to off-the-shelf DC/DC converters (TracoPower, 2010a). From an energy efficiency perspective, Chapter 7 has indicated a consistent advantage for HFAC/DC converters of approximately 100W compared to DC/DC modules for a power rating from 1kW to 2kW. Based on this expected benefit of HFAC, and that the loads have an intermittent duty cycle, a total power saving between 120W and 360W (for a duty cycle of 0.1 and 0.3, respectively) can potentially be achieved.

- second, if high-torque AC machines are utilised, the mass and efficiency of 12 DC/AC and HFAC/AC modules should be compared. As with the first aspect, discussed above, it is assumed that the mass of DC/AC and HFAC/AC modules is approximately equal for the same circuit power rating. From an energy point of view, it has been argued in Chapter 7 that the HFAC/AC converter losses are approximately double compared to a DC/AC drive. In particular, for a power rating from 1kW to 2.4kW, the losses within the HFAC module are expected to exceed the DC circuit losses by 50W to approximately 430W. Considering a duty cycle variation from 0.1 to 0.3 for the present analysis, Table 9.7 indicates that the HFAC/AC converter losses for all the 12 high-power loads is between 384W and 1,152W.

Table 9.7 Power losses of HFAC/AC converters

Power rating (kW)	No. loads	Difference between HFAC/AC and DC/AC converter losses (W) (see Table 7.2 in Chapter 7 for reference)	Average losses attributed to the HFAC/AC drive (W)
0.45	4	18W, for each converter	7.2W to 21W (for a load duty cycle from 0.1 to 0.3)
3	6	550W, for each converter (based on the same power calculation as described in Chapter 7, Section 7.3)	330W to 990W
0.8	1	50W	5W to 15W
2.4	1	427W (see Table 7.2 in Chapter 7)	42W to 126W
		Total	**384 to 1,152**

Therefore, at the power conversion stage, HFAC/DC power modules can potentially save between 120W and 360W in supplying DC machines. However, if AC motor actuators are connected to the HFAC bus, the disadvantage can potentially extend from 384W to 1,152W.

For the case study of high power electrical loads, the electrical loads sub-system is not relevant. The reason is that there are yet no potential HFAC substitutes for high-torque motors.

In conclusion for the high-power electrical loads case study:

- the disadvantage of the HFAC system is expected to be of approximately 7kg compared to the 42V DC system, and
- from the perspective of power losses, the DC bus is potentially more efficient by at least 1kW and up to 1.6kW.

Therefore, based on the current technology, HFAC is not a feasible substitute for the proposed 42V DC system for high-power loads. However, future technological improvements in the efficiency and mass of HFAC power modules may provide an incentive to reiterate the analysis presented within this Section. If this is the case, and

the HFAC technology proves to be a better alternative to DC systems for high-power loads, aspects such as the cost, complexity and reliability of the new technology should also be taken into consideration.

9.4.2 400Hz AC motor loads

The study presented in Chapter 8 highlighted the following advantages associated with the replacement of low-torque DC motors (up to 2Nm, 200W) with 400Hz AC induction machines:

- an approximate mass saving of 0.6kg per device (based on an average actuator mass of 1kg, and potential mass reduction of 60%), and
- a potential energy saving between 10W and 30W for intermittent and continuously operating machines, respectively.

For the present case study of 98 electrical loads, Table 9.8 lists the applications that can potentially benefit from the two advantages above. The Table also indicates the power rating of the systems, based on the measurements described in Chapter 6 and also on the figures presented in the studies by (Lukic and Emadi, 2002, Lukic and Emadi, 2003).

Power generation sub-system

The cumulative power of the loads in Table 9.8 equals 1,358W. In addition, for passenger vehicles with a small engine capacity (up to 1.6L), the engine electric cooling fan (with a power rating of 200W) can also be included in the analysis. For vehicles with a more powerful engine, the electric cooling fan can have a power rating of up to 800W (Lukic and Emadi, 2002, Lukic and Emadi, 2003).

Table 9.8 Applications integrating low-power DC motor actuators [5]

---

[5] The numbers in the Table are consistent with the initial numeration in Table 9.3, in order to identify the loads within the HFAC system layout in Figure 9.10

No.	Load name	Power rating (W)	No.	Load name	Power rating (W)
1	Blower motor	200	15	Fuel pump	150
2	Front power window 1	50	16	Electric roof	100
3	Front power window 2	50	17	Seat 1, motor 1	30
4	Rear power window 1	50	18	Seat 1, motor 2	30
5	Rear power window 2	50	19	Seat 1, motor 3	50
6	Central locking motor 1	20	20	Seat 1, motor 4	50
7	Central locking motor 2	20	21	Seat 2, motor 1	30
8	Central locking motor 3	20	22	Seat 2, motor 2	30
9	Central locking motor 4	20	23	Seat 2, motor 3	50
10	Central locking motor 5	20	24	Seat 2, motor 4	50
11	Front wipers motor	55	25	Throttle-by-wire motor	50
12	Front washer pump	45	26	Boot open motor	50
13	Rear wiper motor	28	27	Electric mirror 1	15
14	Rear washer pump	30	28	Electric mirror 2	15

Total: 1,358 (1,558 incl. engine radiator cooling fan)

Apart from two applications with a continuous duty cycle (the fuel pump and the throttle-by-wire actuator), the remaining actuators are operated on an intermittent basis. Based on a duty cycle variation from 0.1 to 0.3, the average power requirement of the set of loads in Table 9.8 fluctuates from approximately 156W to 468W. Consequently, based on Figure 9.1, a HFAC power supply for the considered group has a mass in the order of 1kg. In addition, up to 51W (or 11% of 468W) can be attributed to the 10% losses in the conversion stage.

Power distribution sub-system

Figure 9.7 shows the location within the vehicle of the 29 electrical loads considered in this Subsection. Based on their cumulative average power below 500W indicated above, and taking into consideration the optimum interval of up to to 2kW (Figure 6.11) for the

HFAC conductor, the most advantageous power distribution topology is possibly an architecture that integrates all the 400Hz AC motor loads within a single loop.
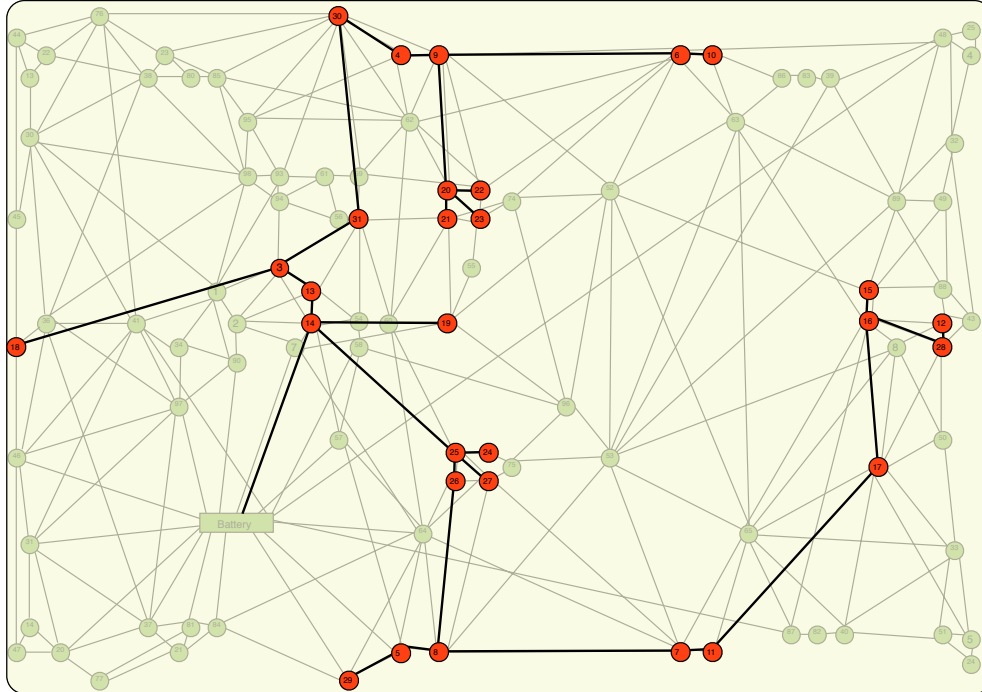
Figure 9.7 Loads integrating low-torque DC motors, location within the vehicle

An alternative HFAC bus topology to the loop or ring configuration is a configuration that minimises the length of the HFAC flat cable connecting the loads. Figure 9.7 presents the conductor network as a result of such a design approach. The purpose of choosing this architecture is to demonstrate the inherent flexibility of the HFAC bus. Specifically, the design of the network can be directed to either a maintenance-friendly approach (in the form of HFAC power rings) or targeted to the minimisation of the conductor copper mass and the maximisation of the distribution energy efficiency.

In order to determine the minimum-length connections between the electrical loads, an optimisation method from the field of computer science has been employed. The technique finds the minimum spanning tree within a graph where the length between all the nodes is known. The algorithm is described in detail in Appendix H.

The result returned by the algorithm is a conductor length of 16m. Taking account of the fact that two conductors are required within a HFAC setup, the resulting total cable length is equal to 32m. Therefore, the copper mass of this configuration is approximately 570 grams (based on a mass of 17.92 g/m of a bespoke HFAC conductor). In addition, the power distribution losses are within the interval from 0.45W to 4W[6] (figures supported by a conductor resistance of 5.8mΩ/m, and HFAC power distribution at 100V, 50kHz). Conversely, Table 9.9 illustrates the conductor copper mass for a comparative 42V DC system supplying the proposed set of loads. The total conductor copper mass is approximately 213g and the power distribution losses between 0.41W and 1.23W (for a duty cycle between 0.1 and 0.3, respectively).

The copper mass of the HFAC system therefore exceeds the equivalent 42V DC layout by approximately 360g, while the power distribution losses appear to be similar for a duty cycle of 0.1. However, for a duty cycle of 0.3, the HFAC resistive losses are higher by about 2.7W.

Table 9.9 Copper mass and resistive losses for 42V DC conductors

Load	DC conductor length (m)	DC conductor copper mass, based on AWG data (g)	Resistive energy losses (mW)
Blower motor	1.5	22.2	355.1
Front power window 1	1	3.6	59.5
Front power window 2	2	7.3	119.0
Rear power window 1	3.5	12.8	208.3
Rear power window 2	2.5	9.1	148.8
Central locking motor 1	1	1.8	19.0
Central locking motor 2	2	3.7	38.1
Central locking motor 3	3.5	6.4	66.7
Central locking motor 4	2.5	4.6	47.6

---

[6] Considering an average power distribution between 156W and 468W, i.e. current of 1.56A and 4.68A, respectively, at 100V.

Load	DC conductor length (m)	DC conductor copper mass, based on AWG data (g)	Resistive energy losses (mW)
Central locking motor 5	4	7.3	76.2
Front wipers motor	1	4.6	56.6
Front washer pump	1	3.6	48.2
Rear wiper motor	4	9.1	118.6
Rear washer pump	4	9.1	136.1
Fuel pump	5	58.5	829.1
Electric roof	2	18.6	238.1
Seat 1, motor 1	2	5.9	68.2
Seat 1, motor 2	2.2	6.5	75.0
Seat 1, motor 3	2.2	8.0	131.0
Seat 1, motor 4	2.5	9.1	148.8
Seat 2, motor 1	1.5	4.5	51.1
Seat 2, motor 2	1.7	5.1	57.9
Seat 2, motor 3	1.7	6.2	101.2
Seat 2, motor 4	2	7.3	119.0
Throttle-by-wire motor	1.5	5.5	89.3
Boot open motor	5	18.2	297.6
Electric mirror 1	2	2.3	33.9
Electric mirror 2	1	1.1	17.0
Electric cooling fan	1.5	22.2	355.1
Total		**212.9**	**4,110.2**

Power conversion sub-system

As discussed in Chapter 8, low-power DC motors do not typically require power converter modules. In fact, the applications considered in this Subsection are connected to the battery via switches, relays or other connector types. The proposed AC machines, however, must be interfaced by HFAC to 400Hz AC frequency converters. As suggested

in Chapter 8, the two methods of interfacing the proposed machines off the HFAC bus are:

    a. to integrate a converter with each motor, as a plug-and-play module, or

    b. to design a topology integrating a single converter, which in turn supplies all the induction machines with the required 400Hz, three-phase AC power.

A potential limitation of the second technique is that the electrical safety standard within vehicles does not allow power distribution at 115V, 400Hz AC. In fact, the highest amplitude allowed at this frequency based on the DIN VDE 0800, Part 1, is only 25V. However, it can be argued that this option may be of interest if future improvements in conductor and insulation material technology lead to new electrical safety regulations.

The implication of option (a) for the present case study is that the mass and energy losses of 29 converters must be reviewed. The weight of these modules can be estimated based on the data presented in Section 9.3, Figure 9.3. With regard to the power losses within the HFAC/AC converter, an example has already been given in Chapter 8 which indicated that the maximum resistive losses are in the order of 0.6W for a load power of 200W, at 115V. Table 9.10 outlines the potential mass and power[7] disadvantage of integrating the 400Hz AC machines with individual frequency converters. The total added mass and power losses are equal to 5.96kg and 2.86W[8], respectively.

Table 9.10 Estimated mass and power losses of HFAC/400Hz AC converters

Supplying the load	Estimated mass (g)	Estimated power loss (W)
Blower motor	800	0.762
Front power window 1	150	0.048
Front power window 2	150	0.048

---

[7] Power losses calculation based on the 12-switch cycloconverter topology presented in Chapter 8, a MOSFET internal resistance of 42mΩ, voltage amplitude of 115V. ZVS is employed.

[8] Value is relevant for a continuous operation of the converters. For a duty cycle of 0.1-0.3, the power losses value is between 0.28W and 0.84W. Fuel consumption calculation of 0.061L/100km takes into account these values.

Supplying the load	Estimated mass (g)	Estimated power loss (W)
Rear power window 1	150	0.048
Rear power window 2	150	0.048
Central locking motor 1	100	0.008
Central locking motor 2	100	0.008
Central locking motor 3	100	0.008
Central locking motor 4	100	0.008
Central locking motor 5	100	0.008
Front wipers motor	150	0.058
Front washer pump	150	0.039
Rear wiper motor	100	0.015
Rear washer pump	120	0.017
Fuel pump	740	0.429
Electric roof	500	0.191
Seat 1, motor 1	100	0.017
Seat 1, motor 2	100	0.017
Seat 1, motor 3	150	0.048
Seat 1, motor 4	150	0.048
Seat 2, motor 1	100	0.017
Seat 2, motor 2	100	0.017
Seat 2, motor 3	150	0.048
Seat 2, motor 4	150	0.048
Throttle-by-wire motor	150	0.048
Boot open motor	150	0.048
Electric mirror 1	100	0.004
Electric mirror 2	100	0.004
Electric cooling fan	800	0.762
Total	**5.96**	**2.86**

Alternatively, the consequences of opting for choice (b) are summarised below:

- First, the mass and energy efficiency of a converter with a rated power of up to 500W[9] should be taken into consideration. Following the same assumptions and steps as for option (a), a mass of 1kg and power losses in the order of 4.76W[10] can be associated with the inclusion of the module.

- Second, the examination of the HFAC power distribution system for 400Hz motor loads is no longer relevant since a lower frequency conductor should replace the flat HFAC conductor. The study conducted by (Miller, 1996) suggested that the potential copper mass saving in a three-phase AC distribution system is one half the mass of a comparative DC distribution network. As a result, based on a total DC conductor mass of 212g for the present case study (see Table 9.9), a mass saving of approximately 106g is potentially feasible.

Electrical loads sub-system

The examination presented in Section 8.3.1, has highlighted the potential mass saving and energy efficiency of 400Hz AC and comparative DC machines. Table 9.11 presents in detail the calculation of the mass and energy benefits of the proposed motors. In particular, the total potential mass saving for the case study presented in this Section is of 9.44kg, while the total in terms of energy saving is in the region of 540W. However, taking into consideration the fact that only two applications are expected to operate continuously (the fuel pump and the throttle-by-wire motor actuator) and that the remaining loads have a typical duty cycle between 0.1 and 0.3, the energy saving interval is 92.6W to 192W.

Conclusively for the case study discussed within this Section:

---

[9] Figure based on the estimated average power consumption of 468W for the present case study.

[10] $6(\text{switches}) \cdot 0.042(\text{MOSFET on resistance}) \cdot \left(\dfrac{500W}{115V} \right)^2 = 4.76W$

- choosing option (a) at the power conversion sub-system, the advantage associated with the used of HFAC can be quantified as a mass and power losses reduction of 2.12kg and 482W, respectively.
- based on option (b) at the power conversion sub-system, the HFAC system mass is expected to be lower by approximately 7.2kg and power losses reduced by about 480W compared to the 42V DC system.

Table 9.11 Potential advantages associated with the use of 400Hz AC motors

No.	Load name	Power rating(W)	Potential mass saving (kg)	Potential energy saving (W)
3	Blower motor	200	0.87	40
9	Front power window 1	50	0.25	17
10	Front power window 2	50	0.25	17
11	Rear power window 1	50	0.25	17
12	Rear power window 2	50	0.25	17
15	Central locking motor 1	20	0.25	17
16	Central locking motor 2	20	0.25	17
17	Central locking motor 3	20	0.25	17
18	Central locking motor 4	20	0.25	17
19	Central locking motor 5	20	0.25	17
26	Front wipers motor	55	0.25	17
27	Front washer pump	45	0.25	17
28	Rear wiper motor	28	0.25	17
29	Rear washer pump	30	0.25	17
35	Fuel pump	150	0.8	26
55	Electric roof	100	0.75	22
66	Seat 1, motor 1	30	0.25	17
67	Seat 1, motor 2	30	0.25	17
68	Seat 1, motor 3	50	0.25	17
69	Seat 1, motor 4	50	0.25	17
70	Seat 2, motor 1	30	0.25	17

No.	Load name	Power rating(W)	Potential mass saving (kg)	Potential energy saving (W)
71	Seat 2, motor 2	30	0.25	17
72	Seat 2, motor 3	50	0.25	17
73	Seat 2, motor 4	50	0.25	17
79	Throttle-by-wire motor	50	0.25	17
88	Boot open motor	50	0.25	17
91	Electric mirror 1	15	0.2	10
92	Electric mirror 2	15	0.2	10
36	Cooling fan	200	0.87	40
Total			**9.44**	**539**

It is observable that the result at the power distribution sub-system for both high-power applications and 400Hz AC loads has an insignificant effect on the overall balance for the two case studies. In fact, compared to the findings for the other sub-systems investigated, the contribution of the power generation sub-system differs by one order of magnitude. Therefore, due to the complexity of the calculations involved for the power distribution sub-system and that the gain is not significant for the outcome of the investigation, a similar examination for the third case study within Section 9.4 has not been undertaken.

9.4.3 Low-power DC loads

Table 9.12 lists the remaining 57 electrical loads and their corresponding power rating, as indicated by OEM Tier 1 suppliers. For reference, Table A9.2 in Appendix H illustrates the typical information available for several electrical applications.

The cumulative power of the loads listed in Table 9.12 is 4,233W, considering a continuous operation for all the applications. However, as indicated by the initials next

to the load names in the Table[11], only 18 loads are continuously active and have a cumulative power rating of 320W. Based on a duty cycle variation from 0.1 to 0.3, and taking into account that the EHC is active only at vehicle start-up[12] (Lukic and Emadi, 2002, Lukic and Emadi, 2003), the average power demand for the intermittent applications is in the region of 201W to 483W.

Table 9.12 Power consumption of the remaining loads

No.	Load name	Power (W)	No.	Load name	Power (W)
1	Brake light 1 (I)	10	30	Rear parking sensor 1 (I)	1
2	Brake light 2 (I)	10	31	Rear parking sensor 2 (I)	1
3	Brake light 3 (I)	15	32	Rear parking sensor 3 (I)	1
4	Heated front screen (I)	350	33	Rear parking sensor 4 (I)	1
5	Heated rear screen (I)	210	34	DVD player 1 (I)	100
6	Main/high beam 1 (I)	50	35	DVD player 2 (I)	100
7	Main/high beam 2 (I)	50	36	GPS navigation system (C)	70
8	Front left indicator light 1 (I)	10	37	Climate control sensor 1 (C)	1.5
9	Front left indicator light 2 (I)	5	38	Climate control sensor 2 (C)	1.5
10	Front right indicator light 1 (I)	10	39	Radio (I)	5
11	Front right indicator light 2 (I)	5	40	Instrument cluster (C)	10
12	Rear left indicator light (I)	10	41	12V cigarette lighter (I)	20
13	Rear right indicator light (I)	10	42	HUD display (I)	10
14	Front fog light 1 (I)	20	43	Interior light 1 (I)	5
15	Front fog light 2 (I)	20	44	Interior light 2 (I)	5
16	Rear fog light 1 (I)	25	45	Interior light 3 (I)	5
17	Rear fog light 2 (I)	25	46	Interior light 4 (I)	5
18	Electric water pump (C)	200	47	Seat 1 heater (I)	50
19	Tire pressure monitoring system 1 (C)	5	48	Seat 2 heater (I)	50

---

[11] The symbols are: I= Intermittent load operation, and C = continuous load operation.

[12] The average power demand of the EHC is approx. 60W, see Table 5.1 in Chapter 5.

No.	Load name	Power (W)	No.	Load name	Power (W)
20	Tire pressure monitoring system 2 (C)	5	49	Lane departure warning sensor 1 (C)	1
21	Tire pressure monitoring system 3 (C)	5	50	Lane departure warning sensor 2 (C)	1
22	Tire pressure monitoring system 4 (C)	5	51	Adaptive cruise control radar (C)	5
23	Airbag sensor (accelerometer) (C)	1	52	Boot 12V supply (I)	200
24	Airbag sensor (accelerometer) (C)	1	53	Electrically heated catalyst (I)	2,500
25	Rear view camera (I)	5	54	Steering angle sensor (C)	5
26	Parking sensor front 1 (I)	1	55	Steering torque sensor (C)	10
27	Parking sensor front 2 (I)	1	56	Barometric air pressure sensor (C)	2
28	Parking sensor front 3 (I)	1	57	Vehicle angular rate sensor (C)	1
29	Parking sensor front 4 (I)	1			

Total: 4,233 (for continuous load operation)

Accordingly, a HFAC power supply rated for an average power demand of up to 800W (320W for the continuous loads plus 483W for the intermittent applications) is required for this particular group of loads. The implication for the proposed power bus is twofold: first, the vehicle mass increases by at least 2kg due to the DC/HFAC inverter; second, 10% power conversion losses are equal to approximately 90W.

Figures 9.8 and 9.9 show two potential topologies of the 42V and 100V HFAC networks, respectively, for the loads considered in this Subsection. Since most of these operate off the existing 14V supply in vehicles, a 42V/14V DC converter is integrated in the DC configuration. Correspondingly, the HFAC architecture can include several such converters, depending on the number and location of the consumers within the vehicle.
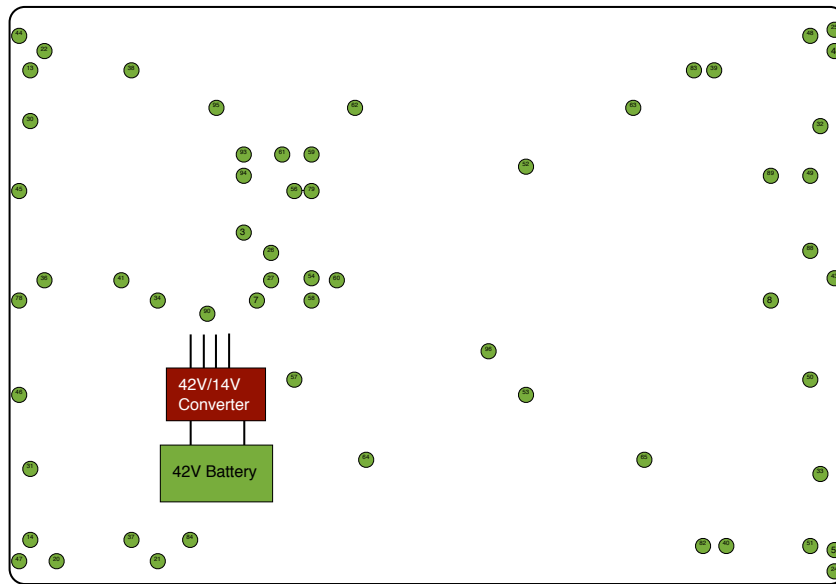
Figure 9.8 42V bus supplying 14V DC loads

As observable in the two Figures, the cabling has been ignored and the power distribution analysis is not included. The rationale, as explained in Section 9.4.2, is that this particular result is expected to have a low impact on the overall system result. In addition, similar to the analysis in Section 9.4.1, no intrinsic advantage of HFAC is expected for the loads considered within this section. Therefore, the remaining of this Section focuses on the power conversion sub-system.

For the specific network in Figure 9.9, it can be assumed that the average power rating of the 57 loads is divided approximately equally between the four HFAC/DC converters. As a result, if the cumulative average power requirement of 800W can be shared equally by the four modules, then the mass and energy efficiency of a 200W converter is of interest for the present examination.

Based on the information previously presented in Figure 9.2, the mass of a 200W AC/DC converter is approximately 500g. Additionally, a power loss value in the order of 2.5W for each 200W HFAC/DC converter is supported by the analysis in Chapter 7 (see Figure 7.8). Following the same steps as above, the 800W DC/DC converter mass is

equal to 1.5kg and the power losses are equal to approximately 75W. Hence, while the power losses are lower by 65W for the HFAC network, the aggregate mass of the four modules is higher by 0.5kg.
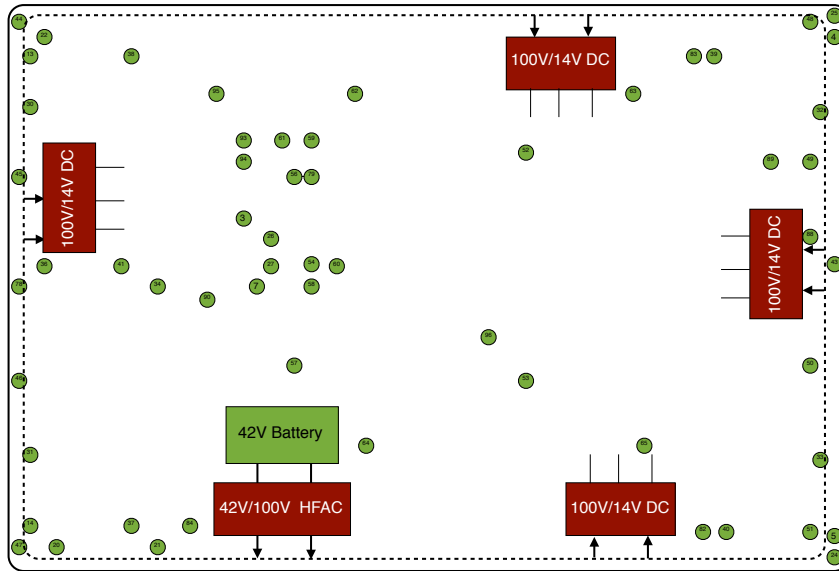
Figure 9.9 HFAC bus supplying 14V DC loads

Conclusively, the maximum potential benefit at the power conversion stage is lower than the disadvantage at the power generation stage. The HFAC system is expected to be 2.5kg heavier than the comparative 42V DC bus and increase the losses by approximately 25W.

9.5 Discussion

The conclusion for the overall system is that a the HFAC bus incurs a comparative disadvantage over a DC bus. Table 9.13 shows the results for the three loads categories presented in the present Chapter, and indicates that the disadvantage of the HFAC system can be quantified by an increased vehicle mass and power losses of approximately 2kg and 1kW, respectively.

Table 9.13. Mass and power losses for the three categories of loads analysed

Group of loads	HFAC system, mass effect	HFAC system, power losses effect
1. High-power loads	Higher by 7kg	Higher by 1kW to 1.6kW
2. Low-torque loads	Lower by 7.2kg	Lower by 480W
3. Remaining loads	Higher by 2.5kg	Higher by 25W

However, the main benefit of the proposed technology is for the low-torque motor actuators where it exhibits a considerable mass and energy efficiency advantage over the 42V DC architecture.

The main unfavourable factors for the HFAC bus at the power generation stage are:

1. the necessity of a DC/HFAC inverter, which adds considerable mass and energy losses, and

2. the present HFAC/AC converter technology, which requires the integration of double the number of power MOSFETs compared to DC drives. As previously discussed in Chapter 7, the power losses in this type of circuit are effectively double compared to DC/AC inverters.

The second aspect is particularly important for the high power loads, since the high current translates into significant resistive losses within the power electronic drive. In fact, for the low-torque motors analysis, similar HFAC/AC converter technology has been considered in order to interface the proposed 400Hz AC induction machines. However, the positive outcome for the latter is partly due to the low current in the HFAC/AC module, owing to:

• first, the high voltage of the induction motors (115V) compared to the 42V high-torque motors, and

• second, to the low power of the rotary actuators (up to 200W).

Therefore, HFAC power is suitable for high-voltage, low-current auxiliary electrical motors. In addition, the result for the group of high-power loads supports the conclusion

in Chapter 8 that HFAC is not yet feasible for high torque (i.e. high-current) motor actuators.

A second feature of the proposed technology that has become apparent during the system-level analysis is that the benefits at the power distribution sub-system are lower by one order of magnitude compared to the contribution of other sub-systems. In particular for the high-power and 400Hz AC motor loads, the contribution of the conductor copper mass and energy efficiency to the overall balance in terms of estimated vehicle fuel consumption can be considered insignificant. Therefore, future improvements in cable technology will probably not generate a significant enhancement for the on-board HFAC bus.

A notable amount of energy is dissipated in power conversion operations. In fact, for the three groups of loads, the total loss value that can be attributed to power transformation is no less than 2kW. As a result, this finding provides a strong incentive to pursue alternative power management strategies within the vehicle, since the present converter technology already allows for very efficient modules (efficiency in excess of 90%).

The on-board electrical system should be based on a single voltage amplitude and frequency. For example, an ISG connected to the motor shaft can supply a constant voltage, constant frequency AC power that the loads can in turn utilise in an unaltered form.

However, technical challenges would have to be overcome for such a concept to be realised, as well as agreement within the industry on a single best approach. Amongst the engineering tasks to be overcome, two main problems that can be perceived include:

1. First, the supply of constant voltage, constant frequency power from an ISG machine connected to the engine. This is potentially difficult to achieve due to the variable rotational speed of the machine, and the irregularity which characterises the regenerative energy cycles (due to the specific driving conditions). Typically, the

method utilised to obtain an invariable voltage and frequency from a variable-speed generator is to transform the power first into DC, and subsequently into the sought-after sinusoidal signal. The only feasible approach is the integration within vehicles of a scaled-down turbine generator as employed within aircraft. These electrical machines operate at a steady speed and therefore the power generated has a constant frequency and amplitude. In fact, a new vehicle prototype has been introduced (October 2010) by Jaguar Land Rover which proposes the integration of micro gas turbines within future HEVs (JaguarLandRover, 2010). For reference, Figures A9.1 and A9.2 in Appendix H give an indication of the proposed concept.

2. Second, the fact that the energy storage within vehicles is in the form of DC power (i.e. batteries). Therefore, surplus energy from the ISG would have to be converted into DC power for storage. Conversely, if the loads power demand exceeds the instantaneous capability of the ISG, battery energy is used which involves yet another conversion process.

Furthermore, the potential for the HFAC architecture to become a viable alternative to the 42V bus may be underpinned by the improvement in packaging technology of power converter units. For the specific case study presented in this Chapter, the total mass of the DC/AC inverters is approximately 13kg. Consequently, lighter power electronic modules can potentially save mass in the order or several kg.

Conclusively, an auxiliary HFAC power bus appears to be an attractive alternative to DC systems for high-voltage and low-torque motor actuators in vehicles. At the system level, due to the high mass and energy losses of existing power converters, the use of HFAC is not yet feasible.

Chapter 10

Conclusions and further work

The critical investigation of HFAC power for the vehicle auxiliary electrical system has indicated that the technology is not expected to be a viable alternative to the 42V DC PowerNet from a mass and electrical energy perspective. Although the latter has not been adopted by the automotive industry as yet, it has been chosen within this analysis as a basis for comparison with the proposed 100V, 50kHz HFAC bus due to their similar power capability.

The present study has argued that the HFAC electrical system is expected to be advantageous for high-voltage, low-torque electrical motor actuators in vehicles. At the system level, the prominent limitation of the proposed system is the requirement for a DC/HFAC power transformation stage, which does not have an equivalent within the DC architecture. It has become apparent during the system-level investigation that the added mass and energy loss at the power generation stage are the principal characteristics negating a favourable prospect for the system-level integration of the proposed technology.

The most notable advantage associated with the use of HFAC is the possibility to replace low-torque DC rotary actuators with 400Hz AC induction machines. The latter are known to be lightweight and compact actuators, and the automotive industry may benefit from the existing component supply base developed for the aircraft industry. Also, the HFAC system offers advantages such as load galvanic isolation and the magnetically-coupled connectors.

HFAC conductors are expected to be lightweight and energy-efficient. Looking at this aspect in isolation indicates that the proposed bus offers considerable benefits in

comparison with 14V DC and 42V DC cables. However, it has been argued in Chapter 9 that this benefit differs by one order of magnitude in comparison to the negative impact of the HFAC power generation sub-system. Therefore, the advantage of HFAC at the power distribution sub-system is not anticipated to be of significance in the overall system balance.

Due to this finding, and based on the fact that characteristics of a state-of-the-art conductor have been used as part of the investigation, it is likely that future improvements in cable technology will not have a noteworthy impact for the prospect of the HFAC system.

The aspects which are expected to make a favourable difference for the proposed electrical bus are the mass and efficiency of the power electronic modules. This is particularly important for the power generation sub-system.

Nevertheless, since the efficiency of the current power electronic circuits is already very high (90% and up to 95%), further progress may be only incremental. In addition, the collected data for the weight of commercially-available power converters is characteristic of optimally designed modules. As a result, the features of the only sub-system that can potentially change the outlook for an on-board HFAC power bus are not expected to improve significantly in the future.

The main limitation of the HFAC system stems from the proposed integration of the technology with the on-board DC power supply, which requires the use of various power transformation modules. As indicated in Chapter 9, the power loss and mass associated with the power electronic circuits are in the order of 2kW and 13kg, respectively.

Consequently, a new integration approach should be adopted as part of future work. Namely, the HFAC bus should become completely detached of the existing DC system

in vehicles, and the loads supplied by the unaltered HFAC power as used for power distribution.

The advantage of such an approach is that the HFAC power conversion stages can be eliminated. Specifically, the HFAC sinusoid can be produced by a micro-turbine generator, for example, while the loads can be attached to the bus in a plug-and-play mode without the need for interfacing power modules. Essentially, the proposed architecture model is similar to the 400Hz AC power network employed in aircraft.

Further work

Further work can investigate such a concept and take the results of the present work as a starting point. In particular, as argued within this study:

- High-torque electrical motors should be supplied by DC power. This aspect is beneficial for the performance of the actuators (such as the torque ripple). In addition, high-torque actuators typically employ a variable speed drive which may require additional power electronics for the integration within the constant-frequency bus concept.
- Due to the on-board energy storage in the form of DC voltage and current, regenerative loads should have a direct connection with the DC bus.
- The most significant impact of AC power distribution at high frequency is in the potential seamless integration of constant-speed AC motors. Therefore, as part of further work, low and medium frequency AC machines can be investigated as potential on-board actuators. A similar actuator profile matching process as presented in Chapter 8 can be conducted.
- although the power conversion efficiency for the particular case of HFAC to 14V DC is more efficient than 42V/14V DC, Chapter 9 has indicated that this beneficial aspect does not have a significant impact for the system-level analysis.

Consequently, the author proposes that further work addresses the potential benefits of an architecture where no power conversion stages are required, and:

- the HFAC power generation function is fulfilled by an aircraft-like micro turbine,
- power is transmitted at high frequency to AC motor loads only, and finally
- the motor actuators are supplied directly with HFAC power.

Provided that the proposed concept becomes a feasible alternative to an equivalent DC system, further research should address the following issues:

- the electromagnetic interference of the HFAC sinusoid with the surrounding electronic equipment;
- power distribution at a frequency and voltage amplitude which are in line with the electrical safety regulations. As indicated in this work, power distribution at 115V 400Hz AC as in aircraft is not yet permitted within vehicles;
- whether the quiescent power loss is significant or not in the overall energy balance of the network;
- the matching of the load impedance to the electrical source impedance, for maximum power transfer to the auxiliary applications from the supply.

References

AFRIDI, K. K. (1998) Evaluation of advanced automotive electrical system architectures using MAESTrO. Power Electronics in Transportation, 1998.

AGRAWAL, V., AGARWAL, A. K. & KANT, K. (1992) A study of single-phase to three-phase cycloconverters using PSPICE. Industrial Electronics, IEEE Transactions on, 39, 141-148.

ANTALOAE, C., MARCO, J. & VAUGHAN, N. (2011) Feasibility of High Frequency Alternating Current Power for Motor Auxiliary Loads in Vehicles. Vehicular Technology, IEEE Transactions on, Pre-Publication, 1-1.

ANTALOAE, C., MARCO, J. & VAUGHAN, N. D. (2010) Investigation of High Frequency AC Power Distribution Benefits for the Automobile Auxiliary Electrical System. SAE Int. J. Passeng. Cars – Electron. Electr. Syst., 3, 109-121.

ANTALOAE, C., MARCO, J. & VAUGHAN, N. D. (2010) High Frequency Alternating Current Power Supply for Automobile Auxiliary Electrical Systems. International Symposium on POWER ELECTRONICS, ELECTRICAL DRIVES, AUTOMATION and MOTION. Pisa, Italy, IEEE.

ARC SYSTEMS (2008) http://www.globalspec.com/FeaturedProducts/Detail/ARCSystems/Aircraft_Style_400_Hz_AC_Induction_Motors/118131/0 (last accessed in November 2010).

BENDYK, M., LUK, P. C. K. & JINUPUN, K. (2007) Direct torque control of induction motor drives using high frequency pulse density modulation for reduced torque ripple and switching losses. IN IEEE (Ed.).

BIANCHI, N. & BOLOGNANI, S. (2000) Design techniques for reducing the cogging torque in surface-mounted PM motors. Industry Applications Conference, 2000. Conference Record of the 2000 IEEE.

BIANCHI, N., BOLOGNANI, S. & DAI PRE, M. (2005) Design of a Fault-tolerant IPM Motor for Electric Power Steering. Power Electronics Specialists Conference, 2005. PESC '05. IEEE 36th.

BOSCH (2004) Bosch automotive handbook.

BOSCHMOTORS (2010) http://www.boschmotorsandcontrols.co.uk/elektromotoren/gleichstrommotoren/ohne-getriebe/index.htm (last accessed in November 2010).

BOSE, B. K., MIN-HUEI, K. & KANKAM, M. D. (1996) High frequency AC vs. DC distribution system for next generation hybrid electric vehicle. Industrial Electronics, Control, and Instrumentation, 1996., Proceedings of the 1996 IEEE IECON 22nd International Conference on.

CAI, W. (2004) Comparison and review of electric machines for integrated starter alternator applications. Industry Applications Conference, 2004. 39th IAS Annual Meeting. Conference Record of the 2004 IEEE.

CALISKAN, V. (2000) A Dual/High-Voltage Automotive Electrical Power System with Superior Transient Performance. Department of Electrical Engineering and Computer Science. Massachusetts Institute of Technology

CHANG, W. S. (2003) An Electromechanical Valve Drive Incorporating a Nonlinear Mechanical Transformer. Department of Electrical Engineering and Computer Science. Massachusetts Institute of Technology

CHIU (2002) Electromechanical actuators, CRC Press.

CORREA, J. M., CHAKRABORTY, S., SIMOES, M. G. & FARRET, F. A. (2003) A single phase high frequency AC microgrid with an unified power quality conditioner. Industry Applications Conference, 2003. 38th IAS Annual Meeting. Conference Record of the.

DALLAS SEMICONDUCTOR (2004) Why drive white LEDs with constant current? (Application Note 3256).

DENSO (2010) http://www.densoproducts.com/product.asp?productCategoryID=8 (accessed November 2010).

DHAR, P., MUSAVI, F., ZHANG, H., JAIN, P., JAIN, D. & BANSAL, N. (2002) Technical Report - A Resonant AC/DC Converter for High Frequency Power Distribution Systems Cistel technology Inc.

DROBNIK, J. (1994) High frequency alternating current power distribution. Telecommunications Energy Conference, 1994. INTELEC '94., 16th International.

DROBNIK, J., HUANG, L., JAIN, P. & STEIGERWALD, R. (1999) PC platform power distribution system-past application, today's challenge and future direction. Telecommunications Energy Conference, 1999. INTELEC '99. The 21st International.

EKI, H., TERATANI, T. & IWASAKI, T. (2007) Power Consumption and Conversion of EPS Systems. Power Conversion Conference - Nagoya, 2007. PCC '07.

EMADI, A. (2005) Handbook of Automotive Power Electronics and Motor Drives, CRC Press, Taylor & Francis Group.

EMADI, A., EHSANI, M. & M.MILLER, J. (2004) Vehicular Electric Power Systems: Land, Sea, Air, and Space Vehicles.
GERBER, M., FERREIRA, J. A., SELIGER, N. & HOFSAJER, I. W. (2005) Design and evaluation of an automotive integrated system module. Industry Applications Conference, 2005. Fourtieth IAS Annual Meeting. Conference Record of the 2005.

GRAOVAC, D., KOPPL, B., SCHEFFER, M., KIEP, A. & PURSCHEL, M. (2008) Optimal PWM method for electric and electro-hydraulic power steering applications. Power Electronics Specialists Conference, 2008. PESC 2008. IEEE.

GRAOVAC, D. A., PÜRSCHEL, M. & KIEP, A. (2006) MOSFET Power Losses Calculation Using the Data-Sheet Parameters (Application Note 1.1). Infineon.

HANSEN, I. G. (1988) Status of 20 kHz Space Station Power Distribution Technology. National Aeronautics and Space Administration Lewis Research Center.

HONEYWILL, T. (2007) Down to the wire. Automotive Engineer. UK, Professional Engineering Publishing Limited (publishing company of the Institution of Mechanical Engineers).

HP7001A (1999) HP 7001A Mainframe Installation and Verification Manual.

HUR, J. (2008) Characteristic Analysis of Interior Permanent-Magnet Synchronous Motor in Electrohydraulic Power Steering Systems. IEEE Transactions on Industrial Electronics, 55.

ILES-KLUMPNER, D., SERBAN, I. & RISTICEVIC, M. (2006) Automotive Electrical Actuation Technologies. Vehicle Power and Propulsion Conference, 2006. VPPC '06. IEEE.

INFINEON (2002) AP32029 - Peak and Hold Current Shape Generated by TriCore Derivative TC 1775. Infineon Technologies.

JAGUAR LAND ROVER (2010) http://www.autocar.co.uk/News/NewsArticle/AllCars/247785/ (last accessed in November 2010).

JAIN, A. K., MATHAPATI, S., RANGANATHAN, V. T. & NARAYANAN, V. (2006) Integrated starter generator for 42-V powernet using induction machine and direct torque control technique. Power Electronics, IEEE Transactions on, 21, 701-710.

JAIN, P. & PINHEIRO, H. (1999) Hybrid high frequency AC power distribution architecture for telecommunication systems. Aerospace and Electronic Systems, IEEE Transactions on, 35, 138-147.

JAIN, P., TANJU, M. C. & BOTTRILL, J. (1993) AC/DC converter topologies for the Space Station. Aerospace and Electronic Systems, IEEE Transactions on, 29, 425-434.
JAIN, P. K. & TANJU, M. C. (1989) A 20 kHz hybrid resonant power source for the space station. Aerospace and Electronic Systems, IEEE Transactions on, 25, 491-496.

JOÃO AFONSO, C. C., JÚLIO MARTINS (2000) Active Filters with Control Based on the p-q Theory. IEEE Industrial Electronics Society Newsletter vol. 47, no. 3, Sept. 2000, ISSN: 0746-1240, pp. 5-10 IEEE.

JOHNSTON, R. H. (1996) A history of automobile electrical systems. Automotive Engineering, 53-66.

JORDAN, H. E. (1994) Energy-Efficient Electric Motors and Their Applications, Plenum Press, New York.

JUICE (2008) Cable designed by Juice Technology Ltd. . UK.

JUN-HYUK, C., SE-HYUN, Y., JIN, H. & HA-GYEONG, S. (2007) The Design and Fabrication of BLDC Motor and Drive for 42V Automotive Applications. Industrial Electronics, 2007. ISIE 2007. IEEE International Symposium on.

KASSAKIAN, J. G., WOLF, H. C., MILLER, J. M. & HURTON, C. J. (1996) Automotive electrical systems circa 2005. Spectrum, IEEE, 33, 22-27.

KEIM, T. A. (2004) 42 Volts - The View from Today. IN ASSOCIATION, C. T. E. (Ed.).

KHAN, I. A. (1999) Automotive electrical systems: architecture and components. Digital Avionics Systems Conference, 1999. Proceedings. 18th.

KLODE, H., OMEKANDA, A. M., LEQUESNE, B., GOPALAKRISHNAN, S., KHALIL, A., UNDERWOOD, S. & HUSAIN, I. (2006) The Potential of Switched Reluctance Motor Technology for Electro-Mechanical Brake Applications SAE Technical Paper Series, 2006-01-0296.

KOKES, M. (1997) Resonantes Wecselspannungsbordnetz für Kraftfahrzeuge und dessen Beschreibung mit Zustandszeigern. Bochum University.

LIU, G., KURNIA, A., LARMINAT, R. D., DESMOND, P. & O'GORMAN, T. (2004) A Low Torque Ripple PMSM Drive for EPS Applications. IN IEEE (Ed.). IEEE.

LOURDES, S. (2010) Isolated Mosfet Module - Test Report. Cranfield University.

LUK, P. C.-K. & NG, A. S. Y. (2008) High Frequency AC Power Distribution Platforms. IN SPRINGERLINK (Ed.) Power Electronics in Smart Electrical Energy Networks. Springer London.

LUKIC, S. M. & EMADI, A. (2002) Performance analysis of automotive power systems: effects of power electronic intensive loads and electrically-assisted propulsion systems. Vehicular Technology Conference, 2002. Proceedings. VTC 2002-Fall. 2002 IEEE 56th.

LUKIC, S. M. & EMADI, A. (2003) Effects of Electrical Loads on 42V Automotive Power Systems. IN INTERNATIONAL, S. (Ed.) Future Transportation Technology Conference & Exhibition, June 2003; Session: Vehicle Power Systems and 42 Volt Technology. Costa Mesa, CA, USA, SAE.

MASRUR, M. A., SITAR, D. S. & SANKARAN, V. A. (1998) Can an AC (alternating current) electrical system replace the present DC system in the automobile? An investigative feasibility study. I. System architecture. Vehicular Technology, IEEE Transactions on, 47, 1072-1080.

MASRUR, M. A., SITAR, D. S. & SANKARAN, V. A. (1998) Can an AC (alternating current) electrical system replace the present DC system in the automobile? An investigative feasibility study. II. Comparison and tradeoffs. Vehicular Technology, IEEE Transactions on, 47, 1081-1086.

MATHWORKS (2009) SimPowerSystems Toolbox, Power Electroncis Library, MOSFET model implementation example.

MEI, Q. & JAIN, P. K. (2002) System performance of a high frequency AC power distribution system. Telecommunications Energy Conference, 2002. INTELEC. 24th Annual International.

MILLER, J. M. (1996) Multiple voltage electrical power distribution system for automotive applications. Energy Conversion Engineering Conference, 1996. IECEC 96. Proceedings of the 31st Intersociety.

MILLER, J. M., EMADI, A., RAJARATHNAM, A. V. & EHSANI, M. (1999) Current status and future trends in More Electric Car power systems. Vehicular Technology Conference, 1999 IEEE 49th.

MILLER, J. M. & NICASTRI, P. R. (1998) The next generation automotive electrical power system architecture: issues and challenges. Digital Avionics Systems Conference, 1998. Proceedings., 17th DASC. The AIAA/IEEE/SAE.

MIZHI, Z. & LITTLE, T. A. (2006) Evaluation on basic resonant structures and voltage clamping techniques. IEEE Industrial Electronics, IECON 2006 - 32nd Annual Conference on.

MUAMER, H., LIANG, C. & LIU, S. (2004) Design and simulation of a moving coil linear actuator for automotive applications. Industrial Technology, 2004. IEEE ICIT '04. 2004 IEEE International Conference on.

MURAKAMI, H., KATAOKA, H., HONDA, Y., MORIMOTO, S. & TAKEDA, Y. (2001) Highly efficient brushless motor design for an air-conditioner of the next generation 42 V vehicle. Industry Applications Conference, 2001. Thirty-Sixth IAS Annual Meeting. Conference Record of the 2001 IEEE.

MURATAPOWER (2010) http://www.murata-ps.com/cgi-bin/cd4power.storefront/EN/ Catalog/1001 (las accessed in November 2010).

NAIDU, M., NEHL, T. W., GOPALAKRISHNAN, S. & WURTH, L. (2003) A semi-integrated sensorless PM brushless drive for a 42 V automotive HVAC compressor. Industry Applications Conference, 2003. 38th IAS Annual Meeting. Conference Record of the.

NG, A. S. Y. (2010) High Frequency AC Power Supply. Power Systems and Drives, PhD Thesis, Cranfield University.

O'DWYER, J., PATTERSON, C. & REIBE, T. (1996) Dual voltage alternator. Machines for Automotive Applications (Digest No. 1996/166), IEE Colloquium on.

PATEL, M. R. (2005) Spacecraft Power Systems, CRC Press.

PRESSMAN, A. I. (1998) Switching Power Supply Design, McGraw-Hill.

QIU, Y. H., PARLIKAR, T. A., CHANG, W. S., SEEMAN, M. D., KEIM, T. A., PERREAULT, D. J. & KASSAKIAN, J. G. (2004) Design and experimental evaluation of an electromechanical engine valve drive. Power Electronics Specialists Conference, 2004. PESC 04. 2004 IEEE 35th Annual.

RAJASHEKARA, K. (2003) 42 V architecture for automobiles. Electrical Insulation Conference and Electrical Manufacturing & Coil Winding Technology Conference, 2003. Proceedings.

RASHID, M. H. (2007) Power Electronics Handbook. IN ACADEMIC PRESS, E. (Ed.) Second Edition ed.

RENZ, D., ROBERT, C., FINKE, N. & OOHN, S., JAMES E. TRINER, AND IRVING6. HANSEN (1983) Design considerations for large space electric power system. NASA Lewis Research Center Clevelnd.

SAE (1999) Electrical Systems: SAE J2232 JUN1999—Vehicle System Voltage—Initial Recommendations. SAE.

SINERGEX (2010) http://www.sinergex.nl/products_purewatts_1500.php.

SL-MTI (2010) http://www.slmti.com/inm/default.asp?metric=true (last accessed in November 2010).

SMITH, C. R. (1991) Review of Heavy Duty Dual Voltage Systems. IN SAE (Ed.) International Off-Highway & Powerplant Congress & Exposition. SAE.

SOOD, P. K. & LIPO, T. A. (1988) Power conversion distribution system using a high-frequency AC link. Industry Applications, IEEE Transactions on, 24, 288-300.

SOOD, P. K., LIPO, T. A. & HANSEN, I. G. (1988) A versatile power converter for high-frequency link systems. Power Electronics, IEEE Transactions on, 3, 383-390.

SUDIPTA, C., MANOJA, D. W. & SIMOES, M. G. (2007) Distributed Intelligent Energy Management System for a Single-Phase High-Frequency AC Microgrid. Industrial Electronics, IEEE Transactions on, 54, 97-109.

TONIUS, N. (2009) MSc Thesis, An electric power-assisted steering test rig. Department of Automotive Engineering, School of Engineering, Cranfield University UK

TRACOPOWER (2010) DC/DC Converter TSC Series 50 - 2500 Watt. http://www.tracopower.com/fileadmin/medien/dokumente/pdf/products/dc_dc_converters/tsc.pdf (accessed on 1/11/2010).

TRACOPOWER (2010) http://www.tracopower.com/AC-DC-Power-Supplies.205.0.html (last accessed in November 2010).

TRIPPLITE (2010) http://www.tripplite.com/en/products/product-series.cfm?txtSeriesID=815 (last accessed in November 2010).

TSUNG-PO, C., YEN-SHIN, L. & CHANG-HUAN, L. (1999) A new space vector modulation technique for inverter control. Power Electronics Specialists Conference, 1999. PESC 99. 30th Annual IEEE.

VENKATESAN, K. & LINDSAY, J. F. (1982) Comparative Study of the Losses in Voltage and Current Source Inverter Fed Induction Motors. Industry Applications, IEEE Transactions on, IA-18, 240-246.

VISHAY (2008) Datasheet, Aluminium Capacitors, Document number 91000.

WANG, C., SHEN, J., JIN, M., LUK, P. C.-K. & FEI, W. (2010) Design Issues of an IPM BLAC Motor Used for Electric Power Steering. Fifth International Conference and Exhibition on Ecological Vehicles and Renewable Energies. Monte Carlo.

WATSON, R., CHEN, W., HUA, G. & LEE, F. C. (1996) Component development for a high-frequency AC distributed power system. Applied Power Electronics Conference and Exposition, 1996. APEC '96. Conference Proceedings 1996., Eleventh Annual.

WHALEY, D. M., SOONG, W. L. & ERTUGRUL, N. (2004) EXTRACTING MORE POWER FROM THE LUNDELL CAR ALTERNATOR. Australasian Universities Power Engineering Conference (AUPEC 2004). Brisbane, Australia.

WIKIPEDIA http://en.wikipedia.org/wiki/Prim%27s_algorithm.

XANTREX (2009) Xantrex Pro Watt 250.

XANTREX (2010) http://www.xantrex.com/power-products/power-inverters/overview.aspx (last accessed in November 2010).

Appendices

Appendix A

Akagi (1983) proposed "The Generalized Theory of Instantaneous Reactive Power in Three-Phase Circuits", known an the *p-q theory*. It is valid for steady state and transitory operation of three-phase power systems as well as for generic voltage and current waveforms. The *p-q theory* consists of an algebraic transformation, known as the *Clarke transformation* of the three-phase voltages and currents in the *a-b-c* coordinates to the $\alpha-\beta-0$ coordinates, followed by the calculation of the *p-q* instantaneous power components:

$$
\begin{bmatrix} v_0 \\ v_\alpha \\ v_\beta \end{bmatrix} = \sqrt{\frac{2}{3}} \cdot \begin{pmatrix} \frac{1}{\sqrt{2}} & \frac{1}{\sqrt{2}} & \frac{1}{\sqrt{2}} \\ 1 & -\frac{1}{2} & -\frac{1}{2} \\ 0 & \frac{\sqrt{3}}{2} & -\frac{\sqrt{3}}{2} \end{pmatrix} \cdot \begin{bmatrix} v_a \\ v_b \\ v_c \end{bmatrix} \quad , \quad \begin{bmatrix} i_0 \\ i_\alpha \\ i_\beta \end{bmatrix} = \sqrt{\frac{2}{3}} \cdot \begin{pmatrix} \frac{1}{\sqrt{2}} & \frac{1}{\sqrt{2}} & \frac{1}{\sqrt{2}} \\ 1 & -\frac{1}{2} & -\frac{1}{2} \\ 0 & \frac{\sqrt{3}}{2} & -\frac{\sqrt{3}}{2} \end{pmatrix} \cdot \begin{bmatrix} i_a \\ i_b \\ i_c \end{bmatrix}
$$

Clarke transformation matrix

$$
\begin{bmatrix} p \\ q \end{bmatrix} = \begin{pmatrix} v_\alpha & v_\beta \\ -v_\beta & v_\alpha \end{pmatrix} \cdot \begin{bmatrix} i_\alpha \\ i_\beta \end{bmatrix}
$$

(1)

The power components of the *p-q* theory in the $\alpha-\beta-0$ coordinates are shown in Figure A2.1 (João Afonso, 2000), where:

$\overline{p_0}$ corresponds to the energy per time unity which is transferred from the power supply to the load through the zero-sequence components of voltage and current

$\widetilde{p_0}$ corresponds to the energy per time unity which is exchanged between the power supply and the load through the zero-sequence components of voltage and current

$\overline{p}$ is the mean value of the instantaneous real power, corresponding to energy per time unity transferred from source to load

$\tilde{p}$ is the alternated value of the instantaneous real power (the energy per time unity exchanged between source and load)

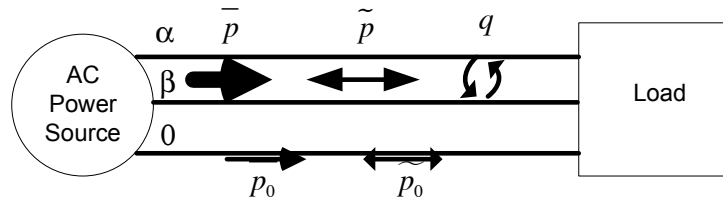q is the instantaneous imaginary power, power exchanged between the phases of the loads.

Figure A2.1 Power components of the *p-q* theory
in $\alpha - \beta - 0$ coordinates (João Afonso, 2000)

The reference compensation currents in the $\alpha - \beta - 0$ coordinates are:

$$\begin{bmatrix} i_{c\alpha}^* \\ i_{c\beta}^* \end{bmatrix} = \frac{1}{v_\alpha^2 + v_\beta^2} \cdot \begin{pmatrix} v_\alpha & -v_\beta \\ v_\beta & v_\alpha \end{pmatrix} \cdot \begin{bmatrix} \tilde{p} - \overline{p_0} \\ q \end{bmatrix} \quad (2)$$

which are transformed as follows to give the reference compensation currents in the *a-b-c* reference system (for a three-phase general system):

$$\begin{bmatrix} i_{ca}^* \\ i_{cb}^* \\ i_{cc}^* \end{bmatrix} = \sqrt{\frac{2}{3}} \cdot \begin{pmatrix} \frac{1}{\sqrt{2}} & 1 & 0 \\ \frac{1}{\sqrt{2}} & -\frac{1}{2} & \frac{\sqrt{3}}{2} \\ \frac{1}{\sqrt{2}} & -\frac{1}{2} & -\frac{\sqrt{3}}{2} \end{pmatrix} \cdot \begin{bmatrix} i_{c0}^* \\ i_{c\alpha}^* \\ i_{c\beta}^* \end{bmatrix} \quad (3)$$

Figure A2.2 HP 70000 Spectrum Analyser Modular System (HP7001A, 1999)

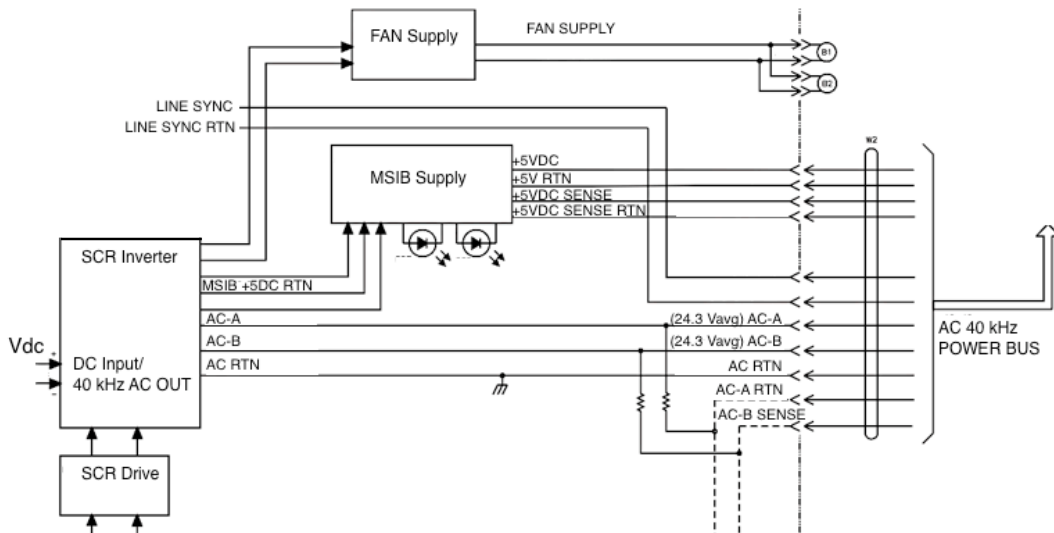Figure A2.3a HP 70000 Spectrum Analyser mainframe power (HP7001A, 1999)

Figure A2.3b HP 70000 A Mainframe Block Diagram -
Section of power supply of 40 kHz (HP7001A, 1999)

Appendix B

In order to understand the equivalent circuit diagrams used in the study to represent the HFAC electrical modules, it is indicated to follow the two-step general process depicted in Figure A3.1 and detailed in Table A3.1. The transformations hold for both AC and DC circuits.

The transformation matrix T, denoted the chain matrix, provides a convenient algebraic way to represent the relationship between currents and voltages on the two sides of a transformer. The voltage in the secondary winding is directly proportional to the voltage in the primary by a ratio n_2 / n_1, which is the proportion of the two winding turns.
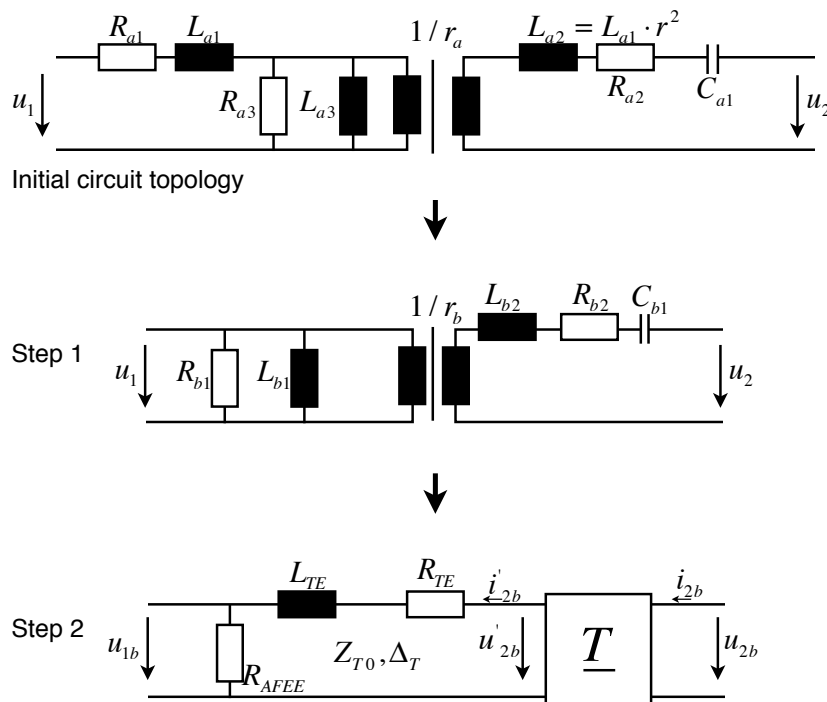

Figure A3.1 The process of obtaining the equivalent
circuit representation (Kokes, 1997)

Table A3.1 Equivalent transformations for the two steps shown in Figure A3.1

Step 1 transformations	Step 2 transformations
$r_b = r_a \cdot \dfrac{L_{a3}}{L_{a1} + L_{a3}}$	$\underline{T} = \begin{pmatrix} 1/r_b & 0 \\ 0 & r_b \end{pmatrix}$
$C_{b1} = C_{a1} \cdot \left(\dfrac{L_{a3}}{L_{a1} + L_{a3}} \right)^2 \cdot r_a^2$	$Z_{T0} = \sqrt{\dfrac{L_{b2}}{C_{b1}}} \cdot \dfrac{1}{r_b^2}$
$L_{b2} = r_a^2 \cdot \dfrac{L_{a1}^2 + 2 \cdot L_{a1} \cdot L_{a3}}{L_{a1} + L_{a3}}$	$\Delta_T = \dfrac{1 - \omega_s \cdot \sqrt{L_{b2} \cdot C_{b1}}}{\omega_s \cdot \sqrt{L_{b2} \cdot C_{b1}}}$
$L_{b1} = L_{a1} + L_{a3}$	$L_{TE} = \dfrac{\pi^2}{4 \cdot r_b^2} \cdot \left(1 + \Delta_T \right)^2 \cdot L_{b2}$
$R_{b2} \approx R_{a2} + r_a^2 \cdot \left(\dfrac{L_{a3}}{L_{a1} + L_{a3}} \right)^2 \cdot R_{a1}$	$R_{TE} = \dfrac{\pi^2}{8 \cdot r_b^2} \cdot \left(1 + \Delta_T \right) \cdot R_{b2}$
$R_{b1} \approx R_{a1} + R_{a3}$	$R_{AFEE} \approx R_{b1}$

The current in the secondary winding is inversely proportional by the same factor to the primary winding current, as indicated by the following relationship:

$$\begin{bmatrix} u'_{2b} \\ i'_{2b} \end{bmatrix} = \underline{T} \cdot \begin{bmatrix} u_{2b} \\ i_{2b} \end{bmatrix} = \begin{pmatrix} 1/r_b & 0 \\ 0 & r_b \end{pmatrix} \cdot \begin{bmatrix} u_{2b} \\ i_{2b} \end{bmatrix} \quad (1)$$

Figure A3.2 shows the equivalent electrical circuit of the inverter. U_{ZW} is the input battery voltage, u_{Nb} is the output square-wave AC voltage and i_{Nb} the sinusoid al output current which is regulated with the factor Δ_A (as previously shown in Table A3.1). The inverter includes a series resonant current converter with clamping diodes. Also, the circuit comprises a boost converter that steps up the battery voltage to a constant value of 435V (U_{ZW}). Table A3.2 presents the parameters of the DC/HFAC inverter.
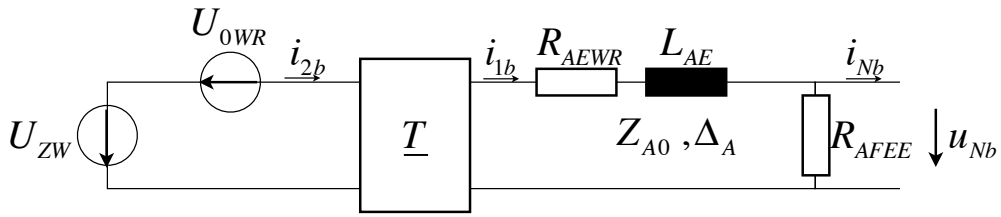
Figure A3.2 Equivalent circuit diagram of feed inverter (Kokes, 1997)

Table A3.2 Parameters of the feed inverter equivalent circuit

$\underline{T} = \begin{pmatrix} 1/5.35 & 0 \\ 0 & 5.35 \end{pmatrix}$	$Z_{A0} = 462 m\Omega$	$\Delta_A = 0.15$
$R_{AEWR} = 11.8 m\Omega$ (AC resistance)	$U_{0WR} = 2.56V$	$L_{AE} = 8.36 \mu H$
$L_h = 570 \mu H$	$R_{AFEE} = 435\Omega$	

The front module can supply 42V DC at a rated power of 1kW, and 13V DC at 500W. The different power ratings of the two submodules yields higher equivalent DC resistance of the 13V circuit (R_{AEGR1}) in comparison to the resistance of the 42V circuit (R_{AEGR2}). Figure A3.3 illustrates the front module equivalent circuit and Table A3.3 lists its parameters.
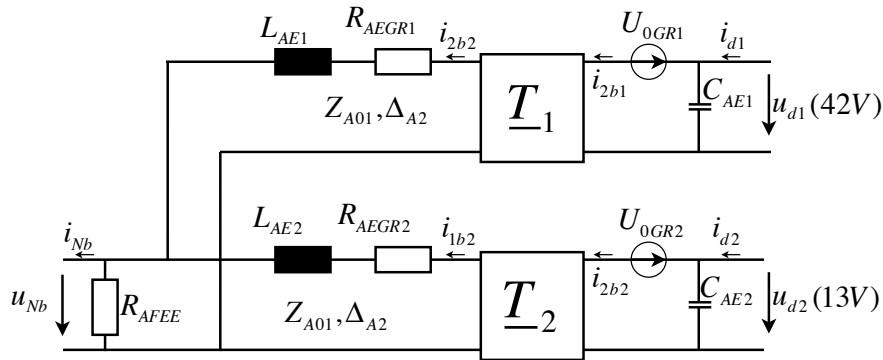

Figure A3.3 Equivalent circuit diagram of front module (Kokes, 1997)

Table A3.3 Parameters of the front module equivalent circuit

$\underline{T}_1 = \begin{pmatrix} 1/0.529 & 0 \\ 0 & 0.529 \end{pmatrix}$	$Z_{A01} = 0.6\Omega$	$\Delta_{A1} = 0.22$
$\underline{T}_2 = \begin{pmatrix} 1/0.166 & 0 \\ 0 & 0.166 \end{pmatrix}$	$Z_{A01} = 1.42\Omega$	$\Delta_{A2} = 0.2$
$R_{AEGR1} = 330m\Omega$	$U_{0GR1} = 0.76V$	$L_{AE1} = 9.3\mu H$
$R_{AEGR2} = 330m\Omega$	$U_{0GR2} = 0.37V$	$L_{AE2} = 22.5\mu H$
$C_{AE1} = 1.41mF$	$C_{AE2} = 13.2mF$	$R_{AFEE} = 650\Omega$
	$L_h = 874\mu H$	

Each of the four high power load modules has an output voltage of 310V DC, rated power of 1.5kW and operates in rectifier mode, as previously mentioned. The equivalent circuit of a high power module is shown in Figure A3.4 and the parameters in Table A3.4.
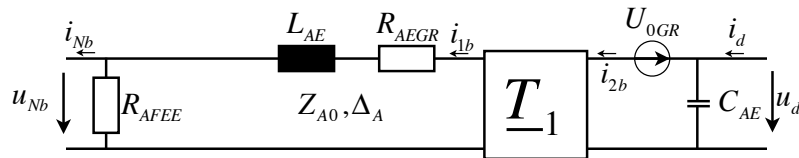

Figure A3.4 Equivalent circuit diagram of high power load module (Kokes, 1997)

Table A3.4 Parameters of the high power module equivalent circuit

$\underline{T}_1 = \begin{pmatrix} 1/3.895 & 0 \\ 0 & 3.895 \end{pmatrix}$	$Z_{A0} = 450m\Omega$	$\Delta_A = 0.18$	
$R_{AEGR} = 80m\Omega$ (DC resistance)	$U_{0GR} = 2.1V$	$L_E = 8.33\mu H$	
$C_{AE} = 440\mu F$	$R_{AFEE} = 1300\Omega$	$L_h = 1.41mH$	

The battery module has an output of 42V DC and a rated power of 1kW. The associated equivalent circuit and parameters are shown in Figure A3.5 and Table A3.5, respectively.
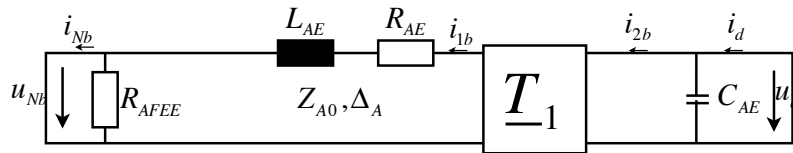

Figure A3.5 Equivalent circuit diagram of battery module (Kokes, 1997)

Table A3.5 Parameters of battery module equivalent circuit

$$\underline{T} = \begin{pmatrix} 1/0.529 & 0 \\ 0 & 0.529 \end{pmatrix} \qquad Z_{A0} = 0.6\Omega \qquad \Delta_A = 0.22$$

$R_{AEGR} = 380\,m\Omega$	$R_{AEWR} = 380\,m\Omega$	$L_{AE} = 9.3\mu H$
$C_{AE} = 1.41\,mF$	$R_{AFEE} = 1300\Omega$	$L_h = 1.35\,mH$

The performance and efficiency of the modules presented are assessed by mathematical models. The validation for the front module consists of comparing simulated and experimental results for DC operation only. Figures A3.6 and A3.7 illustrate the stationary electrical characteristics for the front module, and demonstrate good agreement between the calculated results and experimental data (Kokes, 1997).
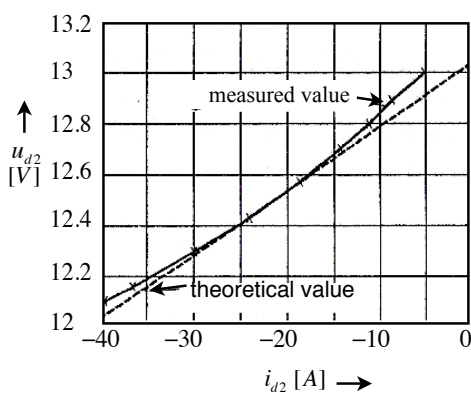

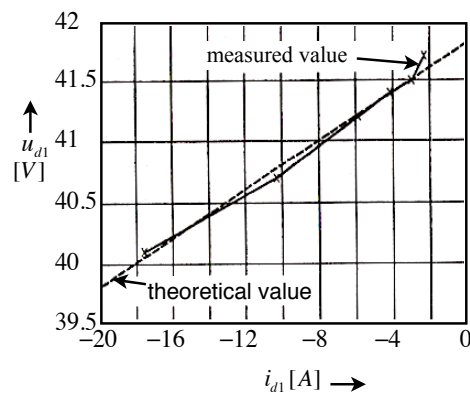Figure A3.6 - Static characteristic of Front module 13 V DC output (Kokes, 1997)

Figure A3.7 - Static characteristic of Front module 42 V DC output (Kokes, 1997)

It is interesting to illustrate the high efficiency curves computed for the network modules. The inverter has an efficiency greater than 90% and is theoretically very close to unity for power output higher than 2kW (Figure A3.8). For the front module, higher efficiency is clearly observable for the 42V DC output (Figure 3.10) in comparison to the 13V DC output (Figure A3.9). Negative power is plotted since the two submodules act as power sources to 42V DC and 13V DC consumers, supplying up to 1kW and 0.5kW, respectively.

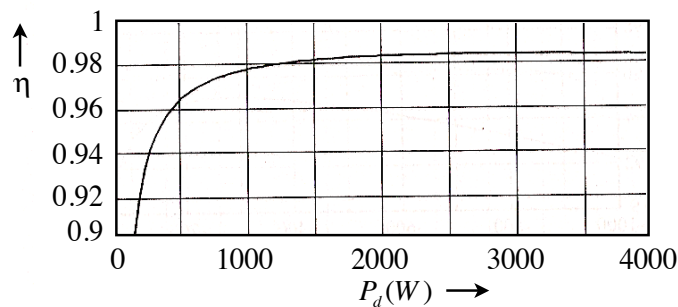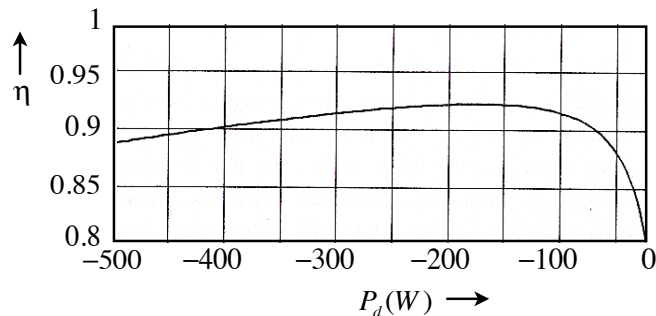Figure A3.8 Calculated static characteristic of inverter efficiency (Kokes, 1997)

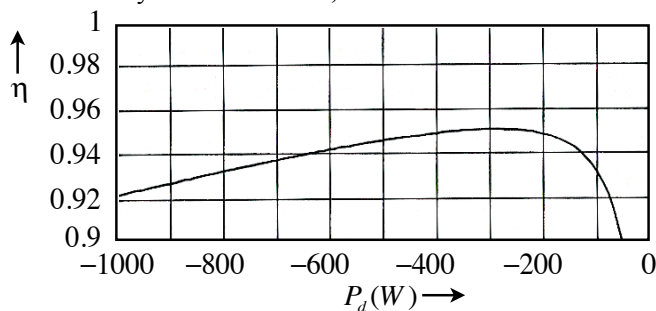Figure A3.9 Efficiency of front module, static characteristic for 13V output (Kokes, 1997)

Figure A3.10 Efficiency of front module, static characteristic for 42V output (Kokes, 1997)

The battery module manages energy flow both to and from the power bus. Efficiency for the two functions (for DC link operation) is approximately symmetrical and is

depicted in Figure A3.11 up to the rated power of 1kW. High calculated efficiency has also been reported for the high power modules, as Figure A3.12 exemplifies.
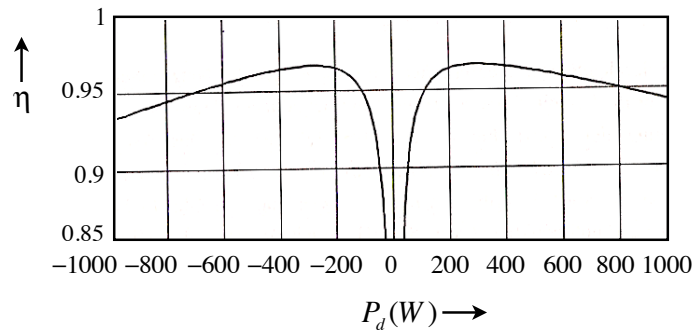
Figure A3.11 Efficiency of battery module, calculated
static characteristic (Kokes, 1997)
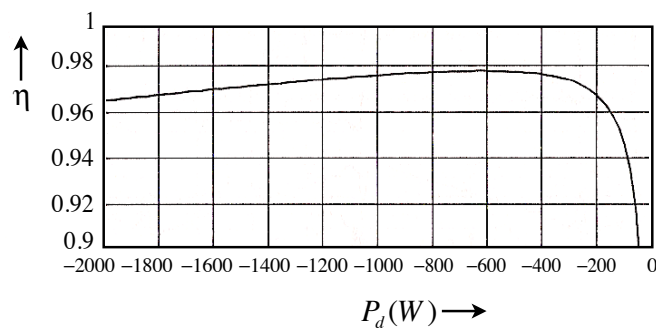
Figure A3.12 Efficiency of high power module,
calculated static characteristic (Kokes, 1997)

The calculated no-load power losses is 49W for DC operation. The value is comparable to the 55W ohmic loss value measured during the experiment. It was pointed out that the no-load power losses for AC components is higher compared to the DC components, although no specific value was given.

Figures A3.14 and A3.15 illustrate the waveforms associated with the HFAC bus variables in steady state operation, for no-load and 800W, respectively. The variables correspond to the inverter schematic diagram in Figure A3.13. These are the bus square

wave voltage u_N, sinusoidal inverter current i_1, clamping diode current i_k and the voltage u_{Ch} over the inverter capacitor C_h.
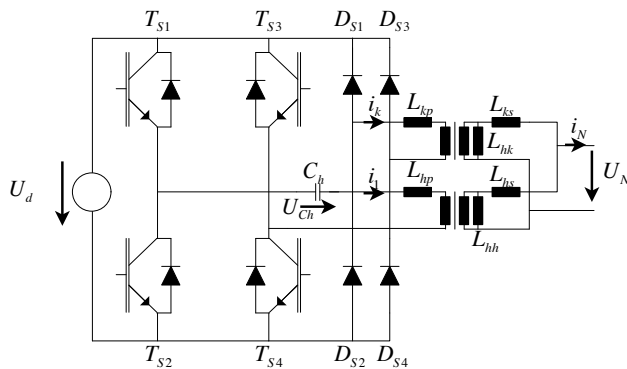
Figure A3.13 HFAC inverter circuit diagram
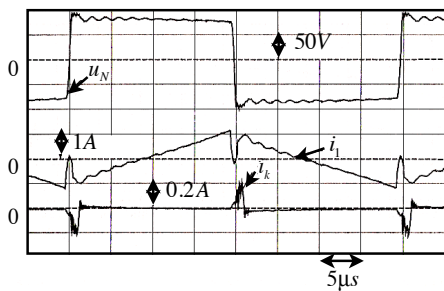
Figure A3.14 Stationary HFAC bus voltage and inverter currents for no-load operation (Kokes, 1997)
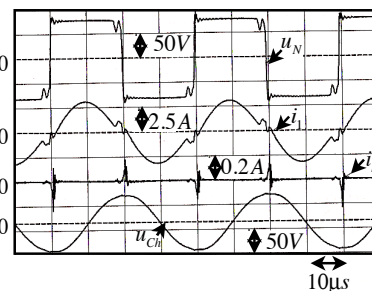
Figure A3.15 Stationary HFAC bus voltage and inverter currents for 800 W load (Kokes, 1997)

For no-load operation, a total bus inductance of 4.4mH was calculated on the basis of a network capacitance of 10.12nF, and a minimum current gap factor of 0.1 (Kokes, 1997). In this situation, a magnetising current is present with a peak of approximately 1A (Figure A3.14).

Figures A3.16 to A3.18 are additional representations of electrical variables for the network in steady state operation. Figure 3.33 shows the waveforms of the bus voltage u_N and current i_N for a front module output power of -420W (at 42V DC). Figures A3.17

and A3.18 illustrate the bus voltage and battery module current for an output power of minus and, respectively, plus 420W.
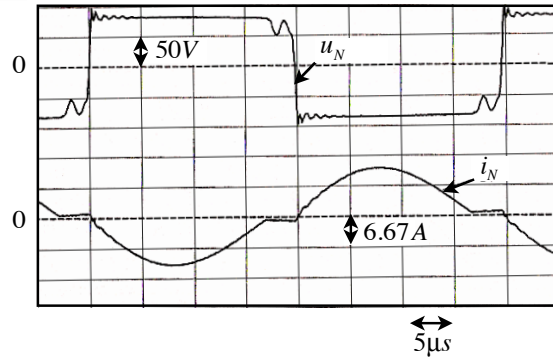
Figure A3.16 Bus voltage and current for -420 W load of front module (Kokes, 1997)
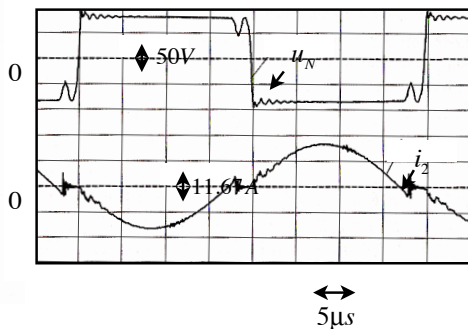
Figure A3.17 Bus voltage and battery module current for -420 W load (Kokes, 1997)
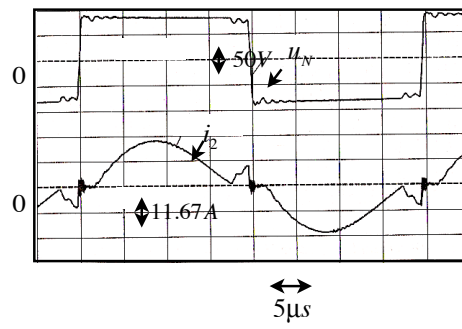
Figure A3.18 Bus voltage and battery module current for 420 W load (Kokes, 1997)

The dynamic behaviour of the HFAC system is first illustrated for a change in power demand for the high power modules, from -800W to -1800W and subsequently from -1800W to -800W. Second, the energy flow in the battery module was reversed from an output of -210W to input power of 420W. Figures A3.19 and A3.20 plot the bus current for the first test. A longer than expected current rise time constant was noticed that has been attributed to the dynamic of the boost converter, which is part of the inverter.
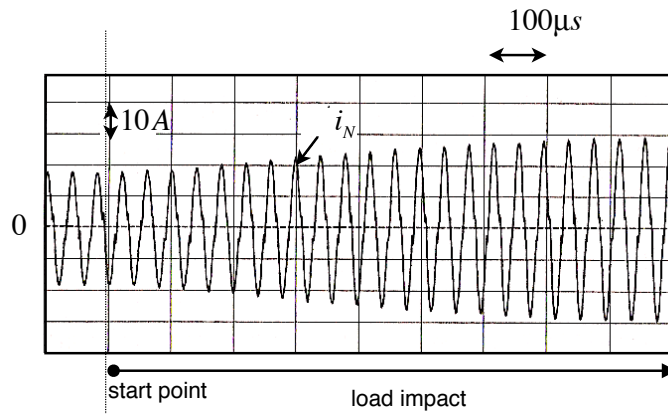
Figure A3.19 Bus current for a load impact from -800 W to -1.8 kW (Kokes, 1997)
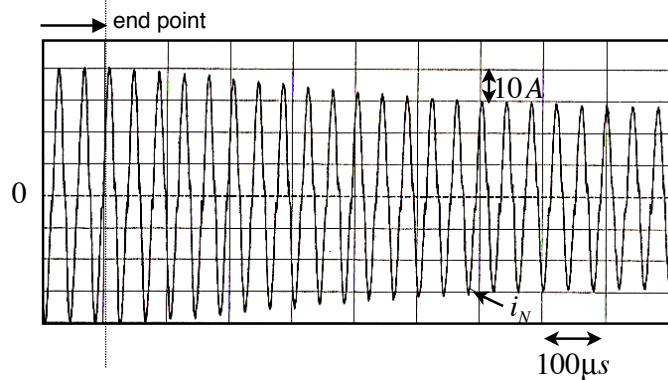
Figure A3.20 Bus current for a load impact from -1.8 kW to -800 W (Kokes, 1997)

Figure A3.21 shows that the dynamic of the network is highly dependent upon the boost converter input current i_E . Also in the Figure are illustrated the waveforms of the DC link voltage u_{ZW} (consistent with the circuit diagram in Figure A3.2). This voltage is the output of the boost converter, kept constant at 435V. Figure A3.21 also illustrates the waveform of the 310V output voltage u_d , from the high power module.

Figure A3.22 shows the bus voltage and the HFAC current for a change in battery module power flow, from -210W to 420W. Also, the Figure captures the increase in the output voltage of the battery module from 42V by one volt. The author further noted that the high dynamic of the system is demonstrated by the swift and smooth change in current that accompanied the change in the battery module energy flow.
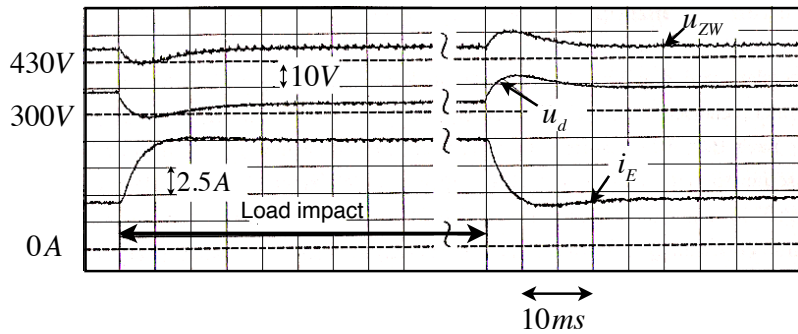
Figure A3.21 Boost converter current and output voltages
for a change in load from -800 W to -1.8 kW (Kokes, 1997)
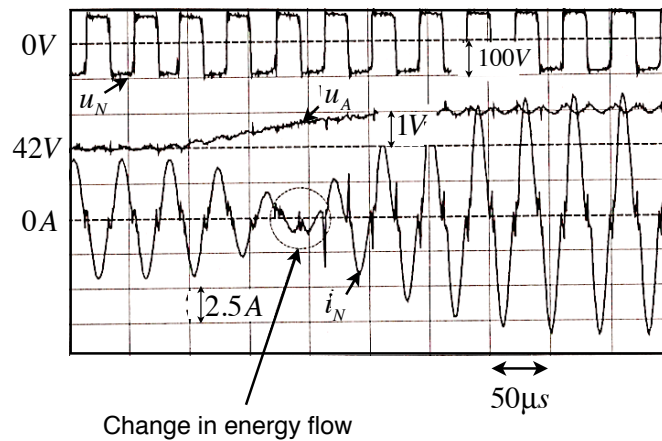
Figure A3.22 Bus voltage (top) and current (bottom), and battery module voltage
(middle) for a change in power flow from -210W to 420 W (Kokes, 1997)

Finally, a bus short circuit with a duration of $210\mu s$ has been evaluated. Initially, the bus load is 800W. Figure A3.23 illustrates the bus voltage and current before, during and after the short circuit test. The Figure demonstrates the operation of the current limiter, which acts at the end of this period to restore the bus operation to an acceptable level.
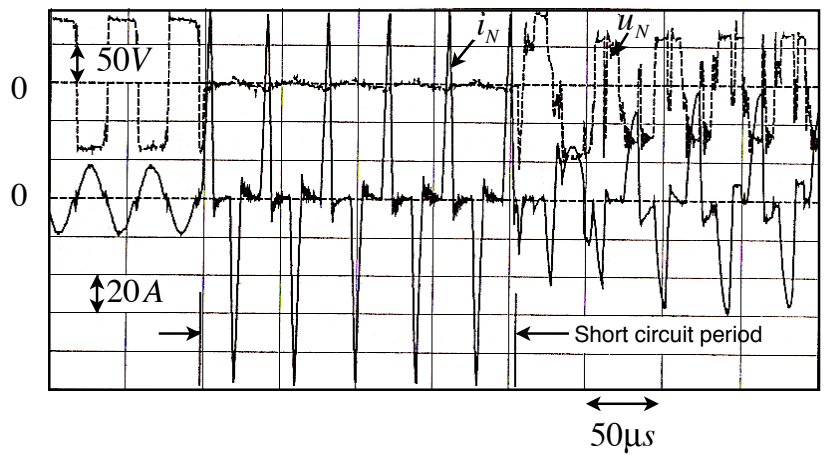
Figure A3.23 Bus voltage (top) and current (bottom), before, during and after a short circuit (Kokes, 1997)

Appendix C

Several effects cause line losses at high frequency: the skin effect, dielectric relaxation in insulators and eddy currents in any metal enclosures (Sudipta et al., 2007). The latter two can be neglected in this analysis because the dielectric loss effect is not significant below 1MHz and eddy current losses can be neglected below 100kHz (Liming and Boggs, 2005). The most significant loss, which will be analysed next, is the skin effect. Figure A4.1 illustrates the attenuation of these losses as a function of frequency for a particular cable used in IGBT motor control applications (i.e. at high frequency) (Liming and Boggs, 2005).
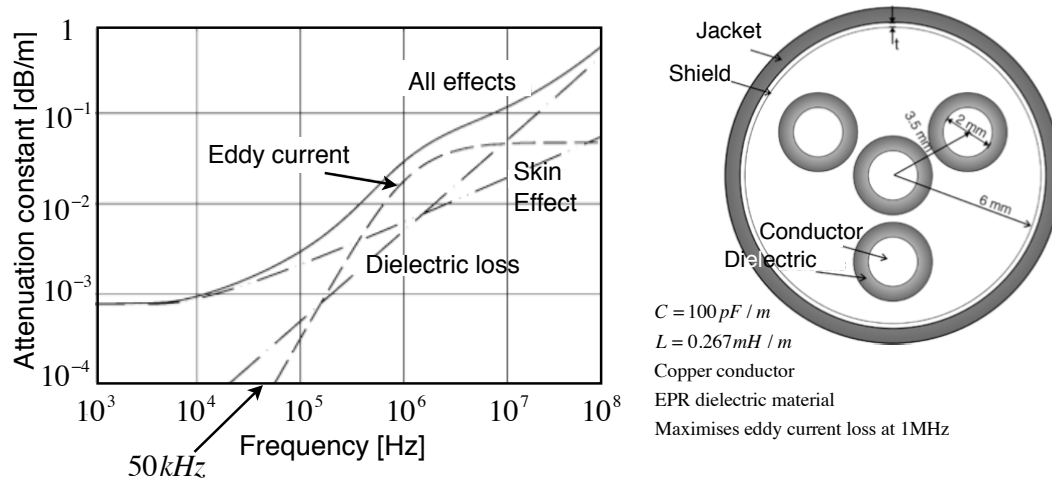
Figure A4.1 Attenuation on high frequency ASD cable shown right (Liming and Boggs, 2005)

The skin effect reduces the area through which the current flows. It is not uncommon for the skin effect to cause the current to flow through a narrower width than that of its carrier cable, which entails greater resistance hence higher I^2R losses along the lines. The following equation yields the skin depth as a function of frequency:

$$\delta_c = \frac{1}{\sqrt{\pi f \mu_0 \sigma}}, \text{ where } \begin{cases} f \text{ is the bus frequency} \\ \mu_0 \text{ is free space permeability} \\ \sigma \text{ is the conductivity of metal} \end{cases} \quad (1)$$

Appendix D

Part D.1

Integrated starter generator (ISG)

Jain et al. (2006) have investigated a direct-torque controlled induction motor for an ISG application. The system was integrated in a 1.4L diesel engine. Experiments show that the total engine cranking torque of 130Nm is achieved within 1.5ms and the process takes approximately 250ms. Figure A5.1 (top) shows the ISG torque and engine speed. Displayed below in the same Figure are the battery voltage and current demand. It is observable that the current exceeds 400A for approximately 250ms during engine cranking.
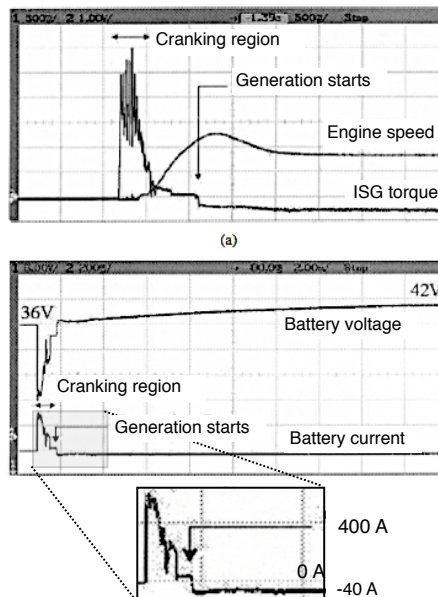
Figure A5.1 (Jain et al., 2006)
(Top) (torque: 30Nm/div, time: 500ms/div). ISG torque vs time; Engine speed vs time
(Bottom) (battery voltage: 6V/div, current: 400A/div, time: 500ms/div). Battery voltage vs time; Battery current vs time

Electromechanical brake (EMB) system

The typical braking force necessary for an electromechanical brake (EMB) system to bring a vehicle to a stop ranges from 1kN to 2kN. These figures are consistent with values quoted for hydraulic braking systems (Klode et al., 2006).

Line et al. (2008) have studied a switched reluctance motor for the EMB system. Figure A5.2 illustrates the DC bus current profile for the motor under brake command. A large current pulse is required at start-up for motor acceleration (40A at 42V, in approximately 5ms). As more brake force input is applied by the driver, the motor develops more torque by increasing the current up to the maximum of 40A in 150ms.
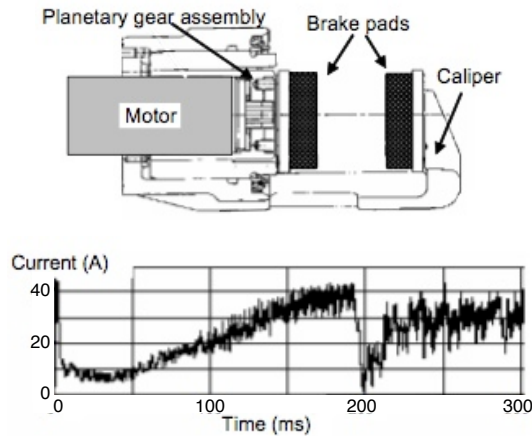
Figure A5.2 Experimental EMB system (top) and motor current during braking (bottom) (Klode et al., 2006)

Electrically heated catalyst (EHC)

The electrical requirements of an electrically heated catalyst (EHC) are shown in Table A5.1 (Bass et al., 1996). Figure A5.3 depicts the EHC voltage and current waveforms during engine cold start, where the peak current demand is approximately 175A at 37V DC (battery voltage 8V). After the 27s heating interval, the alternator resumes normal operation, i.e. charging the battery and maintaining a constant bus voltage level.

Table A5.1 EHC electrical requirements (Bass et al., 1996)

Characteristic	Power levels		
	Low	Medium	High
Current [A]	100-200	200-300	300-400
EMF at load [V]	12	10.5-12	9-10.5
Time at load [s]	15-30	8-15	4-8
Calculated Power Avg. [kW]	1.8	2.8	3.4
Calculated Energy Avg.[Wh]	11.3	9.2	5.7
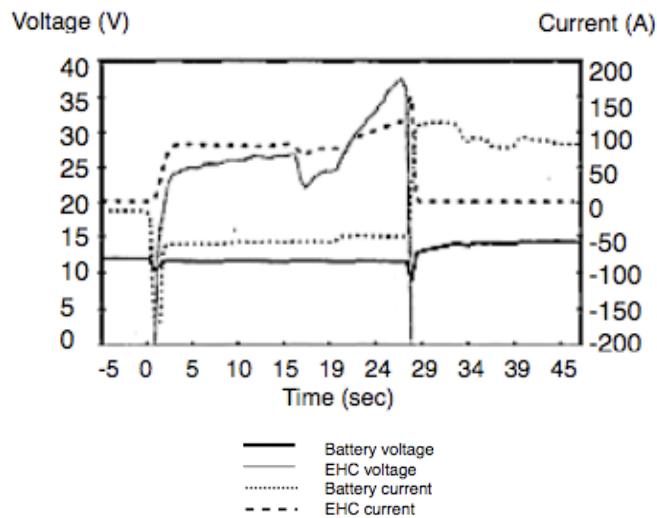
Figure A5.3 EHC current and voltage waveforms during engine cold-start
(Bass et al., 1996)

Variable valve actuation (VVA) system

The final example briefly illustrated is the VVA application. Chang (2003) and Qiu et al. (2004) have investigated a DC motor as actuator for a fully flexible VVA system. Figure A5.4 shows the experimental and simulation current profile during valve transition mode. Current reaches a peak of 18A in less than 1ms, making the VVA application one of the most demanding amongst vehicle auxiliary loads.
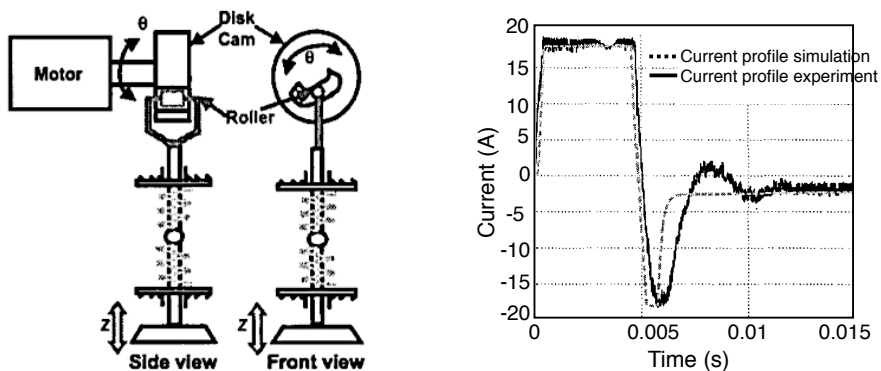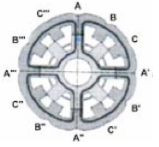
Figure A5.4 (Chang, 2003, Qiu et al., 2004)
(left) VVA system (for one valve) actuated by DC motor with
translational mechanical transformer
(right) Current profiles during transition mode for the DC motor

Table A5.2 Comparison between AC electric machines for the ISG application (Cai, 2004)

Electric Machine Type	Claw Pole Lundell	Induction Motor	Sinusoidal PMAC	Switched Reluctance Machine
Picture				
Efficiency and compactness			✓	
Low torque ripple and noise	✓	✓	✓	
Wide speed range	✓	✓	✓	✓
High power application		✓	✓	✓

Part D.2

The pulsating DC voltage (stage 2, as shown in Figure 5.13) is generated by the equivalent circuit depicted in Figure A5.5, where:

- the voltage source V_{dc} is the equivalent of a generator, AC/DC converter and lead-acid battery combination,
- R_r represents the internal resistance of the resonant network inductor L_r,
- C_r is the resonant network capacitor.
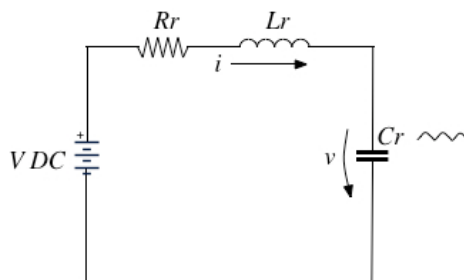
Figure A5.5 Simplified representation of the resonant circuit [1]

---

[1] The pulses over the resonant capacitor shown in the Figure are the sinusoidal DC pulses specified at the stage 2 of the inverter in the previous Section (see Figure 5.13)

Since a pulsating DC voltage is required over capacitor C_r, a representation of the relationship between V_{dc} and the C_r voltage (V_c) is necessary. A suitable method to represent this correlation is the Laplace or frequency-domain analysis of the circuit, based on the fact that the circuit elements are linear. Transforming the time-domain equation of the resonant circuit into the frequency domain, the following second order transfer function yields a convenient instrument for manipulating the dynamics of the circuit:

$$\frac{V_c(s)}{V(s)} = \frac{1}{L_r C_r \cdot s^2 + R_r C_r \cdot s + 1} \tag{1}$$

Figure A5.6 illustrates the transient response of the voltage over C_r ($V_c(s)$) for a DC voltage step input. The role of Figure A5.6[2] is to illustrate the typical response of a second-order system, and to highlight the variables which will be used in the present analysis of the inverter: the natural frequency ω_n, the overshoot χ and the decay ratio δ of $V_c(s)$.

The natural frequency ω_n of the voltage oscillations is determined by Equation 2. The oscillations are progressively reduced due to the damping effect of the inductor resistance R_r. In fact, the influence of this component on the decay ratio δ of $V_c(s)$ is expressed by Equations 3-5. The link between R_r and δ is variable ζ, which is the damping ratio of the transfer function in Equation 1.

---

2. The waveform represents voltage amplitude vs. time, and the actual units for the Figure are dependent upon the values of the circuit components. The Figure aims to highlight main characteristics of the voltage step response and therefore the actual units are not relevant at this stage of the analysis.
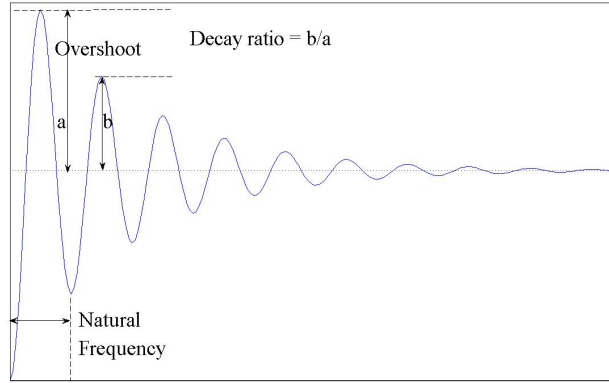
Figure A5.6 *Vc* voltage waveform for step DC voltage input

$$\omega_n = \frac{1}{\sqrt{L_r C_r}} \tag{2}$$

$$\delta = e^{\frac{-2\pi\zeta}{\sqrt{1-\zeta^2}}}, \tag{3}$$

$$\chi = \sqrt{\delta} = e^{\frac{-\pi\zeta}{\sqrt{1-\zeta^2}}} \tag{4}$$

$$\zeta = \frac{R_r}{2}\sqrt{\frac{C_r}{L_r}}, 0 \le \zeta \le 1 \tag{5}$$

The aim is to find the values of L_r and R_r that minimise the decay voltage (or set the decay ratio δ equal to unity) for the first resonant cycle. By reducing δ at time $t = \frac{2\pi}{\omega_n}$, the shape of a positive half sinusoid can be obtained (as in Figure 5.13, stage 2), which becomes the building block of the HFAC output sinusoid and makes ZVS possible.

A value of δ close to unity yields the desired output for the first resonant cycle only, while the decay ratio for the kth cycle of $V_c(s)$ will be $k\delta$. To maintain the decay ratio of the first cycle and the ZVS capability, switches S_1 and S_2 of the H-bridge are turned on simultaneously for a short time period, denoted by Δ, at the beginning of each

resonant cycle. This technique, shown in Figure A5.7, allows the current in the resonant inductor to increase sharply for a finite time and thus, the circuit is energized continuously to maintain its resonating or pulsating pattern.
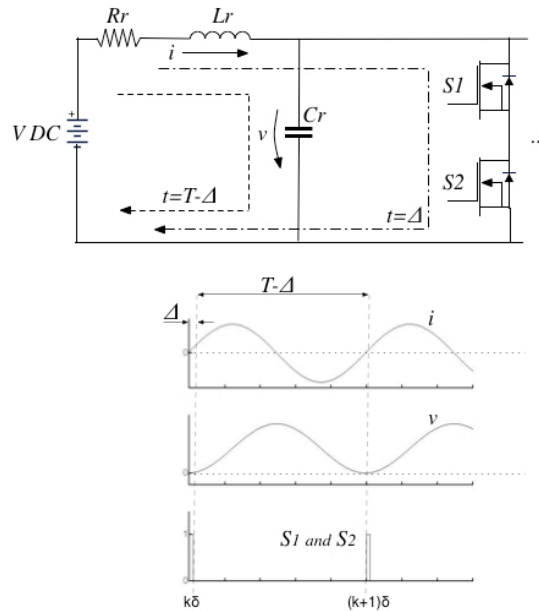
Figure A5.7 Diagram and waveforms illustrating the resonant principle [4]

Since the decay ratio is maintained at a value close to unity, the implication is that the voltage overshoot (variable χ in Equation 4) is also approximately equal to 1, or 100%. Therefore, the amplitude of the resonant DC pulses is expected to be twofold the input DC voltage amplitude, i.e. 84V or 59.4Vrms.

Resonant circuit design

The analysis includes a generic load in the form of a resistor R_L connected in parallel with the resonant capacitor C_r. The new transfer function, corresponding to Equation 1 and reflecting the added load becomes:

---

[4] Only the switches of the first H-bridge leg (see Figure 5.14) are shown in the diagram.

$$H(s) = \frac{V_c(s)}{V(s)} = \frac{1}{s^2 + \frac{1}{L_r C_r} \cdot \frac{L_r + R_r R_L C_r}{R_L} \cdot s + \frac{R_r + R_L}{R_L} \cdot \frac{1}{L_r C_r}} \tag{6}$$

This analysis illustrates the steps in determining, and the constraints related to, the parameters of *H(s)* for a preset decay voltage or decay ratio δ. As previously mentioned, the decay voltage should be as close to zero as possible to allow for ZVS. For an input DC voltage V_{DC}, preset decay voltage V_0 and based on Equation 5 and Figure A5.6, the following relationship determines the decay ratio δ:

$$V_{DC} \cdot \sqrt{\delta} - V_{DC} \cdot \sqrt{\delta} \cdot \delta = V_0 \tag{7}$$

Amongst the three real roots of Equation 7 (where the variable is $\sqrt{\delta}$ or χ, the voltage overshoot), let δ_0 denote the one closest to unity, satisfying the condition $0 < \delta_0 < 1$. This value is next used to calculate the damping ratio ζ (corresponding to the preset decay voltage) required for *H(s)*. Replacing δ_0 in Equation 3 yields the following value for the damping ratio corresponding to the decay voltage V_0:

$$\zeta = \frac{|\ln \delta_0|}{\sqrt{4\pi^2 + \ln^2 \delta_0}} \tag{8}$$

The values of L_r and C_r satisfying Equation 8 are the solution of the following system, based on the equivalent representation of *H(s)* in Equation 10 as a standard second order system:

$$\begin{cases} \omega_n^2 = \frac{R_r + R_L}{R_L} \cdot \frac{1}{L_r C_r} \\ 2\zeta\omega_n = \frac{1}{L_r C_r} \cdot \frac{L_r + R_r R_L C_r}{R_L} \end{cases} \tag{9}$$

$$H(s) = \frac{1}{s^2 + 2\zeta\omega_n s + \omega_n^2} \tag{10}$$

Solving system 9 (above) yields the quadratic equation below for the inductance L_r:

$$L_r^2 - 2\zeta \frac{R_r + R_L}{\omega_n} \cdot L_r + \frac{R_r(R_r + R_L)}{\omega_n^2} = 0 \tag{11}$$

where C_r is a function of L_r:

$$C_r = \frac{R_r + R_L}{R_L} \cdot \frac{1}{\omega_n^2} \cdot \frac{1}{L_r} \tag{12}$$

The condition for the existence of real roots for Equation 11 is the constraint that the parameters R_r and R_L must satisfy for the given decay ratio δ_0, or decay voltage V_0:

$$\frac{R_r}{R_r + R_L} \leq \zeta^2 \tag{13}$$

Equation 13 sets the limit for the inverter output power and input DC voltage, and has a direct effect on the dissipation losses in the inverter. In particular, the output power that the inverter can handle for a given δ_0 is expressed in the form of the lower bound on the load resistance R_L, derived from Equation 13:

$$R_L \geq \frac{R_r(1 - \zeta^2)}{\zeta^2} \tag{14}$$

Replacing ζ with its equivalent from Equation 8, the lower limit on R_L can be expressed directly in terms of the circuit design parameter δ_0 as in Equation 15:

$$R_L \geq \frac{4\pi^2 R_r}{\ln^2 \delta_0} \tag{15}$$

The second constraint imposed by Equation 13 is an upper bound on the inductor winding resistance R_r:

$$R_r \leq \frac{\ln^2 \delta_0}{4\pi^2} R_L \qquad (16)$$

R_r has a role in determining the value of L_r as in Equation 17, which is the expression of the larger of the two roots of equation 11: the upper limit on R_r translates into a low value for L_r.

$$L_r = \zeta \frac{R_r + R_L}{\omega_n} + \frac{1}{2}\sqrt{\zeta^2(R_r + R_L) - R_r} \qquad (17)$$

Since $I_{Lr} = \frac{V_{DC}}{\omega_n L_r}$, a low R_r ultimately sets a requirement for the inductor to have a high current withstanding capability. Furthermore, since the dissipation losses in the inductor are proportional to the square of the current, a high current may generate undesirable I^2R losses.

Output voltage control

Two sets of signals are constructed by the control sub-system; first, diagonal switches of the H-bridge are closed simultaneously every resonant cycle to transfer the C_r voltage pulses with alternate polarities to the output filter (inverter stage 3, in Figure 5.13). Second, at the beginning of each time period, the two switches of the first inverter leg are closed concurrently in order to maintain the energy in the resonant circuit, as previously shown in Figure A5.7.

While the first set of signals is a repetitive pulse sequence synchronised with the output frequency, the second set of signals are adapted by the control structure to the load conditions: for higher load currents, the duration Δ while MOSFETs S_1 and S_2 are switched on is longer in order to draw more current from the DC source. For low current load conditions, Δ will be minimised.

Since Δ is the control variable in the circuit, its influence on the energy stored in the resonant circuit can be described with reference to the diagram in Figure A5.8, where

$2R_{DS}$ represents the combined *ON* resistance of power switches S_1 and S_2. During Δ the current through inductor L_r increases according to the transfer function:

$$G(s) = \frac{I(s)}{V(s)} = \frac{2R_{DS}C_r s + 1}{2R_{DS}L_r C_r s^2 + (L_r + 2R_{DS}R_r C_r)s + R_r + 2R_{DS}} \qquad (18)$$
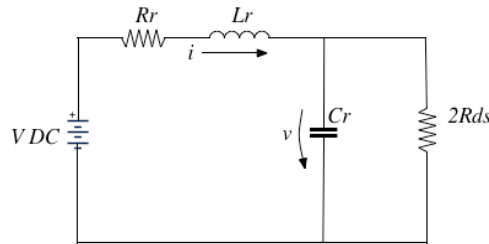
Figure A5.8 Equivalent circuit diagram for time duration Δ

G(s) can be approximated by a first order transfer function since the coefficients $2R_{DS}L_r C_r$, $2R_{DS}R_r C_r$ and $2R_{DS}C_r$ are very small in comparison with R_r and R_{DS}, and therefore can be neglected. The step response of *G(s)*, alike for both the detailed and approximate representations, is depicted in Figure A5.9. The Laplace transfer function and the time-domain equivalent representation of *G(s)* are expressed by Equations 19 and 20, respectively.
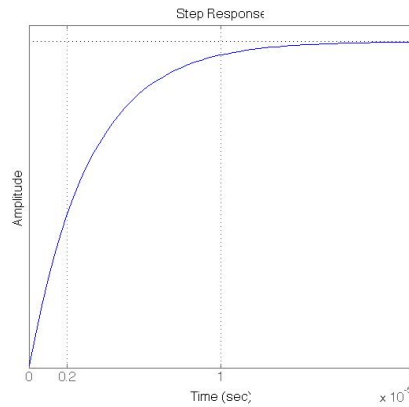
Figure A5.9 Step response of current over inductor L_r

$$G(s) = \frac{I(s)}{V(s)} \approx \frac{1}{L_r \cdot s + R_r + 2R_{DS}} \qquad (19)$$

$$i(t) = \frac{V_{DC}}{L_r} \cdot (1 - e^{-\frac{R_r + 2R_{DS}}{L_r} \cdot t}) \tag{20}$$

Figure A5.9 shows that for the first 2μs the curve is approximately linear. In fact, the control variable Δ is not expected to exceed this duration. For the output voltage frequency of 50kHz, 2μs represents 20% of the half-sinusoid time period (or 20% of the resonant DC voltage time period). Consequently, the exponential function in Equation 20 can be approximated by the first two terms in its equivalent Taylor series. The expression of the current for the linear region becomes:

$$i(t) = \frac{V_{DC}}{L_r} \left[1 - \left(1 - \frac{R_r + 2R_{DS}}{L_r} t \right) \right] = \frac{V_{DC}(R_r + 2R_{DS})}{L_r^2} t \tag{21}$$

Under varying load conditions, Δ must satisfy the following equality every resonant cycle of time period *T/2* (where *T* is the time period of the 50kHz sinusoid), based on the requirement for the voltage over capacitor C_r to be equal to the inverter reference voltage V_{ref}:

$$V_{ref}(t) = \frac{1}{C_r} \int_0^{\Delta} i(t)dt + \frac{1}{C_r} \int_{\Delta}^{T/2} (i_{L_r}(t) - i_{load}(t))dt \tag{22}$$

As a result, based on Equations 21 and 22, the time duration control Δ is varied by the control sub-system in order to satisfy the following equality:

$$V_{ref}(t) = \frac{V_{DC}(R_r + 2R_{DS})}{C_r L_r^2} \frac{\Delta^2}{2} + \frac{1}{C_r} \int_{\Delta}^{T/2} (i_{L_r}(t) - i_{load}(t))dt \tag{23}$$

which is calculated at the beginning of each cycle and makes use of the measured load current (i_{load}) and resonant inductor current (i_{L_r}).

Part D.3
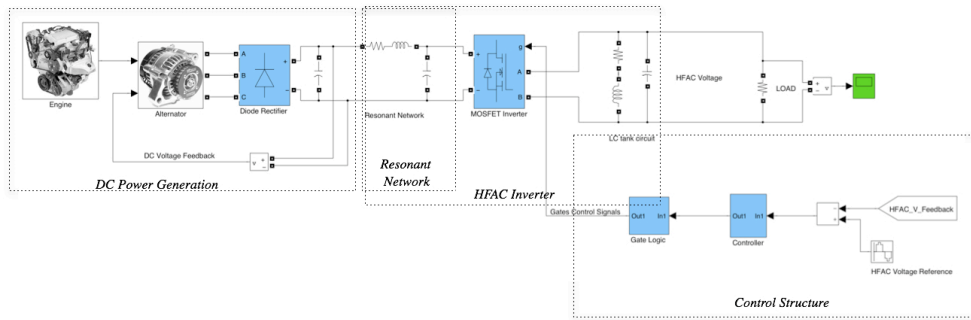
Figure A5.10 Matlab Simulink model of the proposed vehicle HFAC power supply. Sub5systems corresponding to Figure 5.14 are highlighted; these include the DC Power Generation, Resonant Network, and HFAC Inverter and Control structure

Appendix E
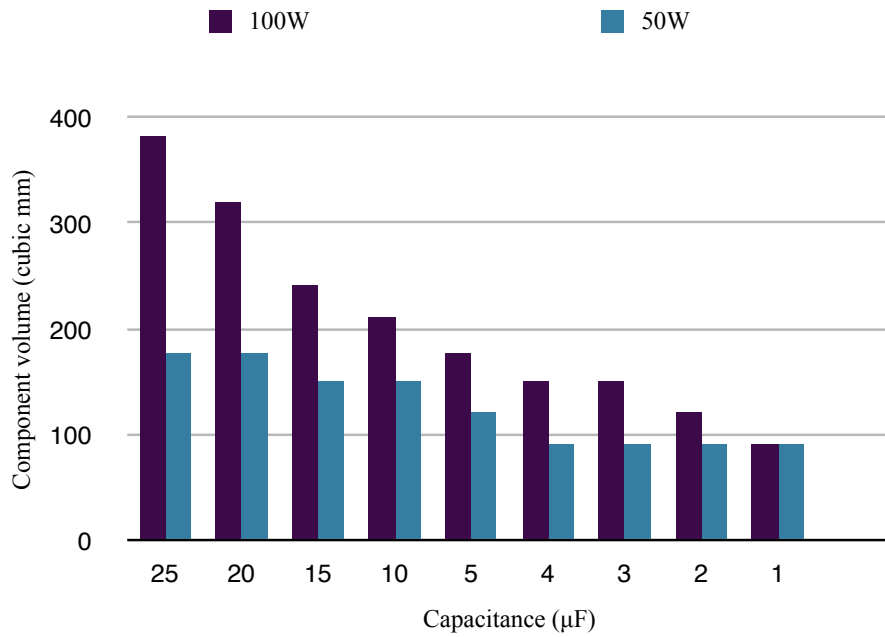
Figure A6.1 Packaging volume (mm3) of a capacitor vs. capacitance (µF), for two different power rating values (Vishay, 2008)

Table A6.1 AWG data for DC conductors

AWG gauge	Conductor Diameter Inches	Conductor Diameter mm	Ohms per 1000 ft.	Ohms per km	Maximum amps for chassis wiring	Maximum amps for power transmission	Maximum frequency for 100% skin depth for solid conductor copper
OOOO	0.46	11.684	0.049	0.16072	380	302	125 Hz

OOO	0.4096	10.40384	0.0618	0.202704	328	239	160 Hz
OO	0.3648	9.26592	0.0779	0.255512	283	190	200 Hz
0	0.3249	8.25246	0.0983	0.322424	245	150	250 Hz
1	0.2893	7.34822	0.1239	0.406392	211	119	325 Hz
2	0.2576	6.54304	0.1563	0.512664	181	94	410 Hz
3	0.2294	5.82676	0.197	0.64616	158	75	500 Hz
4	0.2043	5.18922	0.2485	0.81508	135	60	650 Hz
5	0.1819	4.62026	0.3133	1.027624	118	47	810 Hz
6	0.162	4.1148	0.3951	1.295928	101	37	1100 Hz
7	0.1443	3.66522	0.4982	1.634096	89	30	1300 Hz
8	0.1285	3.2639	0.6282	2.060496	73	24	1650 Hz
9	0.1144	2.90576	0.7921	2.598088	64	19	2050 Hz
10	0.1019	2.58826	0.9989	3.276392	55	15	2600 Hz
11	0.0907	2.30378	1.26	4.1328	47	12	3200 Hz
12	0.0808	2.05232	1.588	5.20864	41	9.3	4150 Hz
13	0.072	1.8288	2.003	6.56984	35	7.4	5300 Hz
14	0.0641	1.62814	2.525	8.282	32	5.9	6700 Hz
15	0.0571	1.45034	3.184	10.44352	28	4.7	8250 Hz
16	0.0508	1.29032	4.016	13.17248	22	3.7	11 k Hz
17	0.0453	1.15062	5.064	16.60992	19	2.9	13 k Hz
18	0.0403	1.02362	6.385	20.9428	16	2.3	17 kHz
19	0.0359	0.91186	8.051	26.40728	14	1.8	21 kHz
20	0.032	0.8128	10.15	33.292	11	1.5	27 kHz
21	0.0285	0.7239	12.8	41.984	9	1.2	33 kHz
22	0.0254	0.64516	16.14	52.9392	7	0.92	42 kHz
23	0.0226	0.57404	20.36	66.7808	4.7	0.729	53 kHz
24	0.0201	0.51054	25.67	84.1976	3.5	0.577	68 kHz
25	0.0179	0.45466	32.37	106.1736	2.7	0.457	85 kHz
26	0.0159	0.40386	40.81	133.8568	2.2	0.361	107 kH
27	0.0142	0.36068	51.47	168.8216	1.7	0.288	130 kHz
28	0.0126	0.32004	64.9	212.872	1.4	0.226	170 kHz
29	0.0113	0.28702	81.83	268.4024	1.2	0.182	210 kHz
30	0.01	0.254	103.2	338.496	0.86	0.142	270 kHz
31	0.0089	0.22606	130.1	426.728	0.7	0.113	340 kHz
32	0.008	0.2032	164.1	538.248	0.53	0.091	430 kHz
Metric 2.0	0.00787	0.200	169.39	555.61	0.51	0.088	440 kHz
33	0.0071	0.18034	206.9	678.632	0.43	0.072	540 kHz
Metric 1.8	0.00709	0.180	207.5	680.55	0.43	0.072	540 kHz
34	0.0063	0.16002	260.9	855.752	0.33	0.056	690 kHz

Metric 1.6	0.0063	0.16002	260.9	855.752	0.33	0.056	690 kHz
35	0.0056	0.14224	329	1079.12	0.27	0.044	870 kHz
Metric 1.4	0.00551	0.140	339	1114	0.26	0.043	900 kHz
36	0.005	0.127	414.8	1360	0.21	0.035	1100 kHz
Metric 1.25	0.00492	0.125	428.2	1404	0.20	0.034	1150 kHz
37	0.0045	0.1143	523.1	1715	0.17	0.0289	1350 kHz
Metric 1.12	0.00441	0.112	533.8	1750	0.163	0.0277	1400 kHz
38	0.004	0.1016	659.6	2163	0.13	0.0228	1750 kHz
Metric 1	0.00394	0.1000	670.2	2198	0.126	0.0225	1750 kHz
39	0.0035	0.0889	831.8	2728	0.11	0.0175	2250 kHz
40	0.0031	0.07874	1049	3440	0.09	0.0137	2900 kHz

Appendix F

(a)

(b)
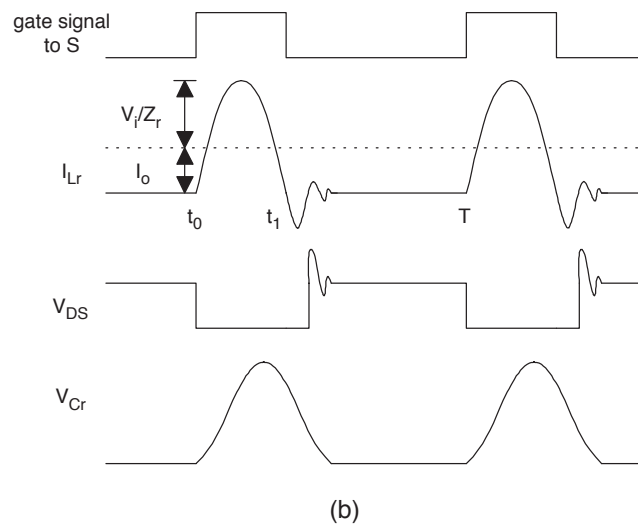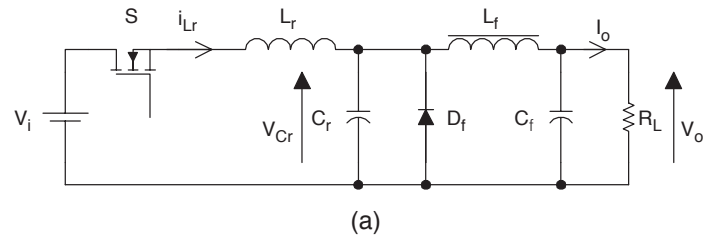
Figure A7.1 Full-wave, quasi-resonant buck converter with ZVS
(a) schematic diagram, (b) circuit waveforms (Rashid, 2007)
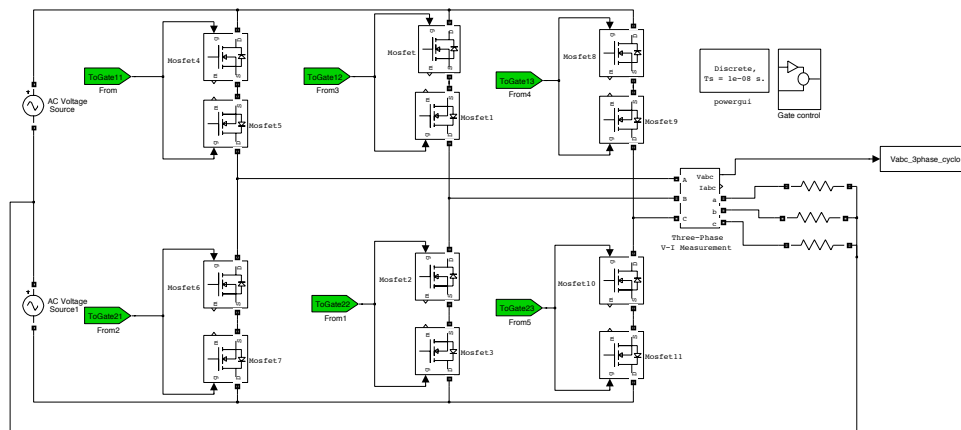
Figure A7.2a Matlab Simulink model of the HFAC to three-phase AC cycloconverter
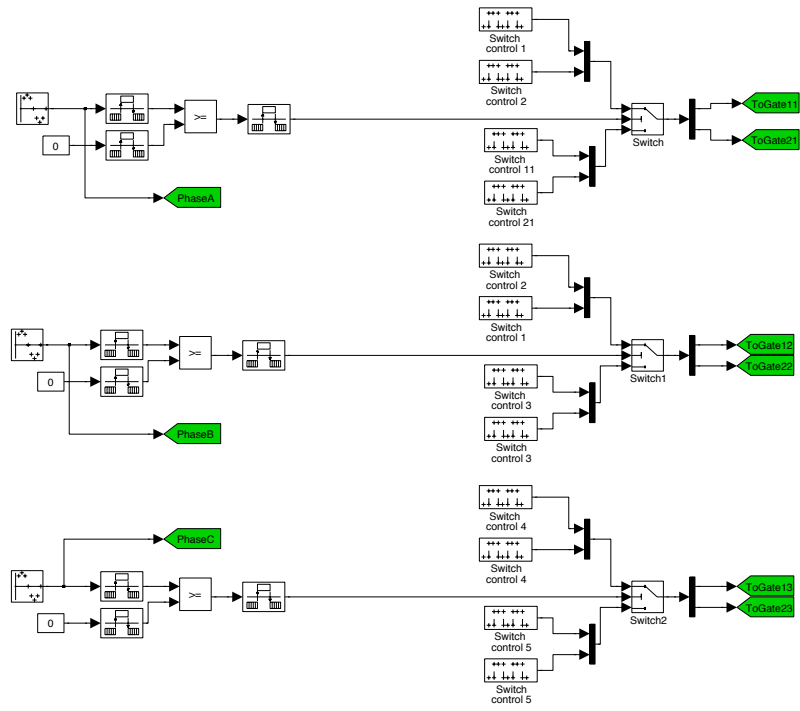
Figure A7.2b Gate control sub-model in the three-phase AC cycloconverter model shown in
Figure A7.2 (a)

Appendix G
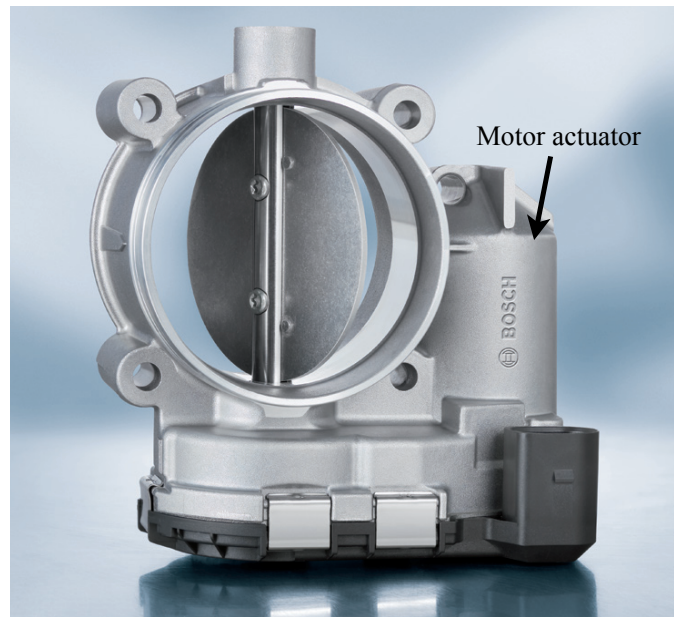
Figure A8.1 Throttle valve system (Bosch)

Figure A8.2 EPAS experimental apparatus (left)
Figure A8.3 Three-phase, permanent magnet synchronous motor (right)
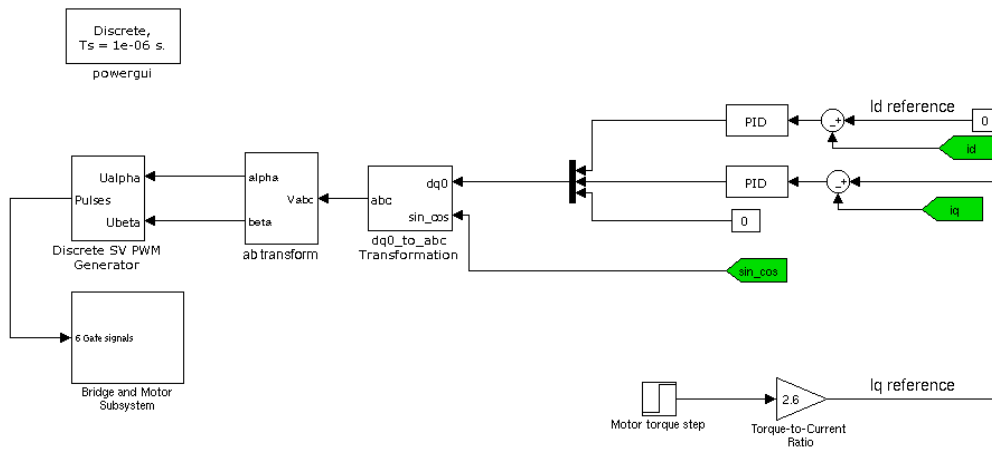
Figure A8.4a Matlab Simulink model of EPAS system
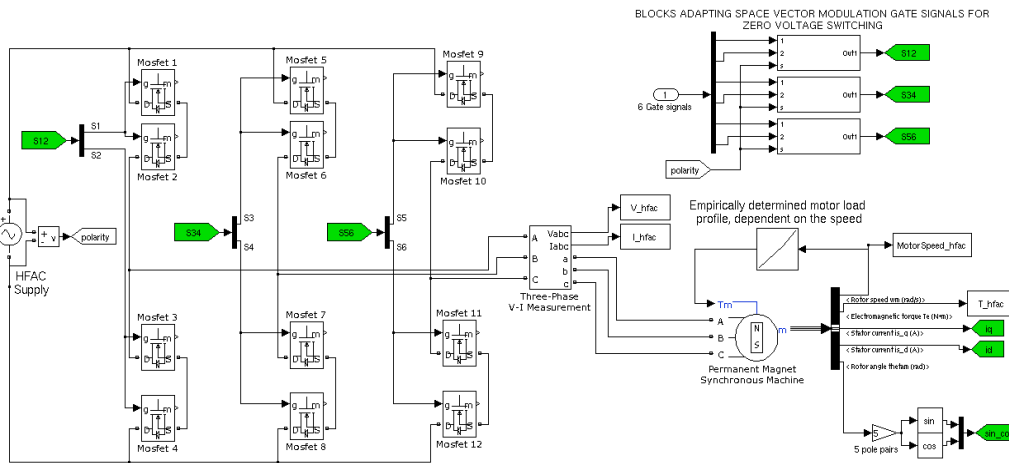
Figure A8.4b HFAC/AC bridge and motor sub-system model in Matlab Simulink (corresponding to the block with the same name in the model shown in Figure A3.a)

Table A81. PMSM parameters

Model	12S10P	Copper loss (W)	152
Slot number	12	Efficiency (%)	73.5
Pole number	10	Wire size (mm)	1.0
Rated current (A)	13.0	Number of turns	30
Rated torque (N-m)	7.03	Current density (MA/m^2)	16.67
Cogging torque, T_{cog}(N-m)	4.42e-3	Slot fill factor (%)	55.57
T_{cog}/T_n(%)	0.063	Stator outer diameter (mm)	75
Open-circuit voltage (V_{phase})	12.5	Stator inner diameter (mm)	41
Iron loss (W)	3.96	Rotor outer diameter (mm)	40

Appendix H

Table A9.1 Acronyms of electrical loads

Acronym	Description	Acronym	Description
AS	Active Suspension	EHC	Electrically Heated Catalyst
FLG	Front Left Fog Lamp	BM	Blower Motor
FRG	Front Right Fog Lamp	EPS	Electric Power Assisted Steering
PW	Power Window	AB	Airbag Sensor
FL	Front Left Indicator	CLM	Central Locking Motor
FR	Front Right Indicator	HFS	Heated Front Screen
MHB1	Main/High Beam 1	FWM	Front Wipers Motor
MHB2	Main/High Beam 2	FWP	Front Washer Pump
FLL	Left Lateral Indicator Light	IC	Instrument Cluster
FRL	Right Lateral Indicator Light	HRS	Heated Rear Screen
TPS	Tire Pressure Sensor	RWM	Rear Wipers Motor
ISG	Integrated Starter Generator	RWP	Rear Washer Pump
VVA	Variable Valve Actuation	FP	Fuel Pump
A/C	Air Conditioning	RMB1	Rear Main Beam 1
RG	Rear Fog Light	RMB2	Rear Main Beam 2
TGM	Tailgate (Boot) Motor	RRB	Rear Right Brake Light
TGL	Tailgate (Boot) Light	RLB	Rear Left Brake Light

Table A9.2 Typical information available for several low power electrical loads

LOAD DESCRIPTION

Climate Control Sensor
Supply Voltage: 8V..18V
Supply Current: 110 mA
Operating conditions: -40..85 degrees C

Differential Pressure Sensor
(for measuring load on diesel particulate filter)
Supply Voltage: 5V
Supply Current: 9mA
Operating conditions: -40..130 degrees C

LOAD DESCRIPTION

Hot-film Air-mass Meter
(for measuring air mass in intake manifold)
Supply Voltage: 6V..17V
Operating conditions: -20..80 degrees C

Accelerator Pedal Sensor
Supply Voltage: 5V
Operating conditions: -40..80 degrees C

Peripheral Pressure Sensor
Supply Voltage: 5V..11V; 8.5V nominal
Supply Current: 30mA..43.5mA; 37mA nominal
Operating conditions: -40..85 degrees C

Steering Angle Sensor
Supply Voltage: 8V..16V
Supply Current: 150mA

Steering Torque Sensor
Supply Voltage: 8V..16V
Supply Current: 400mA

Accelerometer
Supply Voltage: 4.75V..5.25V; 5V nominal
Supply Current: 8mA, max 10mA

Barometric Air Pressure Sensor
(for engine management)
Supply Voltage: 4.75V..5.25V; 5V nominal
Supply Current: 12.5mA
Operating conditions: -40..130 degrees C

Angular Rate Sensor
(for rollover applications)
Supply Voltage: 4.75V..5.25V
Supply Current: <30mA
Operating conditions: -40..85 degrees C

Transmission Range Selection Sensor
Supply Voltage: 5V (+/- 0.25V)
Operating temperature: -40..150 degree C

Minimum-length optimisation algorithm

For the total of 29 electrical loads analysed in Section 9.4.2, an optimisation method has been utilised, based on a *greedy algorithm* (WIkipedia).

The technique finds the minimum spanning tree in a graph of interconnected nodes. The required information to run the algorithm is a matrix indicating the length between each and all the elements of the graph.

For the specific analysis in Section 9.4.2, the matrix below indicates the estimated length between the electrical loads within the vehicle. Matrix element M(i,j) represents the estimated conductor length between loads denoted by the numbers *i* and *j*.

Matrix M:

0	2	2	3	3	3	2	3	4	6	0	1	5	6	5	2	2	2	1	2	2	3	2	3	3	6	2	3	1
0	0	2	2	3	2	0	2	4	4	2	2	3	4	5	4	2	1	1	1	2	2	2	2	4	2	0	2	
0	0	0	3	2	0	2	4	2	4	2	2	3	4	3	4	2	5	4	5	3	1	1	1	1	4	0	2	2
0	0	0	0	2	3	1	0	2	3	3	3	2	3	3	5	4	2	2	2	2	3	3	3	3	3	3	1	3
0	0	0	0	0	1	3	2	0	3	3	3	3	2	2	5	4	3	3	6	5	2	2	2	2	3	1	3	4
0	0	0	0	0	0	2	3	1	4	2	2	3	3	3	4	2	4	4	5	3	1	1	1	1	4	0	2	2
0	0	0	0	0	0	0	1	3	4	2	2	3	4	5	4	2	1	1	1	1	2	2	2	2	4	2	0	2
0	0	0	0	0	0	0	0	2	2	3	3	2	3	3	5	4	2	2	2	2	3	3	3	3	3	3	2	3
0	0	0	0	0	0	0	0	0	2	3	3	2	2	1	5	4	3	3	6	5	2	2	2	2	2	2	3	4
0	0	0	0	0	0	0	0	0	0	5	6	1	1	1	8	7	5	5	5	5	6	6	6	6	0	6	4	5
0	0	0	0	0	0	0	0	0	0	0	0	0	5	5	6	2	1	2	2	2	2	1	2	2	2	6	1	1	1
0	0	0	0	0	0	0	0	0	0	0	0	0	5	5	5	2	1	2	2	2	2	1	2	2	2	6	1	1	1
0	0	0	0	0	0	0	0	0	0	0	0	0	0	1	8	7	5	5	5	5	6	6	6	6	1	6	4	5
0	0	0	0	0	0	0	0	0	0	0	0	0	0	1	8	7	5	5	5	5	5	6	5	6	1	6	4	5
0	0	0	0	0	0	0	0	0	0	0	0	0	0	0	7	6	5	4	8	7	4	4	4	4	1	4	5	6
0	0	0	0	0	0	0	0	0	0	0	0	0	0	0	0	3	5	5	5	5	5	5	5	5	8	4	4	5
0	0	0	0	0	0	0	0	0	0	0	0	0	0	0	0	0	2	2	2	2	2	2	2	3	4	4	2	
0	0	0	0	0	0	0	0	0	0	0	0	0	0	0	0	0	0	0	0	0	2	2	2	2	3	3	1	1
0	0	0	0	0	0	0	0	0	0	0	0	0	0	0	0	0	0	0	0	0	2	2	2	2	3	3	1	1
0	0	0	0	0	0	0	0	0	0	0	0	0	0	0	0	0	0	0	0	0	2	2	2	2	3	3	1	1

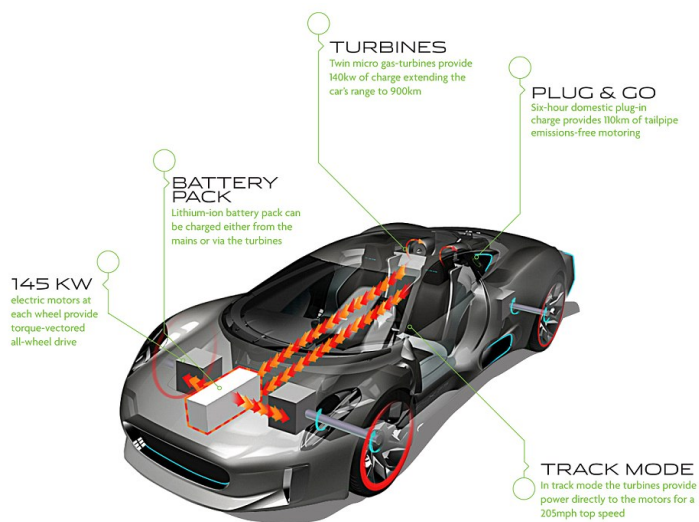|																														
0	0	0	0	0	0	0	0	0	0	0	0	0	0	0	0	0	0	0	0	0	0	0	2	2	2	2	3	3	1	1
0	0	0	0	0	0	0	0	0	0	0	0	0	0	0	0	0	0	0	0	0	0	0	0	0	0	0	3	1	3	2
0	0	0	0	0	0	0	0	0	0	0	0	0	0	0	0	0	0	0	0	0	0	0	0	0	0	0	3	1	3	2
0	0	0	0	0	0	0	0	0	0	0	0	0	0	0	0	0	0	0	0	0	0	0	0	0	0	0	3	1	3	2
0	0	0	0	0	0	0	0	0	0	0	0	0	0	0	0	0	0	0	0	0	0	0	0	0	0	0	3	1	3	2
0	0	0	0	0	0	0	0	0	0	0	0	0	0	0	0	0	0	0	0	0	0	0	0	0	0	0	0	4	4	5
0	0	0	0	0	0	0	0	0	0	0	0	0	0	0	0	0	0	0	0	0	0	0	0	0	0	0	0	0	3	2
0	0	0	0	0	0	0	0	0	0	0	0	0	0	0	0	0	0	0	0	0	0	0	0	0	0	0	0	0	0	1
0	0	0	0	0	0	0	0	0	0	0	0	0	0	0	0	0	0	0	0	0	0	0	0	0	0	0	0	0	0	0

Figure A9.1 Concept of vehicle integrating micro gas turbines (Jaguar Land Rover)

Figure A9.2 Micro gas turbine concept for the next generation of HEVs (Jaguar Land Rover)